**NATIONAL TECHNICAL UNIVERSITY OF ATHENS**

SCHOOL OF CHEMICAL ENGINEERING – INTERDISCIPLINARY PROGRAM OF POSTGRADUATE STUDIES "MATERIALS SCIENCE & TECHNOLOGY"

# MASTER THESIS

---

CRASHWORTHINESS BEHAVIOR OF THIN-WALLED ALUMINIUM SQUARE TUBES UNDER OBLIQUE IMPACT

---

**KONSTANTINA D. KARANTZA**

Supervisor Professor: D. MANOLAKOS

Athens
September 2022

*In the memory of my beloved late grandmother Barbara*

*whose soul will be my eternal teacher*

# Abstract

The aim of current master thesis is to investigate the crushing behavior of thin-walled aluminium AA6060-T6 square tubes subjected to both axial and oblique loading in order to evaluate their crashworthiness efficiency and energy absorption capacity. A parametric analysis in loading angle lying up to 15$^{o}$ and in initial type of contact between impactor and tube are examined in order to assess their effect on plastic collapse initiation and energy absorption. The examined initial contact types contain a contact-in-edge case and a contact-in-corner one between impactor and tube regarding the oblique loading scenarios. In order to evaluate the energy absorption capability and the characteristics of the occurred collapse mechanism, both experimental tests and numerical finite element simulations are carried out providing the force-displacement curve and the main crashworthiness response parameters, while further different collapse states are captured during plastic deformation.

At first, the experimental compression tests are conducted in quasi-static conditions under a constant loading rate of 10 mm/min by adjusting properly the loading angle representing off-axis oblique crushing conditions. For each examined case, two compression tests are carried out in order to secure the reliability of experimental results. At next, numerical simulation are carried out in LS DYNA software by developing the finite element models for each examined case. The numerical simulations consider dynamic conditions by adjusting a crushing speed of 1 m/s. The square tubes are modelled via 4-node shell elements, while at each examined configuration the bottom tube end was considered as fixedly supported. The experimental and the numerical results were firstly compared between each other to validate the created finite element models, while also both were taken into account in order to evaluate the crashworthiness performance and assess the loading angle and initial type of contact effects on crushing efficiency.

Both experiments and simulations showed a sufficient agreement in both plastic collapse mechanism and crashworthiness response parameters. All examined cases revealed an inextensional collapse mode, while slight tearing occurred around tube corners. The tearing effect seemed stronger at lower loading angles compared to the one of crushing angle, while in contrast the crushing angle effect revealed greater magnitude at higher loading angles. The increase in loading angle resulted in energy absorption decrease and lower peak crushing force which however flattened out at high angles. Cornered oblique loading revealed greater peak force and energy absorption at all loading angles compared to edged oblique loading. Finally, 5$^{o}$ cornered oblique crushing was proved as the most beneficial revealing the greatest energy absorption capacity.

# Acknowledgements

I would like to deeply thank my thesis supervisor professor D. Manolakos for entrusting me and providing me with such an interesting subject, as well as for his valuable guidance, advice and constant encouragement and guidance throughout both my undergraduate and postgraduate studies.

Also, I would like to express my grateful thanks to the technical staff of the Manufacturing Technology Lab of NTUA for their useful help on specimens' productions and preparation.

Finally, I would like to specially thank my family for their continued encouragement and support during my studies and throughout my life

# Contents

# List of Figures

# List of Tables

# 1. Introduction

## 1.1 Introduction to crashworthiness

The desire of designers and engineers to increase occupant safety in vehicle structures has brought the need of improving the crashworthiness characteristics of structures. Crashworthiness is a design philosophy applied in every vehicle structure of the current transportation field, from automobiles and trains to aircrafts and helicopters. The overall objective of designing for crashworthiness is to reduce the impact of crash on the passengers resulting in increased structure safety levels. The reduction of crash impact aims to eliminate injuries and fatalities in the case of mild impacts, and minimize them in severe collisions. Also, modern crashworthy vehicles are designed to control the extent of crash impact damage by dissipating large amounts of crushing energy, while an adequate space for the passengers has to be maintained in addition. Thus, the design of crashworthy structures targets in absorbing the greater possible amount of energy produced during the crash. However, the energy absorption is preferable to be accomplished with controllable collapse in the event of a collision, and within certain constraints, such as limits on force transmission, permissible deformations and failure.

More specifically, if only small deformations are permitted regarding to occupant space, then large amounts of momentum transfer and force levels will be occurred, which may be unacceptable to be experienced from the passengers. On the other hand, a limit in permanent deformations must be enforced to retain a minimum volume for survival. So, in order to achieve an optimal combination of permitted frame deformation and transmitted forces to passengers, specific energy absorbing devices, strategically placed in the appropriate frame positions, are applied to vehicle structures to improve their crashworthiness behavior. Energy absorbers are mainly constructed by metals (steel, aluminum etc.), polymers, composite or bi-metallic materials. The two latter materials are widely used in current technology, as they provide light structures capable of absorbing large amounts of impact energy under axial crushing, bending and/or combined loading conditions. Further, research studies and experiments propose that thin-walled structures are more beneficial for use as energy absorbers, as they provide devices with high energy absorption capability and reduced total weight. The greater energy absorption capacity of a thin-walled structure is based on the fact that a thin-walled structure requires lower crushing loads to behave plastically and dissipate amounts of energy. In contrast, compact structures require greater loads to receive plastic deformations, which may keep them behaving completely elastic without dissipating any energy, or deform them in low strain levels, reducing the energy absorption capability in every case. As a result, the energy absorbers are preferable to be thin-walled structures.

In general, crashworthiness behavior and survivability can be improved by modifying the structural geometry or by introducing specifically designed energy absorbing devices. Both research directions have been investigated from the designers to produce crashworthy structures which dissipate the kinetic energy of crash in the most effective way. Figure 1 illustrates typical frame positions in which energy absorbers are usually placed for both automobile and aircraft's fuselage cases. As shown, energy absorbers are used in modern structures as collapsible tubular rails in the front end of automobiles, or in the case of aircrafts, as collapsible floor stanchions and beams.

The new design philosophy of crashworthiness has replaced more traditional design approaches, which considered strong, massive and stiff structures as the better ones. Such approaches have been rejected by current design trends as they fail to dissipate energy during impact, conveying it to the occupants and the cargo. In contrast, crashworthy structures are designed to provide a progressive controllable collapse, during of which they ensure a safe dissipation of adequate amounts of kinetic energy.

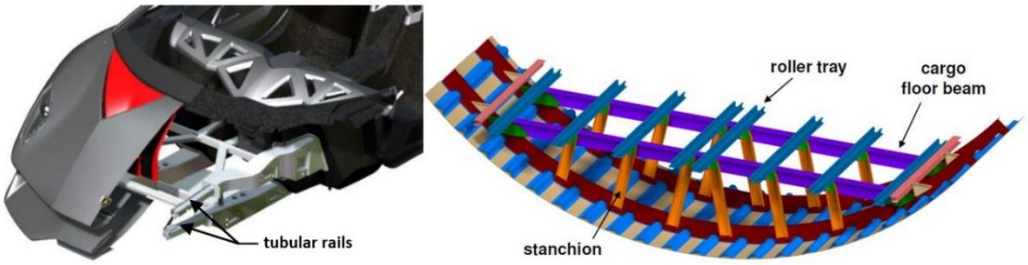


**Figure 1 Energy absorbers positions in automobile and aircraft's fuselage structures, [1]**

A structure designed to satisfy the main crashworthiness requirements must ensure five conditions for survival which are:

- Maintaining sufficient and survivable occupant space
- Providing adequate occupant restraint
- Limiting acceleration and loads experienced from the occupants by employing energy absorbing devices
- Providing protection from the release of items of mass
- Allowing for a safe post-crash egress from the vehicle

Regarding to aircraft structures, crashworthiness regulations have been set in Advisory Circular (AC) of Federal Aviation Administration (FAA) as suggested in [2]. The regulations were introduced based on experiences gained during actual aircraft operations. In order to set the appropriate regulations, FAA considered the impact response characteristics of the fuselage to examine the crashworthiness efficiency of aircrafts. On the other hand, regarding to automobiles, the crashworthiness regulations are set based on either past experience from incidents and accidents or according to safety rules.

The need of designing for crashworthiness has turned the research interest into investigating how structures response in crushing conditions. The complexity of understanding how factors, such as structure materials, geometry, failure mechanisms and crushing modes, affect the energy absorption capability of the structures, has led the engineering community to carry out several research works. As a result, many studies on crashworthiness behavior and energy absorption capability of structures have been carried out by conducting experimental crash tests and by using finite element analysis (FEA) numerical simulations.

## 1.2 Aim of this thesis

Current Master thesis investigates the crashworthiness behavior of thin-walled square aluminium tubes subjected to axial and oblique impact until $15^{o}$ crushing angle. This study aims to reveal the effect of crushing angle on energy absorption capability and plastic collapse stability, while also the effect of initial contact between tube and impactor is examined in order to capture its influence on peak crushing force and plastic collapse initiation. Regarding the initial contact between tube and impactor, two different types of contact are examined for the loading cases of oblique impact; at first, the impactor is in contact with the tube alongside its top edge, while secondly the initial contact is around the top corner of square tube cross-section.

The investigation is carried out in both experimental and numerical level in order to validate the numerical models and evaluate the crashworthiness performance by providing the force-displacement curves and calculating the crashworthiness response metrics. Also, different states of plastic collapse are captured in order to identify the occurred failure mechanism from the characteristics of the deformation mode. Finally, the experimental tests are conducted under quasi-static conditions, while numerical simulations are also carried out by developing finite element models and utilizing the non-linear explicit dynamic LS-DYNA code.

## 1.3 Scope

Current part of present Master thesis introduces shortly the basic meanings of crashworthiness design philosophy in a preliminary and theoretical level. The main reasons considered as most responsible for designing crashworthy structures are pointed out, describing in parallel the advantages which can be brought from this design trend. So, the aim of current chapter is to highlight the need and importance of implementing the crashworthiness philosophy in the design of every transportational structure such as vehicles, aircrafts, ships, trains etc. For this reason, some main regulations and requirements which a crashworthy structure must satisfy are described in order to define some metrics which are taken into account for evaluating the crashworthiness behavior of such

structures. Finally, this initial part ends with the presentation of the aim of current thesis.

Chapter 2 presents the main characteristics of crashworthiness behavior of structures in more detail and from a more technical point of view. Also, the way many factors affect the energy absorption capability is described, followed by a detailed description of the failure mechanisms and crushing modes which can be observed during plastic collapse. At next, the two main types of experimental crush tests which can be conducted for crashworthiness analysis are described by presenting the benefits and the drawbacks of each one. Finally, chapter 2 summarizes and reviews a number of research studies on crashworthiness response in both axial and oblique impact, presenting also a theoretical analysis to calculate the mean crushing load which is considered one of the most significant metrics for evaluating crashworthiness efficiency and energy absorbing capability.

Chapter 3 presents the experimental procedure of the quasi-static tests carried out for assessing the crashworthiness behavior of examined thin-walled aluminium square tubes and providing the necessary data for the validating procedure of the created finite element models. The experimental results contain both stage-by-stage observations of the collapse in order to obtain the occurred failure mechanism, and the estimating of critical crashworthiness response characteristics provided by the experimental data for evaluating the energy absorption capacity in each case.

Chapter 4 presents the modelling approach followed to simulate each test case. Initially, a short description of LS-DYNA software is presented, followed by the finite element models development for the purpose of current work. After that, the numerical results are presented and assessed by both calculating the main crashworthiness metrics and identifying the occurred collapse mode for each examined case.

Chapter 5 consists of the respective comparisons between the experimental and the numerical results with the relative errors to evaluate their level of agreement. The comparison offers the opportunity to provide useful conclusions for the crashworthiness behavior of the examined thin-walled tubes and to examine the accuracy and validity of the numerical simulations. After the comparison between experimental and numerical results in terms of crashworthiness response characteristics, the occurred collapse mode for each case is also captured and coupled to the revealed results regarding the collapse stability and energy dissipation capability which are offered. Finally, the effect of crushing angle and the one of the types of initial contact between tube and impactor are also discussed and compared in order to extract the proper conclusions and evaluate their impact on crashworthiness efficiency.

Finally, chapter 6 contains a short summary of the aim of this thesis, the utilized modelling tool and the conducted experiments and numerical simulations followed by the provided results. Critical conclusions are next extracted for both crashworthiness response characteristics and collapse mechanisms, while finally some recommendations about future work are made.

# 2. Crashworthiness

## 2.1 Principles of crashworthiness design

The main goal of crashsworthiness design philosophy regarding every transportational or structural construction can be summarized in converting the greater possible amounts of crushing kinetic energy to plastic deformation ones. This specific capability of structures must be achieved under a stable and safe mode, maintaining a sufficient and survivable structural volume and limiting the inertial forces experienced from the passengers/occupants. Therefore, some of the most significant objectives of a crashworthy structure can be described by the main below aims:

*a) Irreversible energy conversion*

In order to achieve the greater possible absorption of crushing kinetic energy, a structure must be capable of deforming plastically for dissipation significant amounts by converting them into plastic strain energy. Therefore, the structure must be designed regarding its geometry and material properties in a way that the crushing load should be sufficient enough to overcome its yield stress and deform it plastically, otherwise the provided elastic strains could not be capable of absorbing any crushing energy amounts as they would result in a "spring back" effect on the structure which would rebound to its initial shape and geometry without dissipating any amounts of crushing kinetic energy.

*b) Constant and stable crushing force*

For minimizing the inertial forces transported to passengers/occupants during collision, a well crashworthy behaving structure should be capable of absorbing amounts of crushing energy by deforming plastically under a constant and stable sustained load, which ideally should be close enough to the peak crushing force applied initially, but also below a threshold amount, resulting that way in the minimum possible injuries caused by sudden decelerations. Thus, an energy absorbing device of high crashworthiness efficiency should possess a rectangular load-displacement characteristic, deforming that way stable under a constant and sustained load during its collapse.

*c) Long stroke*

Increasing the useful crushing distance by compressing the structure under long strokes, results in dissipating greater amounts of crushing kinetic energy, as the more the structure deforms the greater amounts of plastic strain energy

requires. Thus, longer deformation levels allow generally higher energy absorption capacity to the designed structures. However, the maximum stroke is often constrained to limits regarding a sufficient and survivable structure volume.

*d) Light weight with high energy absorption capacity*

Structures weight is commonly treated as one of the most significant design parameters for both transportational and structural constructions. Therefore, designing under low weights is always considered as a significant feature, turning that way the crashworthiness design trend into thin-walled structures. In addition, thin-walled structures facilitate the plastic deformation initiation, resulting in greater amounts of absorbed crushing energy under low weight in fact. Thus, thin-walled structures are widely preferred in crashworthiness design as they provide high specific energy absorption levels.

## 2.2 Crashworthiness Indicators

The main aim of designing crashworthy structures is to improve their capability in absorbing the amount of energy produced during a crush event. A typical response of a crushed structure in terms of applied crushing force versus shortening (or stroke) of the crushed structure is depicted in Figure 2. The initial collapse stage contains the elastic deformation until the maximum crushing force which reflects the plastic collapse initiation followed by the post-buckling region in which the plastic deformation progresses under a sustained force formulating local peaks and lows in crushing force reflecting the formulation of plastic convolutions during the collapse. In that way, the crushing kinetic energy is dissipated by being transformed into plastic deformation energy in which the energy absorption mechanism contains the bending energy which is dissipated during the bending of the rotated folds and the membrane energy which is in turn dissipated by the extension of the formulated folds.

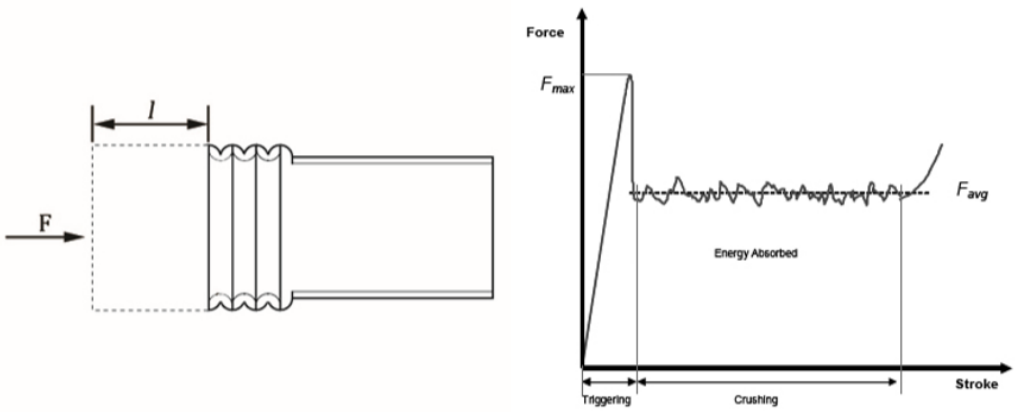


**Figure 2 Load-displacement curve of a crushed structure, [3]**

Some widely used crushing response parameters which are taken into account for the evaluation of energy absorption capacity, plastic collapse initiation and crushing efficiency are peak crushing force (PCF), mean crushing force (MCF), energy absorption (EA) and specific energy absorption (SEA), crushing force efficiency (CFE) and stroke efficiency (SE). In more specific, EA refers to total energy absorption which is dissipated during plastic collapse as the kinetic energy is transformed into plastic deformation energy. Considering F(x) as the instantaneous crushing force and d as the maximum impactor displacement, EA is computed as the total area below force-displacement curve as expressed following:

$$EA = \int_0^d F(x)dx \tag{1}$$

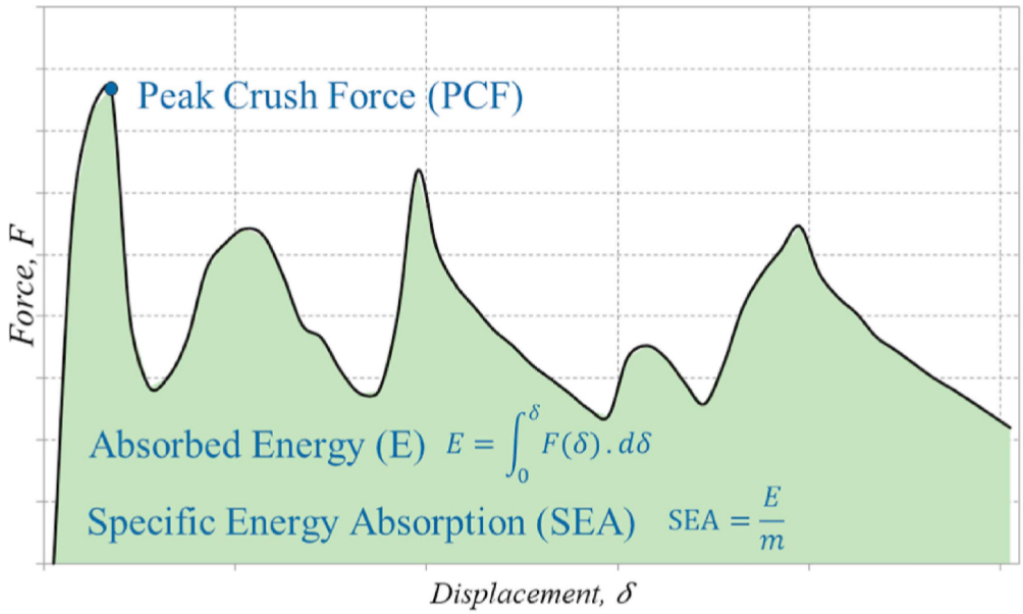


**Figure 3 Energy absorption basic terms referring to load-stroke diagram, [4]**

However, a more reliable indicator for assessing the energy absorption capacity of structures is SEA which expresses the absorbed energy per unit mass of crushed structure (m). Thus, SEA reflects a more indicative parameters than EA for comparing the crashworthiness performance for structures of different material, dimensions and cross-section geometry. So, for a crushed structure of ρ material density, A cross-sectional area and d maximum crushing shortening, SEA is expressed as:

$$SEA = \frac{EA}{m} = \frac{EA}{A \cdot \rho \cdot d} \tag{2}$$

Regarding the crushing force indicators, PCF and MCF contain the two main metrics which reflect the plastic collapse initiation and the energy absorption capability respectively. In more detail, PCF refers to maximum crushing force required for plastic collapse initiation and is responsible for the initial formulation of the first plastic convolution. However, PCF can also be captured sometimes by one of the local force peaks during post-buckling region of plastic collapse due to a low enough required initial maximum force which may be overpassed by the required force for the formulation of an external fold. In contrast, MCF is defined as the ration of energy absorption to the maximum impactor displacement representing a constant sustained force around of which the plastic collapse progresses formulating local peak and lows in crushing force which reflect the formulation of external and internal plastic folds respectively. So, PCF and MCF can be expressed as follows:

$$PCF = \max\{F(x)\} \tag{3}$$

$$MCF = \frac{EA}{d} \tag{4}$$

Finally, CFE expresses the uniformity of crushing force distribution defined as the ration between MCF and PCF, while SE reflects the ration of maximum crushed structure longitudinal shortening d to its initial length $l_o$.

$$CFE = \frac{MCF}{PCF} \tag{5}$$

$$SE = \frac{d}{l_0} \tag{6}$$

Structures of high energy absorption capability can be described as efficient ones in terms of crashworthiness. However, the specific energy absorption (SEA) is the main parameter for the evaluation of material efficiency. As a result, the comparison of two structures in terms of energy absorption capability is made comparing their SEA values. Obviously, the structure with greater SEA is the more efficient one. Additionally, a parameter of high importance is the peak crush force (PCF). PCF must be a reasonable value because if peak load is too great, the crush load may not reach the required force level, which is the PCF, to deform the structure plastically, meaning that the structure will retain behaving completely elastic without absorbing any energy. PCF is a function of geometric (thickness in case of thin-walled structures) and material characteristics of the structure.

Further, the crushing force efficiency (CFE) is an important factor representing the decelerating force which is applied to the passengers as the structure is loaded from maximum load to sustained one. A CFE of 100% is an ideal value as it provides a completely uniform applied load of high energy absorption. Finally, stroke efficiency (SE) is preferred to be as great as possible, resulting in high plastic deformations which increase the energy absorption capability of the structure and make the use of the material efficient in terms of crashworthiness behavior. A representative example of the effect of SE on energy absorption capacity is the comparison between brittle and ductile materials. As shows, ductile materials are characterized by greater SE as they can be deformed plastically without failing, resulting in greater energy absorption capacity compared to brittle.

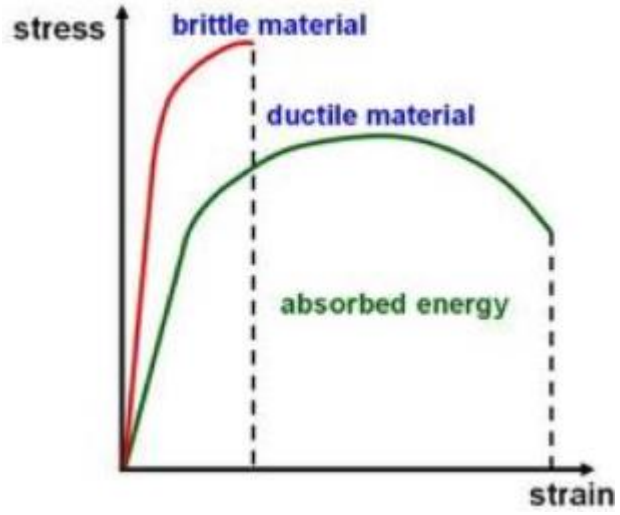


**Figure 4 Energy absorption for brittle and ductile materials, [5]**

Summarizing, an ideal energy absorber is characterized by high specific energy absorption (SEA), a reasonable peak load, a crushing force efficiency (CFE) of 100% and a stroke efficiency (SE) as closer to 100% as possible. The following figures depict typical energy absorbing devices for frontal longitudinal crushes in case of automobiles.

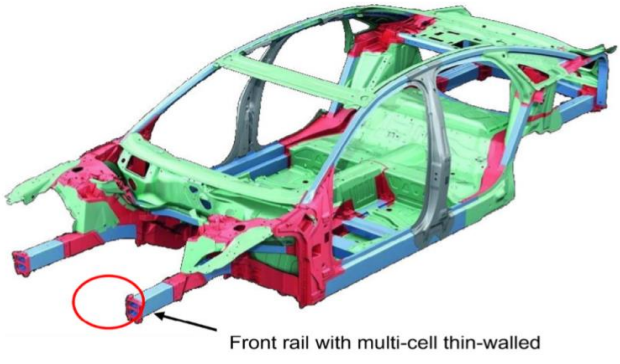


**Figure 5 Frontal longitudinal energy absorbers of typical automobile, [6]**

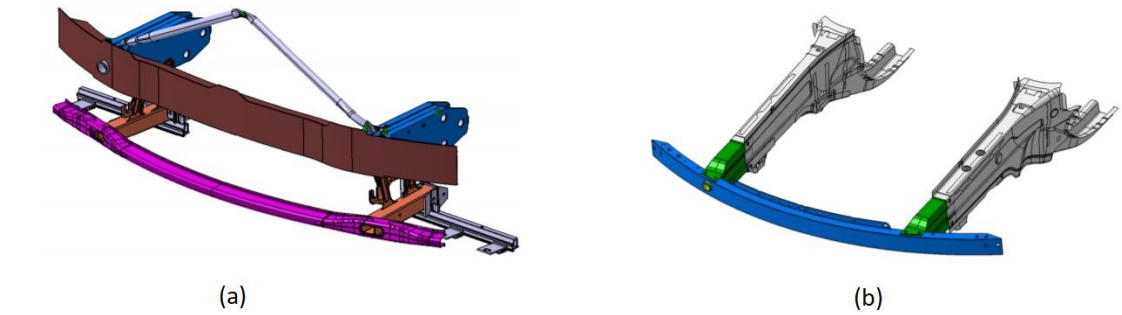


**Figure 6 Energy absorbing system of front end of automobiles, (a) BMW 3 series model and (b) Mercedes C Class, [7]**

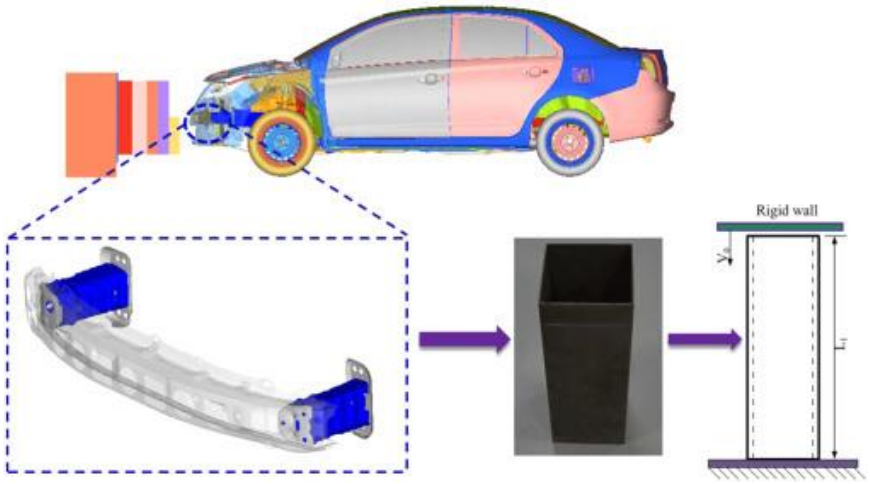


**Figure 7 Energy absorbing system of front end of automobiles, [7]**

The two next figures show the crashworthiness design of the fuselage of aircrafts, in which energy absorbing devices (beams and stanchions) are located in order to dissipate the necessary amounts of energy under loading, during vertical crushing conditions of the fuselage.

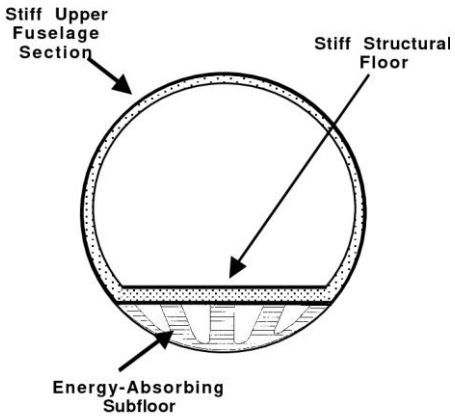


**Figure 8 Crashworthiness design of aircraft's fuselage, [8]**

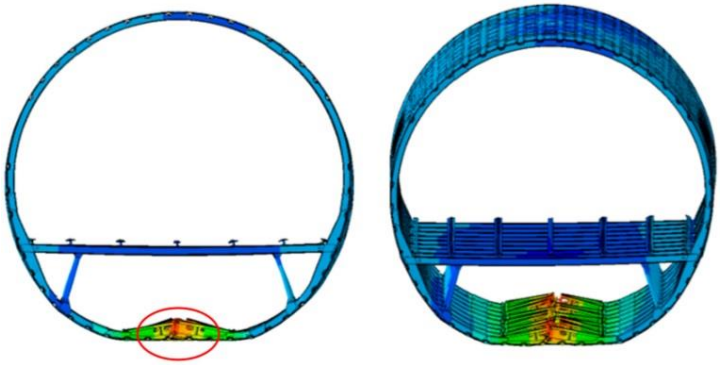

**Figure 9 Aircraft's fuselage crushing behavior, [8]**

## 2.2 Energy absorption and failure mechanisms

The specific energy absorption, which is the main parameter characterizing the energy absorption capability of a structure, strongly depends on the mode the structure fails. In fact, two different crushing modes can occur; the catastrophic failure mode and the progressive failure mode.

The catastrophic failure mode occurs when unstable interlaminar crack growth occurs and it is characterized by a sudden increase in load until the peak load, followed by a low post-failure load. This type of failure mode is also described as uncontrollable.

In contrast, the progressive failure mode is controllable and progresses through the material at the loading speed. In this case, a triggering mechanism is provided at the one of the structure ends, as a stress concentrator, and causes the failure initiation. A reduction of peak load is observed down to a lower, almost constant, sustained load, under of which a stable collapse is provided. The advantages of a progressive failure mode are that the energy absorption is larger in a progressive crush compared to a catastrophic failure, while structures designed to response to loads by progressively failing have proved to be lighter than the ones which are designed to react to loads by catastrophically failing. Thus, the progressive failure mode is more beneficial compared to the catastrophic one because it provides lighter structures of higher energy absorption capability, or on other words structures of higher SEA.

According to Farley and Jones [9], the crushing mode is an indicator of how efficiently the structure is being crushed. The prediction of crushing response includes the understanding of how the energy absorption is affected by both material mechanical properties and specimen structure (geometry). Farley and Jones suggest that the crushing speed affects the energy absorption capability of a structure in the same way the strain rate affects the mechanical response of a material (Figure 10). As a result, the amount of absorbed energy depends on the crushing speed in a proportional way.

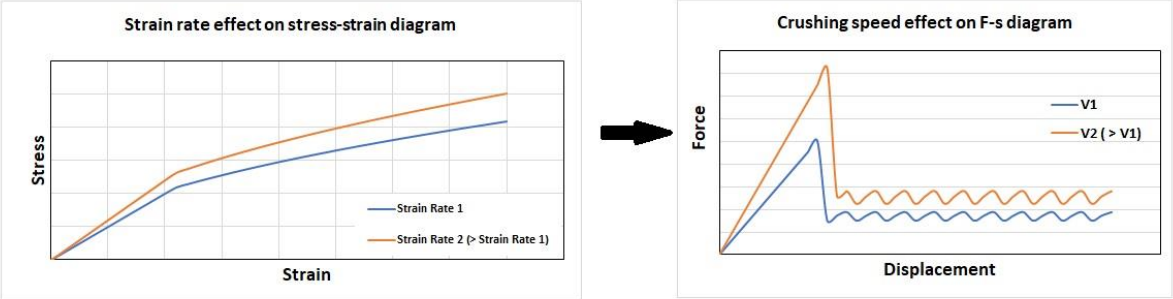


**Figure 10 Effect on crushing speed on energy absorption according to [9]**

Referring to the studies of Farley and Jones (1989), four different crushing modes have been identified considering composite materials. These four proposed crushing modes are presented below. All of them are exhibited by brittle composite materials, but the last crushing mode is the only one which can be also exhibited by ductile materials.

1. *Transverse shearing and fragmentation mode*
   It is characterized by laminate cross-section with short interlaminar and longitudinal cracks that form partial lamina bundles (Figure 11). The main energy absorption mechanism is the fracturing of lamina bundles; when the fragmentation occurs, the length of interlaminar and longitudinal cracks is lower than that of the lamina. The mechanism is observed when the crushed material length is short. The mechanism that controls the crushing process is the transverse lamina bending strength, which is a function of fiber stiffness and strength in case of composite materials. As Farley and Jones suggested, if the fiber mechanical response depends on the strain rate, then the energy absorption depends on crushing speed in a similar way.

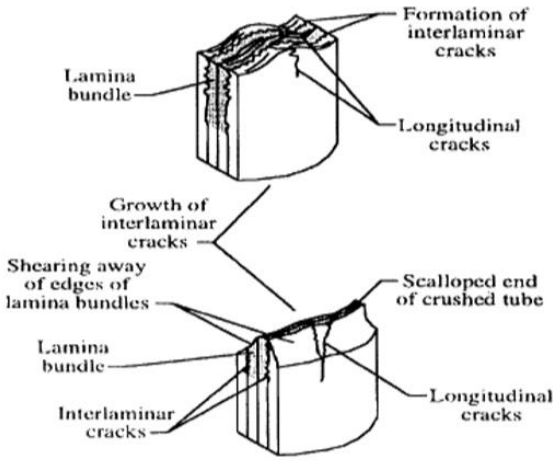


**Figure 11 Transverse shearing and fragmentation crushing mode, [3]**

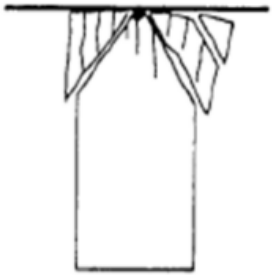

**Figure 12 Fragmentation crushing mode,** [1]

*2. Brittle fracturing*

The brittle fracturing crushing mode exhibits the same energy absorption mechanism like the fragmentation mode, which is the failure of lamina bundles. However, the length of interlaminar cracks in brittle fracturing lies from one to ten times the lamina thickness. The longer the fractured lamina bundle is, the less efficient the crushing mode is. Lamina bundles in brittle fracturing mode often exhibit some bending and usually fracture near the base. When the first lamina bundles fracture, the load is redistributed resulting in cracks growth and further lamina bundles fracturing. The controlling mechanisms in brittle fracturing mode, for composite materials, are the matrix stiffness and the lamina bundle tensile strength. The first controls the interlaminar and parallel-to-fiber crack growth, while the second controls the fracture of lamina bundle.

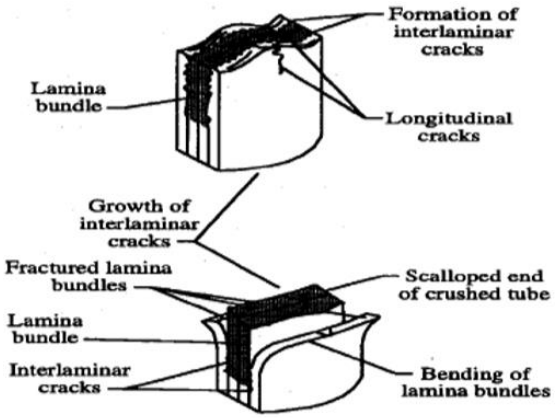


**Figure 13 Brittle fracturing crushing mode,** [3]

*3. Lamina bending or splaying mode*

Splaying mode is characterized by very long interlaminar and parallel-to-fiber cracks, but the lamina bundle does not fracture. The energy absorption mechanism here is crack growth. The respective cracks length is greater than ten times the lamina thickness. In splaying crushing mode, the lamina bundles exhibit significant bending deformation but do not fracture. The not fractured long lamina bundles result in an inefficient crushing mode. The matrix strength is the controlling mechanism of the splaying mode, as it controls the cracks

growth. Once again, the way the strain rate affects the mechanical response of a material, is the same to the way the crushing speed affects the lamina bending and in consequence the energy absorption.

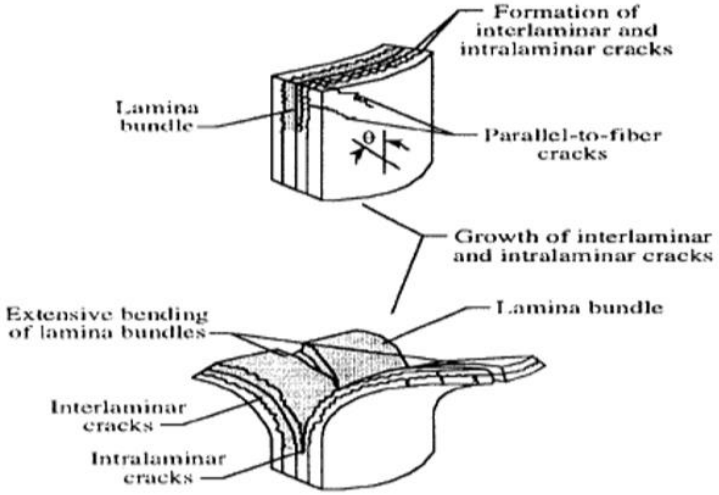


**Figure 14 Splaying mode,** [3]

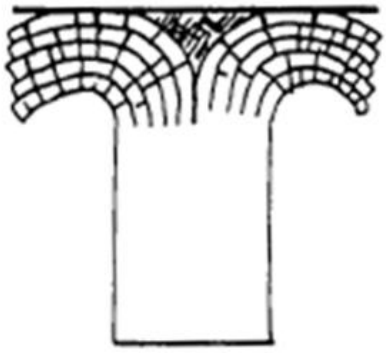

**Figure 15 Splaying mode, [3]**

4. *Local buckling or progressive folding*

The progressive folding crushing mode is characterized by the formation of local buckles, or folds, by means of plastic material deformation. This mode is exhibited by both brittle and ductile materials. The ductile fiber-reinforced composites remain intact after the crush due to the fiber and matrix plasticity and fiber splitting. In the case of brittle composite materials, the structure collapses in folding mode when matrix has higher failure stress than the one of the fibers. The mechanisms that control the progressive folding crushing mode is the plastic yielding of the fiber and/or the matrix. More specifically, the matrix non-linear stress-strain response controls the local buckling progress in case of brittle materials, while the matrix or fiber stiffness controls the progress of local buckling in case of ductile materials.

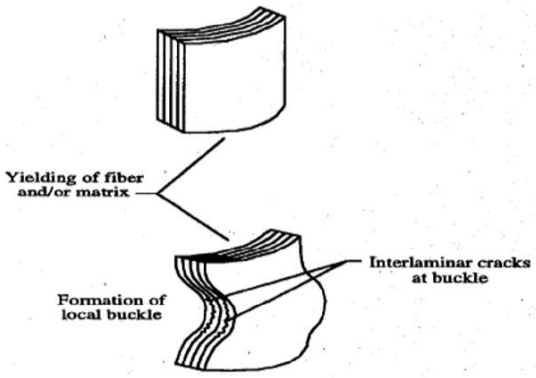


**Figure 16 Local buckling or progressive folding mode,** [3]

Further crushing modes referring to specific materials and geometries can be found in many studies of open literature, which have examined certain structures. A typical example is the study carried out by Bisagni [10] who observed the failure modes occurred in crushed circular carbon fiber tubes.

The energy absorption capability of a structure is a function of both geometry and material properties. In addition, energy absorption capacity of a structure depends strongly on the failure mechanism (crushing mode) which is observed during the collapse. So, regarding to composite materials, progressive crushing with microfragmentation is associated with the larger amount of absorbed crush energy according to Mamalis et al. [11]. However, when the fragmentation is quite intense providing large debris which have the tendency to concentrate in the interior of the tube, the fragmented and compacted debris limit the available stroke, resulting in lower stroke efficiency and in consequence lower levels of energy absorption capability. Furthermore, structures which collapse according to the crushing mode of progressive folding and hinging, are characterized by medium energy absorption capacity, while brittle fracturing mode results in very little levels of energy absorption providing a catastrophic failure. Finally, in every failure mode, environmental factors react in the same way on crashworthiness behavior. An important factor is the ambient temperature which reduces the amount of energy absorption according to Ptak et al. [12], as the force levels decrease in higher temperatures, moving the force-displacement curve downwards, reacting on lower energy absorption. The same paper underlined also the effect of crushing speed concluding that increased crushing speeds increase in turn the energy absorption as Figure 10 shows.

More emphasis will be given to local buckling and progressive folding crushing mode, as different types of folding modes can be occurred in the case of an axial crushed structure. The progressive folding and hinging are oftenly observed failure modes. The four main types of progressive folding crushing mode are:

1. Concertina mode or ring mode
2. Diamond mode (3 lobes, 4 lobes etc.)
3. Mixed mode
4. Euler-type buckling mode

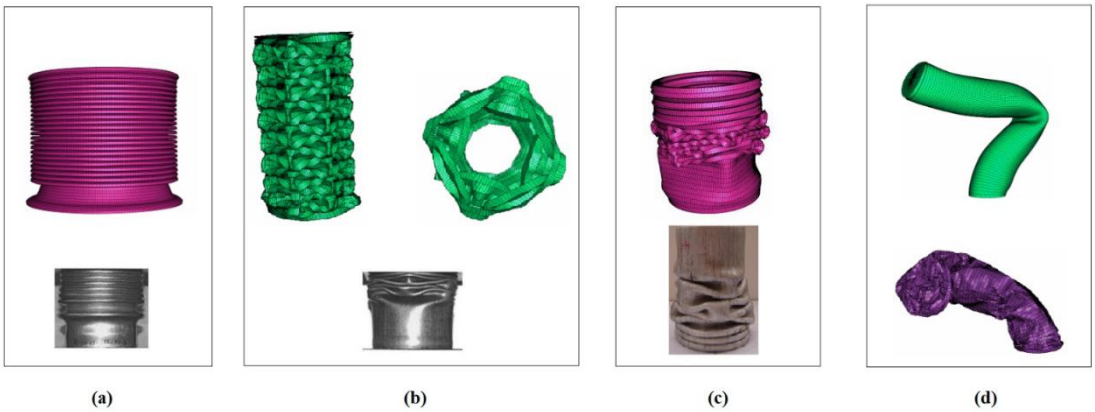


**Figure 17 Progressive folding crushing mode, (a) concertina mode, (b) diamond mode, (c) mixed mode and (d) Euler-type buckling mode**

The type of folding crush mode in which a structure is expected to collapse strongly depends on geometric characteristics. Specifically, a thin-walled tube will collapse under axial crushing load either axisymmetrically or non-asymmetrically, depending on the ratio of diameter to thickness (D/t) and the ratio of the length to the diameter (L/D). The axisymmetric mode is often called as concertina mode (or ring mode), while the non-symmetric one as diamond mode. For a certain D/t ratio, a tube may start collapsing in concertina mode and switch to diamond mode, exhibiting in that way a mixed crushing mode. Finally, a tube can also collapse in Euler-type buckling mode, which is a catastrophic and uncontrollable collapse provided by large bending of the tube resulting in significant loss in energy absorption capacity.

As mentioned before, the energy absorption capability strongly depends of failure mode. In case of folding and hinging crushing mode, research studies and experimental works have shown that concertina mode seems to be the best folding mode providing the highest energy absorption levels. A little lower energy absorption capability is provided by diamond mode, while the Euler-type buckling mode is characterized by very low energy absorption levels due to its catastrophic and unstable collapse progress.

Regarding to geometric characteristics which have a strong influence on expected type of folding, Florent et al. [13] examined aluminium tubes, suggesting that thick and short tubes are expected to collapse in concertina mode. As the tube thickness reduces and the length of the tube increases, a mixed mode is more expected to be observed, while even thinner and longer tubes may collapse in diamond mode. However, for extremely thin and long tubes, Euler-type buckling mode may be occurred. So, the length of the crushed structure or specimen must be very carefully selected in order to avoid the uncontrollable and catastrophic collapse of Euler-type buckling mode. For this reason, extremely long tubes must be avoided. Figure 18 illustrates the expected type of folding for aluminium tubes according to [13].

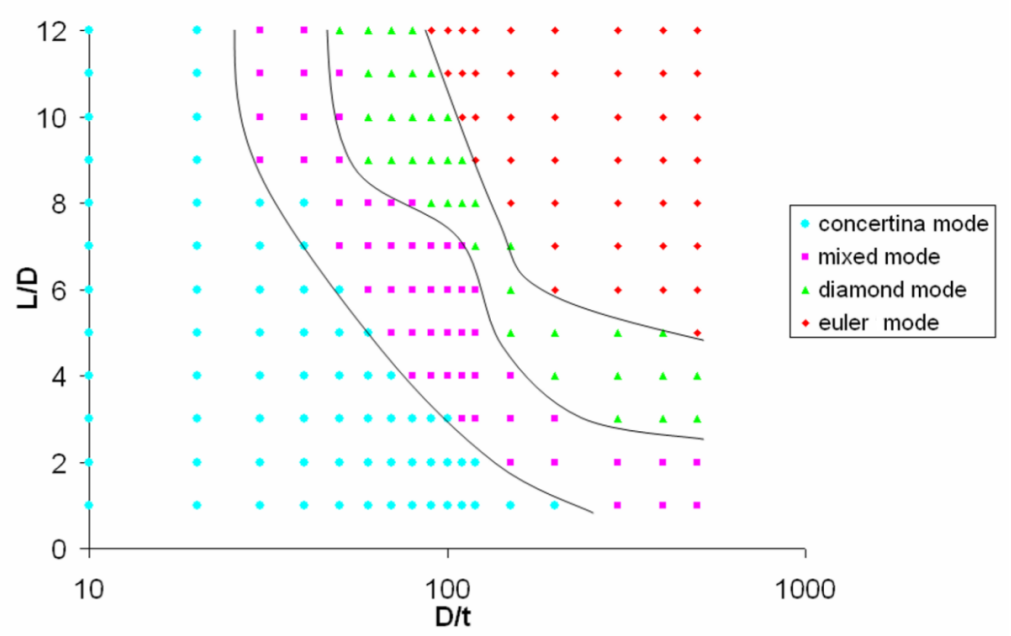


**Figure 18 Folding mode classification for aluminium tubes, [13]**

In addition, an important parameter in designing energy absorbers is their cross-section. Recent studies have examined single cross-sectioned tubes, concluding that circular tubes provide the highest energy absorption capability. A little lower levels of energy absorption capability are provided by square cross-section, and even lower by rectangular ones. In general, for cross-sections with corners (square, hexagonal, octagonal etc.), the energy absorption levels increase as the number of corners is getting higher. For example, the energy absorption capability of a circular tube is higher than an octagonal, which in turn is higher than a hexagonal one, which in turn is higher than a square one etc.

Finally, Florent et al. [13] investigated the effect of the type of support applied at structure ends. Specifically, the examined support types were tie constraint, roller and fixed, while four different boundary conditions were examined; (1) tie constraint-roller, (2) fixed-fixed, (3) fixed-roller and (4) roller-roller. The first support type refers to the bottom of the tube, while the second one refers to the top of the tube. For an examined specimen which was expected to collapse in concertina folding mode, the four types of support which were examined affected the folds formation as the next figure shows. A key-factor is that at symmetric supports, (2) and (4), the folds formation was also symmetric, as folds appeared at both ends of the specimen (aluminium tube).

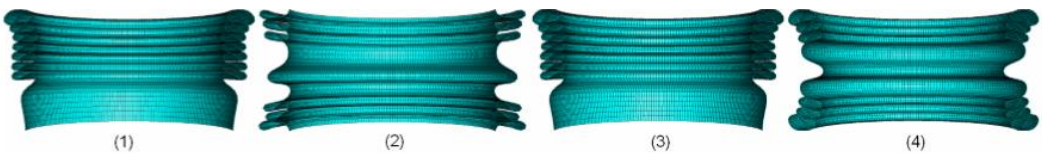


**Figure 19 Effect of support types on specimen expected to collapse in concertina mode, (1) tie constraint-roller, (2) fixed-fixed, (3) fixed-roller and (4) roller-roller, [13]**

Following, an examined specimen in [13], expected to collapse in mixed folding mode, in fact collapsed in concertina mode for fixed-roller supports as shown in next figure, suggesting that when the one of two tube ends is fixed, the concertina folding mode is occurred.

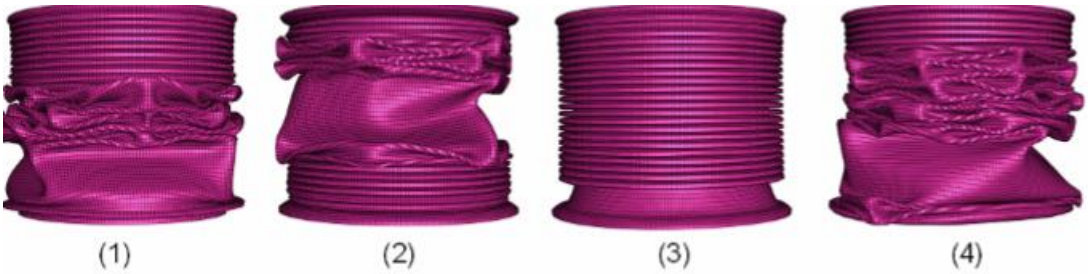


**Figure 20 Effect of support types on specimen expected to collapse in mixed mode, (1) tie constraint-roller, (2) fixed-fixed, (3) fixed-roller and (4) roller-roller, [13]**

Finally, the same study examined a specimen expected to collapse in Euler-type buckling mode. It was concluded that the end of specimen which was fixed or tied to the plate, was remained in contact to the plates after the collapse, while the end in which a roller boundary conditions was applied, was losing its contact to the plate by sliding over it. Summarizing on the effect of support types on folding collapse mode, when at least one end is fixed, more axisymmetric folds are created, providing so the best supported structure in terms of energy absorption capability which is at the higher levels. In contrast, when both ends are free, the energy absorption is significant low.

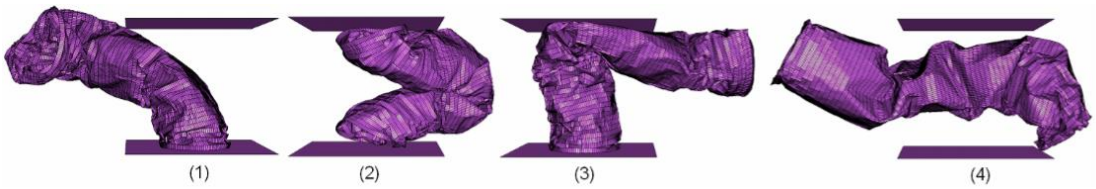


**Figure 21 Effect of support types on specimen expected to collapse in Euler-type buckling mode, (1) tie constraint-roller, (2) fixed-fixed, (3) fixed-roller and (4) roller-roller, [13]**

Comparing however the circular and the square tubes between each other in practical applications, the use of circular tubes in automobile structures have met various difficulties and constraints associated with mounting them to other structural members. Thus, square tubes have received a noticeable attention for fabrication of crashworthy components. In general, square tubes have been proved to be less effective as energy absorbers compared to circular tubes, as severe deformation is concentrated in zones around the corners of the squared cross-section of tubular structures providing so lower energy absorbing levels about even 30% as Tang et al. [14] (2013) proposed founding that the structural effectiveness of square tubes under crushing loads is about 0.7 of the one of circular tubes. Similar to circular tubes, the deformation mode observed in square

tubes during their plastic collapse depends on cross-section dimensions and is mainly affected by width to thickness (b/t) ratio. The collapse mechanisms which occur during plastic deformation of square tubes under impact loading are shown in the following figures and they can be divided to:

- Extensional mode
- Inextensional mode
- Mixed mode
- Non-compact crushing mode
- Euler-type buckling mode

As Reid [15] (1993) observed, square tubes subjected to impact loading can collapse either under a progressive and controllable mode or under an unstable inelastic way. Regarding the progressive plastic deformation modes occurred during collapse, an extensional collapse mode can be observed at $b/t < 7.5$ deforming the plastic hinges by stretching them externally or internally. Also, an inextensional collapse mode can be captured at $b/t > 40.8$, while as b/t lies between the range of 7.5 to 40.8 a mixed collapse mode is observed formulating initially extensional convolutions followed by inextensional ones. During the formulation of an inextensional convolution, the two opposite sides of the squared cross-section are bended and stretched externally, while the two other sides are bended and stretched internally, maintaining so the initial circumferential length of the cross-section but changing thus its geometrical shape.

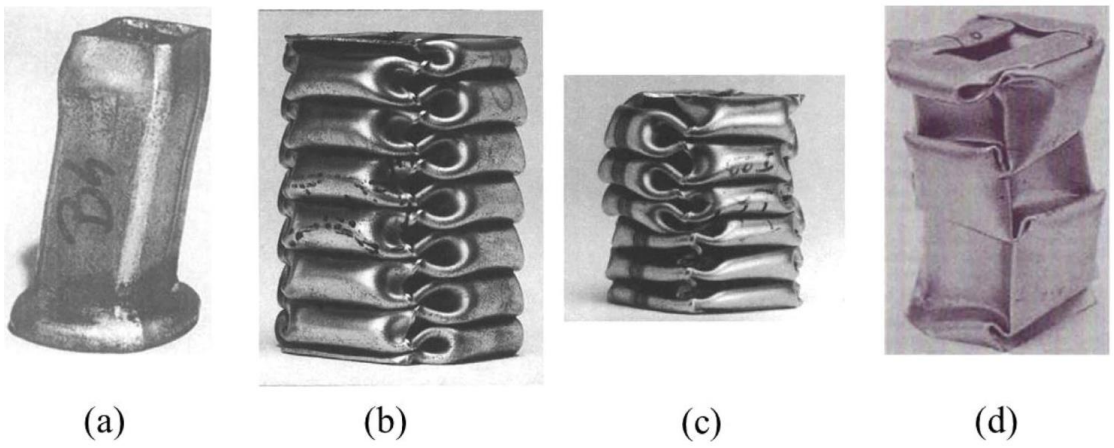


**Figure 22 Axial progressive deformation modes of square tubes: (a) extensional mode, (b) inextensional mode, (c) asymmetric mixed mode, (d) non-compact crushing mode, [15]**

Moreover, very thin square tubes about $b/t > 100$ may adopt a non-compact collapse mode which provides less energy absorption capacity than the previous modes. However, the lowest energy absorption capacity is revealed when Euler-type buckling mode is occurred during plastic collapse as its unstable and inelastic behavior do not allow for dissipating significant amount of energy.

Following figure depicts a possible view of Euler-type buckling collapse mode, knows also as bending mode, in the case of square and circular tubes. In more specific, Reyes et al. [16] (2002) studied the bending collapse mode of square tubes identifying different mechanisms during the initiation of bending collapse mode emphasizing on the formulation of the initial folds around of which the crushed structure was bended at next. The possible mechanisms depicted in Figure 24 contain the formulation of one external or internal fold – mechanisms A and C respectively – around of which the crushed tubular structure was at next bended, while mechanism B indicates the initial formulation of two inextensional lobes from which the first one is stretched externally and the second one internally regarding the side of the cross-section in which the structure is bended on.

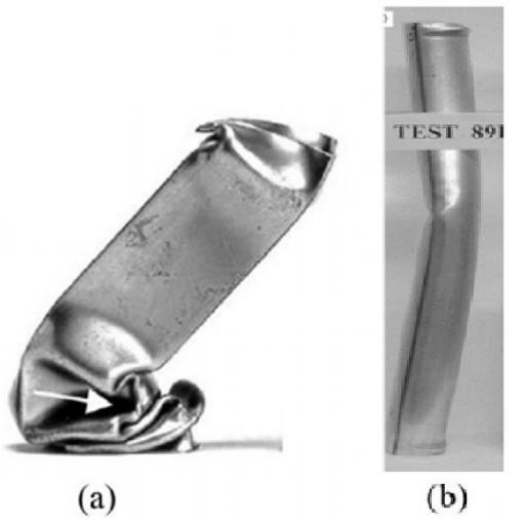


**Figure 23 Euler-type buckling collapse mode: (a) square tube, (b) circular tube**

Finally, as Figure 25 shows, a progressive and controllable mode of plastic collapse allows for greater energy absorption capacity due to its collapse stability under of which the crushing energy is dissipated by the folding deformation of the crushed structure which requires a highly maintained force distribution for the formulation of the external and internal convolutions. In contrast, a bending collapse mode causes a significant drop in energy absorption capability as the crushing force seems to decrease with the collapse progress, as the unstable and inelastic behavior facilitate both the initiation and the progress of plastic collapse without requiring high crushing force levels.

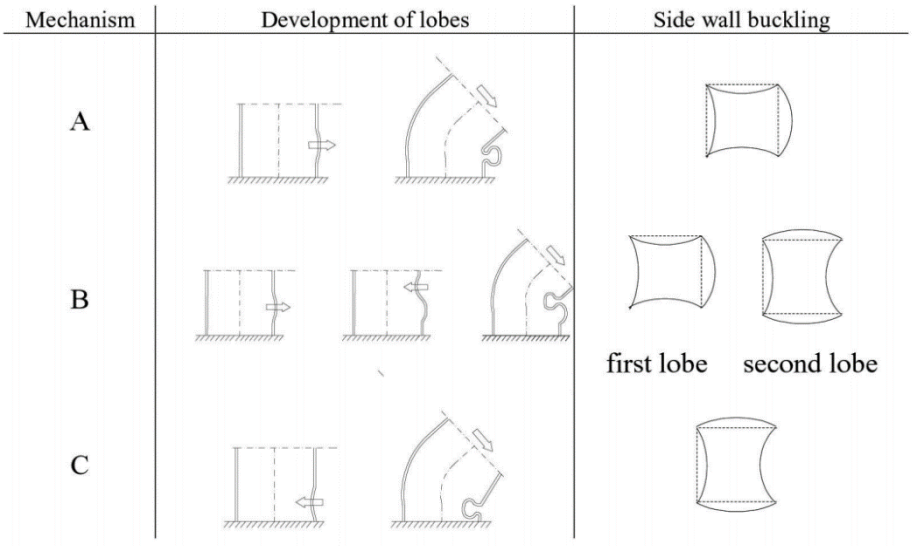


**Figure 24 Initial formulation stages of Euler-type buckling mode, [16]**

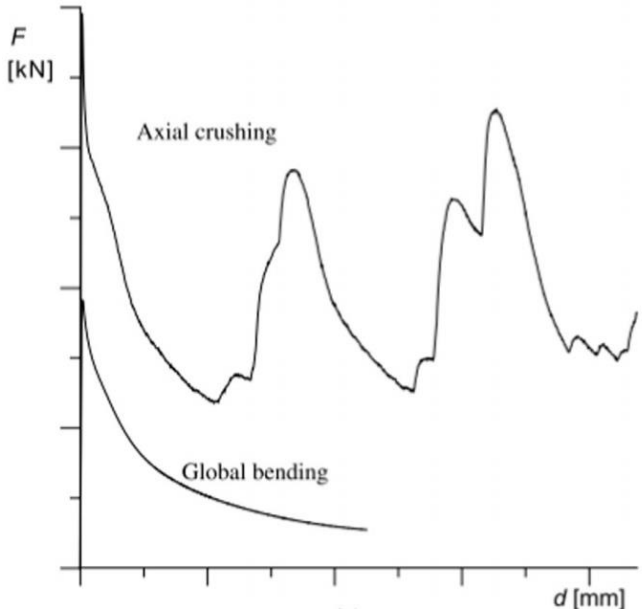


**Figure 25 Force-displacement curve of progressive vs. bending collapse, [17]**

## 2.3 Crush tests

The crashworthiness behavior of a structure and its main characteristics can be studied through numerical simulations or experimental tests. The experimental tests often provide more accurate results in every aspect; prediction of energy absorption capability, maximum load, maximum specimen shortening, force-displacement curve, failure mode etc. The experiment tests, oftenly called as crush tests, can be conducted in two different ways: quasi-static and impact conditions.

**Figure 26 Impact crush test of aircraft's fuselage, [8]**

In quasi-static conditions, the specimen is crushed at constant speed. However, quasi-static conditions do not represent a true simulation of crush conditions, because in real crush conditions the structure is subjected to a decrease in crushing speed, from the initial impact to rest. Given that many materials are strain rate sensitive and the energy absorption capability depends on crushing speed according to Farley and Jones [9], the quasi-static tests may not lead to an accurate prediction of the amount of absorbed energy. Although, the advantages of quasi-static tests are that they are simple and easy to control without requiring expensive equipment to record the crush events.

On the other hand, the impact tests represent a true simulation of real crushing conditions, as the crushing speed decreases from the initial impact velocity to rest because of the energy absorption by the specimen. The benefit of impact tests is their accuracy in predicting the collapse mode and the main crashworthiness characteristics (energy absorption capability, maximum load, maximum specimen shortening, force-displacement curve, failure mode etc.). Their major disadvantage though is that they require expensive equipment, such as high-speed cameras, data recorders of very high frequency etc., as the crushing process takes place in a fraction of second.

## 2.4 Previous research studies

A plenty of research studies on crashworthiness have been carried out through the recent years utilizing numerical simulations with finite element analysis software or experimental crush tests. The main emphasis has been paid on investigating different materials (aluminium, composite materials etc.), cross-section designs, support types, the effect of triggering mechanisms for crush initiation or finally the loading conditions such as the crushing angle in case of axial or oblique impact loading. The metrics used by the majority of the studies to evaluate the crashworthiness efficiency are parameters such as specific energy

absorption (SEA), mean crushing force (MCF), peak crushing force (PCF) and crushing force efficiency (CFE). Further, the observation of the occurred failure mechanism is always of significant importance affecting the collapse stability and in subsequence the energy dissipation capability.

Florent et al. [13] (2007) examined the impact of support types and foam filling on the crashworthiness behavior of aluminium thin-walled tubes, and more specifically on exhibited crushing modes. The study utilized as modelling tool the LS-DYNA software. The examined support types were tie-constraint end of tube, fixed end and roller in the tube end. The boundary conditions (support types combination for the two tube ends) have been referred to previous subsection of this chapter (2.2). It was concluded that for a specimen expected to collapse in concertina failure mode, both shell elements model and solid elements model predicted correctly the failure mode. However, given that a certain initial tube length can be formed in a standard number of folds, the shell elements model predicted more accurately the number of folds compared to the solid elements model (Figure 27). Additionally, the impact of boundary conditions in terms of support type of each tube end was examined providing the conclusions referred to subsection 2.2 of this chapter. Finally, the aluminium foam filled tubes showed higher energy absorption levels. However, the aluminium foam filling resulted in shortening the folding length (Figure 28), while a change in collapse failure mode from diamond mode to concertina or Euler-type was occurred. The last observation is considered to be disadvantageous as it may cause unstable collapse (Euler-type buckling mode).

**Figure 27 Bare tube folds prediction (shell elements model, experimental specimen, solid elements model), [13]**

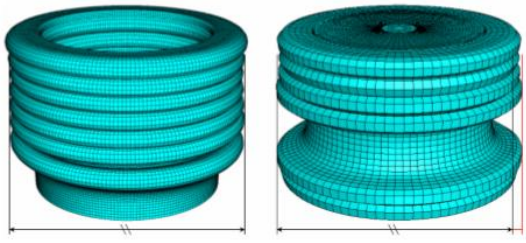

**Figure 28 Effect of aluminium foam filling on exhibited number of folds, [13]**

Mamalis et al. [11] (2009) studied square tubes of vinyl-ester and fiberglass composite material, internally reinforced with aluminium or polyurethane foam. Both experimental tests and numerical simulation in LS-DYNA software were conducted to observe and analyze the collapse mechanisms. The numerical simulations in LS-DYNA predicted correctly the failure mode, while mean deviations in predicted F-s curve of 20% and 15% were observed in the case of

bare tube and tube reinforced with foam (both aluminium and polyurethane cases), respectively. It was concluded that the energy absorption was higher for the foam filled tubes compared to the bare ones. In fact, the aluminium foam filled tube was the one of higher SEA. Also, filling with aluminium foam provided better stabilization of the collapsed specimen and the crush energy was absorbed in completely plastic way in form of heat energy. In contrast, polyurethane foam filling provided an elastoplastic behavior during energy absorption, retransferring the amount of absorbed energy back to the crushing system.

Suzhen et al. [6] (2016) examined the effect of multi-cell cross-section designs on the crashworthiness characteristics of aluminium square tubes. The finite element analysis models which were developed for the needs of the study were initially validated by both quasi-static experimental tests. A typical representation of the study results is shown in the next two figures, where the collapsed specimens are depicted in the first figure, and the influence of multi-cell cross-section on energy absorption is depicted in the second figure. As Figure 30 shows, all SEA, PCF and MCF parameters increase as the number of cells increases too.

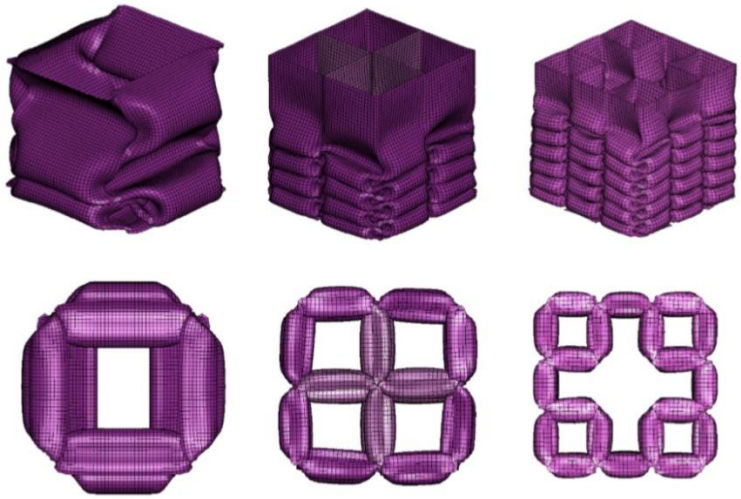

**Figure 29 Collapsed specimens (single-cell, four-cell and five-cell cross-sectioned square tubes), [6]**

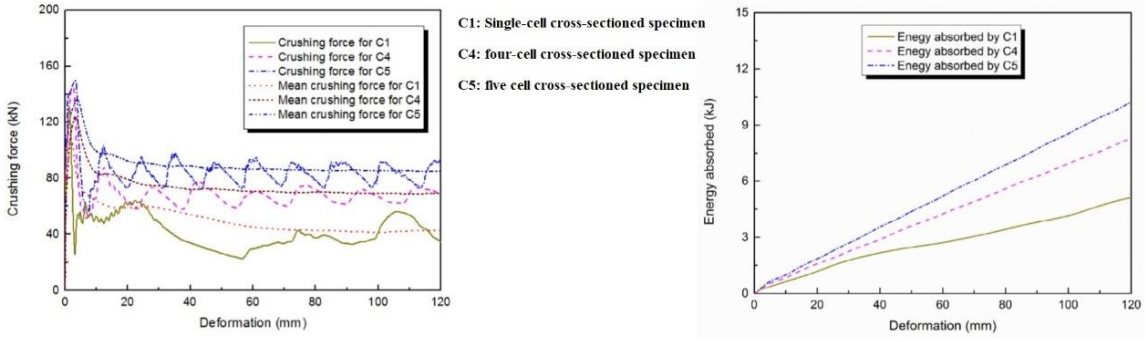


**Figure 30 Effect of multi-cell cross-sections on energy absorption, [6]**

Nikkhah et al. [4] (2019) studied the crashworthiness behavior of thin-walled windowed tubes made of aluminium. Different multi-cell cross-section designs were also considered in this research work too. It was concluded that the windowed thin-walled tubes were characterized by lower peak crush force (PCF) and lower specific energy absorption (SEA). The first consequence is positive, considering that PCF must be a reasonable value in order to the specimen be able of being deformed plastically absorbing energy. However, low SEA means in turn reduced energy absorption capability.

Acar et al. [18] (2019) examined different designs of multi-cell cross-sectioned thin-walled aluminium tubes, too. An optimization of crashworthiness response considering the CFE and SEA parameters was performed. The finite element models which were developed for the needs of the study were initially validated with experimental results. For the optimization, the same weighting factors were considered in the objective function for both CFE and SEA, paying in that way the same importance on maximizing both parameters. It was concluded that designs of thinner and larger in diameter tubes were provided for CFE maximization compared to the ones provided for SEA maximization.

Although most research works have been performed on crashworthiness analysis of simple composite structures such as tubes, Mamalis et al. [19] (1991) studied the effect of specimen geometry of thin-walled conical shells on energy absorption capability. Specifically, geometry characteristics like thickness, shell length and apical angle were investigated both experimentally and analytically. A standard crushing speed of 10mm/min was applied at all test cases until a deformation of 63mm being reached. The examined specimens were fiber-reinforced thin-walled composite conical shells with the semi-apical angle lying in the region of $5^o$ to $30^o$. The failure mode of collapse and the effect of geometry characteristics (shell length, thickness of thin-walled shell, apical angle, diameter) on energy absorption capability were obtained. In general, thin-walled shells revealed a more efficient crashworthy behavior compared to thin-walled tubes. The experimental data provided that the specific energy absorption is a linear function of diameter to thickness ratio, or SEA (kJ/kg) = $1469.4 \cdot t/D - 6.8$. For axial compression of thin-walled composite shells, it was concluded that catastrophic brittle fracture and elastic instability must be prevented in order to achieve stable collapse during crushing conditions. In case of conical shells, stable collapse may be developed with absence of external trigger mechanism, as conical shells develop self-triggering mechanism with fracture initiating at regions of highest stress. The transition from stable to unstable collapse mode regarding to semi-apical angle was found to be in the region of $15^o$ to $20^o$. Finally, the results showed that specific energy absorption decreases as semi-apical angle of shell increases, as thickness increases or as diameter decreases. In fact, though, large diameter shells may collapse under catastrophic failure.

Regarding oblique impact conditions, Shivdayal et al. [20] (2019) examined circular polymer tubes under both axial and oblique impact loading aiming to investigate the effect of various design variables on crushing response of road vehicle structures. Carbon and glass fiber reinforced plastic (CFRP / GFRP) composite tubes were evaluated respectively through their crashworthiness

behavior examining homogeneous and heterogeneous ply orientation of $0^o$, $\pm 45^o$ and $90^o$ for the laminated tubes. Non-linear crushing analysis was carried out by implementing finite element modelling in ABAQUS software for assessing peak crushing force (PCF), deformation length and energy absorption capability through the revealed failure mode. A Continuum Damage Mechanics (CDM) approach was taken into account introducing an effective damage tensor for estimating material plastic response during collapse according to Hashin damage criteria. The above approach offered the capability of estimating the damage propagation and possible delamination of composited tubes, allowing that way to predict their effect on the revealed crashworthiness. More, the upper edge of examined tubes was $45^o$ beveled behaving as a triggering mechanism which facilitates the initiation of a progressive failure. The created finite element models were initially validated against experimental data provided from $10^o$ oblique loading tests of CFRP tubes, while the numerical simulations carried out concerned about both axial and oblique loading in various angles with uniform or non-uniform contact between tube and impactor.

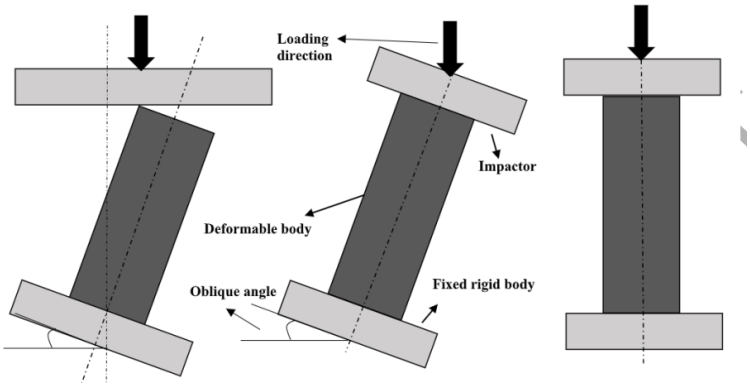


**Figure 31 Axial and oblique loading conditions of uniform and non-uniform contact, [20]**

The simulation results showed that CRFP tubes revealed greater energy absorption capability, while the heterogeneous ply orientation structures proved to be more efficient structures. Finally, axial loading provided higher energy dissipation levels for the collapsed tubes compared to oblique one, in which higher loading angles resulted in lower energy absorption levels as the failure mechanism proved to be less progressive, which was amplified more in oblique loading with non-uniform contact.

Zarei [21] (2019) examined hybrid composite aluminum tubes under both dynamic and oblique impact loadings. The examined specimens consisted of 6060 aluminum alloy tubes with external composite layers varying in number from one to three in total, consisted of E-glass fiber and epoxy resin. The crashworthiness behavior was evaluated through experimental tests under dynamic conditions and also finite element analysis carried out in LS-Dyna software. The thin-walled tubes were modelled utilizing shell elements, while Chang-Chang failure model was accounting for material plastic response. In every case, the specific energy absorption was considered as the main metric for the assessment of crashworthiness efficiency for each structure. The results

revealed a decrease in maximum and mean crushing forces as loading angle gets higher, while the greater energy absorption capacity revealed by the hybrid aluminum tube of one composite external layer, as in that case the structure collapsed maintaining the adhesion between the tube and the external layer which was not observed in the case of two or three external composite layers.

Further, Fauzan et al. (2016) [22] investigated a design optimization of foam-filled circular 6060 T4 aluminum tubes regarding their crashworthiness response under both axial and oblique impact loading. The examined structures contained of an empty double tube, an internally foam-filled double tube and a fully foam-filled double tube. The finite element models were developed in ABAQUS software and were validated via experimental data. Single 4-node shell elements were utilized for tubes modelling, and 8-node solid elements for aluminium foams. In each examined configuration, the bottom tube end was considered fixed, while oblique loading angles were adjusted to the range of $0^o$ to $40^o$. Fully foam-filled double tubes proved as the more crashworthy structures revealing the greatest energy absorbing levels since they could withstand an oblique impact load as effectively as an axial compression and bending mode.

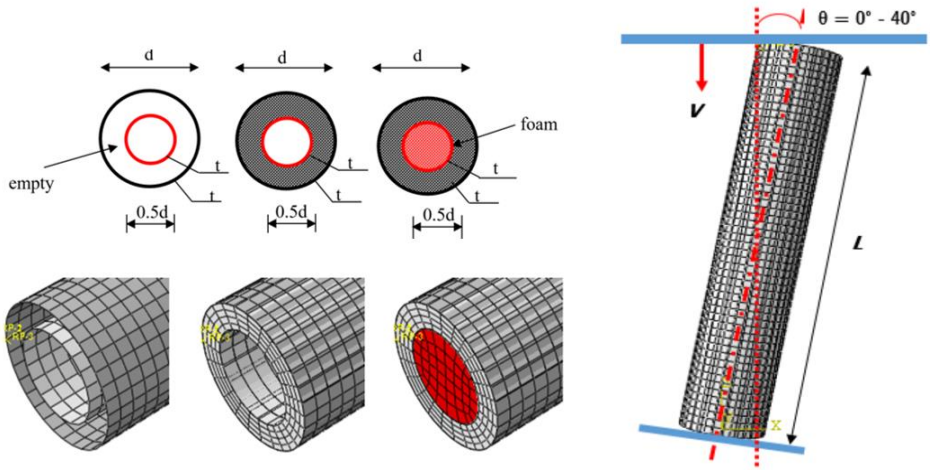


**Figure 32 Foam-filled examined double tubes under oblique collapse, [22]**

Kim and Wierzbicki [23] identified two different cases of oblique impact loading; angled loading and off-axis loading. In the first case, the tube is supported to the impactor and moving with its velocity towards the crushing surface which is positioned in an oblique angle. In the second case, the tube is supported in a bottom holder, both positioned in an oblique angle compared to the impactor which moves vertically crushing the tube. For this purpose, square and rectangular section beams were examined through non-linear finite element analysis in PAM-CRASH software. Their work highlighted the different loading conditions which the examined tube faces in the above two oblique loading cases, calculating a critical angle which defined the more preferable loading case. Finally, their research concluded further that the loading angle revealed a significant effect on collapse mode, as below a critical angle of bending moment

with respect to axis-symmetry of section, the initial fold would formulate in the weaker side of the tube section revealing lower energy absorption capacity.

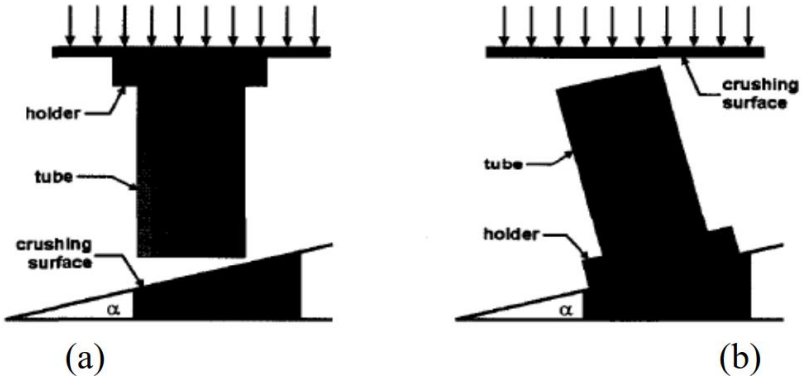


**Figure 33 types of oblique crushing: (a) angled loading, (b) off-axis loading, [23]**

Moreover, Han and Park [24] (1999) used the angled loading type, depicted above, in their numerical analysis of oblique loading of mild steel square columns. The examined columns were simulated assuming frictionless conditions under a crushing velocity of 30 mph to an inclined wall. The results revealed that above a critical loading angle, a transition of axial collapse to Euler-type buckling mode takes place decreasing significantly the energy dissipation levels of the impacted structure. Finally, their work utilized normalized numerical results from multiple simulations cases in order to derive an approximate expression for mean crushing force and critical angle for the modelled steel tubes.

Reyes et al. [16] (2002) studied the crashworthiness behavior of AA6060 aluminum extruded thin-walled square columns under subjected to off-axis oblique loading. Both experimental tests under quasi-static conditions and numerical analyses via finite element models in LS-Dyna were conducted in order to assess the effect of wall thickness, initial length, loading angle and impact velocity, while all examined structures were clamped to their bottom end. All columns revealed an unstable bending collapse mode with significant decrease in mean crushing force for loading angles greater than $5^o$. The energy absorbing levels seemed to flatten out in the range of $15^o$ to $30^o$ loading angle, while the wall thickness and initial length proved additionally to be the dominant parameters in structure response.

Crutzen et al. [25] (1996) indicated a possible solution through numerical analysis results for avoiding the unstable Euler-type bending mode during oblique impact, by redistributing the specimen mass along its length properly causing a more stable and progressive collapse. In that direction, columns of variable thickness or cross-section were proposed instead of straight columns, dissipating greater amounts of crushing energy due to their progressive failure. Pirmohammad et al. [26] (2016) studied also multi-cell tubes until $27^o$ oblique quasi-static loads through FEA code in LS-DYNA, while COPRAS method was utilized for indicating the best energy absorbing configuration among different geometries. Circularly multi-cell tubes proved to be the most efficient ones with a scaling factor of 0.5 regarding the dimensioning of interior cells. Liu et al. [27]

(2020) conducted numerically a multi-objective crashworthiness optimization of tapered star-shaped aluminum tubes subjected to oblique crushing, where the optimization criteria contained the peak crushing force (PCF) minimization and the specific energy absorption (SEA) maximization. The results highlighted that an optimum star-shaped cross-section design could bring an almost 10% increase in SEA and a slight reduction in PCF, while greater thickness and taper angle showed to increase the critical loading angle from $10^o$ up to $15^o$.

Moreover, the effect of foam-filling together with different cross-sectional shapes on axial and oblique crushing response has been studied by Tarlochan et al. (2013) [28]. Energy absorption, crushing efficiency, ease of manufacture and cost were the criteria for indicating the optimal configuration, while foam-filling and wall thickness contained the design parameters. Further, foam-filled conical and circular aluminum tubes subjected to oblique loading have been investigated by Qi et al. (2014) [29] via FEA models. PCF and SEA proved to be improved for conical tubes reaching a maximum increase of 106.6% in SEA considering the case of foam-filled ones. The optimal design of conical tubes was affected by the loading angle regarding which a $10^o$ critical value was revealed. Borvik et al. (2003) [30] studied aluminum empty and foam-filled circular tubes subjected to axial and oblique crushing up to $30^o$ angle. Quasi-static tests and simulations in LS-DYNA were conducted considering shell elements for the tubes and brick elements for the foam following an elastoplastic approach of isotropic strain hardening for material modelling. The provided results showed that foam-filling increased the crashworthiness performance, while the energy absorption drop in increased angles seemed to affect stronger the foam-filled tubes compared to the empty tubes. Additionally, the crushing response of foam-filled ellipse tubes under oblique loading has also been investigated by Gao et al. (2016) [31] conducting a multi-objective optimization for foam-filled ellipse tubes via FEA simulations. The provided results revealed a 3% drop in PCF and 27% increase of SEA compared to conventional square and circular tubes.

Finally, more novel tubular configurations have been also investigated under oblique impact loading conditions, such as multi-cell tubes and windowed tubes. In specific, Qi et al. [32] (2012) examined the crashworthiness behavior of tapered square tubes under oblique impact loading by studying numerically several geometrical configurations such as single-cell and multi-cell tubes, concluding that multi-cell tapered tubes revealed more efficient crashworthy structures. Additionally, Song [33] (2013) studied the crushing response of obliquely loaded square windowed tubes by conducting numerical finite element analysis. The examined parameters contained of the loading angle, tube windows dimensions and impact velocity. The results of his work highlighted that the windowed tubes revealed lower energy absorbing levels under oblique impact compared to conventional tubes, while a novel design of windowed tubes was then proposed by varying windows dimensions along the tube in order to increase the critical angle achieving a more stable collapse mode, maintaining however the absorbed energy high enough, proving that way this design more efficient in terms of crashworthiness response. Further, the response of additional novel designs against oblique loading has been examined such as the

one of functionally graded thickness (FGT) tubes. Baykasoglou et al. [34] (2019) studied the effect of FGT and cross-section shape on crashworthiness performance under angles up to 30$^o$ via non-linear explicit FEA models validated against experimental and theoretical data. A critical angle value of 15$^o$ was obtained for circular aluminum tubes, while the FGT effect seemed stronger in high loading angles where a maximum increase in SEA about 93% was revealed. The effect of variable thickness distribution on energy absorption of obliquely crushed tubes was also studied by Mohammadiha et al. [35] (2016) concluding that the optimal design is affected by the crushing angle.

## 2.5 Analytical expressions of mean crushing load for axial collapse

Efforts during the past have been made in order to calculate an analytical and theoretical expression for the mean crushing load of structures axially collapsed by formulating convolutions. One of the first works was carried out by Alexander [36] made in 1960. That research work was conducted considering thin-walled cylindrical shells which were expected to collapse in concertina mode under axial loading, formulated that way straight-sided convolutions consisted of 3 stationary plastic hinges. The mean collapse load is calculated by equating the internal deformation work to the external loading one. In specific, as required work considered the one which would deform the metal in one straight-sided convolution causing bending at circular joints and stretching the metal between them, as depicted following. From that study, Alexander suggested the following expression for mean collapse load.

$$\bar{P} = M_0 \cdot (20{,}73 \cdot \sqrt{2R_0/h_0} + 6{,}283) \tag{7}$$

In the above equation, let $M_0$ be the fully plastic bending moment, $h_0$ the initial wall thickness and $R_0$ the tube mean radius.

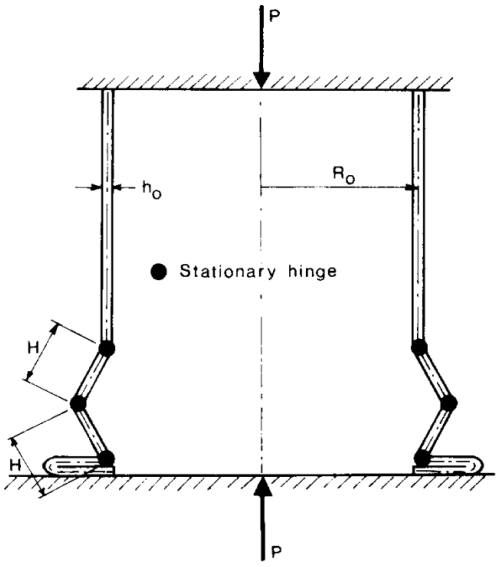


**Figure 34 Alexander's model for axisymmetric axial crushing of circular tube, [36]**

Further, Abramowicz and Jones [37] improved afterwards the Alexander solution by introducing a correction for the effective crushing distance. The internal energy dissipation was computed according to Alexander's approach, utilizing a rigid-perfectly plastic material idealization with stationary plastic hinges. However, in the improved approach the work of external forces was estimated based on a linear strain-hardening material behavior. Thus, Abramowicz and Jones' proposed theory predicts more accurately the magnitude of mean crushing force over a wide range of wall thickness to width ratio, allowing for an estimation for both symmetric and non-symmetric collapse modes as cited below by equations (8) and (9) for concertina and diamond mode respectively.

$$\bar{P} = M_0 \cdot \frac{20{,}79 \cdot \sqrt{2R/h} + 11{,}9}{0{,}86 - 0{,}568\sqrt{h/2R}} \tag{8}$$

$$\bar{P} = M_0 \cdot 86{,}14 \cdot \sqrt[3]{2R/h} \tag{9}$$

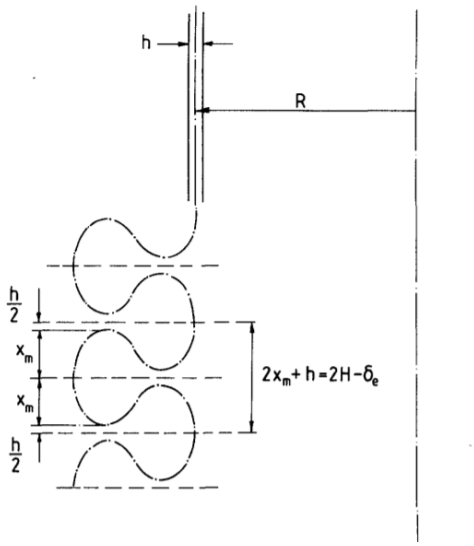


**Figure 35 Effective crushing distance $\delta_e$ (Abramowicz and Jones), [37]**

Moreover, Abramowicz and Jones developed in the same work a theorical expression for mean crushing force of square tubes taking into account the strain hardening effect proposing that:

$$\bar{P} = 13.06 \cdot \sigma_0 \cdot b^{1/3} \cdot t^{5/3} \tag{10}$$

More, Wierzbicki et al. [38] proposed additional improvements replacing the stationary plastic hinges of Alexander's theory with moving hinges representing that way a more realistic shape of deformed convolutions formulated during collapse. According to this treatment, two folding waves are being created in an active crush zone considering two different cases. In the first one, a model with two straight elements constrained by stationary hinges was analyzed, while in the second case two S-shaped superfolding elements were taken into account revealing a more realistic prediction for the mean crushing load, capable also of predicting the existence of intermediate peaks in load-displacement response. Each treatment revealed the following expressions for the two straight elements consideration constrained by stationary hinges and for the S-shaped superfolding elements respectively:

$$\bar{P} = M_0 \cdot 22{,}27 \cdot \sqrt{2R/h} \tag{11}$$

$$\bar{P} = M_0 \cdot 31{,}74 \cdot \sqrt{2R/_h} \tag{12}$$

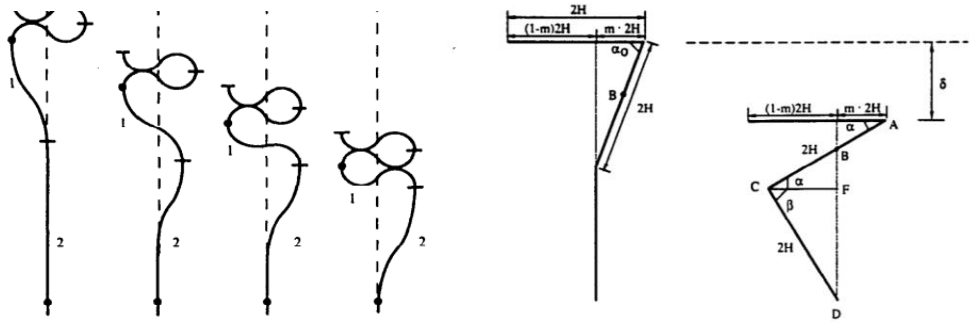


**Figure 36 Superfolding elements assumption (Wierzbicki), [38]**

Furthermore, Wierzbicki and Abramowicz expanded the initial theory into two specific types of superfolding elements; type I and type II. Both types are capable of predicting accurately the idealized collapse behavior of square tubes, as the combination between them offers sufficient estimations for both symmetric and non-symmetric modes. So, for symmetrically formulated convolutions the mean crushing load can be estimated as:

$$\bar{P} = M_0 \cdot 52{,}22 \cdot \sqrt[3]{c/_h} \tag{13}$$

while for non-symmetrically formulated convolutions:

$$\bar{P} = M_0 \cdot \{42{,}92 \cdot \sqrt[3]{c/_h} + 3{,}17 \cdot \sqrt[3]{(c/_h)^2} + 2{,}04\} \tag{14}$$

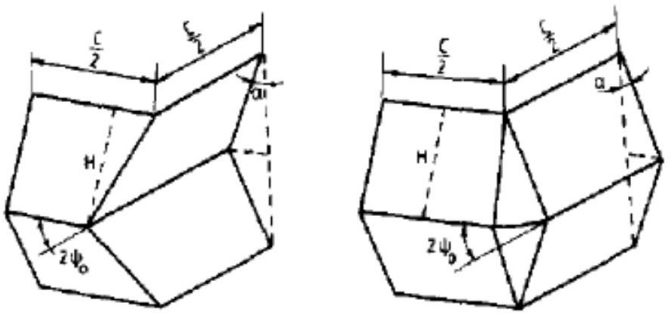


**Figure 37 Superfolding elements; type I (left) and type II (right), [38]**

Additionally, more studies have been carried out aiming to estimate the mean crushing load of an axially collapsed tubular structure. Specifically, Johnson et al. [39] studied the inextensional collapse modes of thin-walled tubes under axial loading. Tubes deformation assumed to take place under folding about fixed hinge lines formulating a number of flat triangular plates. The proposed failure mechanism accounts for a progressive collapse starting from the one tube end and following then a passage of a travelling hinge, resulting in the formulation of horizontal stationary hinges as depicted below.

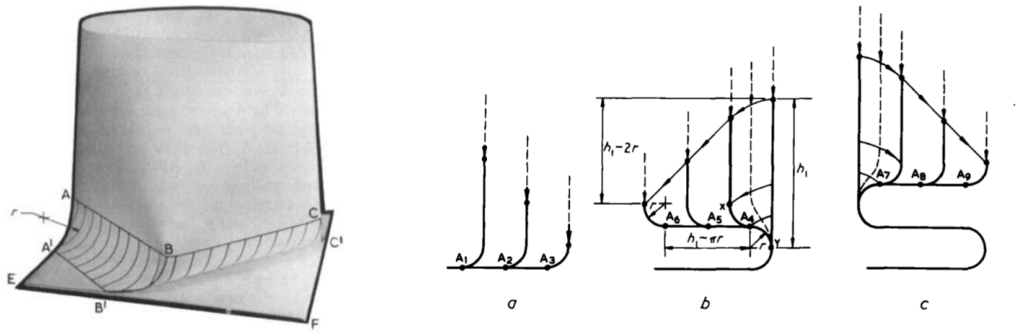


**Figure 38 Horizontal stationary hinges formulation from travelling hinge assumption, [39]**

The above model considers also the number of circumferential lobes *n* (n=2 for 2D-diamond mode, n=3 for 3-D diamond mode etc.) and the number of axial lobes *m*, proposing the following expression for the mean crushing force:

$$\bar{P} = 2\pi M_0 \cdot (1 + n \cdot cosec\frac{\pi}{2n} + \frac{m-1}{m} \cdot n \cdot cot\frac{\pi}{2n}) \quad (15)$$

Also, Mamalis et al. [40] studied the crushing response of thin-walled bi-material tubes under extensible collapse, providing an analytical expression for the mean crushing force by equating the internal deformation work to the one of the external forces required to formulate a convolution. Considering thus, common material properties for the internal and external shells, the revealed analytical expression can be summarized following considering *Y* as the material yield stress, *t* the tube wall thickness and *D* its external diameter:

$$\bar{P} = 5{,}6Y \cdot t \cdot \sqrt{D \cdot t} \quad (16)$$

The above expression revealed sufficient agreement with Alexander's theory, while both took into account Tresca's yield criterion for the plasticity initiation during collapse.

Regarding the case of oblique impact loading, Tran et al. [41] (2014) developed a theoretical approach for energy absorption prediction validated via FEA modelling for multi-cell square tubes subjected to oblique crushing. In more specific, their study introduced an oblique impacting coefficient ″λ″ which is defined as the ratio of mean crushing force (MCF) obtained under oblique loading to the one of axial loading. In fact, λ revealed to be affected by the crushing angle ″a″, the wall thickness ″t″ and the tube side length ″b″ as the following expression shows, while ″c″ refers to a constant based on the geometrical configuration of multi-cell tube varying from 1.1 to 1.24. Moreover, λ coefficient showed a decrease as the loading angle gets higher, while at angles greater than $10^o$ the decrease in λ coefficient proved to be significantly greater highlighting $10^o$ as the critical crushing angle which results in a significant drop of MCF and in consequence of energy absorption capacity.

$$\lambda = \frac{MCF_{oblique}}{MCF_{axial}} = (10 \cdot \frac{t}{b} + c) \cdot cosa \tag{17}$$

Furthermore, their work highlighted that the applied crushing force during oblique impact loading reacts to axial compressive and lateral loads, while the last ones result in additional bending moment around tube bottom end. That bending moment ″M″ increases with the increase in crushing angle ″a″ (18) facilitating both the plastic collapse initiation and its progress, resulting that way in lower peak crushing force and lower energy absorption for a crushed structure. In addition, at high crushing angles when the introduced bending moment due to the angled loading gets greater than the one required for bending deformation mode, an unstable Euler-type buckling mode will occur during collapse dropping significantly the energy absorption capacity due to its unstable inelastic behavior.

$$M = P_h \cdot x = P \cdot sina \cdot (L_o - \frac{b - t}{2tana}) \tag{18}$$

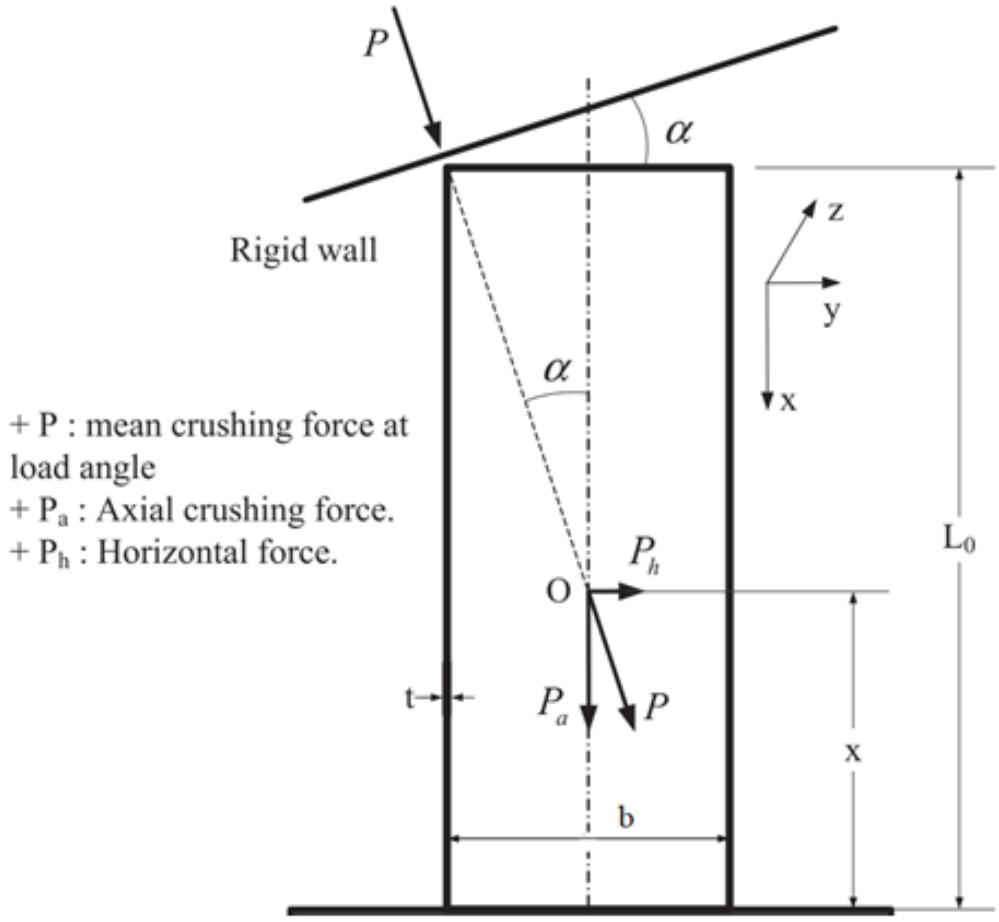


**Figure 39 Forces acting in oblique impact loading,** [41]

Finally, regarding the Euler-type buckling failure mode, the crushing load resulting in this mechanism has not been yet computed with similar accuracy due to its unstable behavior which leads to significantly lower energy absorbing levels. However, semi-empirical criteria have been developed based on experimental data considering the effect of geometrical parameters such as tube length, diameter and wall thickness. Although, Kecman [42] proposed bending collapse mode is usually localized at plastic hinges while the other tube sections behave as rotating rigid bodies. Kecman studied prismatic tubes collapsed under Euler-type buckling, observing that this mechanism takes place in four phases; a) a bulge is initially forming without any apparent rolling deformation, b) rolling deformations starts then to occur, c) the rolling deformations are jammed creating new bending line and d) two buckled halves coming in contact followed by the total jamming of the original hinge causing the initiation of an adjacent secondary hinge, as depicted in the following figure.

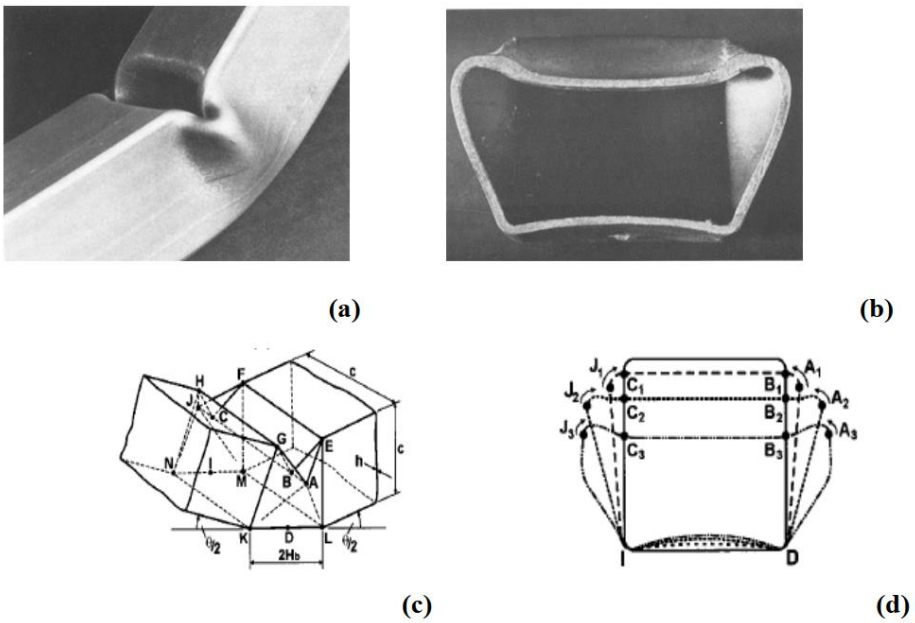


**Figure 40 Euler-type buckling model by Kecman, [42]**

The theory developed by Kecman was emphasized in the second stage of bending collapse, proposing that the absorbed energy can be estimated through its dependence to hinges rotation angle (19), as shown in Figure 40 (c). Finally, the bending zone width was also estimated based on rectangular tube width and wall thickness (20).

$$EA = \sum_{i=1}^{8} EA(\theta_i) \tag{19}$$

$$H_b = 1{,}276 \cdot c^{2/3} \cdot h^{1/3} \tag{20}$$

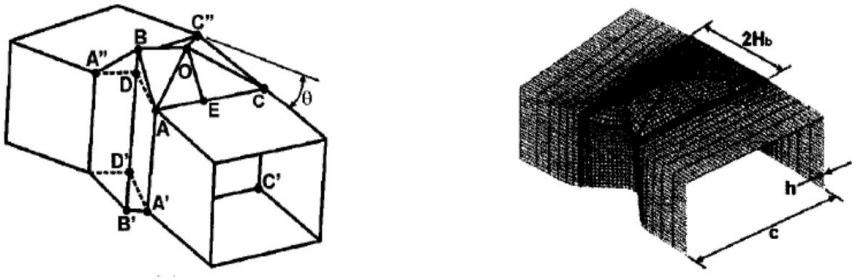


**Figure 41 Bending zone width, [42]**

# 3. Experimental Investigation of Crashworthiness Behavior

## 3.1 Introduction

Current chapter contains the experimental investigation of crashsworthiness response under axial and oblique impact loading for the examined thin-walled tubes. The conducted tests carried out in quasi-static conditions for a range of oblique crushing angles up to $15^{o}$ under two different types of initial contact between impactor and tubular specimen. In specific, an initial contact alongside tube top edge was examined at first, while secondly the initial contact was occurred around top corner of tube for the oblique loading cases. The experimental investigation of the above examined test cases aims to assess the effects of crushing angle and initial type of contact on the crushing response efficiency. In each test case, the main crashworthiness metrics were computed via the force-displacement curve provided from the experimental data, while the occurred collapse mechanism was also captured. Finally, the experimental results are analyzed for both the evaluation of the crashworthiness performance and the validating procedure of the developed finite element models.

## 3.2 Experimental Tests

This study carries out both experimental tests and numerical simulations in order to assess the response of thin-walled aluminium tubes under both axial and oblique crushing loads. The main goal of each analysis is to obtain the main response characteristics of a crashworthy structure and observe the crushing mode occurred during the collapse. Peak crushing force (PCF), mean crushing force (MCF), crushing force efficiency (CFE), specific energy absorption (SEA) and the amount of absorbed energy (EA) are some critical key parameters. These parameters together with the appeared collapse mechanism are considered as the appropriate metrics for comparisons between the provided experimental and numerical results. The conducted experimental tests can be used for two main reasons; the first one is to observe the crashworthiness behavior of the structure during the collapse and extract critical conclusions for key response characteristics, while in addition, the results from experimental tests can be utilized as a validating source to assess the accuracy of developed numerical models. The last ones are widely used as they provide useful results in predicting the collapse mode and crashworthiness response characteristics of a crushed

structure when they have been validated and their accuracy has been proved by sufficient matching against experimental data. The important advantage of carrying out numerical simulations is that they require less cost than conducting experimental tests where the necessary equipment (machine, high-frequency data recorders and high-speed cameras) is oftenly of high cost.

As reported previously in subsection 2.3, the experimental tests which can be conducted are either quasi-static or dynamic tests. The first ones require less expensive equipment but they provide less accurate results, as they are conducted at lower loading speeds than the appeared conditions in real crushes. In contrast, the dynamic crush tests represent more real crushing conditions and provide more accurate results as they are conducted at high loading speeds. However, the cost of such tests is quite higher and they are rarely preferred due to that.

For the purposes of current study, the examined tubular specimens are tested to assess their crashworthy behavior under both axial and oblique impact loading. The experimental tests are conducted in quasi-static conditions by compressing each specimen in a pressing machine with a loading rate of 10 mm/min. For each one of the tested specimens, different states are captured during their collapse, while stress and strain measurements are recorded providing the experimental force-displacement curve. From the provided experimental curves, parameters which characterize the structure response in crashworthiness - such as peak crushing force (PCF), mean crushing force (MCF), energy absorption (EA), specific energy absorption (SEA) and crushing force efficiency (CFE) - can be computed.

## 3.3 Examined Test Cases

The examined specimens consist of thin-walled aluminium tubes of 50 x 50 mm squared cross-section, 1.5 mm wall thickness and 100 mm initial length as depicted in revealing a total specimen mass about 78.57 gr. The thin-walled square tubes are of 6000 series aluminium alloy AA6060-T6 containing according to EN573-3 about 0.4% Si, 0.34% Fe, 0.02% Cu, 0.47% Mg, 0.004% Cr, 0.06% Zn and 98.706% Al. Each examined configurations consisted of the tested tubular specimen, a bottom base and an upper plate moving downwards vertically in order to load the specimen under the compressive forces applied from the pressing machine. The bottom base was further able to rotate by the implementation of a screwed adjustment in order to position the tube to the proper crushing angle with respect to the impactor. In addition, an external configuration was placed on the top of the bottom base supporting the tube in order to avoid any sliding during the oblique impact loading.

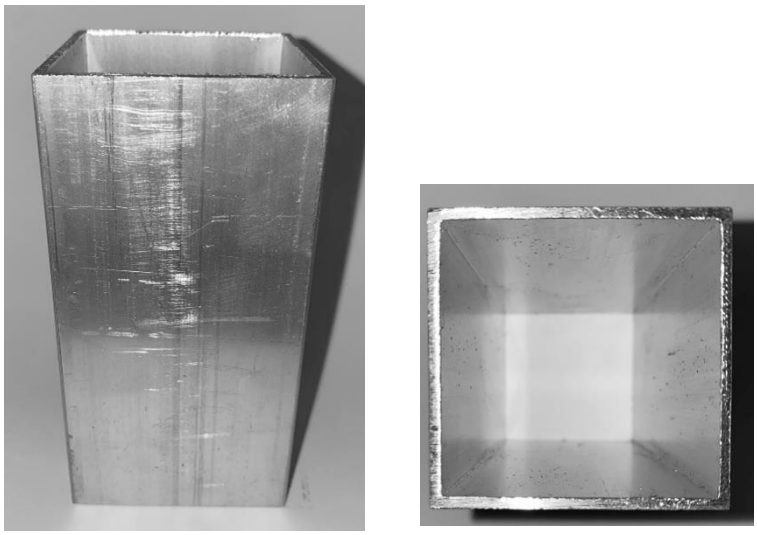

**Figure 42 Initial specimen aspects**

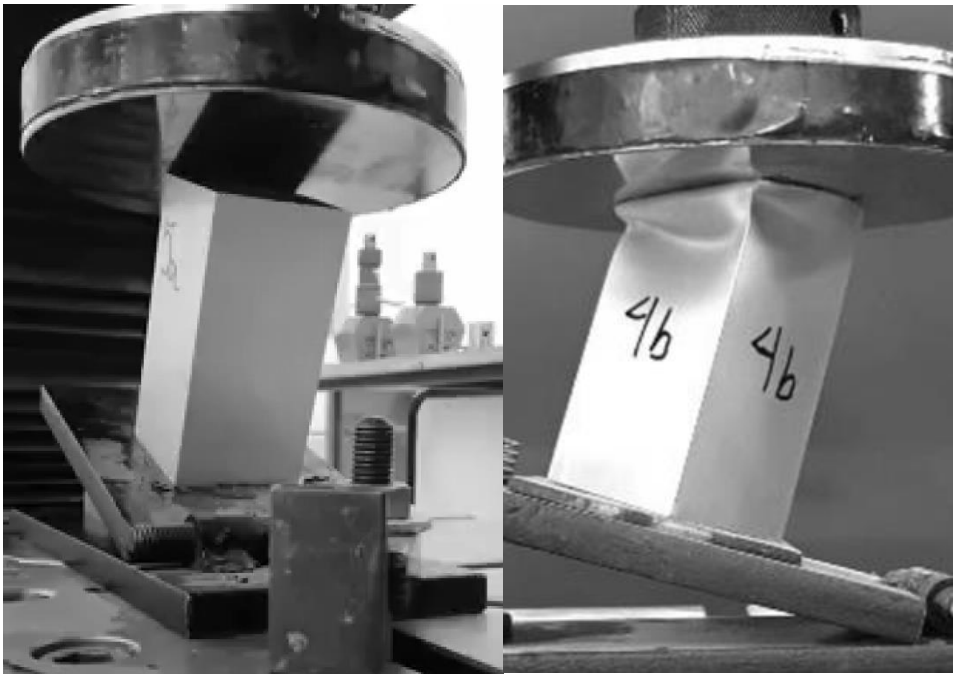


**Figure 43 Examined oblique loading test configurations regarding tube-impactor initial contact: contact in edge (left), contact in corner (right)**

The conducted tests carried out in INSTRON 4482 pressing machine with which the MTL of NTUA is equipped. The above pressing machine is capable of 10 kN nominal load with 250 mm/min maximum loading velocity under peak load and so its adequate power made it a proper tool for the experimental investigation together with a data recording system with which is equipped regarding the measurement of the applied forces and displacements. Each experimental compression test carried out in quasi-static conditions under a constant loading rate of 10 mm/min until a maximum displacement about 60

mm, while the specimens are subjected to both axial and oblique compressive loads by examining various crushing angles lying from $0^o$ to $15^o$ in order to assess their effect on crashworthiness response and energy absorption capability of the crushed tubes. The loading angle was adjusted properly by rotating the bottom base together with the tube representing in that way off-axis oblique loading conditions. In addition, two different types of initial contact between the impactor (upper pressing plate) and the tube were examined regarding the oblique impact loading cases. In more specific, at first the tube was obliquely positioned to the impactor such that their initial contact being occurred alongside the tube top side edge of its cross-section providing so a linear initial contact, while at the second test case the tube was obliquely positioned to the impactor such that their initial contact occurring in tube top corner of its cross-section. Thus, the two different types of initial contact between impactor and tube are described as “contact in edge” and “contact in corner” respectively. The experimental investigation thus aims to both provide the necessary test data for the validating procedure of the finite element models and contribute to the total evaluation of the crashworthiness performance under the examined cases focusing on identifying the effect of crushing angle and initial type of contact on energy absorption capability and the stability of plastic collapse.


**Figure 44 INSTRON 4482 pressing machine**

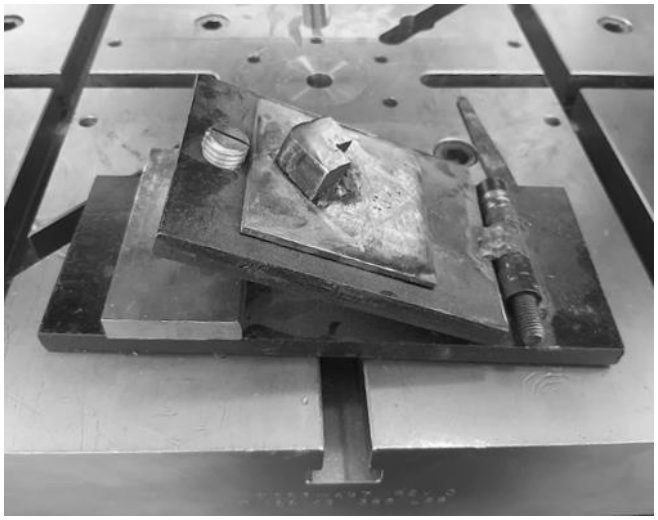

**Figure 45 Bottom base external configuration**

Each test case is conducted twice for the same specimen and loading condition aiming to provide more reliable results avoiding any possible deviations due to material defects, data recording errors, varied environmental testing conditions etc., labelling thus the conducted tests as “a” and “b”. Moreover, each oblique loading case is also examined under contact-in-edge and contact-in-corner scenarios regarding the initial type of contact between impactor and specimen. Finally, the conducted tests are numbered from 1 to 4 regarding the examined crushing angle which varies from $0^o$ to $15^o$ as shows Table 1 which also depicts the crushed mass of the deformed specimen section taken into account for SEA assessment. For the test cases of oblique loading, the crushed mass of collapsed specimen is referred for both types of initial impactor-specimen contact mentioned as “contact-in-edge” and “contact-in-corner”.

**Table 1 Examined test cases**

| Test case | Loading angle (deg) | Initial impactor-specimen contact case |
|---|---|---|
| **1** | 0 | - |
| **2** | 5 | in edge / in corner |
| **3** | 10 | in edge / in corner |
| **4** | 15 | in edge / in corner |

Finally, the provided experimental results are offered for both crashworthiness evaluation of the examined conditions regarding their effect on structures energy absorption capacity, and numerical models validating procedure. In every case, the results analysis consists of estimating the main crashworthiness response characteristic parameters from the revealed load-displacement curve and the observing the occurred collapse mechanism the mode of which affects significantly the energy absorption capability of the crushed structure.

## 3.4 Experimental Results

Current section presents the experimental results as provided by the conducted compression quasi-static tests for each examined loading case. The presented results were provided by the crashworthiness analysis of the recorded force-displacement (F-x) test data from which the respective curves were extracted together with the main crashworthiness response parameters like peak crushing force (PCF), mean crushing force (MCF), energy absorption (EA) and specific energy absorption (SEA) and crushing force efficiency (CFE).

Furthermore, for each case proper deformation states were captured in order to identify the occurred plastic collapse mechanism and its characteristics which affect the energy absorption capacity of the crushed structure reacting on force distribution during post-buckling region of force-displacement diagram. The examined axial and oblique loading test cases are labelled as 1–2–3–4 regarding the loading angles of $0^o$–$5^o$–$10^o$–$15^o$ respectively, while in the case of obliquely compressed specimens two types of initial contact between impactor and tube are examined; a contact-in-edge type and a contact-in-corner one. Each test case was carried out twice providing “test a” and “test b” scenarios in order to avoid any data recording errors or possible material defects securing thus more reliable experimental results. Finally, all quasi-static tests are conducted under a 10mm/min constant loading rate until 60 mm maximum impactor vertical displacement.

### 3.4.1 Axial Loading – Test Cases 1a – 1b

In the first test case of this study, the aluminium tubes are subjected to axial compressive loading until maximum shortening of about 60 mm. The recorded experimental data during the test revealed the force-displacement (F-x) and energy absorption-displacement (EA-x) curves for the examined specimens as depicted in Figure 46 and Figure 47 respectively. Table 2 shows the estimation of crashworthiness response parameters as revealed by the experimental data analysis. As shown below, the two experimental tests revealed a sufficient agreement in PCF providing it about 45 kN reflecting the plastic collapse

initiation under the formulation of first plastic fold. During plastic collapse progress, both axially compressed specimens revealed local tearing around their cross-section corners due to stress concentration which reacted to a force reduction until the shortening of 40 mm and 30 mm regarding test 1a and test 1b respectively. After that point, the concentrated crushed mass of plastically deformed tubes behaved as more compact structure achieving to formulate more folds as shown by the local force peaks in F-x curves.

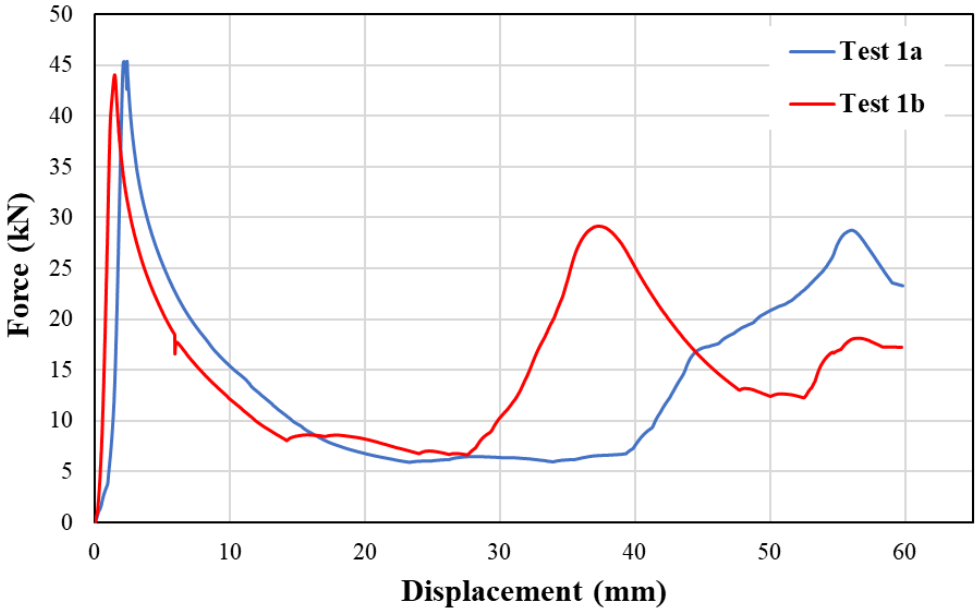


**Figure 46 Experimental F-x curves of axial loading tests**

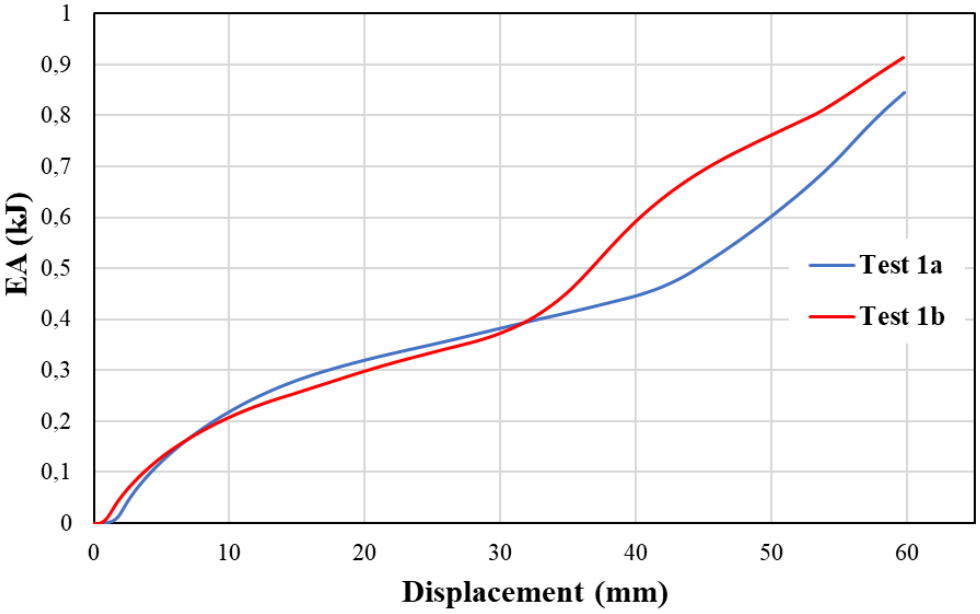


**Figure 47 Experimental EA-x curves of axial loading tests**

In fact, although the two tests showed a deviation of 3% in PCF revealing a sufficient agreement, energy absorption capacity was slightly higher deviated about a 7.5% error in EA between the two tests as in test 1b the formulation of second plastic fold occurred earlier than in test 1a due to a lighter tearing around tube corners allowing for greater energy absorption after 30 mm of shortening as depicted in Figure 47.

**Table 2 Crashworthiness response parameters for tests 1a-1b**

| | **Test 1a** | **Test 1b** | **Deviation (%)** |
|---|---|---|---|
| **PCF (kN)** | 45.36 | 44.02 | 3.0 |
| **MCF (kN)** | 14.13 | 15.28 | 7.5 |
| **EA (J)** | 844.9 | 912.7 | 7.4 |
| **SEA (kJ/kg)** | 17.92 | 19.36 | 7.4 |
| **CFE (-)** | 0.31 | 0.35 | 10.2 |

Moreover, as depicted by the following figures regarding plastic collapse states and final views of crushed specimens, both specimens started to collapse controllably under inextensional mode by formulating one inextensional fold reflected by PCF, after of which local tearing was occurred around square cross-section's corners. The above observation was captured more intensively in test 1a, while test 1b revealed a lighter corner tearing mode. Thus, test 1b resulted in greater MCF and in consequence higher EA and SEA levels, as during its plastic collapse progress two further inextensional folds were formulated as captured also by the two local force peaks of test 1b at the final stages of collapse. In contrast, test 1a revealed a greater tearing magnitude not allowing to the crushed specimen to formulate more plastic folds except the last stage of collapse where an inextensional fold tended to be formulated as captured also by the force increase during the last stage of impactor displacement. Thus, test 1b allowed for greater energy absorption capacity revealing a more controllable and progressive collapse formulating 3 inextensional folds with a light tearing occurance in contrast to test 1a results which showed a greater tearing magnitude around tube corners which reacted to lower EA. However, PCF seemed to be matched sufficiently by the two tests as both revealed the plastic collapse initiation under an inextensional fold.

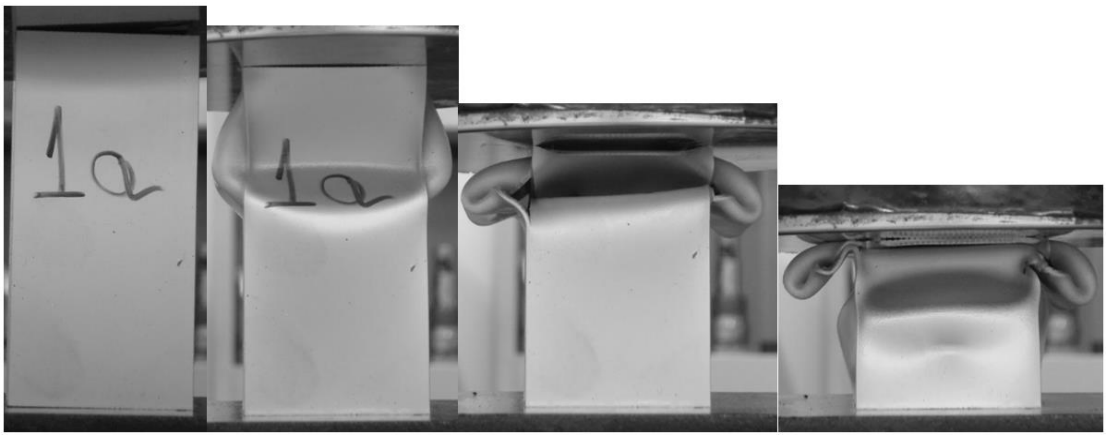


**Figure 48 Collapse states of test 1a**

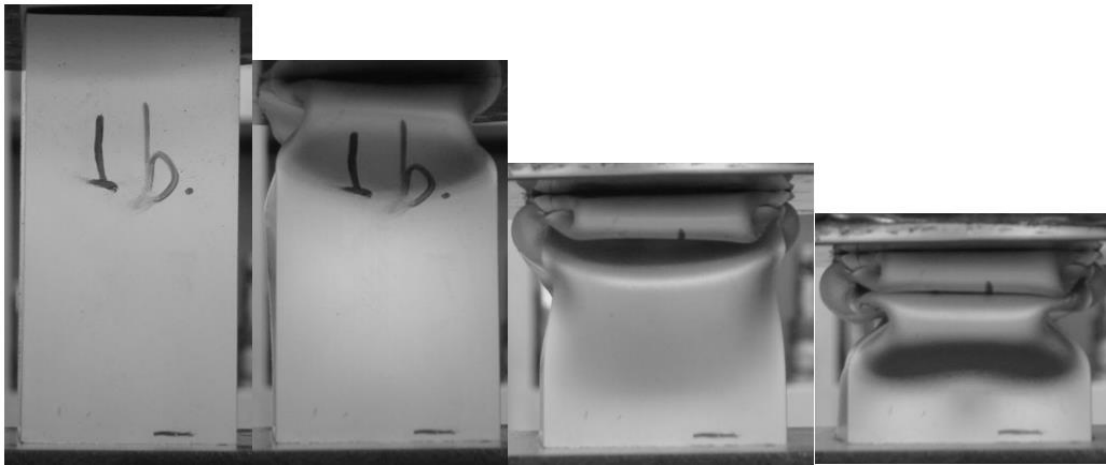


**Figure 49 Collapse states of test 1b**

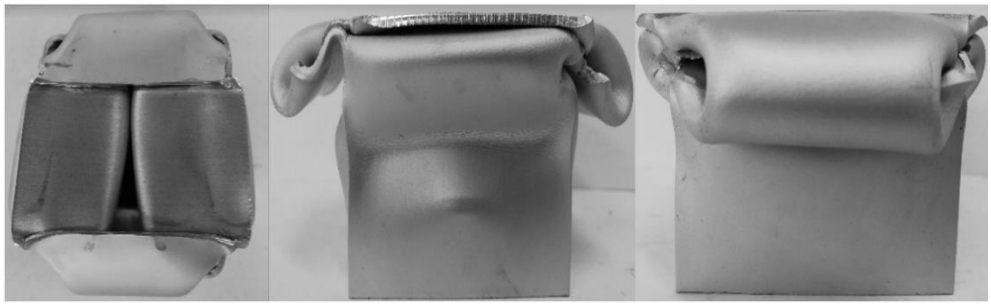

**Figure 50 Final views of crushed specimen in test 1a**

**Figure 51 Final views of crushed specimen in test 1b**

## 3.4.2 Oblique Loading under 5º angle – Test Cases 2a – 2b

### 3.4.2.1 Initial contact in edge

In current test cases, the behavior of aluminium tubes subjected to 5º oblique compressive loading is examined with the initial contact between impactor and tube being around tube top side edge. The recorded experimental data during the test revealed the force-displacement (F-x) and energy absorption-displacement (EA-x) curves for the examined specimens as depicted in Figure 52 and Figure 53 respectively. As presented following, the two experimental tests showed a sufficient agreement in PCF revealing it about 25.5 kN reflecting the collapse initiation through plastic deformation. During plastic collapse progress, both obliquely compressed specimens revealed a progressive and controllable collapse mode formulating inextensional folds, while a slight tearing around tube corners was observed in both tests without however significant magnitude. As a result, the two tests revealed great energy absorption capability keeping high enough MCF due to the stable progress of plastic collapse under folding mode which is depicted by the local peaks and lows in force distribution along post-buckling region of F-x curves depicted in Figure 53.

Moreover, the oblique loading reacted on lower PCF compared to axial compressive loading of tests 1a and 1b, as the lateral crushing force component introduced additional bending moments to the collapsed structure. Thus, the reach of plastic bending moment required lower axial longitudinal crushing force as part of the developed bending moment was undertaken by the additional moments introduced by lateral forces of oblique loading resulting so in lower PCF Facilitating the initiation of plastic deformation. Furthermore, the progressive collapse mode of obliquely compressed tubes allowed for greater MCF than the one of axial loading tests where more significant tearing was occurred, reacting thus in higher CFE in consequence.

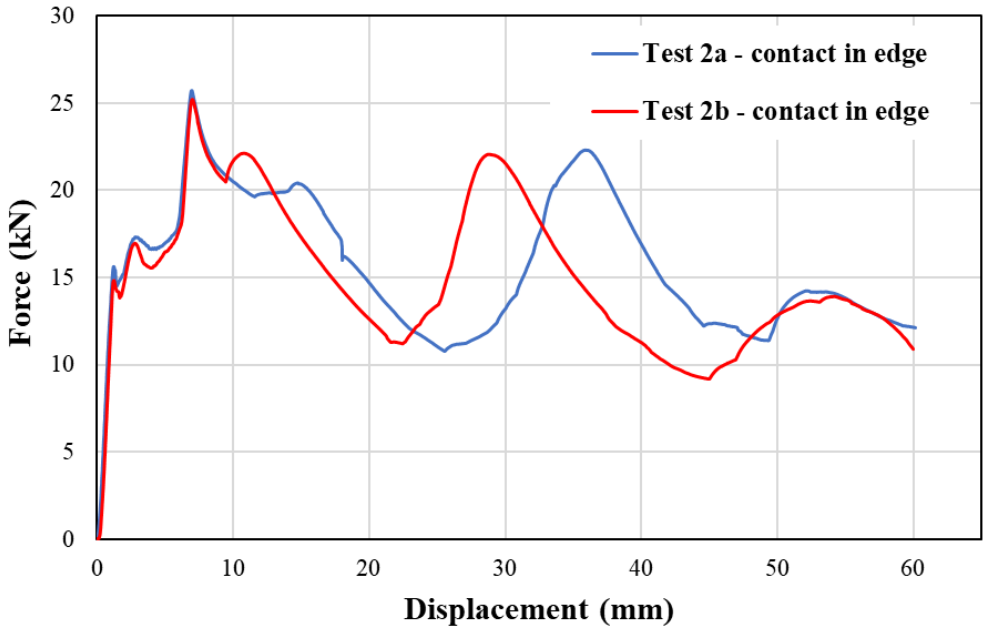


**Figure 52 Experimental F-x curves of 5º oblique loading tests under contact in edge**

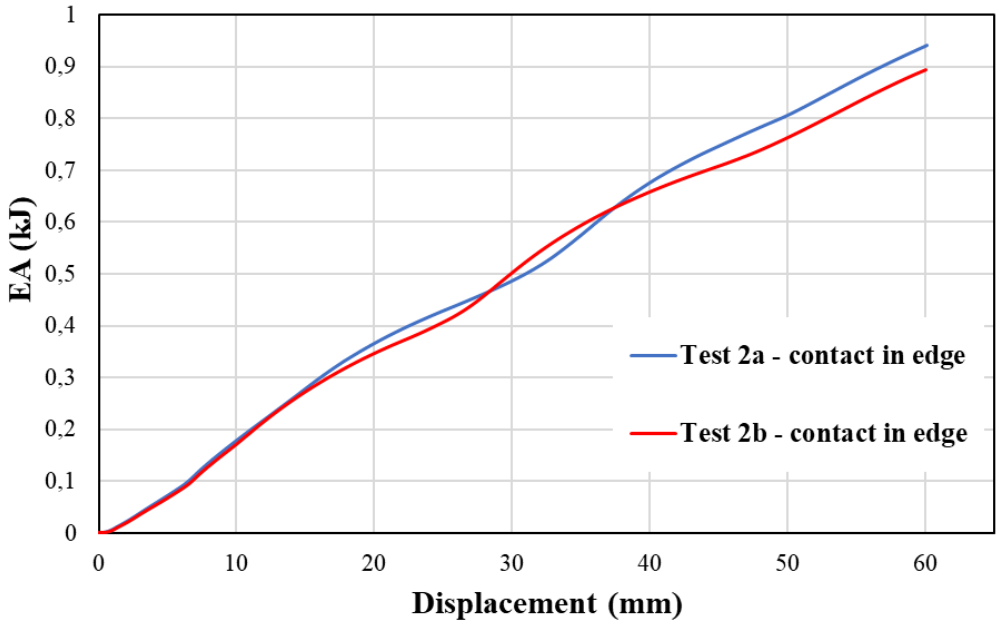


**Figure 53 Experimental EA-x curves of 5º oblique loading tests under contact in edge**

**Table 3 Crashworthiness response parameters for tests 2a-2b under contact in edge**

| | Test 2a - edge | Test 2b - edge | Deviation (%) |
|---|---|---|---|
| **PCF (kN)** | 25.75 | 25.21 | 2.1 |
| **MCF (kN)** | 15.68 | 14.90 | 4.9 |
| **EA (J)** | 942.1 | 894.2 | 5.1 |
| **SEA (kJ/kg)** | 19.98 | 18.97 | 5.1 |
| **CFE (-)** | 0.61 | 0.59 | 2.9 |

Regarding the provided errors between the two experiments, the two tests revealed a sufficient agreement in PCF showing a deviation about 2.1%, while also regarding the two tests captured sufficiently the force distribution during plastic collapse progress revealing an error about 5% in MCF and in consequence in the estimated energy absorption capacity.

Moreover, as depicted by the following figures regarding plastic collapse states and final views of crushed specimens, both tests revealed a progressive deformation mode formulating 3 inextensional folds as confirmed by the local force peaks in F-x curves. In addition, slight tearing was occurred around tube corners in both tests which however proved to be not of significant magnitude.

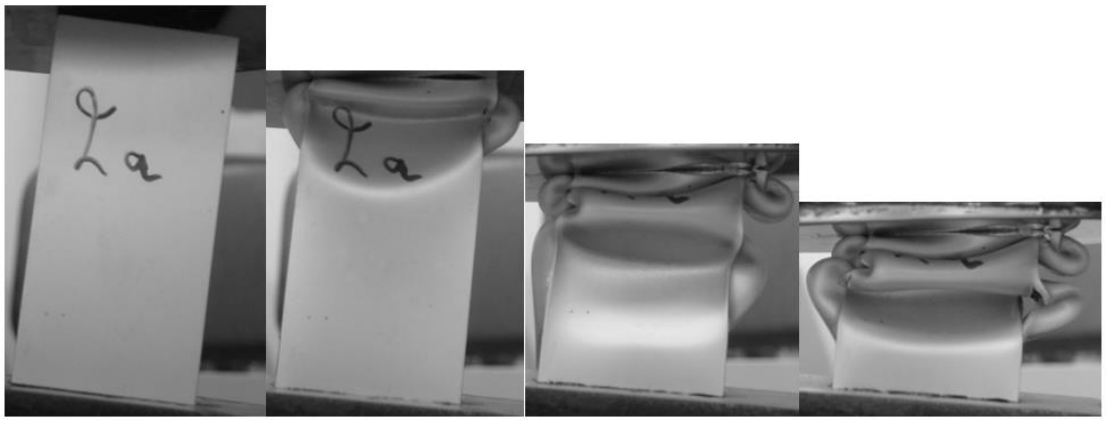

**Figure 54 Collapse states of test 2a under contact in edge**

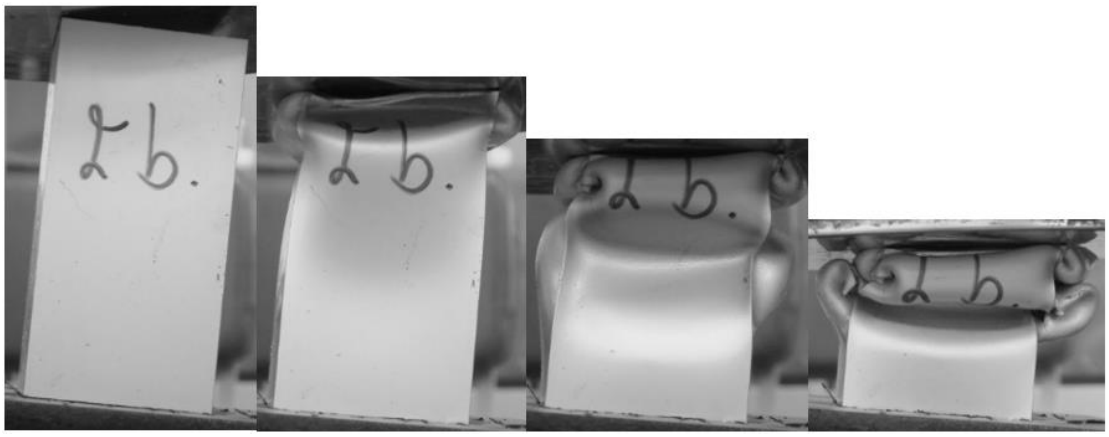


**Figure 55 Collapse states of test 2b under contact in edge**

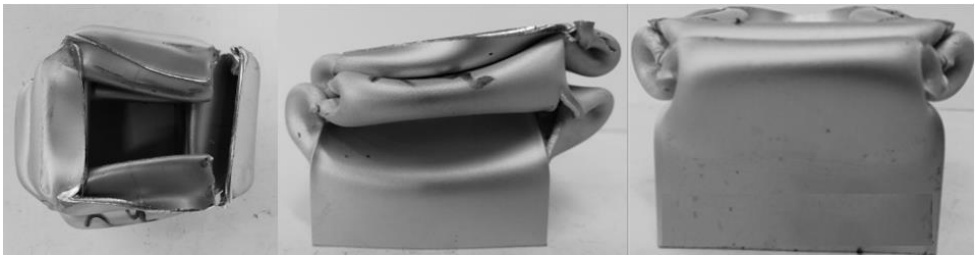

**Figure 56 Final views of crushed specimen in test 2a under contact in edge**

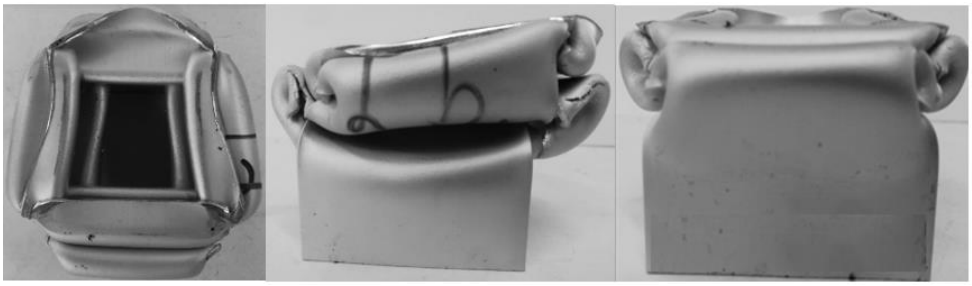

**Figure 57 Final views of crushed specimen in test 2b under contact in edge**

### 3.4.2.2 Initial contact in corner

In 5$^{o}$ oblique loading test with the initial contact between impactor and tube being around tube top corner, the recorded experimental data revealed the force-displacement (F-x) and energy absorption-displacement (EA-x) curves depicted in Figure 58 and Figure 59 respectively. As shown following, the two tests showed a sufficient agreement in PCF revealing it about 25.5 kN reflecting the plastic collapse initiation. During plastic collapse progress, both obliquely compressed specimens revealed a progressive and controllable collapse mode

formulating inextensional folds, while a slight tearing around tube corners was observed in both tests with a greater magnitude regarding the compressed specimen in test 2a. The two tests revealed high enough energy absorption capacity maintaining MCF around 17.5 kN by the formulation of plastic folds which reflect the local peaks and lows in force distribution. The above observation is also captured from the linear increase in EA as Figure 59 depicts, confirming the progressive behavior of the plastic deformation.

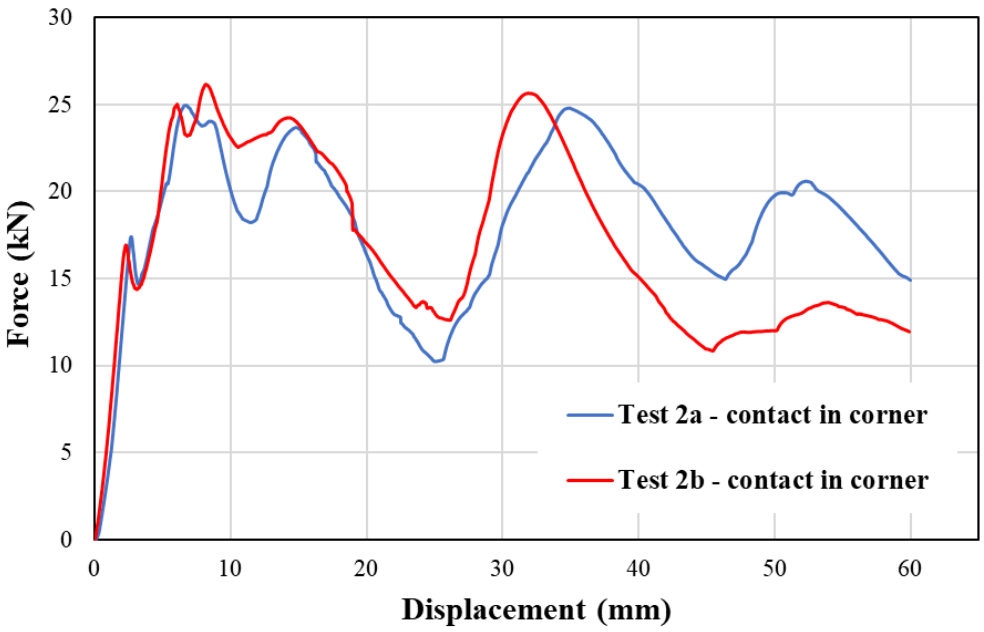


**Figure 58 Experimental F-x curves of 5º oblique loading tests under contact in corner**

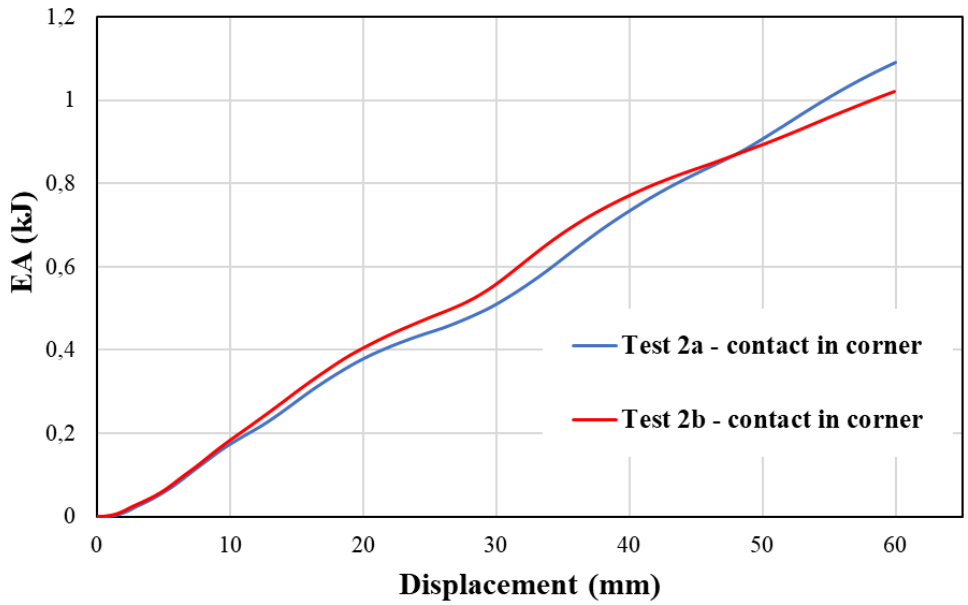


**Figure 59 Experimental EA-x curves of 5º oblique loading tests under contact in corner**

In addition, the oblique loading under an initial contact-in-corner between impactor and tubular specimen revealed a greater EA compared to the previous $5^o$ oblique loading test case under a contact-in-edge, as the contact-in-corner scenario provided greater additional bending moment due to oblique loading resulting in more effective folding deformation mode. In contrast, PCF was captured at the same magnitude like the contact-in-edge test case. Thus, CFE parameter proved to be increased when the initial contact between impactor and tube was taken place around tube top corner as greater MCF was allowed while PCF was maintained in the same level. Regarding the provided errors between the two experiments, the two tests revealed a sufficient agreement in PCF showing a deviation about 4.8%, while also regarding the two tests captured sufficiently the force distribution during plastic collapse progress revealing an error about 6.3% in EA estimation.

**Table 4 Crashworthiness response parameters for tests 2a-2b under contact in corner**

| | **Test 2a - corner** | **Test 2b - corner** | **Deviation (%)** |
|---|---|---|---|
| **PCF (kN)** | 24.95 | 26.14 | 4.8 |
| **MCF (kN)** | 18.17 | 17.06 | 6.1 |
| **EA (J)** | 1090.4 | 1021.9 | 6.3 |
| **SEA (kJ/kg)** | 23.13 | 21.68 | 6.3 |
| **CFE (-)** | 0.73 | 0.65 | 10.4 |

Regarding the observed deformation states, the following figures depict that both tests agreed on the occurred plastic collapse mechanism revealing a progressive deformation mode formulating 3 inextensional folds as confirmed by the local force peaks in F-x curves. Finally, significant tearing was occurred around tube corners of test 2a specimen, while in contrast the tearing of test 2b specimen was less obvious as it was captured in significantly lower extent.

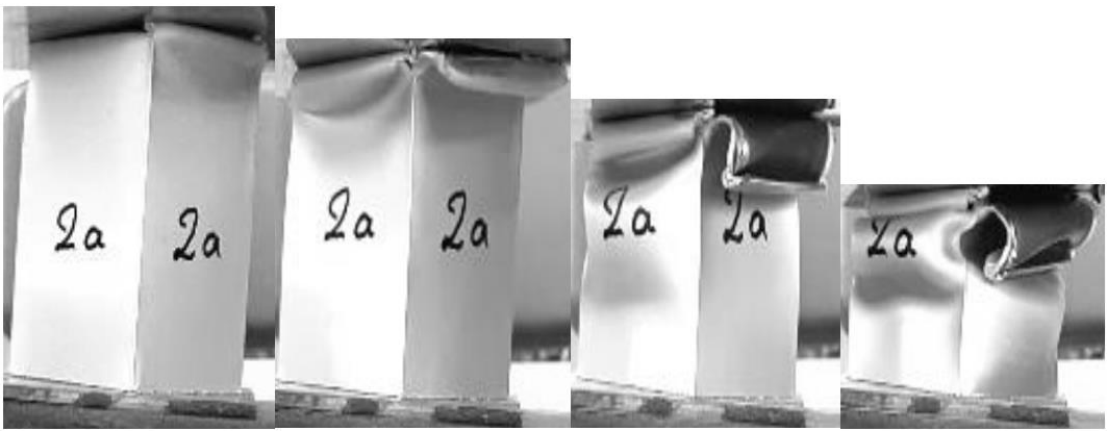


**Figure 60 Collapse states of test 2a under contact in corner**


**Figure 61 Collapse states of test 2b under contact in corner**

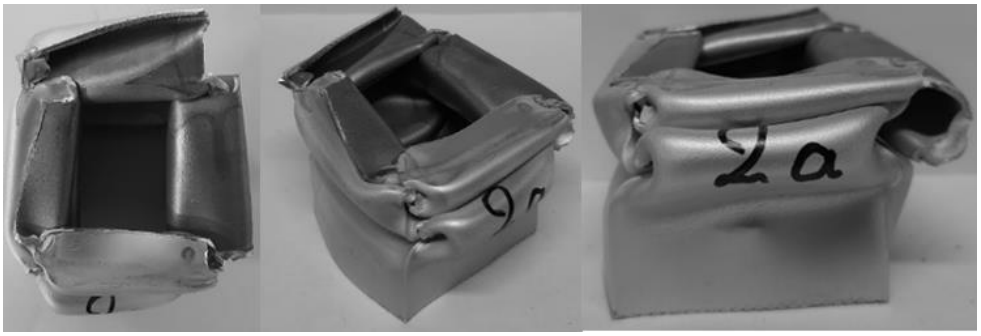


**Figure 62 Final views of crushed specimen in test 2a under contact in corner**


**Figure 63 Final views of crushed specimen in test 2b under contact in corner**

### 3.4.3 Oblique Loading under 10º angle – Test Cases 3a – 3b

#### 3.4.3.1 Initial contact in edge

Loading case 3 examines the behavior of aluminium tubes subjected to 10º oblique compressive loading. Current subsection studies the response of 10º obliquely compressed tubes with an initial contact to the impactor around their top side edge. The recorded experimental data during the test revealed the force-displacement (F-x) and energy absorption-displacement (EA-x) curves for the examined specimens as depicted in Figure 64 and Figure 65 respectively. The two experimental tests showed a sufficient agreement in PCF revealing it about 23 kN reflecting the collapse initiation through plastic deformation. During plastic collapse progress, both obliquely compressed specimens revealed a progressive collapse mode formulating inextensional folds, while tearing was further observed around tube corners in both tests during the final stages of collapse without however being capable of changing the energy absorption characteristics of the crushed specimens. Tests 3a-3b revealed the lower levels in energy absorption capability and PCF among the previously presented test cases of axial and 5º oblique loading, mainly due to the increased loading angle which reacts in additional bending moments and due to the stronger magnitude of corner tearing observed in the collapsed specimens at about 35 mm of impactor displacement above from which EA increase rate with displacement reveals a slight drop as Figure 65 depicts.

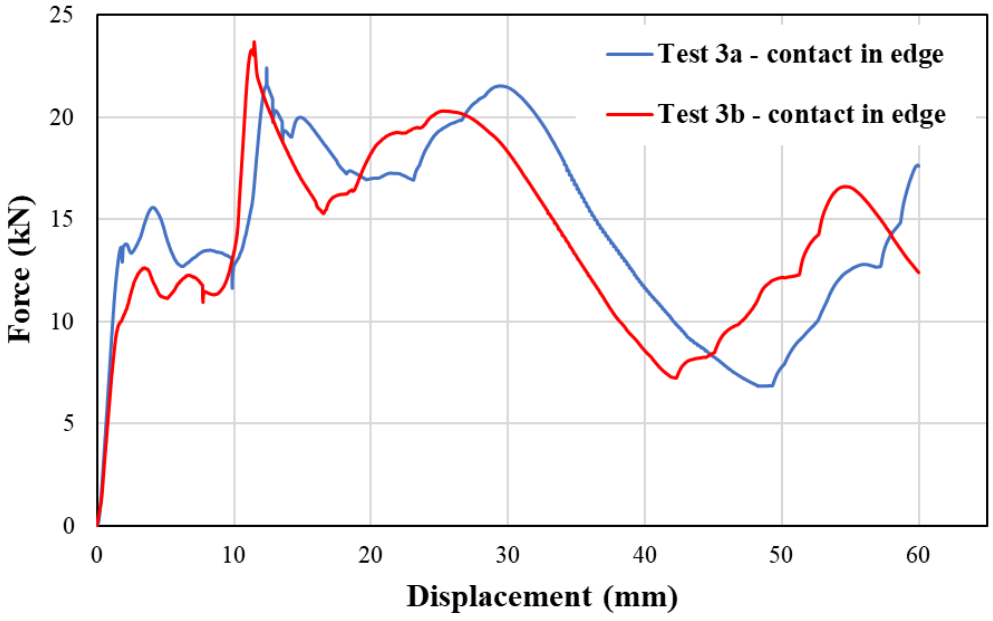


**Figure 64 Experimental F-x curves of 10º oblique loading tests under contact in edge**

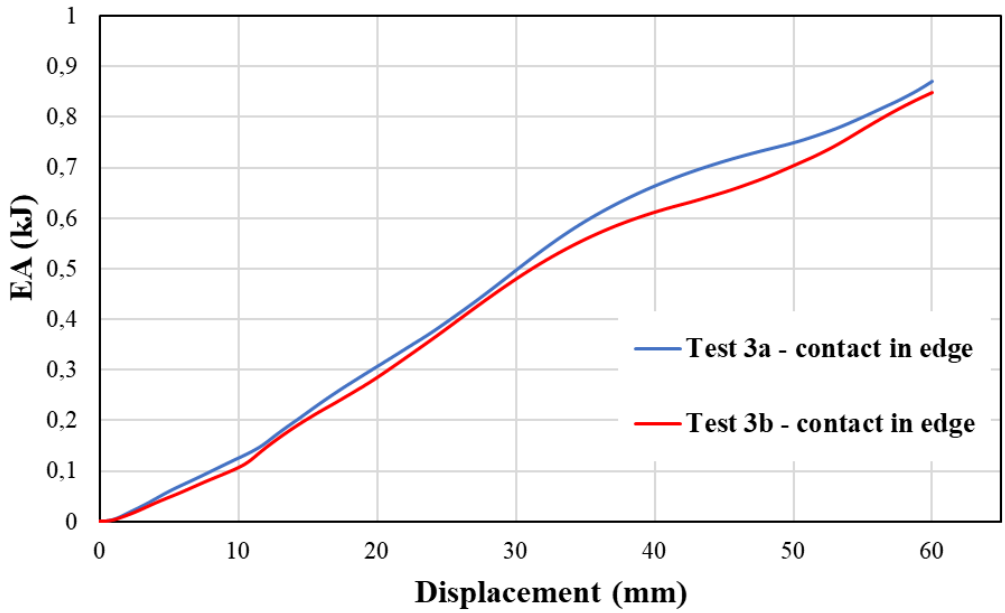


**Figure 65 Experimental EA-x curves of 10º oblique loading tests under contact in edge**

**Table 5 Crashworthiness response parameters for tests 3a-3b under contact in edge**

| | Test 3a - edge | Test 3b - edge | Deviation (%) |
|---|---|---|---|
| **PCF (kN)** | 22.40 | 23.65 | 5.6 |
| **MCF (kN)** | 14.53 | 14.15 | 2.6 |
| **EA (J)** | 871.6 | 849.0 | 2.6 |
| **SEA (kJ/kg)** | 18.49 | 18.01 | 2.6 |
| **CFE (-)** | 0.65 | 0.60 | 7.8 |

Regarding the provided errors between the two experiments, the two tests revealed a sufficient agreement in PCF showing a deviation about 5.6%, while also the two tests captured sufficiently the force distribution during plastic collapse progress revealing an error about 2.6% in MCF and in consequence in the estimated energy absorption capacity of the obliquely crushed tubes. Moreover, as depicted by the following figures regarding the plastic collapse states and the final views of crushed specimens, both tests revealed a progressive deformation mode formulating 3 inextensional folds as confirmed by the local force peaks in F-x curves. In addition, tube corners tearing was occurred in both tests at about 35 mm of impactor displacement which however did not seem to affect significantly the energy absorption characteristics.

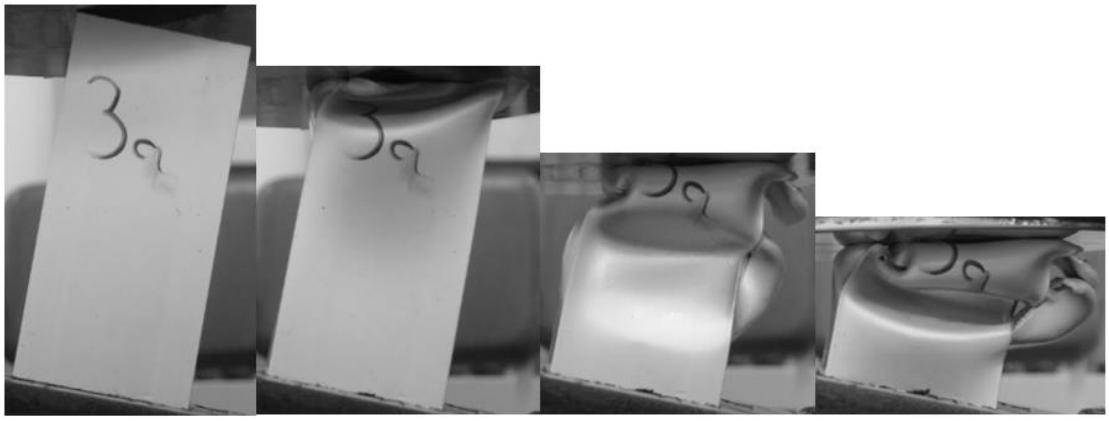


**Figure 66 Collapse states of test 3a under contact in edge**

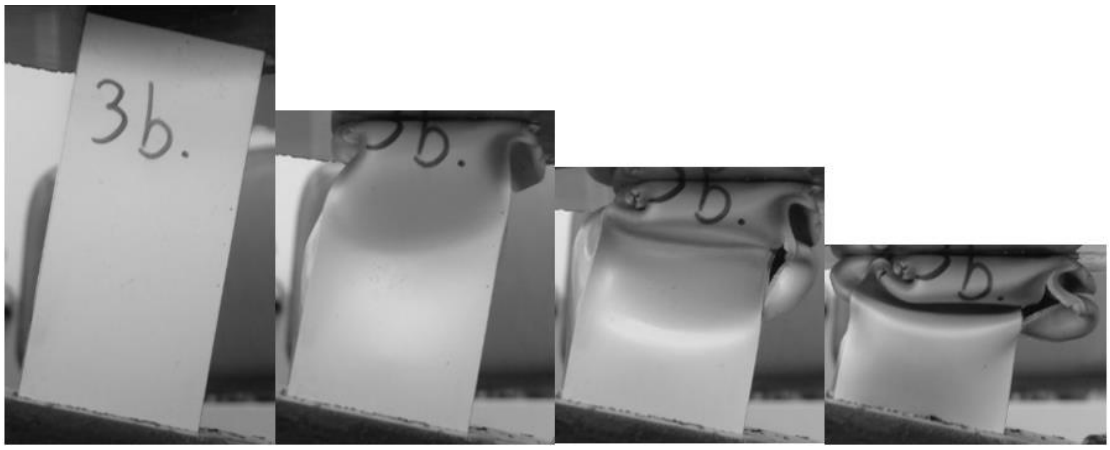


**Figure 67 Collapse states of test 3b under contact in edge**

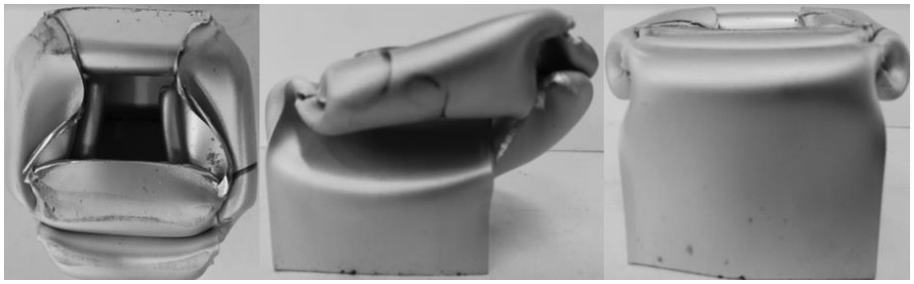

**Figure 68 Final views of crushed specimen in test 3a under contact in edge**

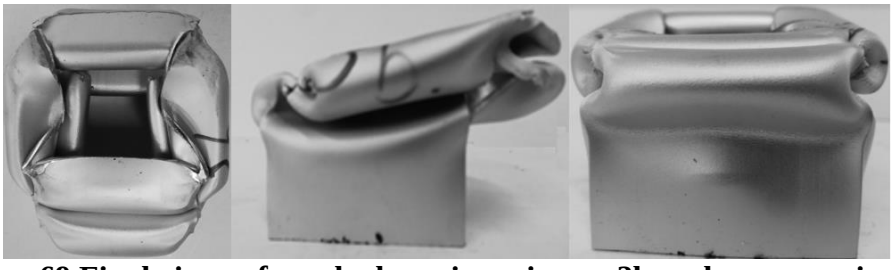

**Figure 69 Final views of crushed specimen in test 3b under contact in edge**

### 3.4.3.2 Initial contact in corner

Current subsection studies the response of 10º obliquely compressed tubes with an initial contact to the impactor around their top corner. The recorded experimental data during the test revealed the force-displacement (F-x) and energy absorption-displacement (EA-x) curves for the examined specimens as depicted in Figure 70 and Figure 71 respectively. The two experimental tests show a sufficient agreement in PCF revealing it about 25 kN reflecting the collapse initiation through plastic deformation. During plastic collapse progress, both obliquely compressed specimens revealed a progressive collapse mode formulating inextensional folds, while tearing was further observed around tube corners in both tests during the final stages of collapse without however being capable of changing the energy absorption characteristics of the crushed specimens.

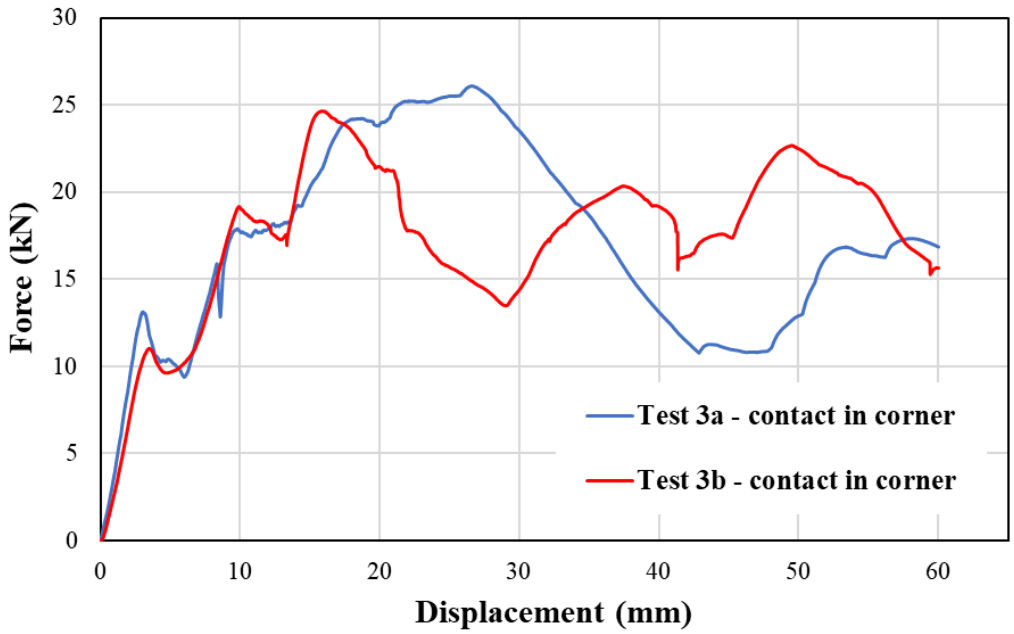


**Figure 70 Experimental F-x curves of 10º oblique loading tests under contact in corner**

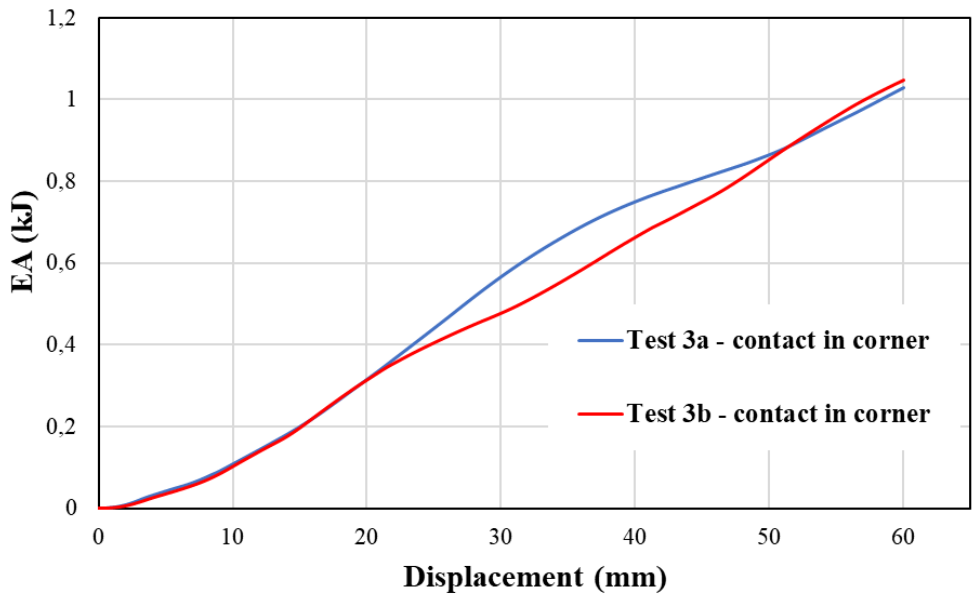


**Figure 71 Experimental EA-x curves of 10º oblique loading tests under contact in corner**

**Table 6 Crashworthiness response parameters for tests 3a-3b under contact in corner**

| | Test 3a - corner | Test 3b - corner | Deviation (%) |
|---|---|---|---|
| **PCF (kN)** | 26.11 | 24.62 | 6.0 |
| **MCF (kN)** | 17.16 | 17.45 | 1.7 |
| **EA (J)** | 1029.8 | 1047.3 | 1.7 |
| **SEA (kJ/kg)** | 21.84 | 22.22 | 1.7 |
| **CFE (-)** | 0.66 | 0.71 | 7.3 |

Regarding the provided errors between the two experiments, the two tests revealed a sufficient agreement in PCF and MCF showing deviations of 6% and 1.7% respectively. Moreover, as depicted by the following figures regarding the plastic collapse states and the final views of crushed specimens, both tests revealed a progressive deformation mode formulating plastic inextensional folds. However, test 3a revealed the formulation of 2 inextensional folds, while in test 3b the collapsed specimen deformed under 3 inextensional folds as confirmed by the local force peaks in F-x curves. For this reason, test 3b provided a greater energy absorption capacity as the compressed tube collapsed under a more progressive and efficient mode formulating more folds and so dissipating larger amount of deformation energy. Finally, tube corners tearing was occurred in both which however did not seem to affect significantly the energy absorption characteristics of the crushed tubes.


**Figure 72 Collapse states of test 3a under contact in corner**


**Figure 73 Collapse states of test 3b under contact in corner**

**Figure 74 Final views of crushed specimen in test 3a under contact in corner**

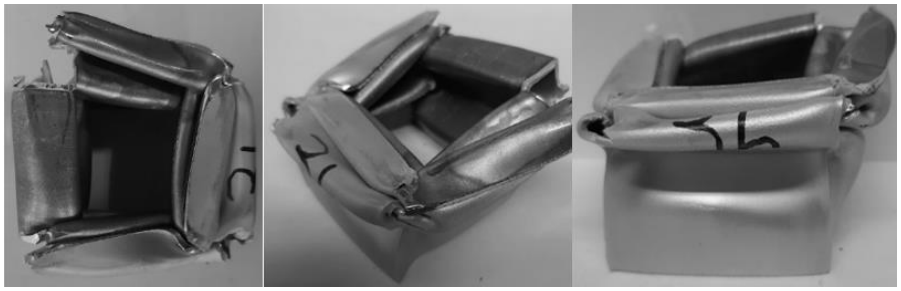

**Figure 75 Final views of crushed specimen in test 3b under contact in corner**

## 3.4.4 Oblique Loading under 15º angle – Test Cases 4a – 4b

### 3.4.4.1 Initial contact in edge

Loading case 4 examines the behavior of aluminium tubes subjected to 15º oblique compressive loading. Current subsection studies the response of 15º obliquely compressed tubes with an initial contact to the impactor around their top side edge. The recorded experimental data during the test revealed the force-displacement (F-x) and energy absorption-displacement (EA-x) curves for the examined specimens as depicted in Figure 76 and Figure 77 respectively.

The two experimental tests showed a sufficient agreement in PCF revealing it about 20.4 kN reflecting the collapse initiation through plastic deformation. During plastic collapse progress, both obliquely compressed specimens revealed a progressive collapse mode formulating inextensional folds, while further tearing was also observed around tube corners in both tests during the final stages of collapse without however affecting strongly the force distribution during plastic collapse and in consequence the energy absorption characteristics of the crushed specimens. Tests 4a-4b with initial contact-in-edge revealed the lower levels in energy absorption capability and PCF among all previously presented test cases of axial and oblique loading, mainly due to the greatest loading angle which reacts in additional bending moments which facilitating the plastic collapse initiation and progress, but also in addition due to the strong magnitude of corner tearing observed in the collapsed specimens which weakened even more the resistance of the compressed structure against its further shortening. Regarding the provided errors between the two experiments, the two tests revealed a PCF error of 6.6%, while also the two tests captured sufficiently the force distribution during plastic collapse progress revealing an error about 1% in MCF and in consequence in the estimated energy absorption capacity of the obliquely crushed tubes.

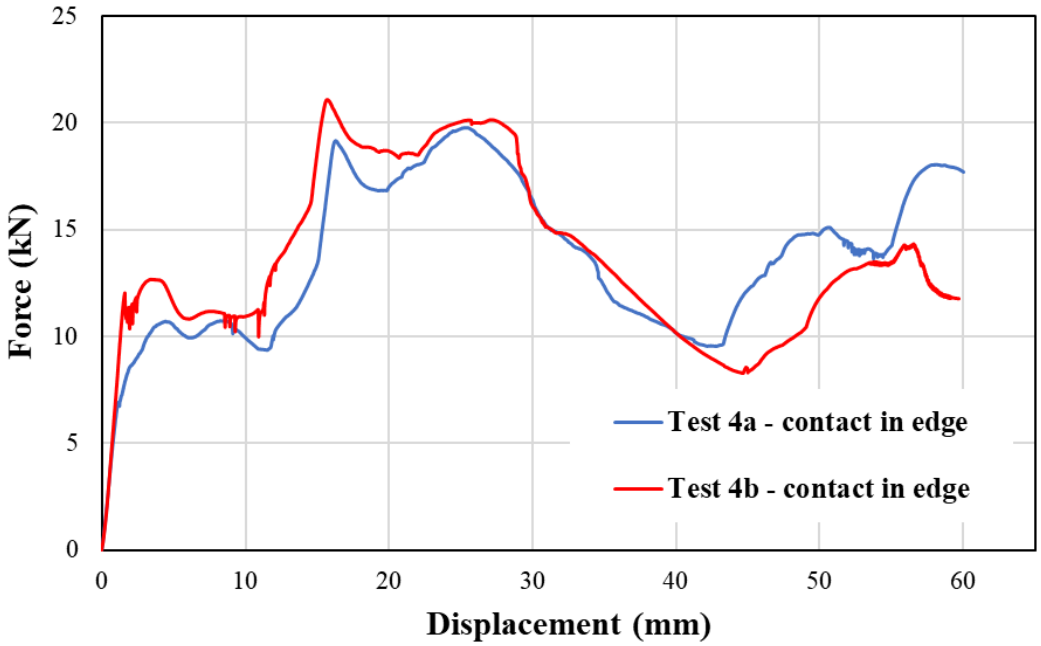


**Figure 76 Experimental F-x curves of 15º oblique loading tests under contact in edge**

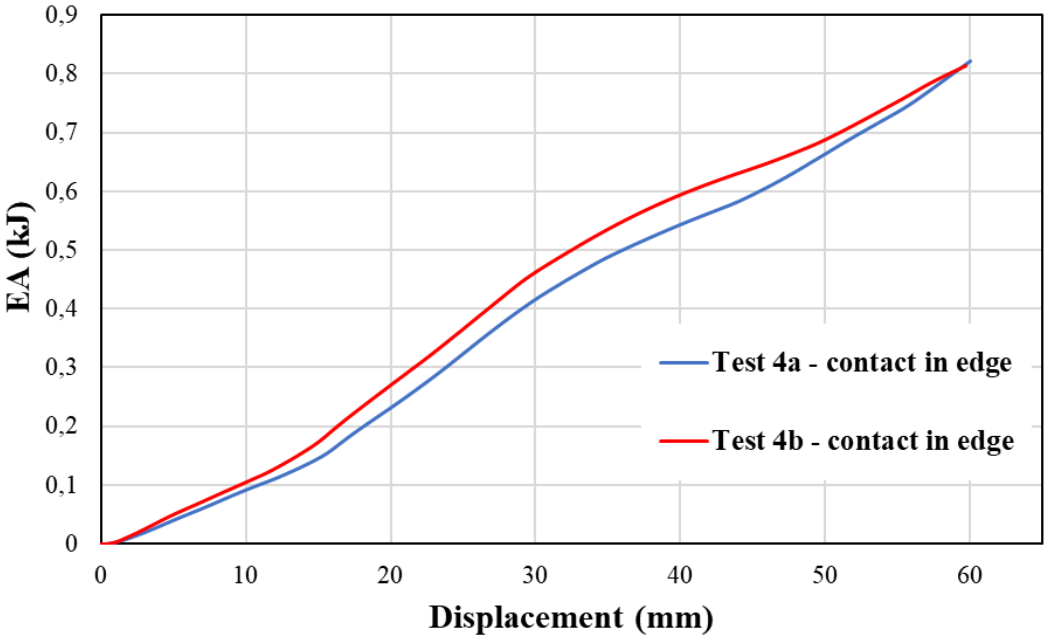


**Figure 77 Experimental EA-x curves of 15º oblique loading tests under contact in edge**

**Table 7 Crashworthiness response parameters for tests 4a-4b under contact in edge**

| | Test 4a - edge | Test 4b - edge | Deviation (%) |
|---|---|---|---|
| **PCF (kN)** | 19.76 | 21.07 | 6.6 |
| **MCF (kN)** | 13.71 | 13.58 | 1.0 |
| **EA (J)** | 822.8 | 814.8 | 1.0 |
| **SEA (kJ/kg)** | 17.45 | 17.28 | 1.0 |
| **CFE (-)** | 0.69 | 0.65 | 7.1 |

Moreover, as depicted by the following figures regarding the plastic collapse states and the final views of crushed specimens, both tests revealed a progressive deformation mode formulating 2 inextensional folds as confirmed by the local force peaks in F-x curves. Finally, tube corners tearing was occurred in both tests which weakened structure resistance against its further shortening dropping so the energy absorption capacity of the examined specimens.

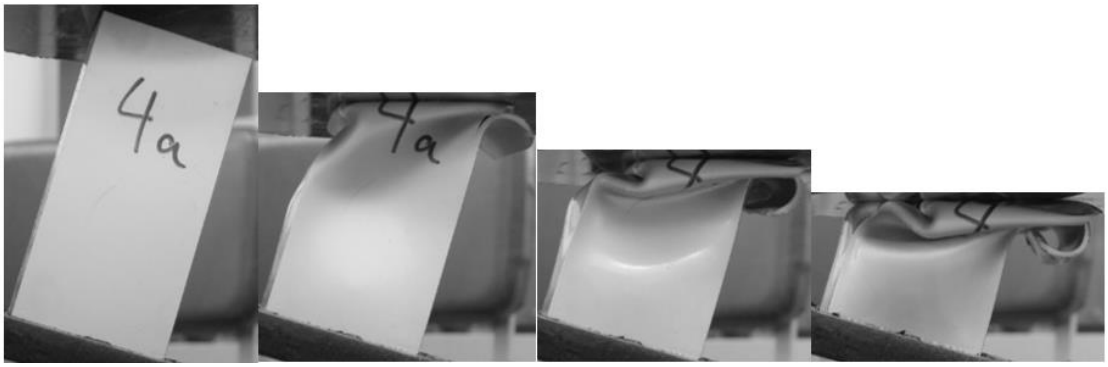


**Figure 78 Collapse states of test 4a under contact in edge**

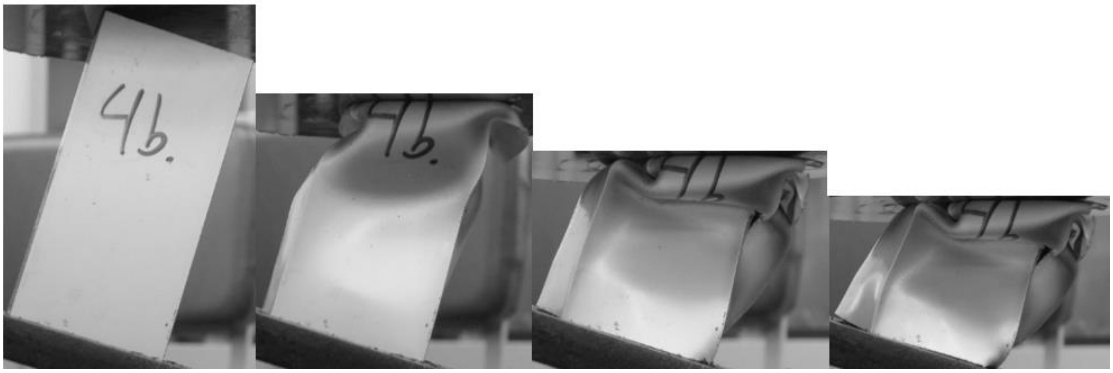


**Figure 79 Collapse states of test 4b under contact in edge**

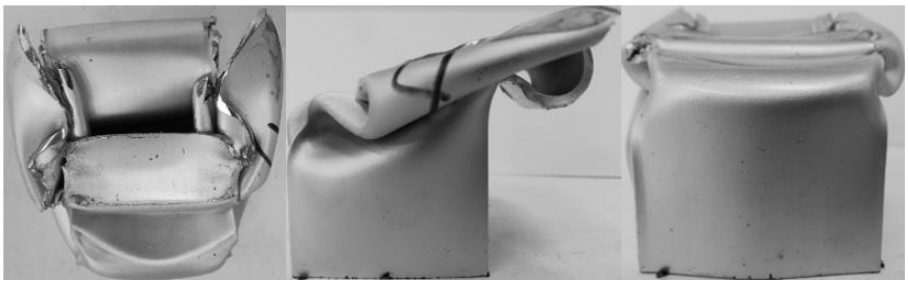

**Figure 80 Final views of crushed specimen in test 4a under contact in edge**

**Figure 81 Final views of crushed specimen in test 4b under contact in edge**

### 3.4.4.2 Initial contact in corner

Current subsection studies the response of 15$^{o}$ obliquely compressed tubes with an initial contact to the impactor around their top corner. The recorded experimental data during the test revealed the force-displacement (F-x) and energy absorption-displacement (EA-x) curves for the examined specimens as depicted in Figure 82 and Figure 83 respectively.

The two experimental tests showed a sufficient agreement in PCF revealing it about 24.2 kN reflecting the collapse initiation through plastic deformation. During plastic collapse progress, both obliquely compressed specimens revealed a progressive collapse mode formulating inextensional folds, while further tearing was also observed around tube corners. Tests 4a-4b with initial contact-in-corner revealed the lower levels in energy absorption capability and PCF among all previously presented oblique loading test cases with contact-in-corner. However, both EA and PCF in oblique loading tests maintained greater in the case of contact-in-corner than the ones of contact-in-edge type. In addition, regarding the oblique loading experimental results under contact-in-corner type, PCF and EA revealed a decrease with the loading angle increase mainly due to the additional bending moments introduced by lateral force components which facilitating the plastic collapse initiation and progress. Regarding the provided errors between the two experiments, both plastic collapse initiation and progress were predicted sufficiently from the two tests which captured the force distribution providing deviations in PCF and EA of 0.1% and 1.4% respectively.

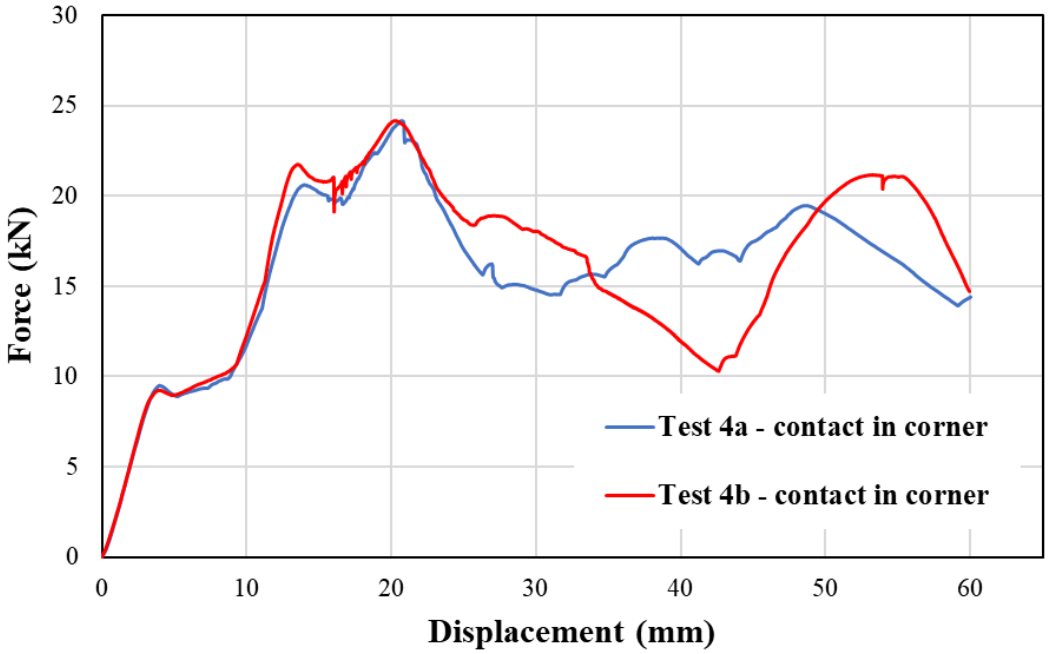


**Figure 82 Experimental F-x curves of 15º oblique loading tests under contact in corner**

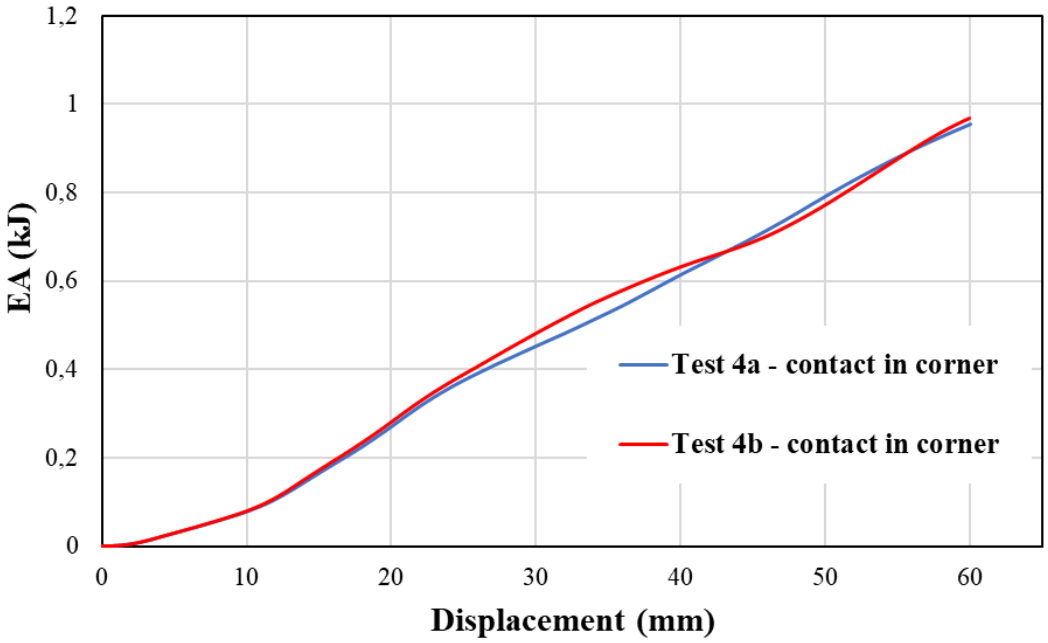


**Figure 83 Experimental EA-x curves of 15º oblique loading tests under contact in corner**

**Table 8 Crashworthiness response parameters for tests 4a-4b under contact in corner**

| | Test 4a - corner | Test 4b - corner | Deviation (%) |
|---|---|---|---|
| **PCF (kN)** | 24.17 | 24.20 | 0.1 |
| **MCF (kN)** | 15.93 | 16.16 | 1.4 |
| **EA (J)** | 955.7 | 968.8 | 1.4 |
| **SEA (kJ/kg)** | 20.27 | 20.55 | 1.4 |
| **CFE (-)** | 0.66 | 0.67 | 1.3 |

Moreover, as depicted by the following figures regarding the plastic collapse states and the final views of crushed specimens, both tests revealed a progressive deformation mode formulating 2 inextensional folds as confirmed by the local force peaks in F-x curves. Finally, tube corners tearing was occurred in both tests which weakened structure resistance against its further shortening dropping so the energy absorption capacity of the examined specimens.


**Figure 84 Collapse states of test 4a under contact in corner**

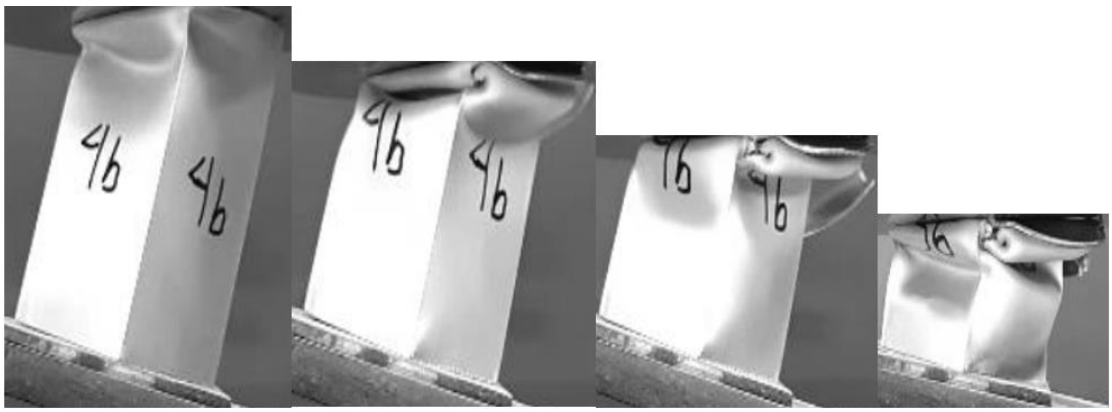


**Figure 85 Collapse states of test 4b under contact in corner**

**Figure 86 Final views of crushed specimen in test 4a under contact in corner**

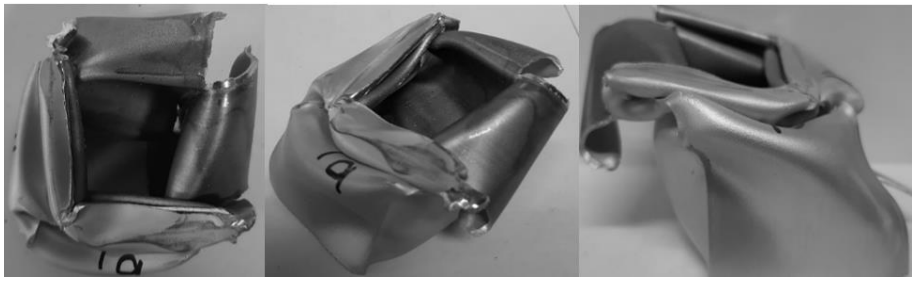

**Figure 87 Final views of crushed specimen in test 4b under contact in corner**

## 3.5 Conclusions

By summarizing the provided experimental results, critical conclusions can be extracted for the crashworthiness response of the examined square tubes subjected to axial and oblique loading regarding the loading angle effect and the effect of initial contact type between impactor and tube. The experimental data analysis carried out for each test case consisted of the provided force-displacement curve and the estimated crashworthiness response parameters, while also the occurred collapse mechanism was further observed by capturing different states of collapse and examining the final crushed structure views. Both stages of the experimental analysis aim to assess the crashworthiness performance of the tested specimens under the specific loading conditions in order to finally evaluate their efficiency under each examined crushing condition and offer the experimental results for the numerical models' validation procedure. The comparison between the tested cases for the final evaluation took into consideration mainly the amount of specific absorbed energy as the most significant parameter because it offers results corrected to specimen geometry, mass or material, and therefore is treated as the most appropriate metric for the final evaluation of the crashworthiness response.

Therefore, summarizing the presented results of previous subsections of current chapter, regarding the occurred collapse mechanism, all specimens deformed formulating inextensional folds while further local tearing was observed around tube corners with the two conducted tests to agree on the occurred collapse mode in each case. In more specific, the specimens subjected

to axial and 5º oblique loading deformed formulating 3 inextensional plastic folds, while the obliquely compressed specimens under 15º angle developed 2 inextensional folds. In the case of 10º oblique loading, the specimen loaded under contact-in-edge formulated 3 inextensional folds, while the case of contact-in-corner the two tests differed revealing 2 (test a) and 3 (test b) folds between each other. Finally, all tested tubes developed tearing around their corners during their plastic collapse. Regarding the revealed crashworthiness response indicators, the two tests revealed a sufficient agreement in both PCF and EA estimation revealing errors below 6.5% in PCF and 7.5% in EA as depicted in Figure 89 and Figure 90.

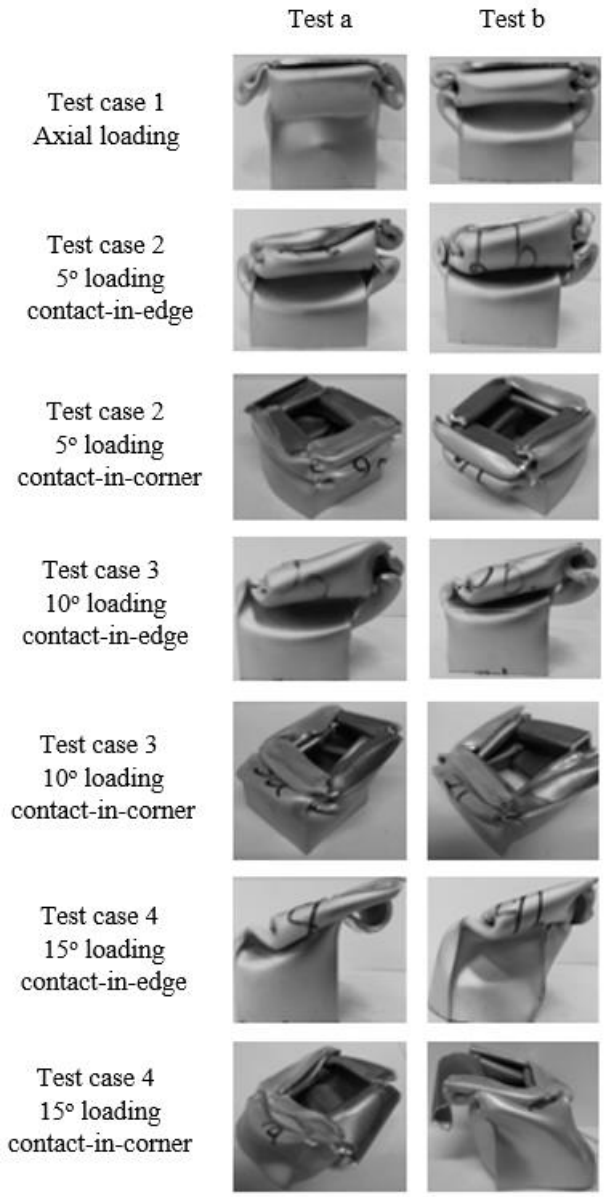


**Figure 88 Final views of crushed tubes**

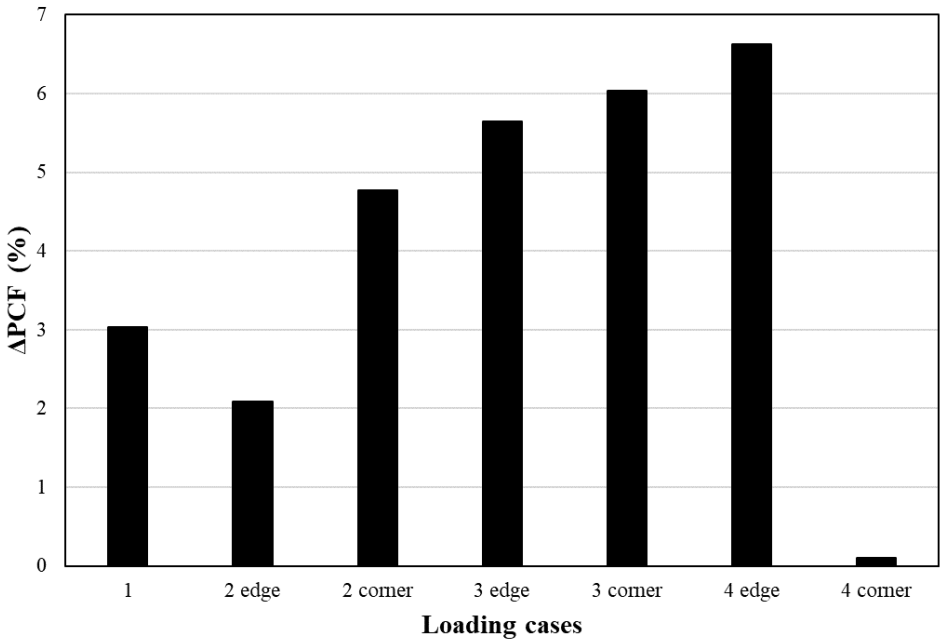


**Figure 89 PCF deviation between experimental tests**

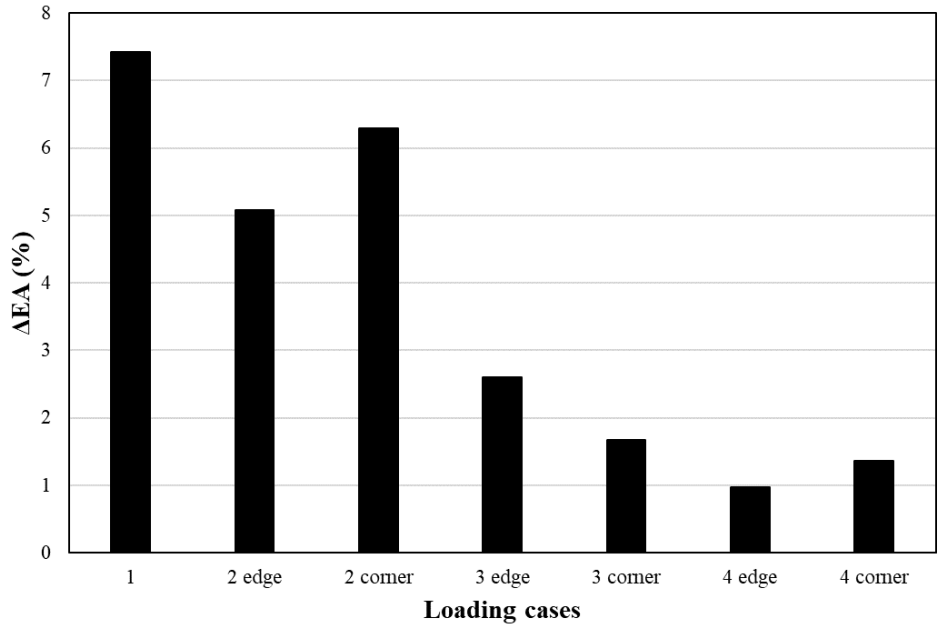


**Figure 90 EA deviation between experimental tests**

Regarding the crashworthiness performance in the examined loading test cases, PCF proved to decrease at higher loading angles which is paid on the additional bending moment introduced by the lateral force component facilitating thus the plastic collapse initiation. In addition, the obliquely loaded tubes under an initial contact-in-corner with the impactor revealed greater PCF compared to the ones with an initial contact-in-edge at all the examined range of

loading angle. In fact, PCF of the obliquely crushed tubes with an initial contact-in-corner with the impactor seem to not vary significantly enough with the loading angle increase, in contrast to the obliquely collapsed tubes with an initial contact-in-edge with the impactor in which PCF decrease proved to be more obvious. Furthermore, axial loading conditions revealed the greatest PCF due to the absence of additional bending moment caused by the oblique loading.

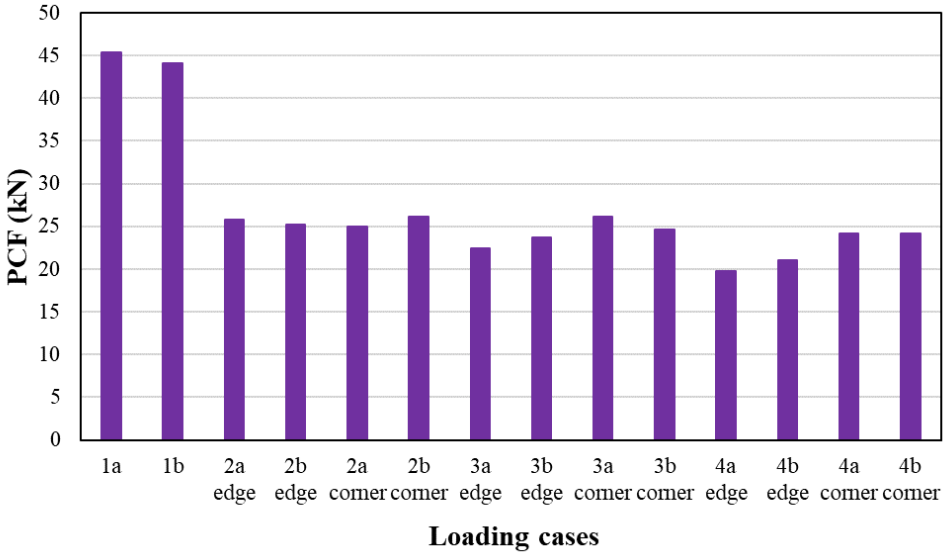


**Figure 91 PCF experimental results**

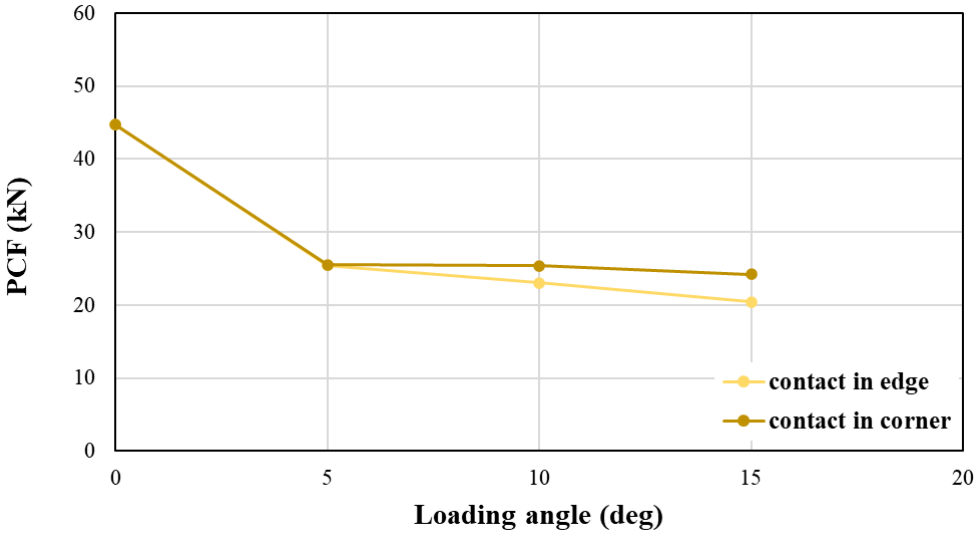


**Figure 92 PCF variation with loading angle and type of initial contact**

Regarding the energy absorption capacity under the examined loading cases, MCF, EA and SEA are treated as the proper indicators in order to evaluate the crashworthiness performance of the tested tubes. The above response parameters

reveal the same tendency with respect to the loading angle and the initial type of contact as they are proportional metrics capturing thus similarly the tendency variations of the energy absorption capability. As depicted in the following figures, the maximum energy absorption capacity is revealed by the 5º oblique loading case while as the loading angles getting higher EA and SEA show a decrease. Axially loaded tubes did not reveal the greatest EA as expected due to the significantly more intense tearing which was observed compared to 5º obliquely loaded tubes where the occurred tearing was of quite lower magnitude. Thus, without considering the tearing effect, the net loading angle effect reacts on an energy absorption decrease as the loading angle gets higher, affecting similarly SEA. In addition, energy absorption capacity seems to be greater in the case of initial contact-in-corner between impactor and tube for all the examined loading angle range revealing greater EA and SEA levels as depicted in Figure 95 and Figure 96.

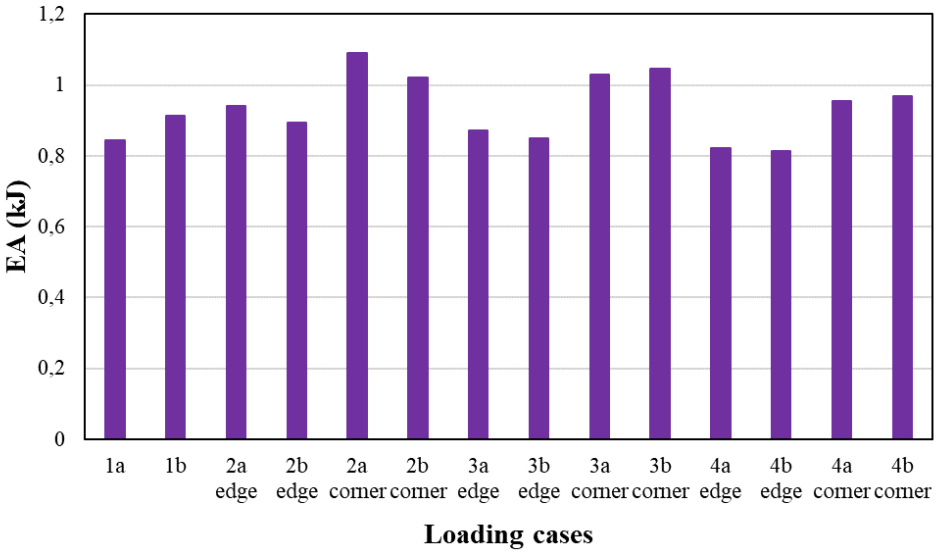


**Figure 93 EA experimental results**

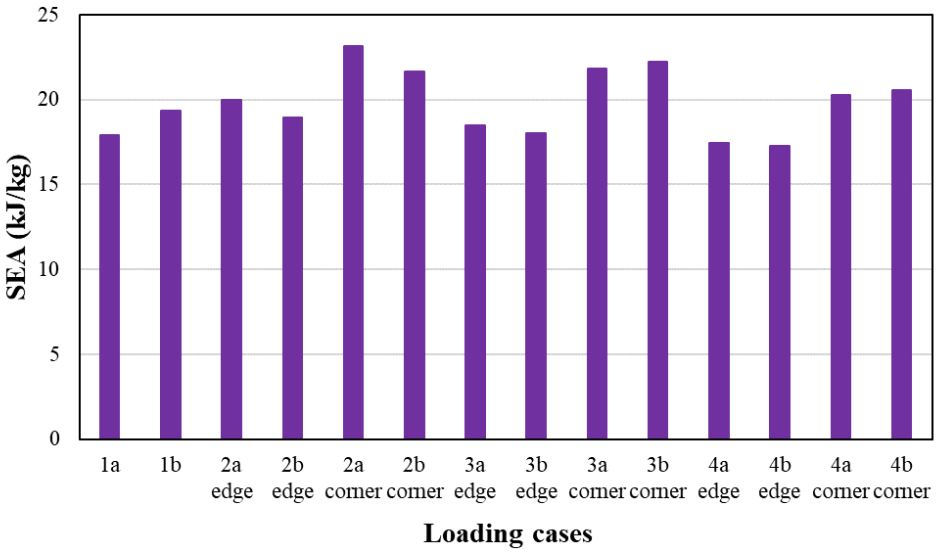


**Figure 94 SEA experimental results**

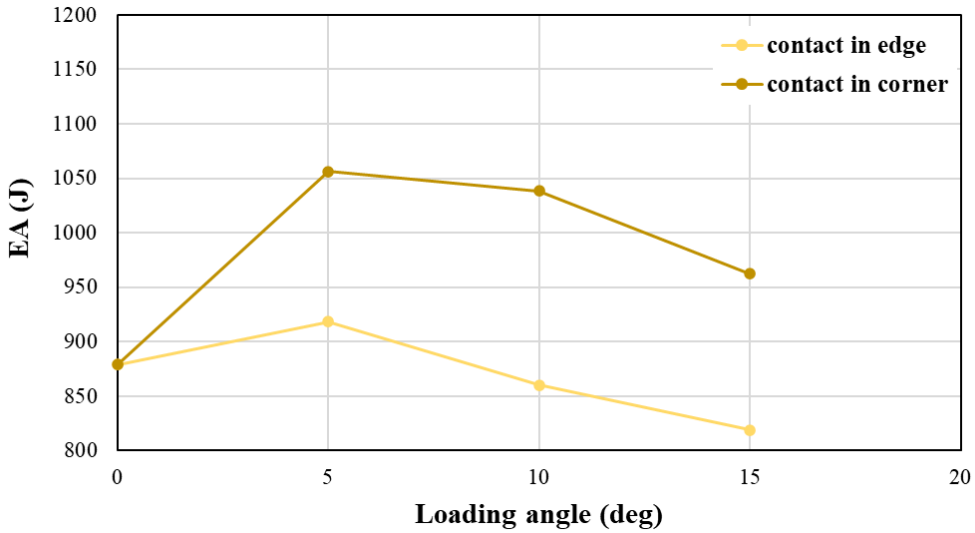


**Figure 95 EA variation with loading angle and type of initial contact**

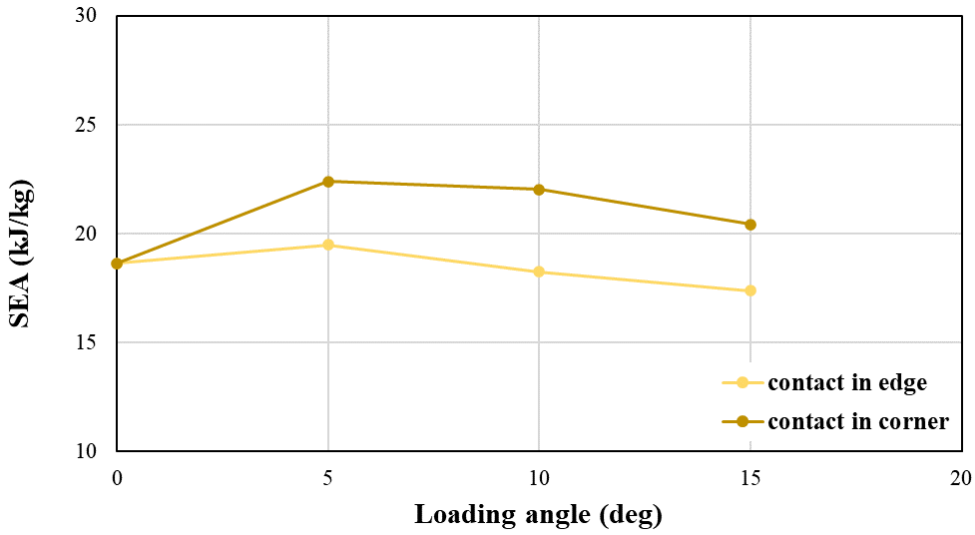


**Figure 96 SEA variation with loading angle and type of initial contact**

Finally, CFE is captured at higher levels in the case of oblique loading cases than axial loading as PCF is significantly higher at axial loading and MCF shows a slight reduction at higher angles resulting thus in greater CFE values. The importance of high enough CFE parameter reflects a sufficient energy absorption capacity under reasonable low PCF and so characterizes crashworthy structures facilitating their plastic collapse initiation and providing them with great enough energy absorption. Also, CFE is captured at higher levels in the case of initial contact-in-corner between impactor and tube where however a CFE decrease is revealed with respect to the loading angle in contrast to the contact-in-edge type where shows a slight increase.

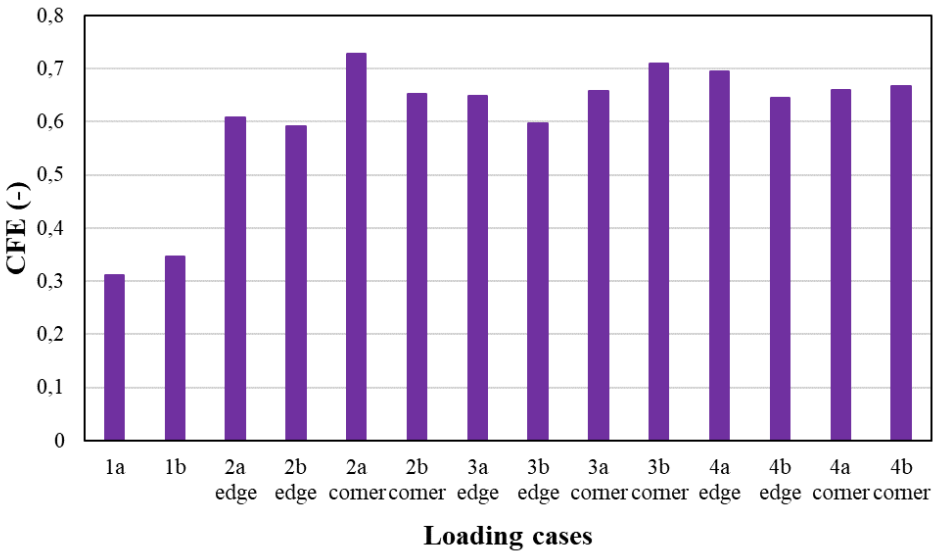


**Figure 97 CFE experimental results**

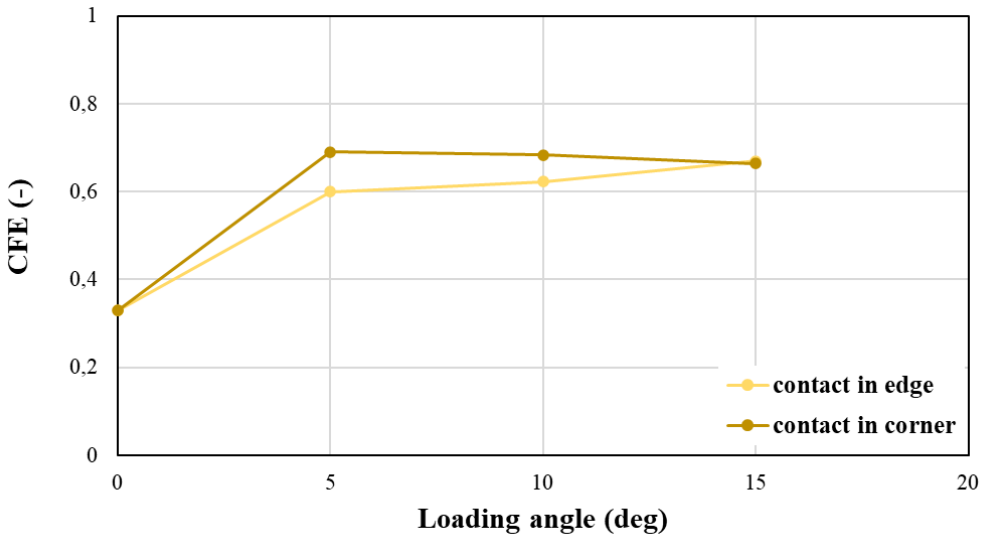


**Figure 98 CFE variation with loading angle and type of initial contact**

# 4. Finite Element Modelling and Simulation Results

## 4.1 Introduction

The aim of this study is to investigate crashworthiness behavior of square thin-walled aluminium tubes by both conducting experimental tests and numerical simulations. The development of appropriate finite element models in software offers the capability to obtain the crashworthiness response characteristics and the failure mode during plastic collapse without spending high costs for experimental equipment. Also, a number of simulations can be carried out in order to predict the effect of various parameters on crushing response of the examined structures by determining both their interaction level and its magnitude. Such important and interesting to analyze parameters can be related to structure geometry, like geometrical shape and dimensions (length, diameter, thickness, cross-section geometry etc.), the material and its mechanical properties and behavior during plastic deformation, special structure configurations (edges, cross-section variation, stress concentration etc.), type of edge supports or loading characteristics like crushing speed, crushing angle, type of initial contact between impactor and specimen etc. However, an important step before carrying out any numerical simulation is the comparison of developed models to experimental data in order to assess their validity and accuracy level.

The study of current Master thesis implements Finite Element Analysis (FEA) for the needs of model development utilizing the non-linear explicit finite element code of LS-DYNA, where inn particular a finite element modelling approach is used in this work in order to create the appropriate models of the examined configurations. LS-DYNA software [43] is utilized as the modelling tool for the purposes of current study. In general, the first step of modelling procedure with FEA is the geometry determination of the structure by defining the structure geometrical shape and its appropriate dimensions. Next, mesh generation usually follows by properly distributing the finite element nodes creating that way the elements mesh. Many softwares offer the capability for an automatic mesh generation, but they allow users to select by their own the preferable mesh density and type of finite elements. Also, the material properties of the created structural model are defined too, by giving information about physical and mechanical properties, like yield stress, Young' modulus, Poisson ratio, density and finally the stress-plastic strain curve during plastic deformation. After that, the support characteristics together with the boundary

conditions must be enforced, while the last stage of modelling is to define the loading characteristics.

The above modelling steps are made in the pre-processor of LS-DYNA. So, by summarizing, the pre-processing procedure includes the following steps:

- ✓ Geometry determination
- ✓ Mesh generation
- ✓ Material properties
- ✓ Support characteristics and boundary conditions
- ✓ Loading characteristics

As soon as the model is developed, LS-DYNA solver computes the response of the examined structure under the defined loading, by solving the equations provided from the implementation of FEA. Finally, when the numerical solution by the solver ends, LS-DYNA post-processor allows to observe the response of crushed structure under loading conditions.

Further, post-processor provides critical data for the crushed structure like crashworthiness characteristics, observed failure mode, load-deflection diagram etc. Thus, the modelling and calculating procedure in LS-DYNA includes the following three stages as Figure 99 depicts. The first and the last stage of the illustrated procedure can be both conducted in LS Pre-Post as made in current work. LS Pre-Post includes both pre-processor and pro-processor of LS-DYNA, but not the solver which is provided by ANSYS software.

Finally, the unit system which LS-DYNA uses is shown in Table 9. Each produced variable is also expected to be described by the respective units, as for example the unit of N·mm=mJ for energy accounting.

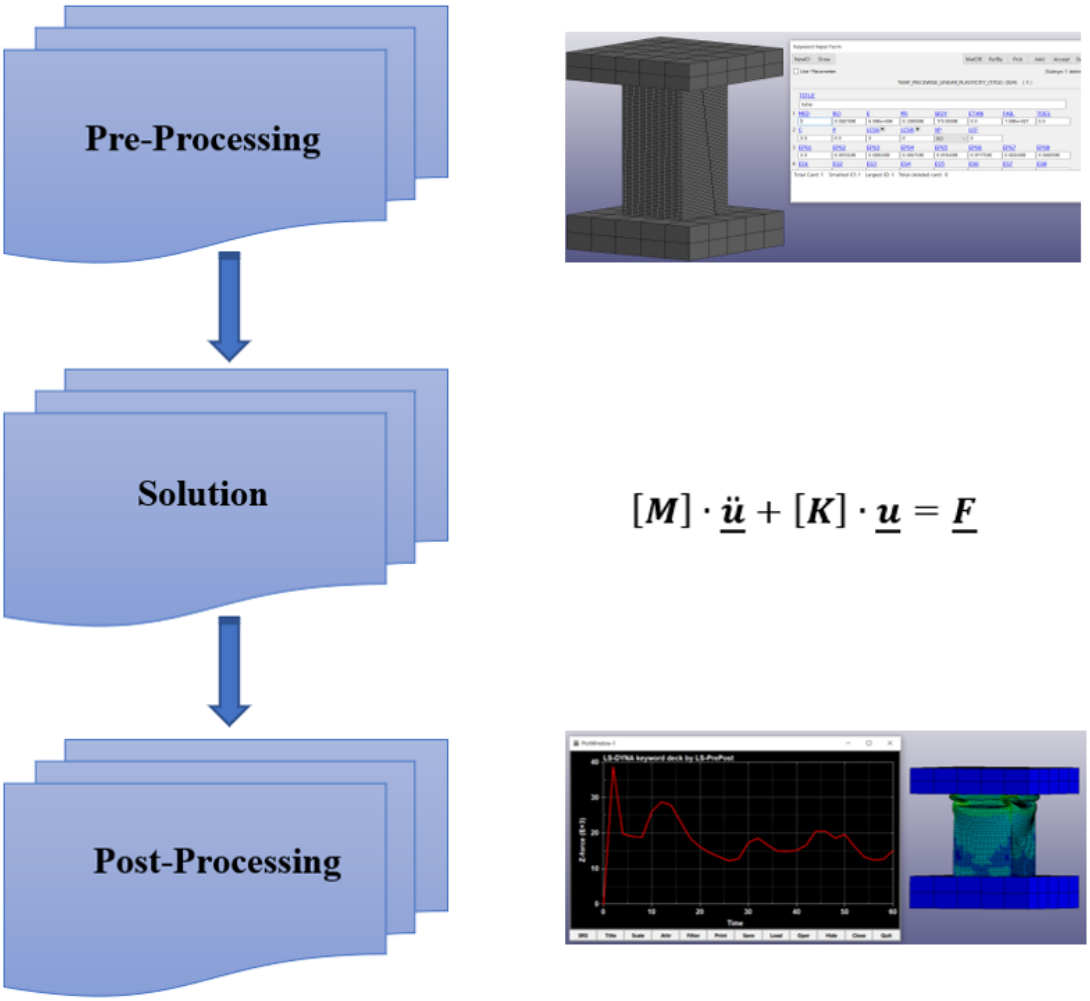


**Figure 99 Modelling and calculating procedure of FEA in LS-DYNA**

**Table 9 Units system in LS-DYNA software**

| Variable | Units |
|---|---|
| Mass | gr |
| Length | mm |
| Time | msec |
| Velocity | mm/msec |
| Force | N |
| Stress | $N/mm^2$ |
| Density | $gr/mm^3$ |

## 4.2 Finite Element Modelling Approach

The study of current work examines the crashworthiness response of thin-walled aluminium square tubes under both axial and oblique loading conditions. The examined tubes are of 50 mm width of square cross-section and 1.5 mm wall thickness. All specimens are 100 mm long and their maximum shortening during test cases lies about 60 mm. Each examined configuration consists of the square tubular specimen, the bottom edge of which is supported to a stationary base with an external configuration offering a fixed support for the bottom tube end in order to avoid any sliding during oblique crushing loading, while an upper plate compresses the tube with constant rate as depicted in Figure 100. Both bottom base and upper plate are considered as rigid bodies, while tube deforms plastically dissipating so amounts of crushing energy during its plastic collapse. Further, rotating the bottom base in which the tube is supported offers the capability to apply oblique compressive loads under the proper crushing angle representing an off-axis oblique loading case. Present work examines both cases of axial and oblique crushing by adjusting $5^o$, $10^o$ and $15^o$ loading angles regarding the oblique impact loading, aiming to assess the effect of crushing angle on energy absorption capability, while a comparison between axial and oblique crushing is carried out to evaluate the collapse mode level of stability and its effect on crushing efficiency. Furthermore, the modelling procedure as conducted in the pre-processor of LS-DYNA (LS Pre-Post) is presented in more detail below.

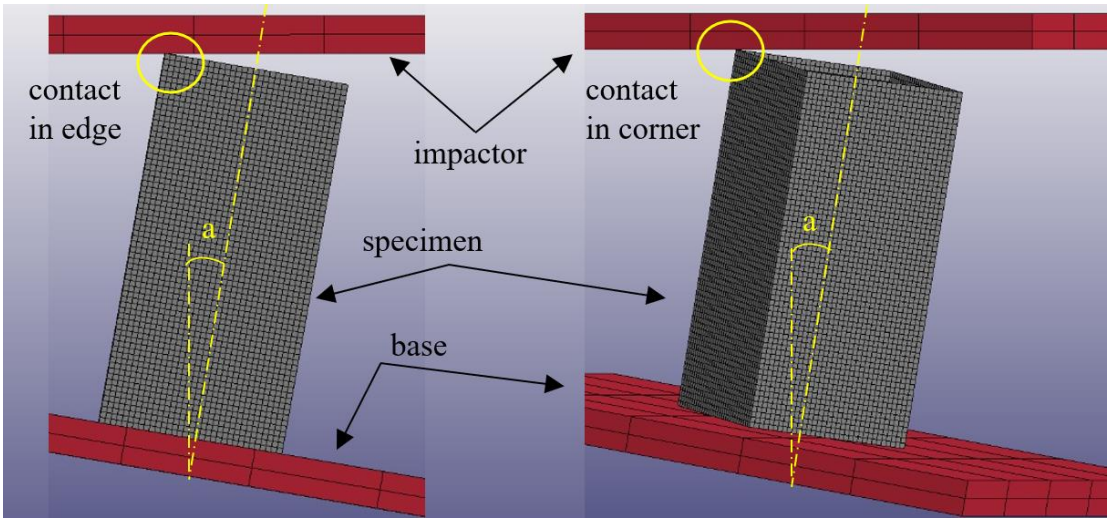


**Figure 100 Examined configurations for modelling in LS-DYNA: initial contact in edge (left), initial contact in corner (right)**

The basic steps of modelling procedure are to initially define the desirable specimen geometry (shape and dimensions) and adjust a finite element mesh by selecting the element type and size for each body. Current work utilizes 2D shell

elements for tubes and 3D solid elements for both bottom base and upper plate – impactor as they are considered as rigid bodies. Following, the material of each body is selected according to its physical and mechanical properties and the appropriate boundary conditions are defined in each interface contact. This study considers the contacts of impactor and bottom base with tube surface and also the contacts between tube convolutions formulated during plastic collapse. Finally, the loading characteristics are selected by adjusting a vertical constant speed to the impactor representing however dynamic crushing conditions considering the impact loading. In the following sections, the modelling procedure is described in more detail.

### 4.2.1 Geometry determination

In the first stage of modelling procedure, the specimen geometry and its dimensions are adjusted for each circular tube specimen. Because of their thin-walled structure, tube models are created using 2D plane finite elements, usually called as *shell elements*. In contrast, the impactor and bottom base which are considered as compact rigid bodies, are modelled with 3D finite elements, usually called as *solid elements*. In each case, the tube models use shell elements as the size of wall thickness compared to the width or the length of the tube, is negligible. So, shell elements provide less nodes, resulting in lower computational time and cost. However, for the appropriate dimensions of tube models, the use of shell elements means that each tube model is developed considering the mean cross-section circumference of width equal to 48.5 mm. Each square tube model is created by selecting the *Box Shell* choice which is included in the *Shape Mesher* of LS Pre-Post, where the mean width and length dimensions are adjusted properly together with elements size. For base and upper plate, the *Box Solid* choice of *Shape Mesher* is selected. Finally, the bottom base and the external configuration are treated as common parts by selecting them and creating a common entity.

### 4.2.2 Mesh Generation

Following, the element type and their size are selected for the bodies of the created models. In particular, the tube is modelled utilizing 4-node plane shell elements, the dimensions of which are adjusted just greater than tube wall thickness in order to make the tube model capable of predicting accurately the type and the number of the formulated folds. In fact, the elements are dimensioned such that their height is selected greater than the ratio of tube length to its wall thickness L/t, and their width similarly greater than the ratio of cross-section width to wall thickness a/t. More specific, the tube elements are adjusted

to square shape accordingly to the above assumption, while their thickness is adjusted properly within *Section Shell* option to 1.5 mm. Further, remaining in *Section Shell* option, the Belytschko-Lin-Tsay element formulation mode is selected to impose the elements deformation behavior during collapse, adjusting the ELFORM parameter equal to 2. The proposed mode of formulation is based on Reissner-Mindlin kinematic assumption, proposed also by Timoshenko, which considers the superposition of mid-surface displacements and rotations to describe plate deformation, treated in that way suitable for plane shell elements. More, Reissner-Mindlin theory assumes that cross section remains straight and unstretched like Bernoulli's theory, while shear deformations are also possible to be taken into account.

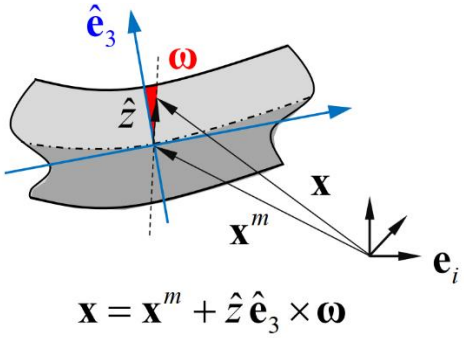


**Figure 101 Reissner-Mindlin bending theory**

As reported, the selected tube finite elements are 4-node shell elements following Belytschko-Lin-Tsay deformation mode which provides 5 degrees of freedom (DOF) in local coordinate system for each node which are the displacements of three axis ($u_x$, $u_y$, $u_z$) and the two rotations ($\theta_x$, $\theta_y$) from bending moments, neglecting in that way only torsional rotation ($\theta_z$). In addition, it has been proved extremely effective as it takes into account the strain rate effect and the Cauchy stresses distribution, while it enforces a bi-linear interpolation between the element nodes, but also retains the computational time in lower levels against the other available options. More, adjusting the number of through shell thickness integration points - regarding the NIP parameter in *Section Shell* option - equal to 5, the computed variables are integrated to reveal their distribution through shell thickness. Finally, a viscous and stiffness *hourglass* control for shell elements is selected for tube body with respect to Flanagan-Belytschko stiffness form setting IHQ parameter equal to 4.

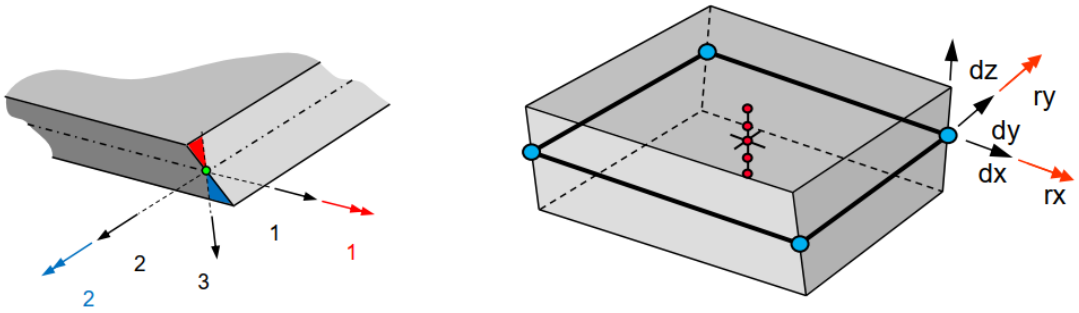


**Figure 102 Belytschko-Lin-Tsay shell element with NIP=5**

For upper plate - impactor and bottom base, 3D solid elements are utilized in *Solid Section*. The respective ELFORM parameter of *solid section* is kept equal to 1 as the default option, while mesh density is significantly lower as the above parts are considered as rigid bodies.

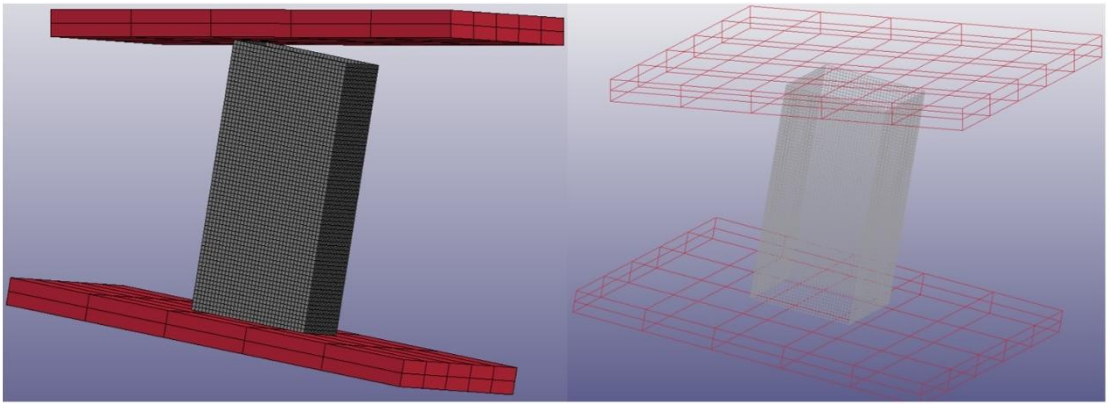

**Figure 103 Mesh generation of created bodies**

### 4.2.3 Material Selection

At next, the appropriate material properties are introduced to the pre-processor. In particular, the material *MAT024_Piecewise Linear Plasticity* option is selected for AA6060-T6 tube modelling, as aluminium plastic behavior can be described by sectionally linear-hardening segments because of its high ductility. *MAT024* describes the material behavior by introducing its density, Young Modulus, Poisson Ratio and yield stress, while it describes the hardening curve in plastic region with 8 points of stress and plastic strain ($\sigma$-$\varepsilon_p$). Specifically, density and poisson ratio of mild steel are selected according to open literature to 2.7 gr/cm$^3$ and 0.33 respectively. On the other hand, Young Modulus, yield stress and stress-plastic strain curve are calculated based on experimental data provided by tension tests of aluminium specimen, while a failure plastic strain penalty of 8% is further implemented in *MAT_024* keyword at tube model corners according to experimental tension test data aiming to capture material failure mainly occurred during tube tearing around its corners.

The test was conducted in a pressing machine applying the tensile load with constant rate of 10 mm/min and recording the measured displacements and loads. The experimental tension test of AA6060-T6 specimen was conducted twice in INSTRON 4482 machine providing the following true stress- true strain curves as Figure 104 depicts. Table 10 presents the mechanical properties utilizing for *MAT024* description according to the experimental data provided from tension test.

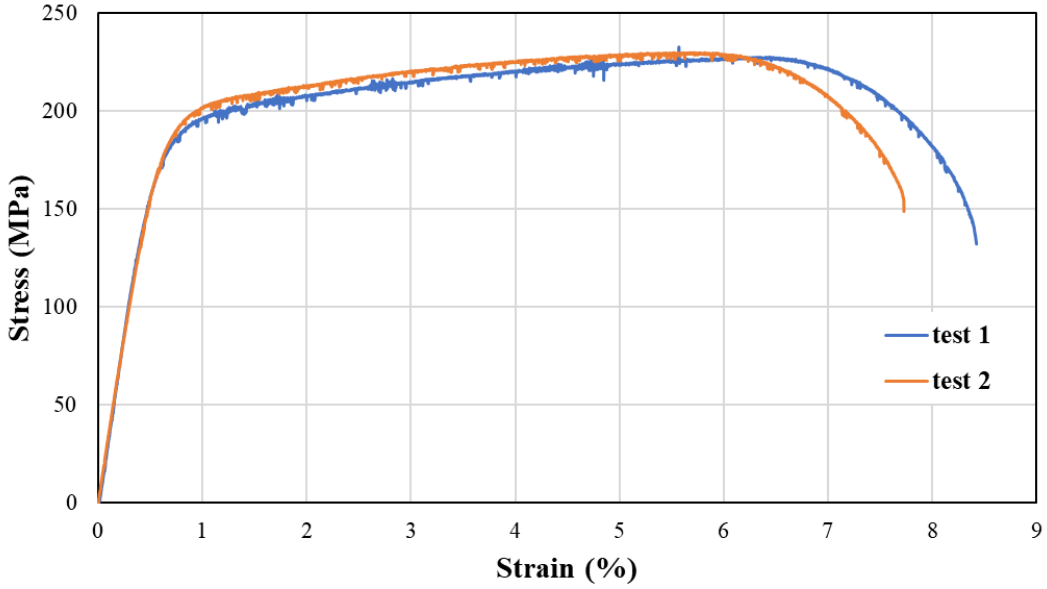


**Figure 104 Stress-strain curve from experimental tension tests of AA6060-T6 tube**

**Table 10 Test data of MAT024 tab for AA6060-T6 tube**

| **AA6060-T6 tube** | | |
|---|---|---|
| ***Young Modulus, E (MPa)*** | | 70000 |
| ***Yield Stress, $\sigma_Y$ (MPa)*** | | 180 |
| ***Failure Plastic Strain, $\varepsilon_{pf}$ (%)*** | | 8.00 |
| | | |
| ***Points*** | ***True plastic strain $\varepsilon_p$ (%)*** | ***True stress $\sigma$ (MPa)*** |
| 1 | 0 | 180 |
| 2 | 0.40 | 200 |
| 3 | 1.05 | 208 |
| 4 | 2.25 | 216 |
| 5 | 2.84 | 220 |
| 6 | 3.92 | 225 |
| 7 | 4.96 | 228 |
| 8 | 5.77 | 229 |

In addition, material option *MAT020_Rigid* is selected to simulate upper plate and bottom base bodies. Both parts are steel considered, with a typical Young Modulus of 205 GPa, Poisson ratio of 0.3 and density of 78.5 gr/cm$^3$. Also, *MAT020* requires the definition of kinematic degrees of freedom (DOF) for each part. CMO parameter is set equal to 1 in order to refer to DOF constraint in global coordinate system, while an appropriate adjustment of CON1 and CON2 parameters represents the constrained displacements and rotations respectively. Thus, for the stationary ringed bottom base, CON1 and CON2 parameters are both set equal to 7 meaning that displacements and rotations are constrained in every direction. However, for the upper plate, CON1 was set equal to 4 and CON2 equal to 7 allowing the upper plate to move vertically downwards crushing the tube specimen.

### 4.2.4 Contacts Definition

After justifying each part properties and characteristics, next step of modelling procedure is to define the type of contact between interface surfaces. For this reason, a *nodes-to-surface contact* and an *automatic single surface contact* are applied to the examined configuration to represent the no penetration boundary conditions in the interfaces.

In particular, the *nodes-to-surface contact* does not allow the penetration of tube nodes into the surface of bottom base and impactor, and so this type of contact is applied twice to the developed model; first for impactor-tube and secondly for the bottom base-tube. In each case, the tube specimen is described as the slave segment because it is considered as the deformable body in the interface, while the in-contact support body is described as the master segment as rigid and non-deformable regarding the bottom base and the impactor. The master segments are stated by their part ID for upper plate and bottom base, selecting the MSTYP parameter equal to 3. The slave segment is also stated by tube part ID by selecting the SSTYP parameter equal to 3 too. Finally, at each type of contact a static friction coefficient (FS) and a dynamic one (FD) are also adjusted to 0.61 and 0.47 respectively in order to estimate the occurred resistances from the relative motion of the two interface surfaces.

Further, *automatic single surface* type of contact is applied in order to avoid the penetration between the developed tube folds formulated during plastic collapse. In this type of contact, only slave segment is defined regarding tube part considering its formulated convolutions by selecting a SSTYP parameter of 3. Static and dynamic friction coefficients of 1.2 and 1.4 are applied respectively for this case too.

Finally, the external configuration of bottom base avoids any sliding of tube surface on the bottom base during oblique impact loading and thus tube bottom end behaves as fixed supported one. So, after the proper node selection of tube bottom end, the selected nodes are constrained against displacements (DOFX=DOY=DOZ=1) and rotations (DOFRX=DOFRY=DOFRZ=1) in

*Boundary SPC Set* option, representing in that way a fixed support for bottom tube end.

### 4.2.5 Loading Conditions Definition

The final step of modelling procedure is to define the loading curve characteristics. The crashworthiness response of the created models is simulated by adjusting a constant vertical crushing velocity of 1 mm/msec to the upper plate until about a maximum displacement of 60 mm reacting to a downwards movement of impactor which crushes tube specimen with constant rate providing the necessary shortening regarding the conducted experimental tests.

The impactor vertical velocity profile u(t) is properly applied in *define curve* option of keyword manager, while it is then adjusted to the upper plate in *Boundary Prescribed Motion Rigid* option, selecting a scaling factor (SF) of -1 to consider that the moving upper plate crushes the tube by moving downwards. Finally, the loading angle is adjusted by rotating both tube specimen and bottom base to the proper crushing angle about x-axis simulating that way the examined oblique crushing angle considering the case of contact-in-edge type of initial contact between impactor and tube. However, in the case of contact-in-corner initial type of contact between impactor and tube, an additional rotation of tube is conducted at first about 45$^{o}$ angle around z-axis and then tube is rotated to the proper crushing angle around x-axis.

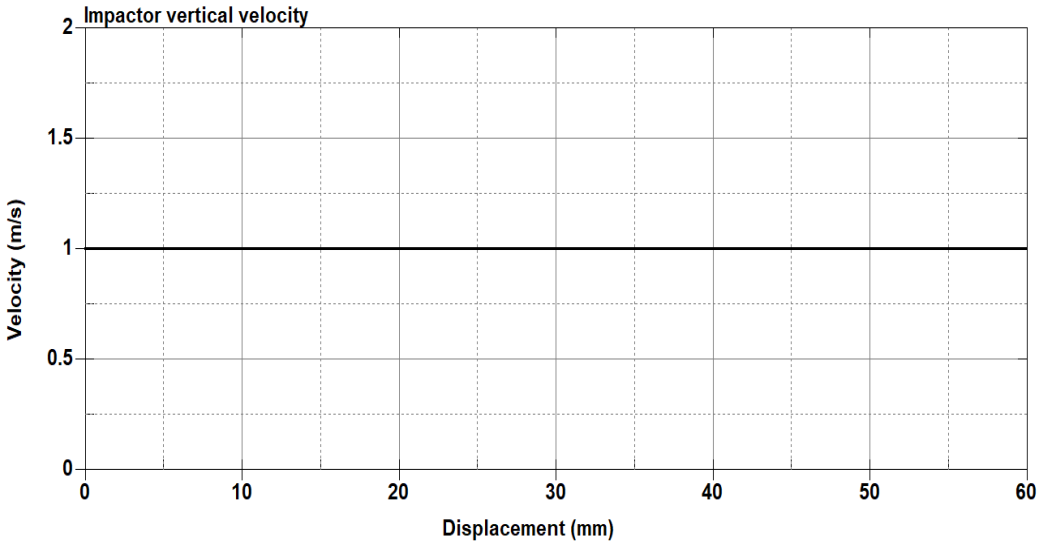


**Figure 105 Loading curve**

### 4.2.6 Database and Termination

As soon as the model is developed, the database timestep is defined at 1 msec. The selected data which solver returns are the forces in the contact surfaces (*rcforc*) and the upper plate movement (*rbdout*). Thus, a load-deflection diagram

is produced from the post-processor by combining the z-force (crushing load or axial compressive load) in the interface between upper plate and tube specimen, and the z-displacement of upper plate. Finally, the termination time is adjusted at proper timing for resulting in the tested specimen shortening regarding the experiments. The developed model is saved as a keyword file and after simulation termination, a *d3plot* file is created and then fed to post-processor where data processing is available, observing different stages of collapse in the same time.

## 4.3 Numerical Simulation Results

The numerical simulations of the developed finite element models are carried out in LS-DYNA software environment by utilizing the explicit non-linear code for the purpose of this study. The provided numerical results are presented and discussed in the following subsections for each examined loading case of current work. All simulations are carried out representing dynamic loading conditions by adjusting a crushing speed of 1 m/s to the impactor until a maximum displacement of 60 mm. The examined axial and oblique impact loading simulation cases are labelled as 1–2–3–4 regarding the loading angles of $0^o$–$5^o$–$10^o$–$15^o$ respectively, while in the case of obliquely crushed specimens two types of initial contact between impactor and tube are examined; a contact-in-edge type and a contact-in-corner one. The analysis of numerical force-displacement curves allowed for the estimation of the main crashworthiness response parameters, while also different states of collapse are recorded in order to capture the failure mechanism and assess its plastic deformation characteristics.

### 4.3.1 Axial Loading – Simulation Case 1

The numerical simulation of the developed finite element model of the axially crushed aluminium square tube revealed the depicted force-displacement (F-x) and energy absorption-displacement (EA-x) curves shown in the following figures, while the numerically estimated crashworthiness indicators are listed in Table 11. As depicted in F-x curve, the plastic collapse initiates at about 44 kN PCF value progressing at next by formulating local peaks and lows in crushing force around MCF of 14.7 kN. In fact, the significantly high enough PCF value results in tearing occurance around tube corners at about a 10 mm length, while at next plastic folds are formulated reacting to a more progressive and controllable plastic deformation mode. The tearing effect causes a light EA drop during plastic collapse progress as shown in Figure 107 which is captured from the slight drop of EA increase rate. In F-x curve, the local peaks and lows of instantaneous crushing force reflect the plastic folds formulation during post-buckling region revealing thus 3 formulated folds. More specifically, as observed in Figure 106, the last formulated fold requires a higher crushing force about 30 kN compared to the second fold which is deformed under 15 kN due to the

increased applied force of the teared tube edges which have been bended compressing the crushed structure. The simulation results revealed an 884.6 J energy absorption capacity for the axially crushed tube with a SEA of 18.76 kJ/kg, while CFE parameter is lied about 0.34 mainly due to the significantly higher PCF compared to MCF.

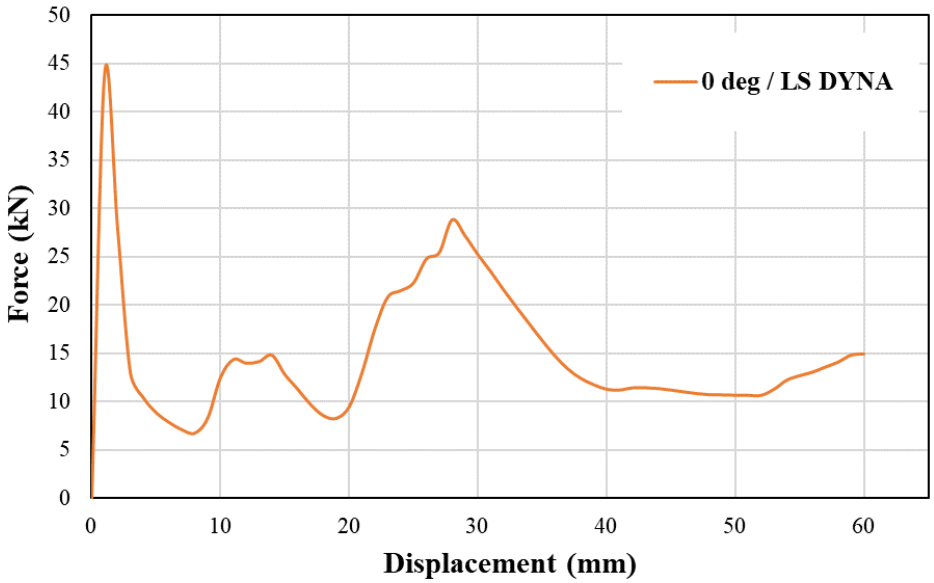


**Figure 106 Numerical F-x curve for axial loading**

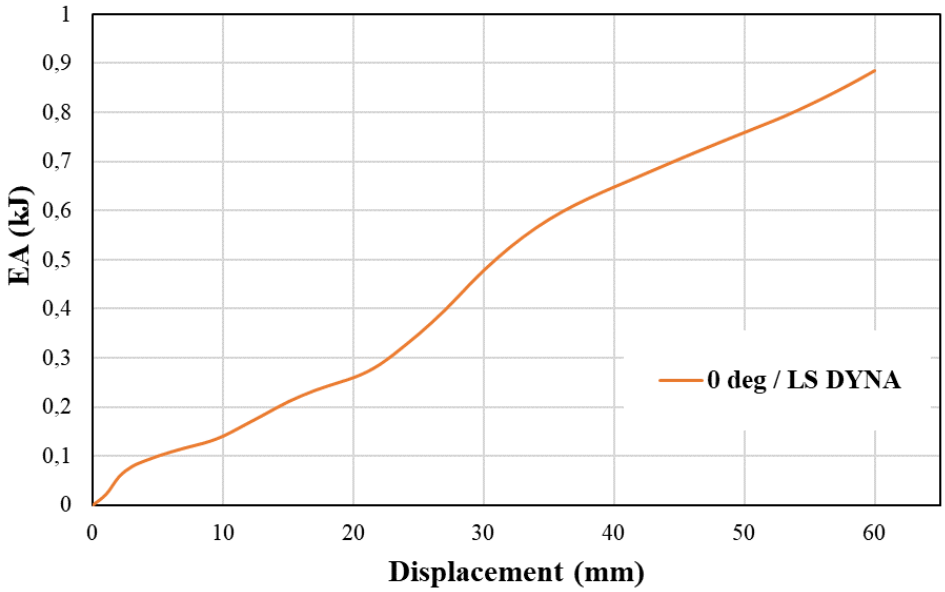


**Figure 107 Numerical EA-x curve for axial loading**

**Table 11 Numerical crashworthiness parameters for simulation case 1**

| *Numerical results – Simulation case 1* | |
|---|---|
| **PCF (kN)** | 43.96 |
| **MCF (kN)** | 14.74 |
| **EA (J)** | 884.6 |
| **SEA (kJ/kg)** | 18.76 |
| **CFE (-)** | 0.34 |

Observing the collapse states of axially crushed tube model, the high enough PCF reacts to a local tearing of the tube top corners which are caused by the great enough bending moments which tended to formulate an extensional plastic fold. Thus, the highly concentrated bending moment around tube top corners (Figure 109) resulted to a local tearing which is captured in the first stages of plastic collapse. At next, the plastic collapse progresses under a more controllable and stable mode formulating two more folds as the local crushing force peaks in F-x curve reflect. Thus, an extensional plastic fold is initially formulated at about 15 kN due to the circumferentially uniform bending moment distribution, while at next an inextensional plastic fold is deformed at about 30 kN due to the non-uniformity of the circumferential bending moment distribution as depicted in Figure 110. In summary so, the axially crushed tube model collapse under a mixed mode formulating an initial extensional fold and an inextensional one at following, while a local tearing around tube top corners was captured at the first stage of plastic deformation due to high enough PCF. Finally, a greater wall thickness could affect the tube strength positively in order to avoid any tearing resulting thus in significantly greater energy absorption capacity.

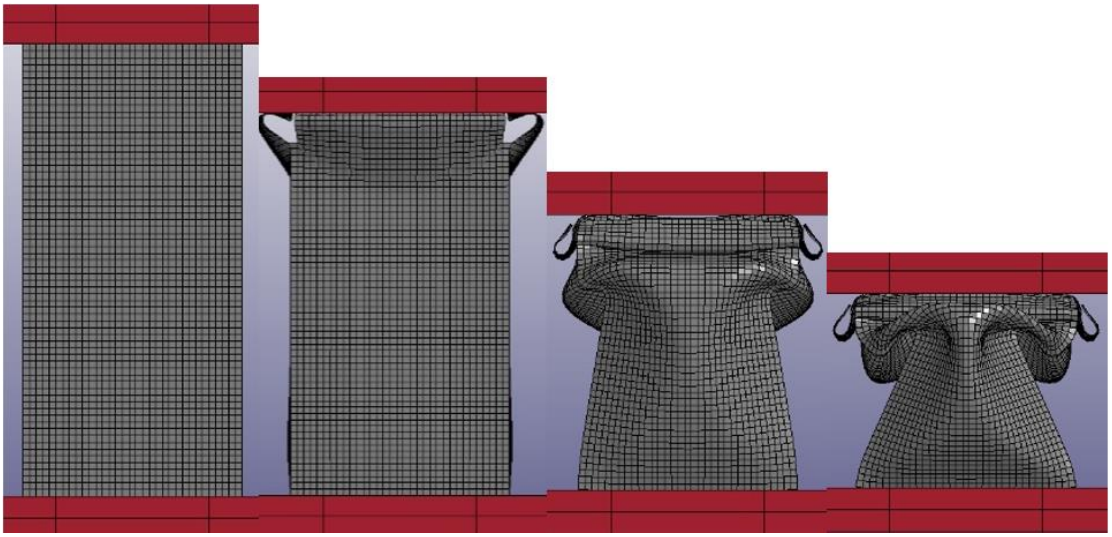

**Figure 108 Collapse states of simulation case 1**

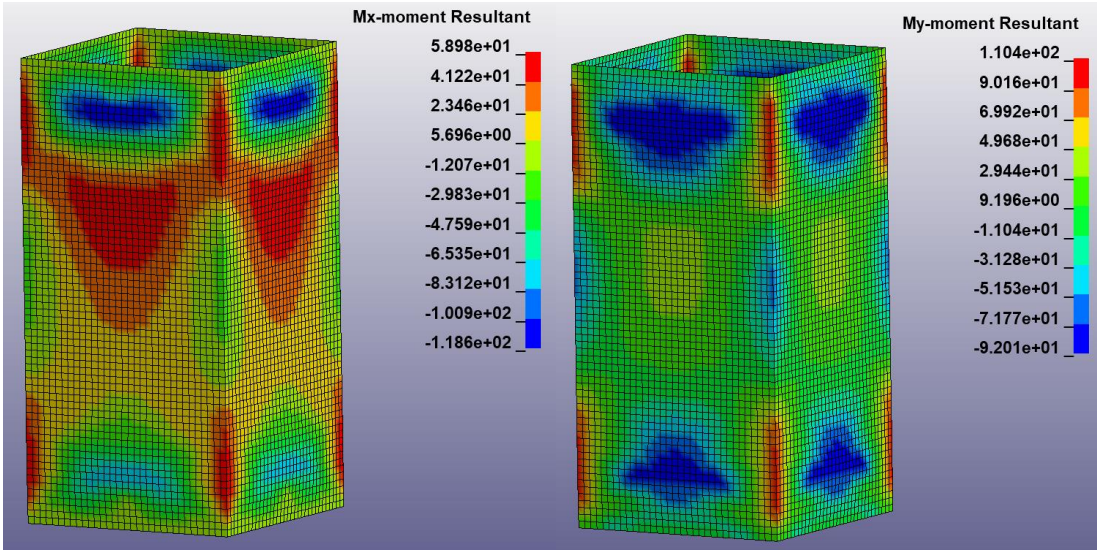


**Figure 109 Bending moment concentration around tube top corners**

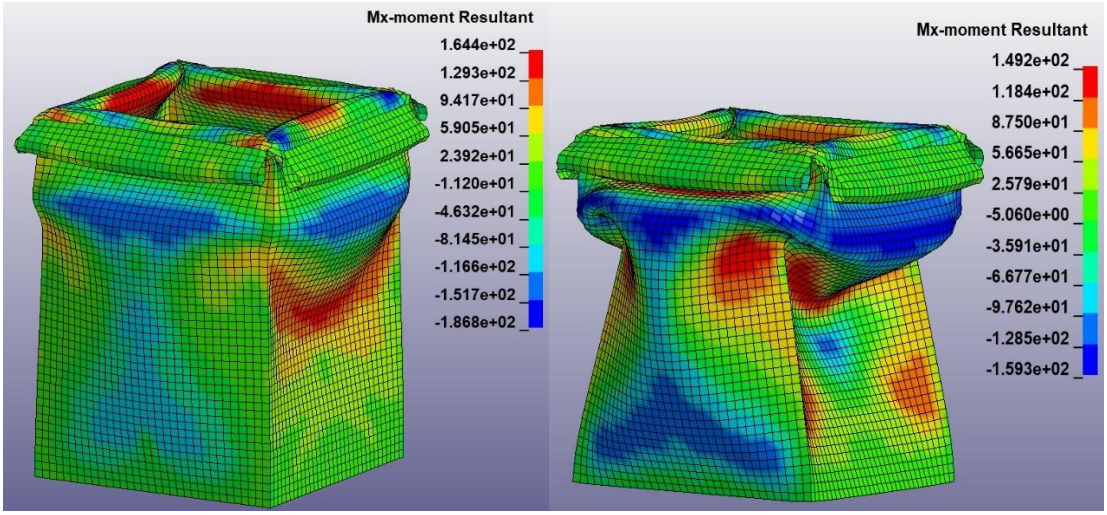


**Figure 110 Effect of bending moment circumferential distribution on extensional (left) and inextensional (right) plastic fold formulation (simulation case 1)**

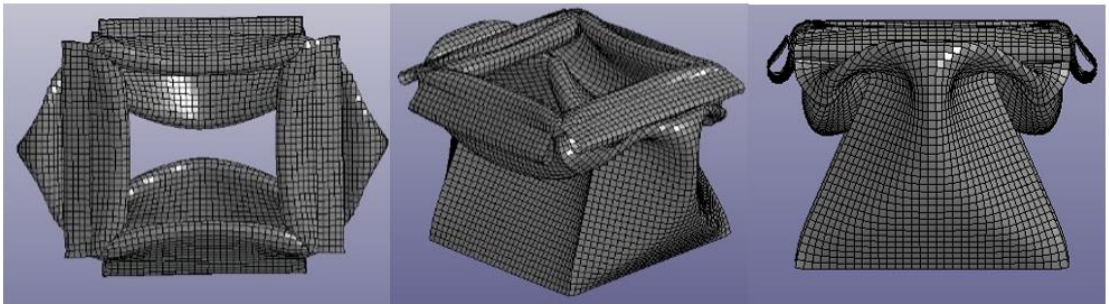

**Figure 111 Final views of crushed tube model in simulation case 1**

### 4.3.2 Oblique Loading under 5º angle – Simulation Case 2

#### 4.3.2.1 Initial contact in edge

The numerical simulation of the developed finite element model for 5º oblique impact loading with an initial contact-in-edge between impactor-tube revealed the depicted F-x and EA-x curves shown in the following figures, while the numerically estimated crashworthiness indicators are listed in Table 12. As depicted in F-x curve, the plastic collapse initiates at about 23 kN PCF value progressing at next by formulating local peaks and lows in crushing force around MCF of 14.6 kN. In F-x curve, the local peaks and lows of instantaneous crushing force reflect the plastic folds formulation during post-buckling region revealing thus 3 formulated folds. The controllable and progressive behavior of plastic collapse by the formulation of 3 inextensional folds is also reflected by the uniform EA increase during collapse. The simulation results revealed an 878 J energy absorption capacity for the 5º obliquely crushed tube under contact-in-edge to the impactor with a SEA of 18.62 kJ/kg, while CFE parameter is lied about 0.63.

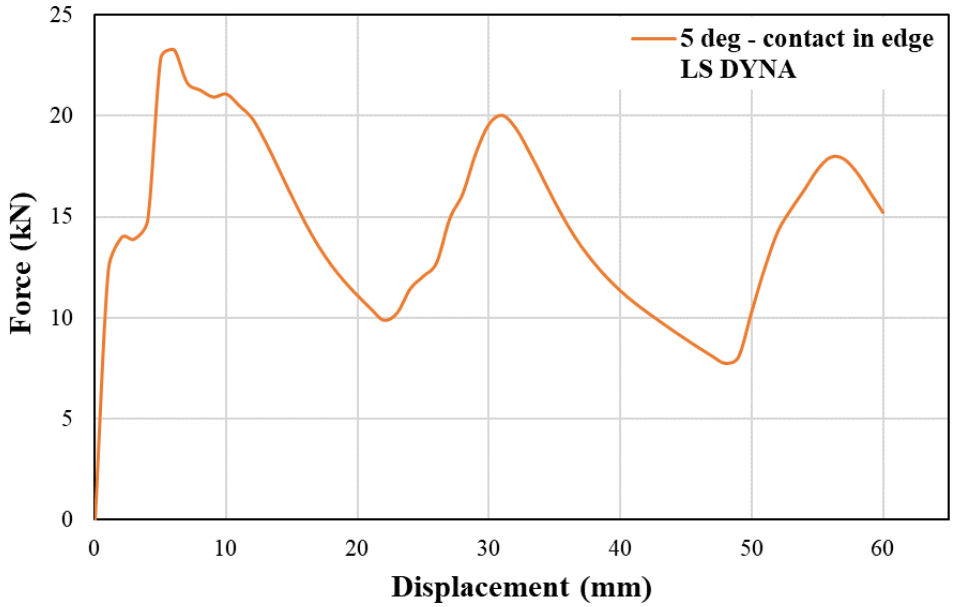


**Figure 112 Numerical F-x curve for 5º oblique loading under contact in edge**

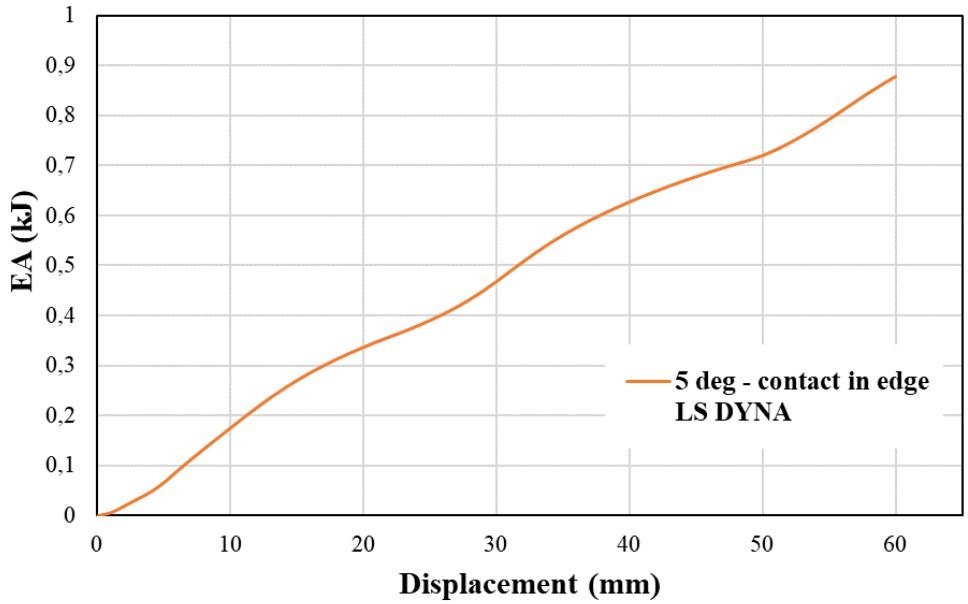


**Figure 113 Numerical EA-x curve for 5º oblique loading under contact in edge**

**Table 12 Numerical crashworthiness parameters for simulation case 2 under contact in edge**

| ***Numerical results – Simulation case 2 - edge*** | |
|---|---|
| **PCF (kN)** | 23.3 |
| **MCF (kN)** | 14.6 |
| **EA (J)** | 878.0 |
| **SEA (kJ/kg)** | 18.62 |
| **CFE (-)** | 0.63 |

Comparing to the axially loaded tube of simulation case 1, the increase in crushing angle to 5º reacted in lower PCF as the lateral crushing force component introduces additional bending moment which facilitate the plastic collapse initiation by formulating the first plastic fold in lower crushing force. Further, the lower PCF compared to the axial crushing does not result in any tearing occurance around tube top corners according to the simulation results. In addition, the increase in crushing angle reacts to lower energy absorption capability due to the additional bending moments which introduces facilitating the collapse progress and thus simulation case 2-edge revealed slightly lower EA and SEA compared to case 1 although the tube tearing occurance in axial crushing which resulted in EA decrease. In fact, the examination of a greater tube wall thickness which would avoid tube tearing would reflect more representatively the crushing angle effect by revealing even more greater EA for the axially crushed tube of simulation case 1. Further, CFE parameter revealed

greater for 5º oblique loading compared to axial impact due to the lower PCF and the sustained MCF value which would be expected to be even lower compared to case 1 if no tearing was observed during the axial collapse of the examined tube.

Observing the collapse states of the 5º obliquely crushed tube model under contact-in-edge with the impactor, the plastic collapse evolves under a controllable and progressive mode formulating 3 inextensional plastic folds as the local crushing force peaks in F-x curve reflect. Thus, the first extensional plastic fold is initially formulated at about 23 kN with the two following folds at 20 kN and 18 kN respectively. The inextensional deformation mode of the formulated folds is paid on the circumferentially non-uniform bending moment distribution as depicted in Figure 115. Thus, the progressive inextensional collapse mode allowed the 5º obliquely tube model to dissipate significant amounts of crushing energy despite the oblique loading and so MCF and in consequence EA and SEA proved to be slightly lower to the ones of axial crushing in which tube tearing was occurred reducing the energy absorption capacity in that case.

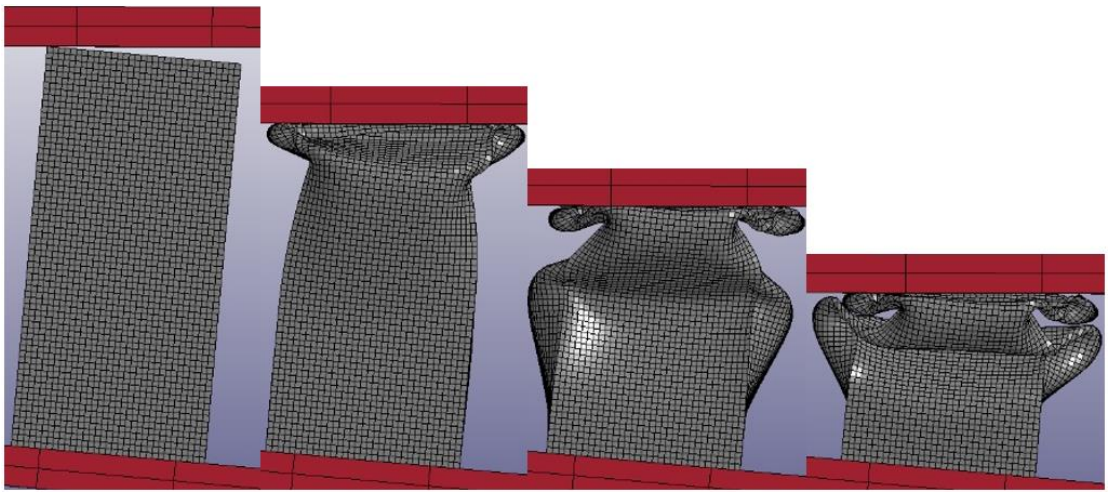

**Figure 114 Collapse states of simulation case 2 under contact in edge**

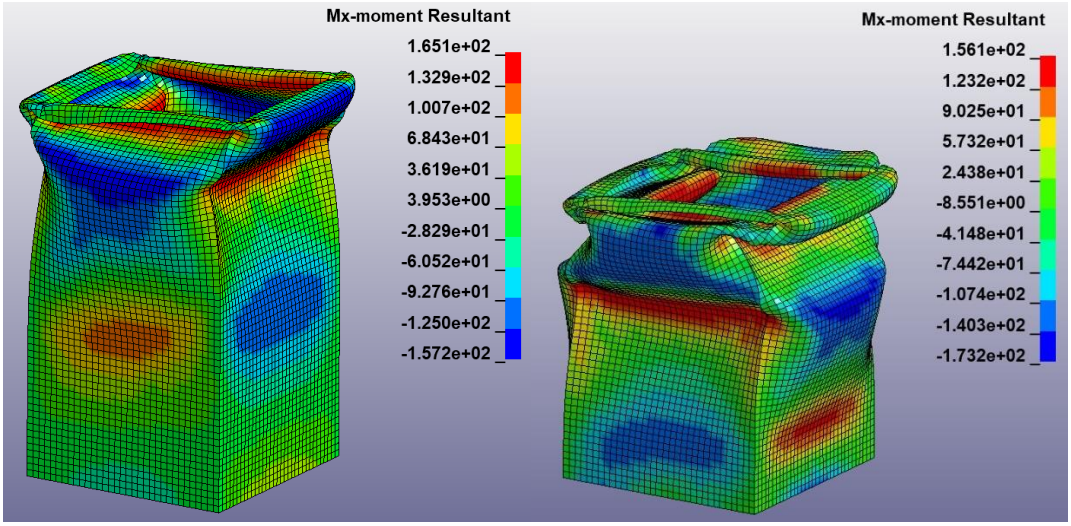


**Figure 115 Effect of bending moment distribution on inextensional folds formulation (simulation case 2-edge)**

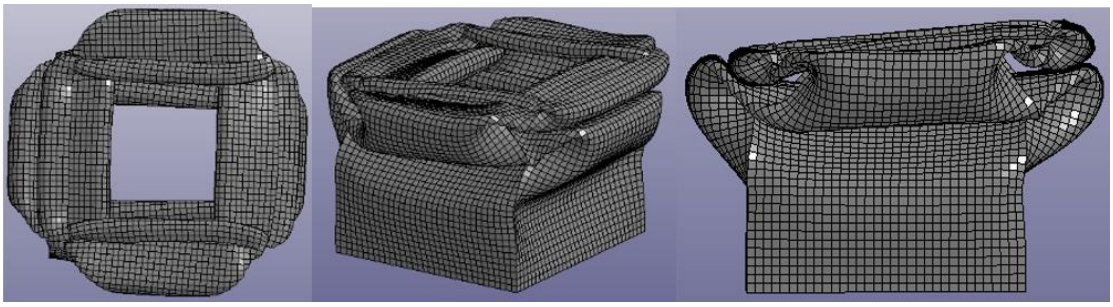

**Figure 116 Final views of crushed tube model in simulation case 2 under contact in edge**

### 4.3.2.2 Initial contact in corner

The numerical results of simulation case 2 for 5$^{o}$ oblique impact loading with an initial contact-in-corner between impactor-tube revealed the depicted F-x and EA-x curves shown in the following figures, while the numerically estimated crashworthiness indicators are listed in

Table 13. As depicted in F-x curve, the plastic collapse initiates at about 25 kN PCF value progressing at next by formulating local peaks and lows in crushing force around MCF of 16.7 kN. In F-x curve, the local peaks and lows of instantaneous crushing force reflect the plastic folds formulation during post-buckling region revealing thus 3 formulated folds. The controllable and progressive behavior of plastic collapse by the formulation of 3 inextensional

folds is also reflected by the linear increase in EA during collapse. The simulation results revealed a 1003.6 J energy absorption capacity for the 5º obliquely crushed tube under contact-in-corner to the impactor with a SEA of 21.29 kJ/kg, while CFE parameter is lied about 0.67.

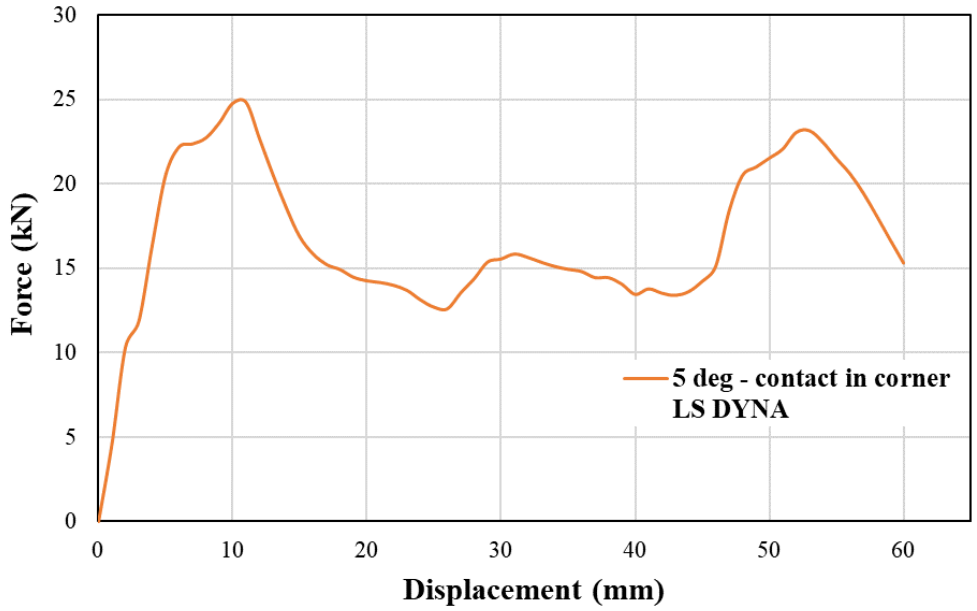


**Figure 117 Numerical F-x curve for 5º oblique loading under contact in corner**

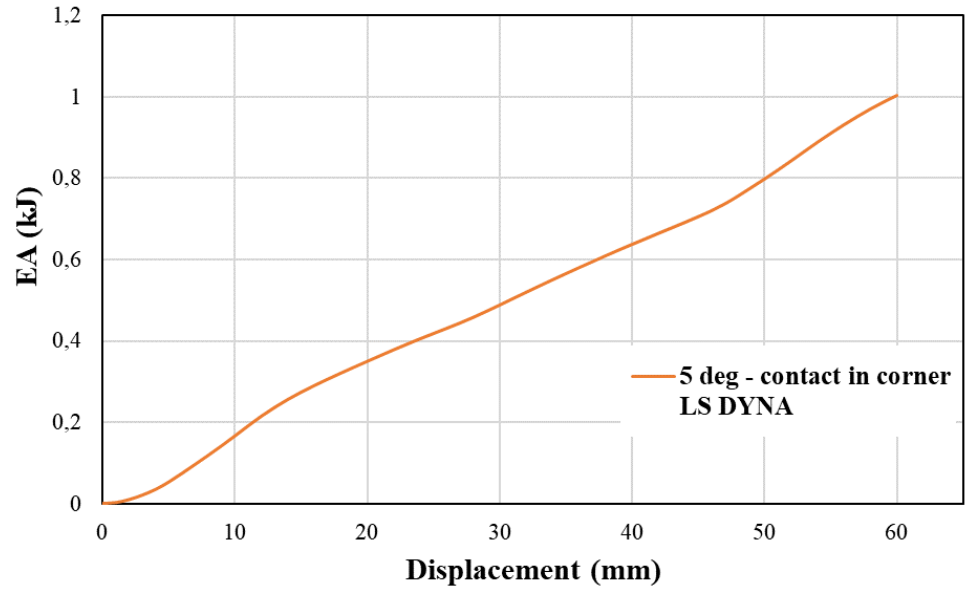


**Figure 118 Numerical EA-x curve for 5º oblique loading under contact in corner**

**Table 13 Numerical crashworthiness parameters for simulation case 2 under contact in corner**

| *Numerical results – Simulation case 2 - corner* | |
|---|---|
| **PCF (kN)** | 24.80 |
| **MCF (kN)** | 16.73 |
| **EA (J)** | 1003.6 |
| **SEA (kJ/kg)** | 21.29 |
| **CFE (-)** | 0.67 |

Comparing to both axially loaded tube (case 1) and 5$^{o}$ obliquely loaded tube with contact-in-edge (case 2-edge), the 5$^{o}$ obliquely loaded tube with contact-in-corner (case 2-corner) revealed greater energy absorption capacity. Thus, compared to case 2-edge the initial contact-in-corner reacts to higher EA and SEA and reflects a more efficient crushing behavior. However, compared to case 1 the greater energy absorption capability is paid on tube tearing occurance in axial crushing due to significantly higher PCF and so 5$^{o}$ oblique crushing under contact-in-corner is proved more beneficial than axial crushing despite crushing angle effect which in the case of oblique impact tends to reduce EA due to additional bending moments which are introduced by the lateral force component. Therefore, case 2-corner reveals greater SEA due to the absence of local tube tearing due to the lower PCF. In contrast though, PCF is revealed lower than case 1 as expected because the additional bending moment due to angled loading facilitates the plastic collapse initiation. However, an initial contact-in-corner between impactor and crushed tube reveals greater PCF than the oblique crushing under contact-in-edge as shown from the comparison between case 2-edge and case 2-corner.

Observing the collapse states of the 5$^{o}$ obliquely crushed tube model under contact-in-corner with the impactor, the plastic collapse evolves under a controllable and progressive mode formulating 3 inextensional plastic folds as the local crushing force peaks in F-x curve reflect. Thus, the first extensional plastic fold is initially formulated at about 24.8 kN with the two following folds at 26 kN and 23 kN respectively. The inextensional deformation mode of the formulated folds is paid on the circumferentially non-uniform bending moment distribution as depicted in Figure 120. Thus, the progressive inextensional collapse mode allowed the 5$^{o}$ obliquely tube model to dissipate significant amounts of crushing energy despite the oblique loading and due to the absence of tube tearing due to lower PCF. Thus, MCF and in consequence EA and SEA proved to be slightly greater than the ones of axial crushing and even higher than

the 5º obliquely crushed tube model with an initial contact-in-edge to the impactor.

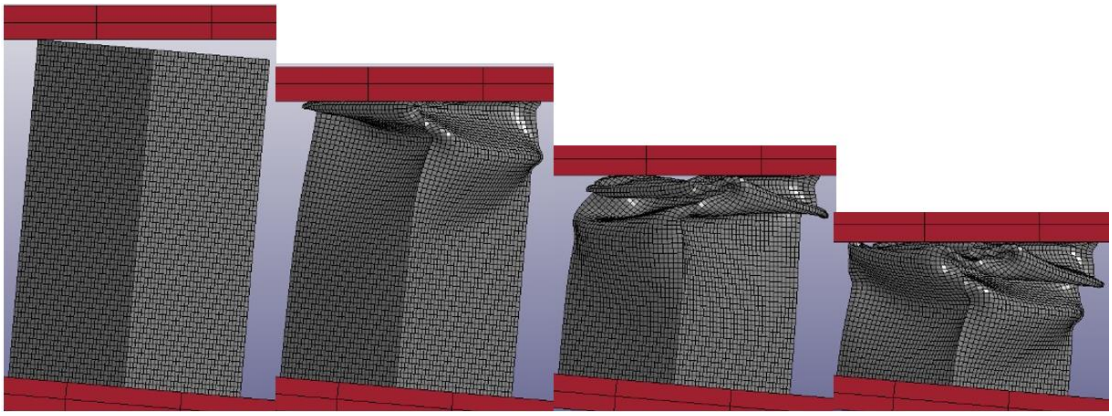

**Figure 119 Collapse states of simulation case 2 under contact in corner**

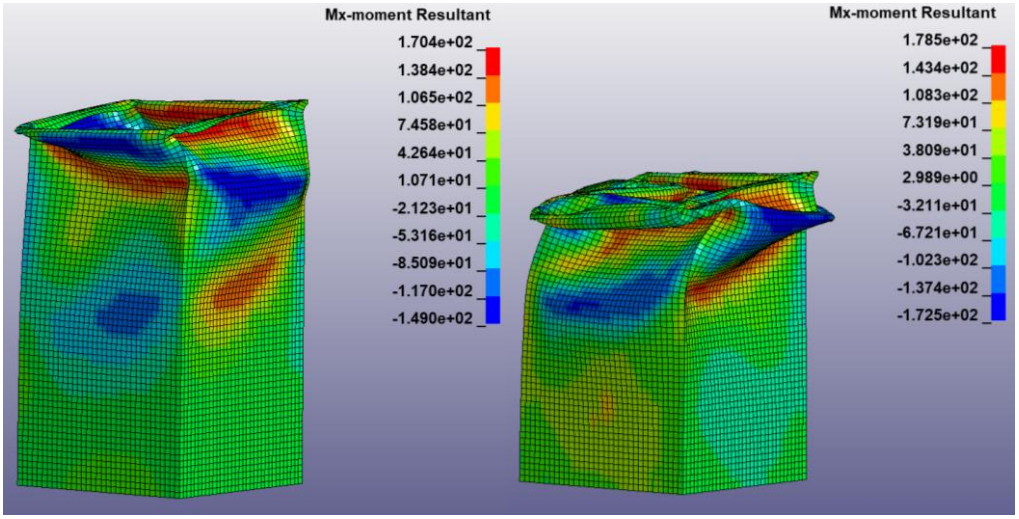


**Figure 120 Effect of bending moment distribution on inextensional folds formulation (simulation case 2-corner)**

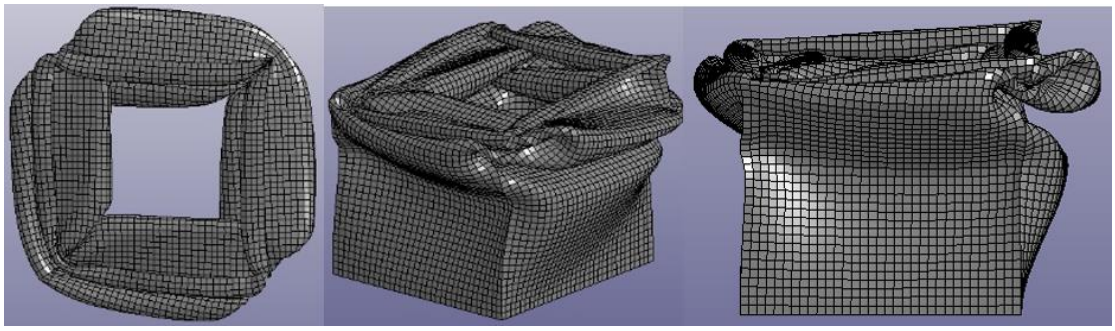

**Figure 121 Final views of crushed tube model in simulation case 2 under contact in corner**

### 4.3.3 Oblique Loading under 10º angle – Simulation Case 3

#### 4.3.3.1 Initial contact in edge

The numerical simulation of the developed tube model subjected to 10º oblique impact loading under an initial contact-in-edge with the impactor revealed the depicted F-x and EA-x curves shown in the following figures, while the numerically estimated crashworthiness indicators are listed in Table14. As depicted in F-x curve, the plastic collapse initiates at about 23.2 kN PCF value progressing at next by formulating local peaks and lows in crushing force around 13.85 kN MCF. In F-x curve, the local peaks and lows of instantaneous crushing force reflect the plastic folds formulated during collapse revealing thus 3 formulated folds. The controllable and progressive behavior of plastic deformation under the formulation of 3 inextensional folds is also reflected by the uniform EA increase during collapse which reaches up to 830.9 J. The simulation results revealed further a 17.62 kJ/kg SEA capacity for the 10º obliquely crushed tube under contact-in-edge to the impactor, while CFE parameter is lied about 0.6.

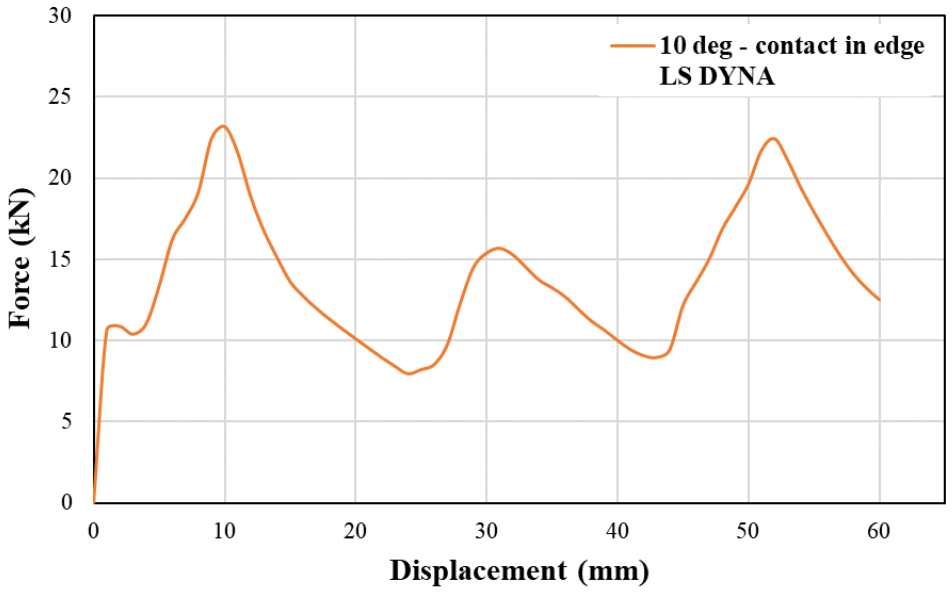


**Figure 122 Numerical F-x curve for 10º oblique loading under contact in edge**

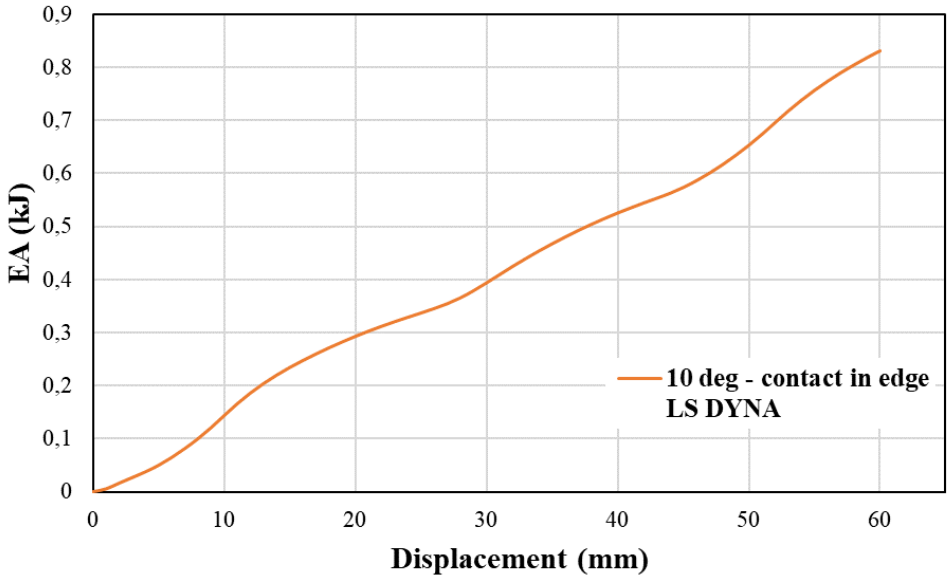


**Figure 123 Numerical EA-x curve for 10º oblique loading under contact in edge**

**Table 14 Numerical crashworthiness parameters for simulation case 3 under contact in edge**

| ***Numerical results – Simulation case 3 - edge*** | |
|---|---|
| **PCF (kN)** | 23.20 |
| **MCF (kN)** | 13.85 |
| **EA (J)** | 830.9 |
| **SEA (kJ/kg)** | 17.62 |
| **CFE (-)** | 0.60 |

Comparing to the simulation case 2, the 10º obliquely crushed tube model revealed lower EA due to the greater crushing angle which introduced higher additional bending moment caused by lateral crushing force component of angled loading. That moment facilitates both plastic collapse initiation and progress reducing so the required plastic deformation force and the necessary plastic bending moment for folding formulation. However, PCF did not seem to affect similarly provided almost lower than the 5º oblique loading case with contact-in-edge. Observing the collapse states of the 10º obliquely crushed tube model under contact-in-edge with the impactor, the plastic collapse evolves under a controllable and progressive mode formulating 3 inextensional plastic folds as the local crushing force peaks in F-x curve reflect. Thus, the first extensional plastic fold is initially formulated at about 23 kN with the two following folds at 16 kN and 22 kN respectively. The inextensional deformation mode of the formulated folds is paid on the circumferentially non-uniform

bending moment distribution which reacts to a plastic fold stretching and compression in opposite direction.

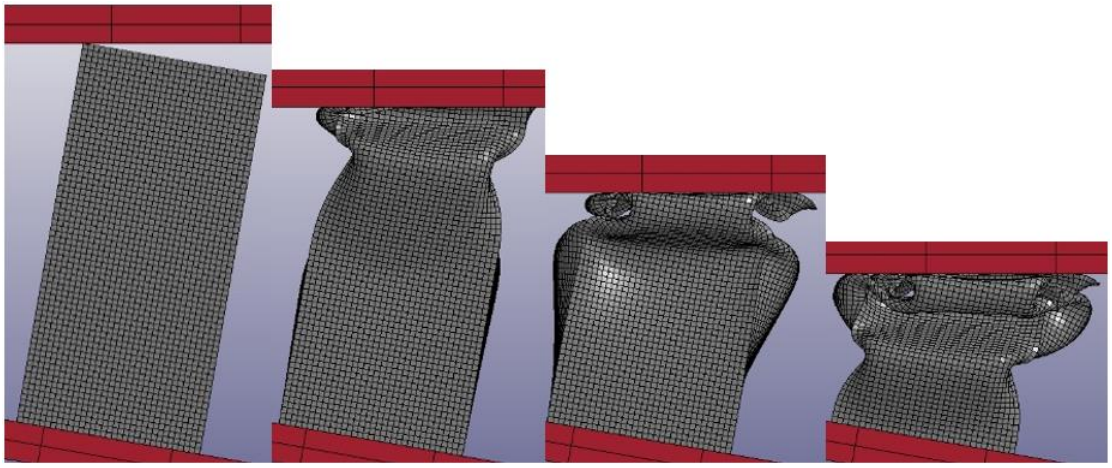

**Figure 124 Collapse states of simulation case 3 under contact in edge**

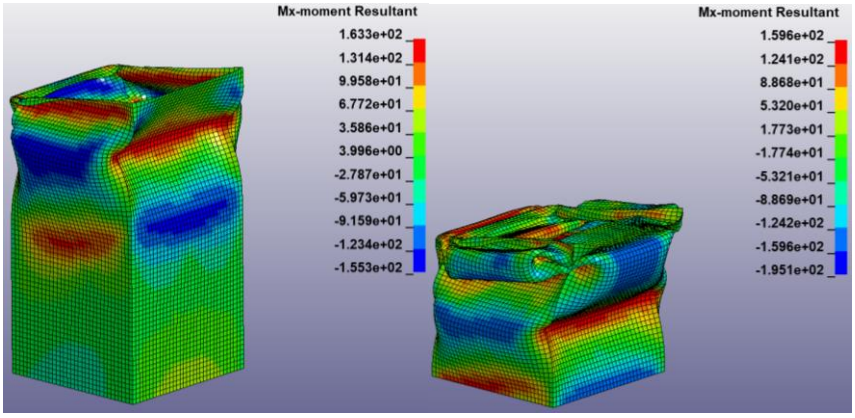


**Figure 125 Effect of bending moment distribution on inextensional folds formulation (simulation case 3-edge)**

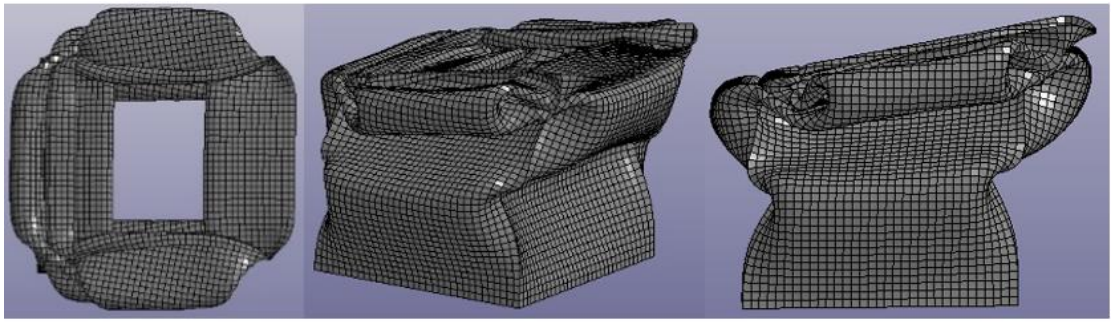

**Figure 126 Final views of crushed tube model in simulation case 3 under contact in edge**

### 4.3.3.2 Initial contact in corner

The numerical simulation of the developed tube model subjected to 10º oblique impact loading under an initial contact-in-corner with the impactor revealed the depicted F-x and EA-x curves shown in the following figures, while the numerically estimated crashworthiness indicators are listed in Table15. As depicted in F-x curve, the plastic collapse initiates at about 24.98 kN PCF value progressing at next by formulating local peaks and lows in crushing force around 15.74 kN MCF. In F-x curve, the local peaks and lows of instantaneous crushing force reflect the plastic folds formulated during collapse revealing thus 3 formulated folds. The controllable and progressive behavior of plastic deformation under the formulation of 3 inextensional folds is also reflected by the EA linear increase during collapse which reaches up to 944.6 J. The simulation results revealed further a 20.04 kJ/kg SEA capacity for the 10º obliquely crushed tube under contact-in-corner to the impactor, while CFE parameter is lied about 0.63.

The 10º obliquely crushed tube model of simulation case 3-corner revealed a similar PCF compared to 5º crushed tube with contact-in-corner, while both cases showed slightly greater PCF compared to the ones under an initial contact-in-edge between impactor and tube. Moreover, the EA capacity reveals a linear decrease with crushing angle under contact-in-corner maintained although in higher levels compared to EA under contact-in-edge for the same crushing angle values. Thus, an initial contact-in-corner shows to react to greater PCF and SEA than the ones under contact-in-edge, while EA drop with respect to crushing angle shows a linear dependence for cornered initial contact in contrast to EA decrease with crushing angle which reveals a sigma variance.

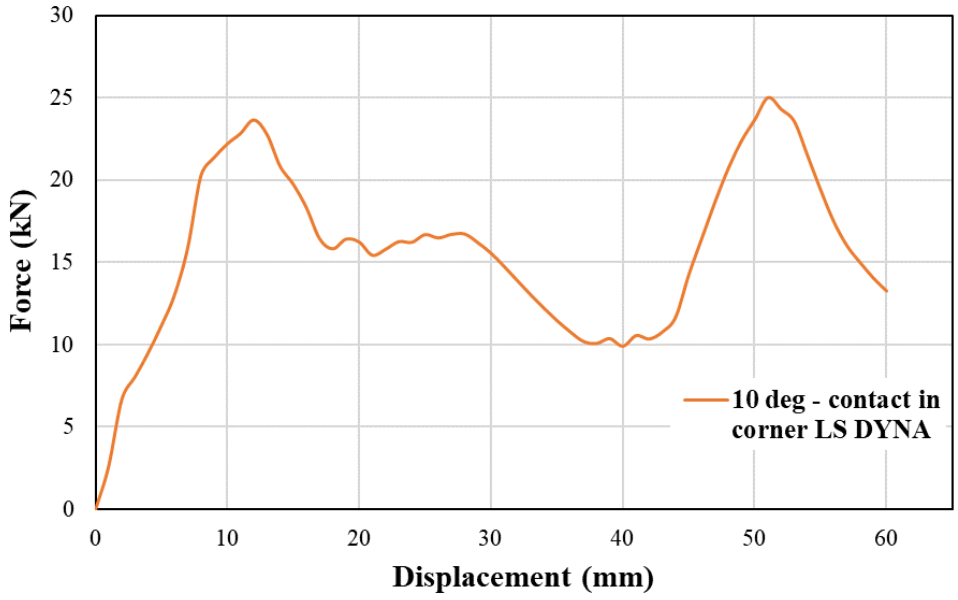


**Figure 127 Numerical F-x curve for 10º oblique loading under contact in corner**

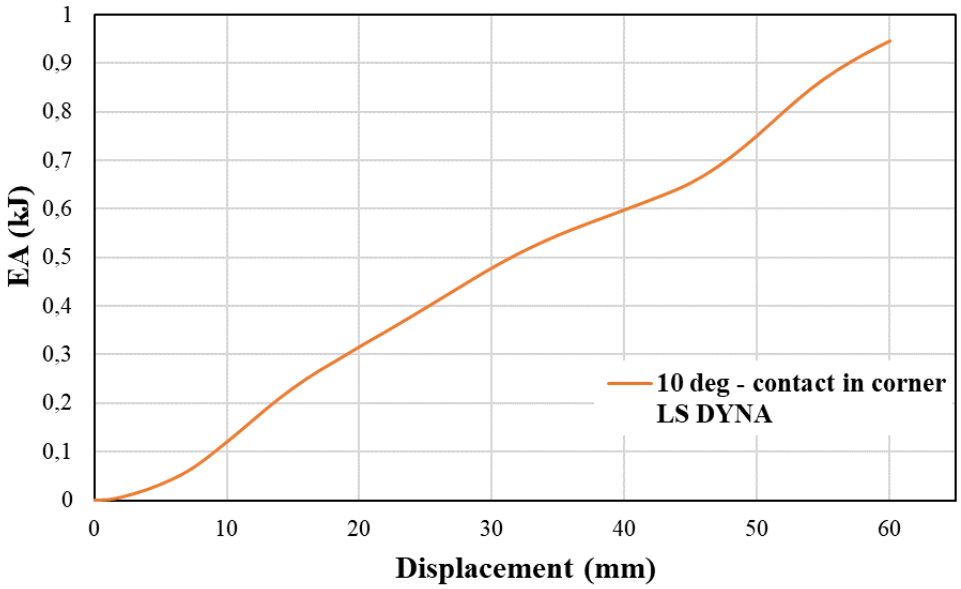


**Figure 128 Numerical EA-x curve for 10º oblique loading under contact in corner**

**Table 15 Numerical crashworthiness parameters for simulation case 3 under contact in corner**

| ***Numerical results – Simulation case 3 - corner*** | |
|---|---|
| **PCF (kN)** | 24.98 |
| **MCF (kN)** | 15.74 |
| **EA (J)** | 944.6 |
| **SEA (kJ/kg)** | 20.04 |
| **CFE (-)** | 0.63 |

Observing the collapse states of the 10º obliquely crushed tube model under contact-in-corner with the impactor, the plastic collapse evolves under a controllable and progressive mode formulating 3 inextensional plastic folds as the local crushing force peaks in F-x curve reflect. Thus, the first extensional plastic fold is initially formulated at about 23 kN with the two following folds at 17 kN and 25 kN respectively. The inextensional deformation mode of the formulated folds is paid on the circumferentially non-uniform bending moment distribution which reacts to a plastic fold stretching and compression in opposite directions.

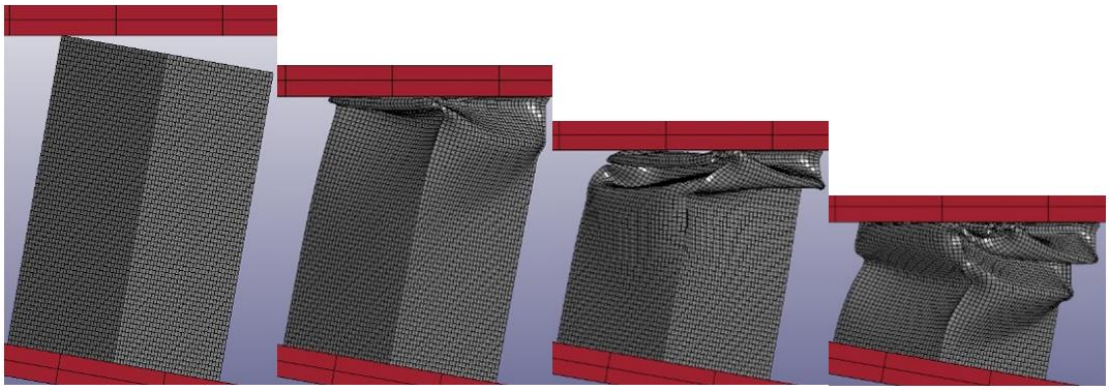

**Figure 129 Collapse states of simulation case 3 under contact in corner**

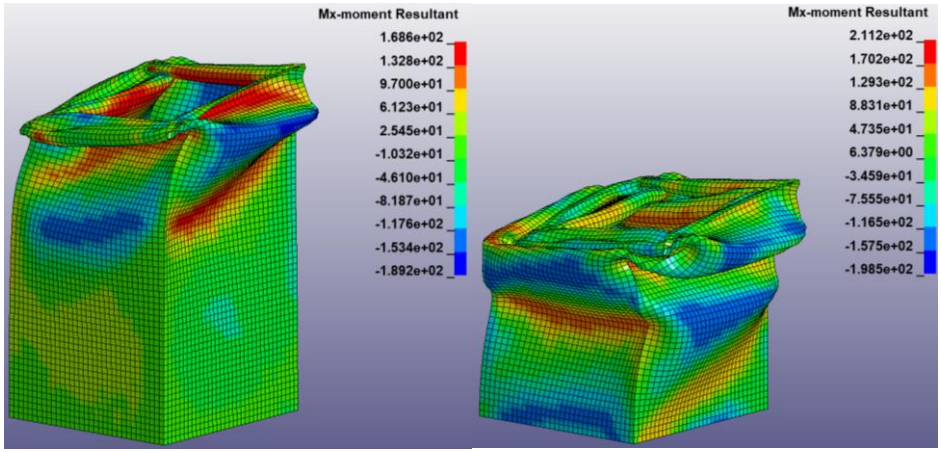


**Figure 130 Effect of bending moment distribution on inextensional folds formulation (simulation case 3-corner)**

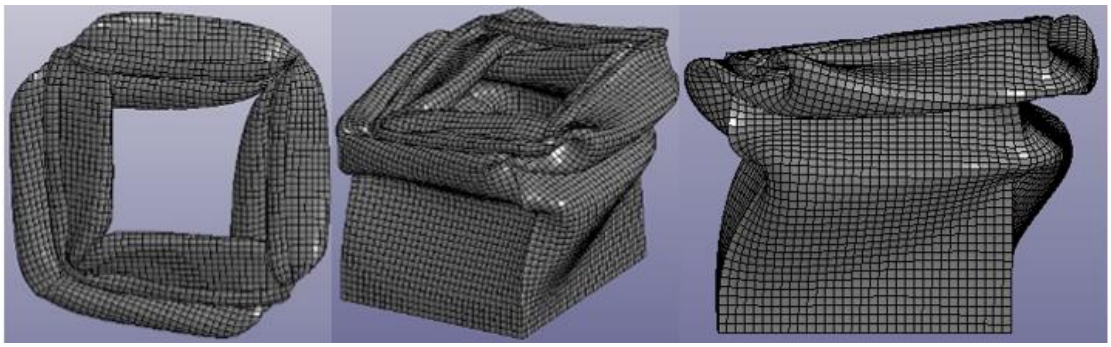

**Figure 131 Final views of crushed tube model in simulation case 3 under contact in corner**

### 4.3.4 Oblique Loading under 15º angle – Simulation Case 4

#### 4.3.4.1 Initial contact in edge

The numerical simulation of the developed tube model subjected to 15º oblique impact loading under an initial contact-in-edge with the impactor revealed the depicted F-x and EA-x curves shown in the following figures, while the numerically estimated crashworthiness indicators are listed in Table16. As depicted in F-x curve, the plastic collapse initiates at about 21.57 kN PCF value progressing at next by formulating local peaks and lows in crushing force around 13.79 kN MCF. In F-x curve, the local peaks and lows of instantaneous crushing force reflect the plastic folds formulated during collapse revealing thus 2 formulated folds. The controllable and progressive behavior of plastic deformation under the formulation of 2 inextensional folds is also reflected by the EA linear increase during collapse which reaches up to 827.5 J. The simulation results revealed further a 17.55 kJ/kg SEA capacity for the 15º obliquely crushed tube under contact-in-edge to the impactor, while CFE parameter is lied about 0.64.

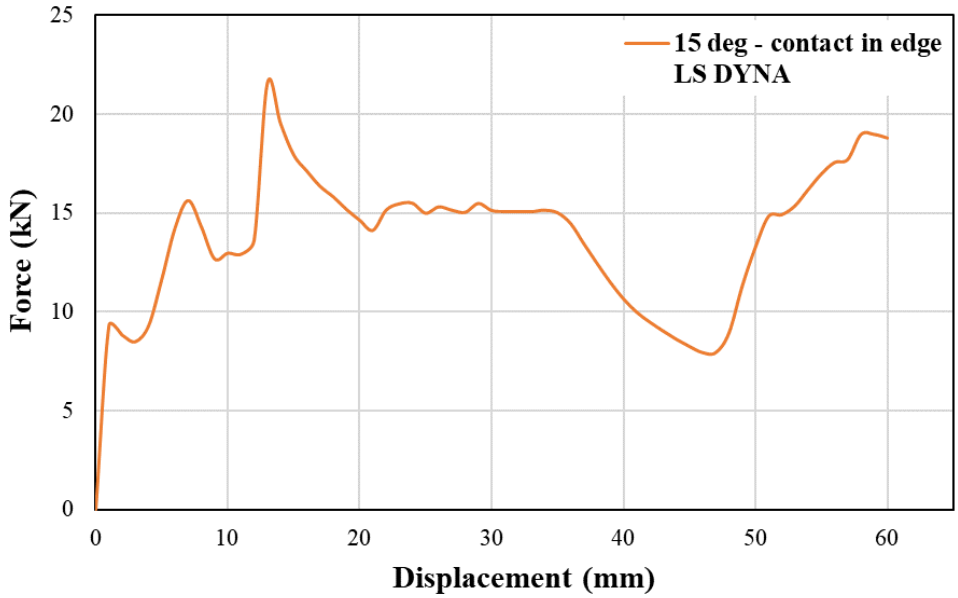


**Figure 132 Numerical F-x curve for 15º oblique loading under contact in edge**

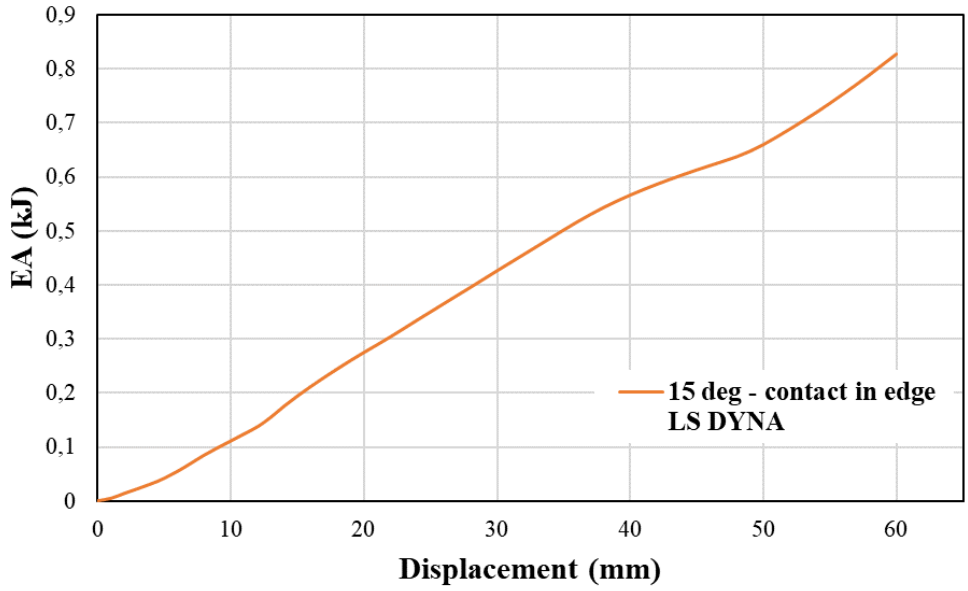


**Figure 133 Numerical EA-x curve for 15º oblique loading under contact in edge**

**Table 16 Numerical crashworthiness parameters for simulation case 4 under contact in edge**

| ***Numerical results – Simulation case 4 - edge*** | |
|---|---|
| **PCF (kN)** | 21.57 |
| **MCF (kN)** | 13.79 |
| **EA (J)** | 827.5 |
| **SEA (kJ/kg)** | 17.55 |
| **CFE (-)** | 0.64 |

Comparing to the simulation case 3-edge, the 15º obliquely crushed tube model revealed slightly lower PCF and EA due to the greater crushing angle the magnitude of which however seems to be flattened out above 10º crushing angle under contact-in-edge conditions. Observing the collapse states of the 15º obliquely crushed tube model under contact-in-edge with the impactor, the plastic collapse is developed under a controllable and progressive mode formulating 2 inextensional plastic folds as the local crushing force peaks in F-x curve reflect, while at following a slight bending of the deformed tube seems to occur in the range of 35 mm to 47 mm of impactor displacement where the crushing force reveals a local drop. The inextensional deformation mode of the formulated folds is paid on the circumferentially non-uniform bending moment distribution which reacts to a plastic fold stretching and compression in opposite directions.

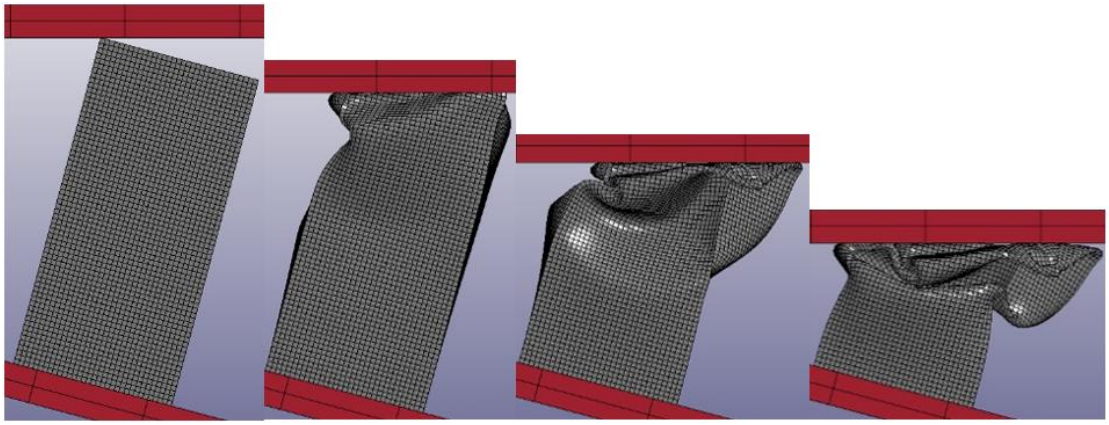

**Figure 134 Collapse states of simulation case 4 under contact in edge**

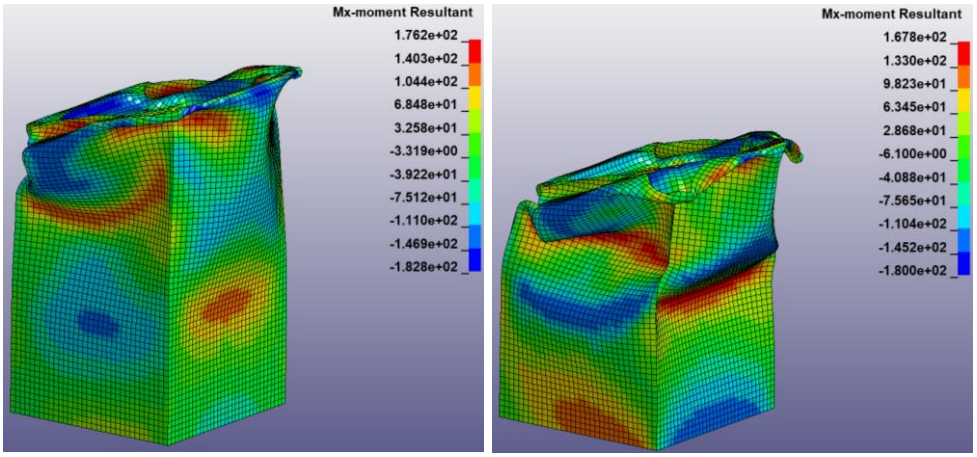


**Figure 135 Effect of bending moment distribution on inextensional folds formulation (simulation case 4-edge)**

**Figure 136 Final views of crushed tube model in simulation case 4 under contact in edge**

### 4.3.4.2 Initial contact in corner

The numerical simulation of the developed tube model subjected to 15$^{o}$ oblique impact loading under an initial contact-in-corner with the impactor revealed the depicted F-x and EA-x curves shown in the following figures, while the numerically estimated crashworthiness indicators are listed in Table17. As depicted in F-x curve, the plastic collapse initiates at about 23.49 kN PCF value progressing at next by formulating local peaks and lows in crushing force around 14.84 kN MCF. In F-x curve, the local peaks and lows of instantaneous crushing force reflect the plastic folds formulated during collapse revealing thus 2 formulated folds. The controllable and progressive behavior of plastic deformation under the formulation of 2 inextensional folds is also reflected by the EA linear increase during collapse which reaches up to 890.5 J. The simulation results revealed further a 18.89 kJ/kg SEA capacity for the 15$^{o}$ obliquely crushed tube under contact-in-corner to the impactor, while CFE parameter is lied about 0.63.

The 15$^{o}$ obliquely crushed tube model of simulation case 4-corner revealed a slightly lower PCF compared to 10$^{o}$ crushed tube with contact-in-corner, while both cases showed slightly greater PCF compared to the ones under an initial contact-in-edge between impactor and tube. Moreover, the EA capacity reveals a linear decrease with crushing angle under contact-in-corner maintained although in higher levels compared to EA under contact-in-edge for the same crushing angle values. Thus, an initial contact-in-corner shows to react to greater PCF and SEA than the ones under contact-in-edge, while EA drop with respect to crushing angle shows a linear dependence for cornered initial contact in contrast to EA decrease with crushing angle which reveals a sigma variance.

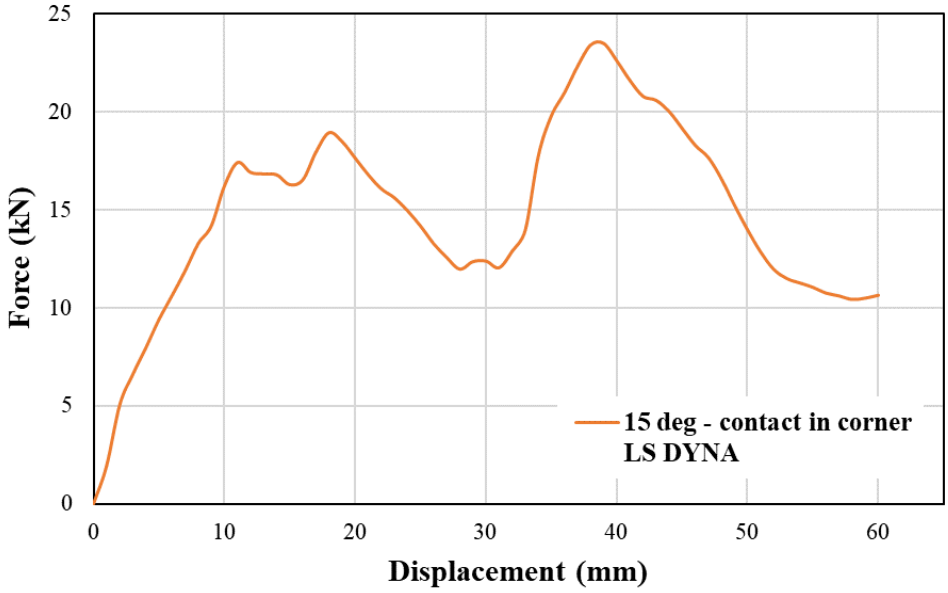


**Figure 137 Numerical F-x curve for 15$^{o}$ oblique loading under contact in corner**

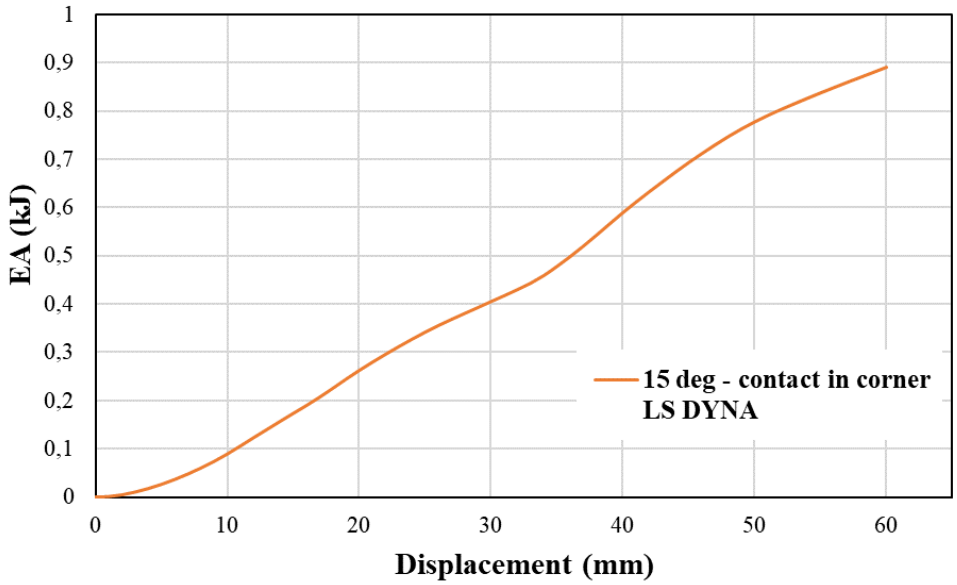


**Figure 138 Numerical EA-x curve for 15º oblique loading under contact in corner**

**Table 17 Numerical crashworthiness parameters for simulation case 4 under contact in corner**

| ***Numerical results – Simulation case 4 - corner*** | |
|---|---|
| **PCF (kN)** | 23.49 |
| **MCF (kN)** | 14.84 |
| **EA (J)** | 890.5 |
| **SEA (kJ/kg)** | 18.89 |
| **CFE (-)** | 0.63 |

Observing the collapse states of the 15º obliquely crushed tube model under contact-in-corner with the impactor, the plastic collapse is developed under a controllable and progressive mode formulating 2 inextensional plastic folds as the local crushing force peaks in F-x curve reflect. Finally, the inextensional deformation mode of the formulated folds is paid on the circumferentially non-uniform bending moment distribution which reacts to a plastic fold stretching and compression in opposite directions.

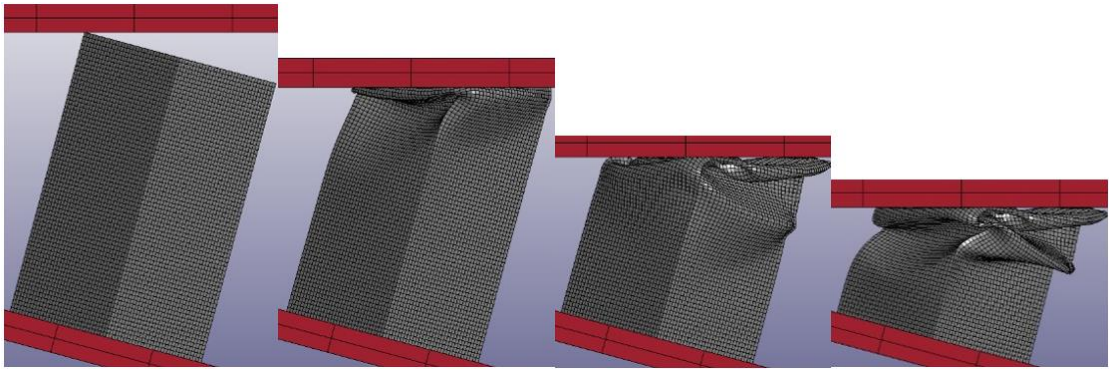

**Figure 139 Collapse states of simulation case 4 under contact in corner**

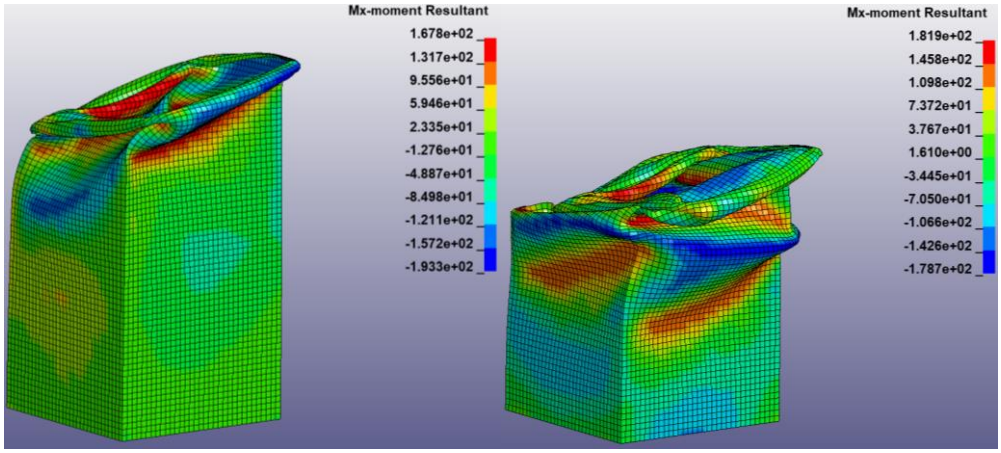


**Figure 140 Effect of bending moment distribution on inextensional folds formulation (simulation case 4-corner)**

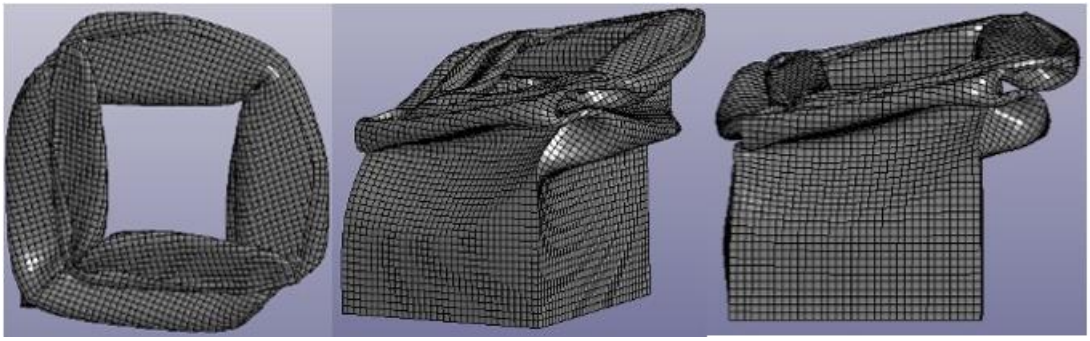

**Figure 141 Final views of crushed tube model in simulation case 4 under contact in corner**

## 4.4 Conclusions

By summarizing the provided numerical results, critical conclusions can be extracted for the crashworthiness response of the examined square tube models subjected to axial and oblique impact loading regarding the loading angle effect and the effect of initial contact type between impactor and tube. Tube model subjected to axial crushing revealed initially a local tearing around tube corners due to high bending moment concentration caused by the high enough PCF, while formulated at next two inextensional folds. In contrast, all obliquely crushed tube models revealed a controllable and progressive collapse mode by formulating inextensional folds avoiding any tearing due to lower PCF magnitude. The progressive inextensional collapse mode in each obliquely crushed tube model is further confirmed by the provided energy absorption distribution during the plastic deformation which increases linearly to the impactor displacement revealing a stable and progressive collapse mode.

In more specific, $5^o$ and $10^o$ obliquely crushed tube models showed 3 inextensional folds, while $15^o$ obliquely collapse models depicted 2 inextensional folds and a slight bending of tube model during the final stages of collapse. The formulation of inextensional plastic folds is also reflected by the local peaks and lows in crushing force distribution during collapse and it is paid on the non-uniformity of the circumferential bending moment distribution which reacts to a stretching and a compression of the tube sides in opposite directions. Regarding the revealed crashworthiness response indicators, Figures 143 and 144 depict the relative errors in PCF and EA between each simulation case and the two experimental tests respectively. As shown, experimental PCF and EA capacity are captured sufficiently by the numerical results providing deviation below 7.5% and 8% respectively.

Simulation case 1
Axial loading

Simulation case 2
5º loading
contact-in-edge

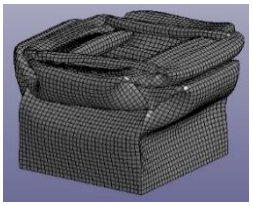

Simulation case 2
5º loading
contact-in-corner

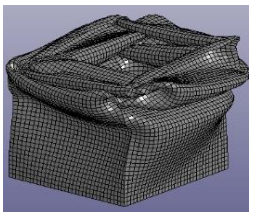

Simulation case 3
10º loading
contact-in-edge

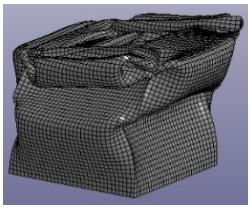

Simulation case 3
10º loading
contact-in-corner

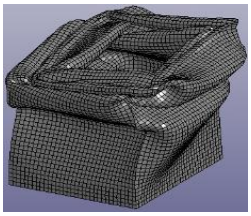

Simulation case 4
15º loading
contact-in-edge

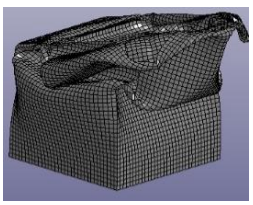

Simulation case 4
15º loading
contact-in-corner

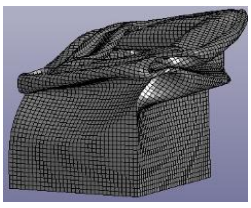

**Figure 142 Final views of crushed tube models**

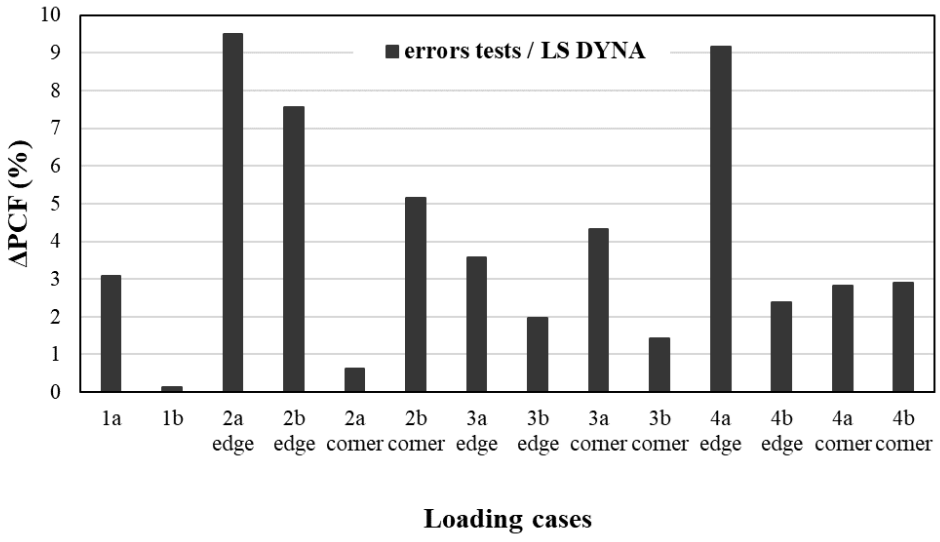


**Figure 143 PCF errors between tests and simulations**

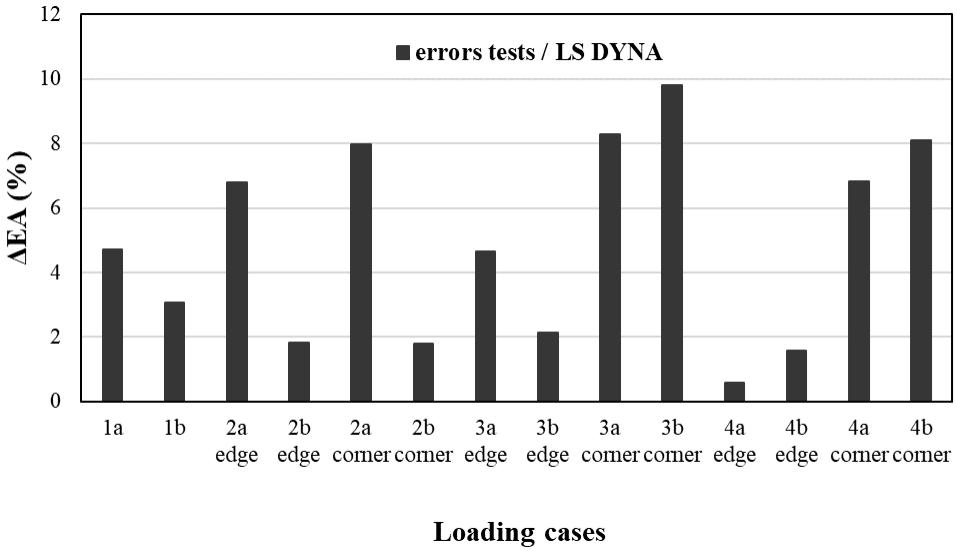


**Figure 144 EA errors between tests and simulations**

Regarding the crashworthiness performance of the simulated tube models, PCF reveals a decrease with respect to crushing angle due to the additional bending moment which is introduced by the lateral force component facilitating the plastic collapse initiation. Also, in all examined crushing angle range, PCF in contact-in-corner conditions is slightly greater than the one under contact-in-edge conditions, while also the oblique crushing cases showed a weakened crushing angle effect on PCF according to the numerical results.

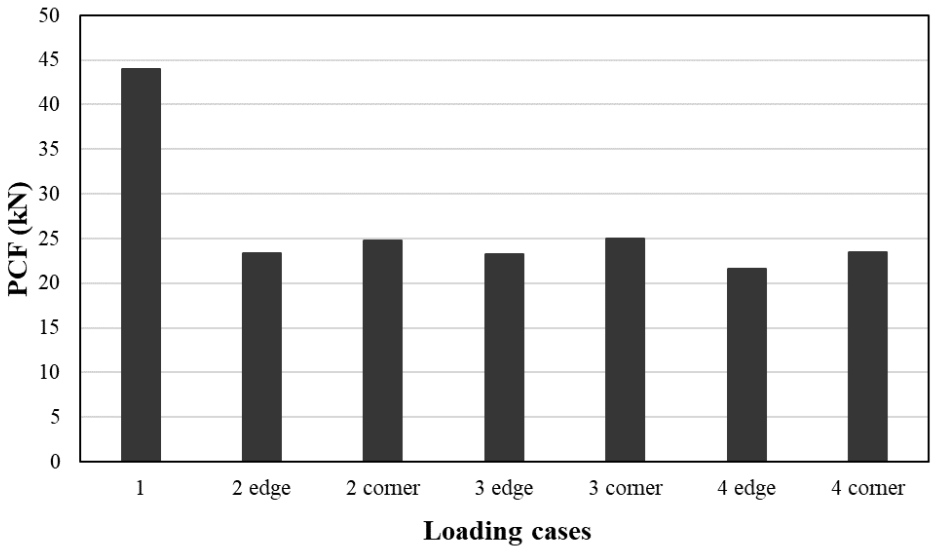


**Figure 145 PCF numerical results**

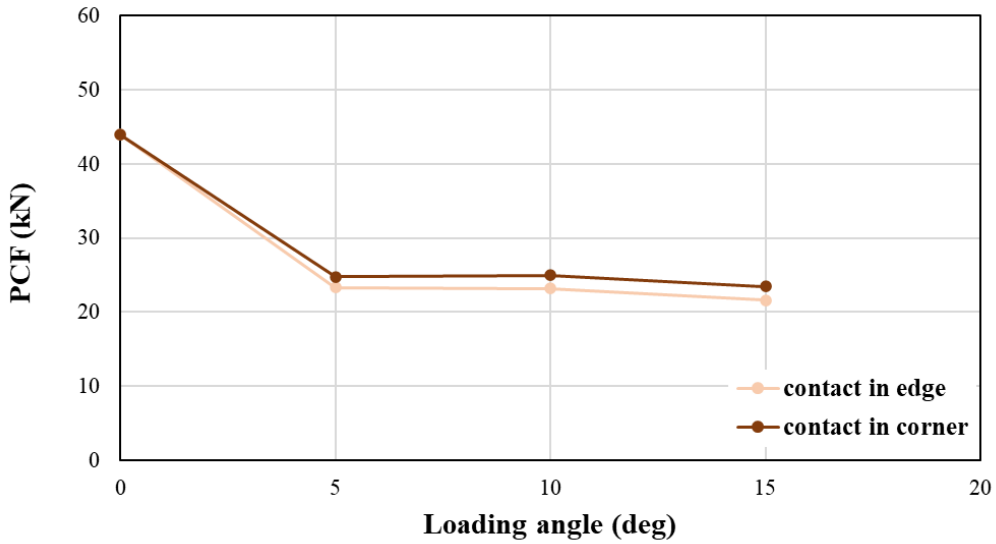


**Figure 146 PCF variation with loading angle and type of initial contact (numerical)**

Regarding the provided energy absorption capacity by the numerical simulations, MCF, EA and SEA are treated as the proper indicators in order to evaluate the crashworthiness performance of the tested tubes. The above response parameters reveal the same tendency with respect to the crushing angle and the initial type of contact as they are proportional metrics capturing thus similarly the tendency variations of the energy absorption capability. As depicted in the following figures, the maximum energy absorption capacity is revealed by the 5° oblique impact loading case under an initial contact-in-corner between impactor and tube. In fact, 5° cornered oblique crushing case revealed a greater EA compared to axial crushing due to tearing occurance in the last one which

caused an EA drop, while 5º edged crushing showed slightly lower EA compared to axially crushed tube model. Furthermore, as the crushing angle getting higher, EA reveals a decrease due to the additional bending moment introduced by lateral crushing force component facilitating both plastic collapse initiation and progress.

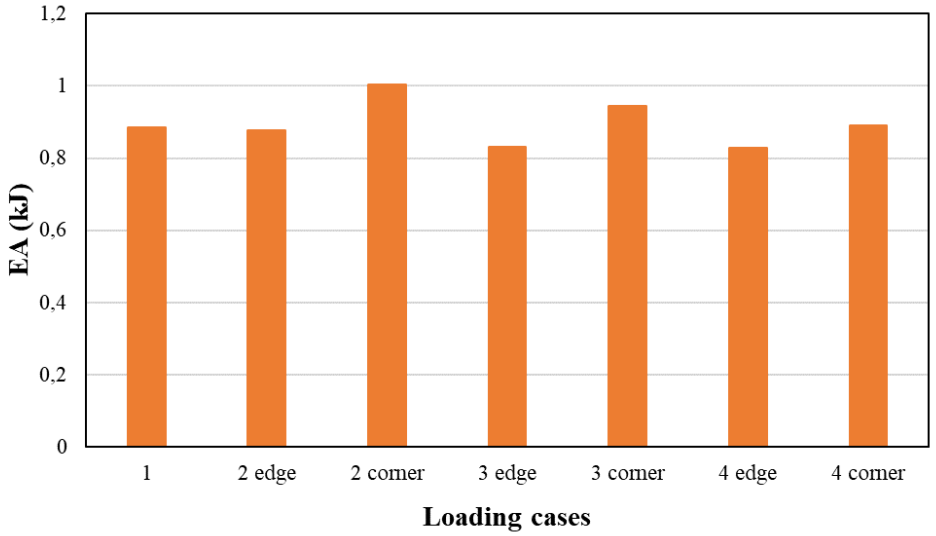


**Figure 147 EA numerical results**

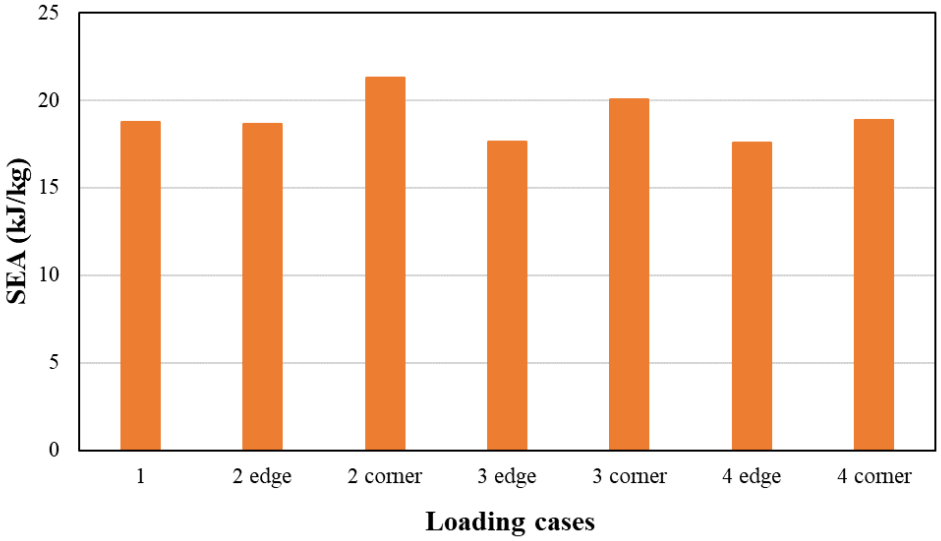


**Figure 148 SEA numerical results**

Moreover, in all examined oblique crushing angles, the contact-in-corner type reveals greater energy absorption capacity compared to the contact-in-edge type. Also, the cornered oblique crushing revealed a linear decrease of EA with respect to crushing angle, while the edged oblique crushing showed a sigma variance in EA reduction revealing a weaker crushing angle effect on energy

absorption. Thus, edged oblique crushing highlighted 10º as the critical crushing angle above from which slight bending mode is occurred during plastic collapse reducing EA, while cornered oblique impact loading does not reveal a critical crushing angle in the examined range until 15º showing a linear drop in EA. Thus, cornered oblique crushing conditions can be considered as more beneficial providing greater energy absorption capacity and an increased critical crushing angle compared to edged oblique loading.

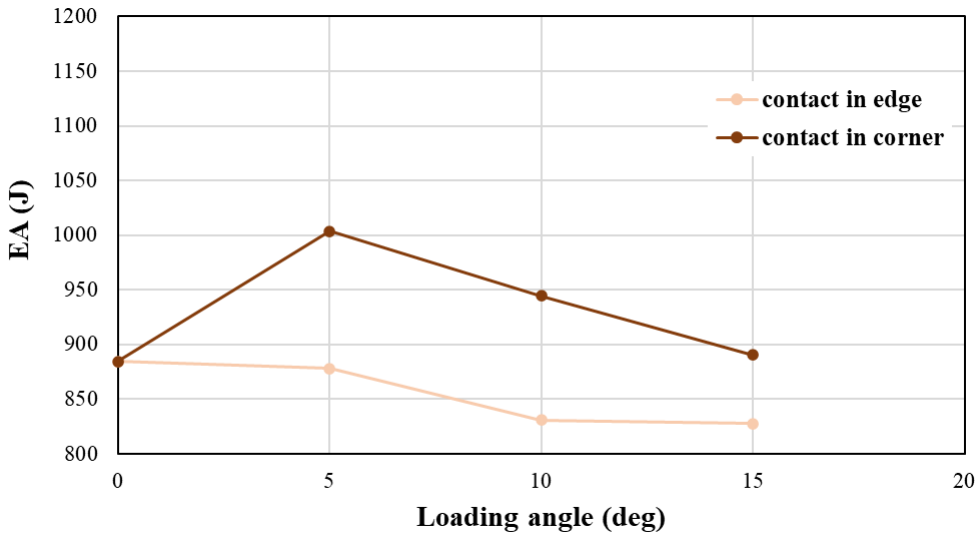


**Figure 149 EA variation with loading angle and type of initial contact (numerical)**

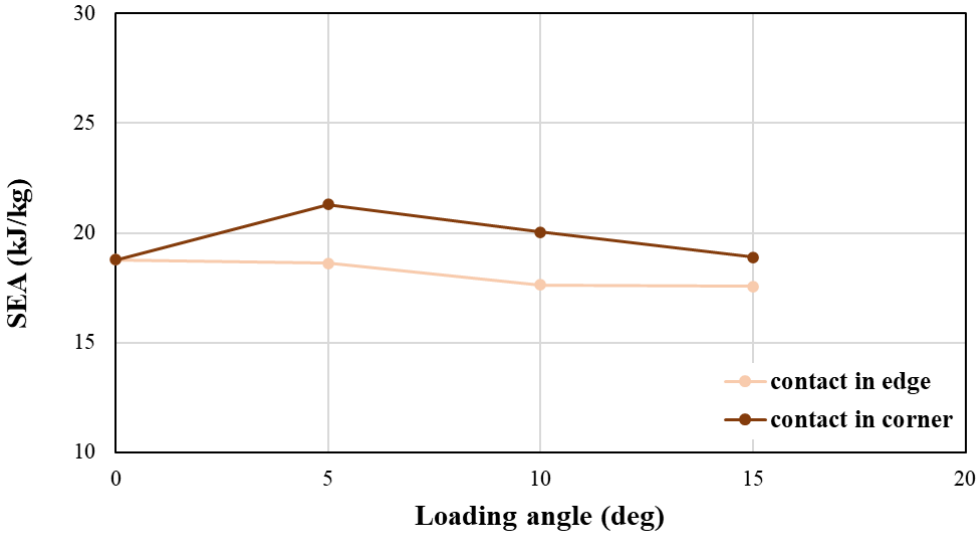


**Figure 150 SEA variation with loading angle and type of initial contact (numerical)**

CFE is captured at higher levels in the case of cornered oblique crushing conditions compared to edged oblique crushing, while as the crushing angle getting higher, the difference in CFE between edged and cornered oblique

loading is eliminated. Finally, a maximum CFE value is revealed for 5º cornered oblique impact as in axial crushing the occurred great enough PCF reacts to lower CFE. Thus, 5º cornered oblique crushing conditions can be considered as the most efficient among the examined ones providing the highest EA, SEA and CFE levels.

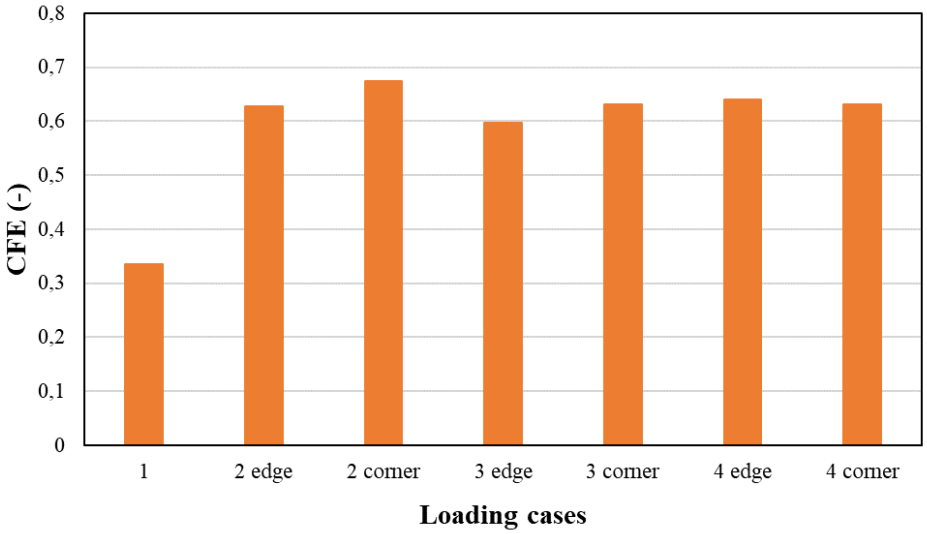


**Figure 151 CFE numerical results**

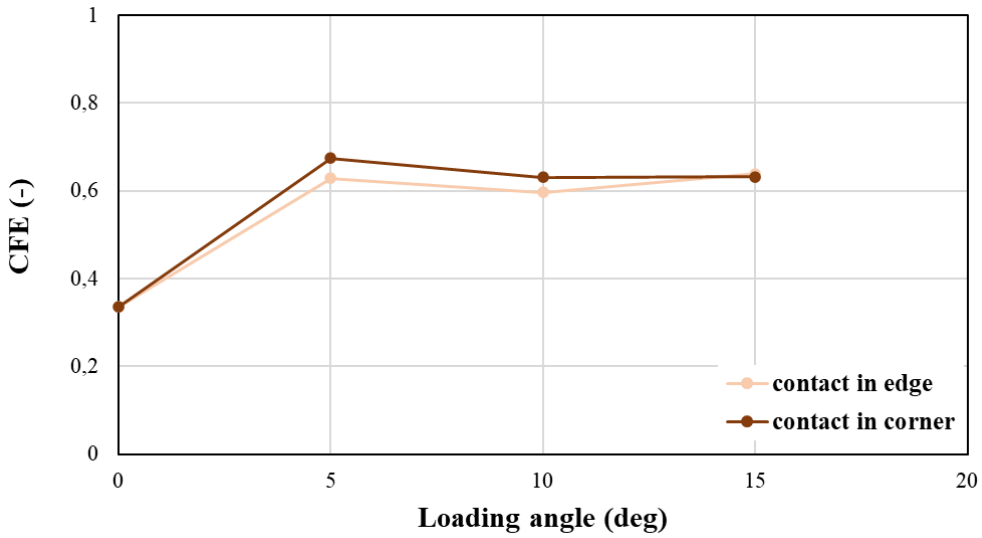


**Figure 152 CFE variation with loading angle and type of initial contact (numerical)**

# 5. Experimental vs. Numerical Simulation Results

## 5.1 Introduction

This chapter contains a comparison between the experimental and numerical results provided by the conducted quasi-static tests and the finite element simulation in LS DYNA respectively. In each examined case, the provided force-displacement curves and the revealed crashworthiness response parameters are presented and set into comparison, while further the final views of the crushed structures are also depicted in order to capture the predicted failure mechanism during plastic collapse.

The comparison between the experimental and numerical results aims to validate the developed finite element models behavior against the experimental data provided by the conducted tests in terms of both crashworthiness response metrics and predicted collapse mode. Finally, both experimental and numerical results are considered in order to evaluate the crashworthiness performance and efficiency of each examined case allowing for useful conclusions regarding the crashworthiness behavior of the designed structures.

## 5.2 Comparison of Experimental and Numerical Results

In the following sections of current chapter, the experimental and numerical results are set into comparison in terms of the revealed force-displacement (F-x) and energy absorption-displacement (EA-x) curves as well as the provided crashworthiness response parameters from the respective analysis. Also, the final views of crushed structures are compared in order to assess the modeling accuracy in predicting properly the occurred collapse mechanism in terms of the type and the number of formulated folds. In each examined case, the numerical results are compared against both conducted tests (test-a and test-b) revealing their relative error in the estimated crashworthiness parameters in order to evaluate their validity and assess the response behavior with the highest level of accuracy and reliance.

### 5.2.1 Axial Loading – Case 1

For the axial loading case of aluminium square tube, simulation seems to capture sufficiently the force distribution as depicted in Figure 153, showing an absolute accuracy in predicted PCF compared to experimental results, while also the force variance during plastic collapse progress is predicted sufficiently revealing a deviation in energy absorption about 3%. In fact, the crushing force

variance tendency is further captured sufficiently as the numerical results capture the force decrease after the initial formulated fold at PCF.

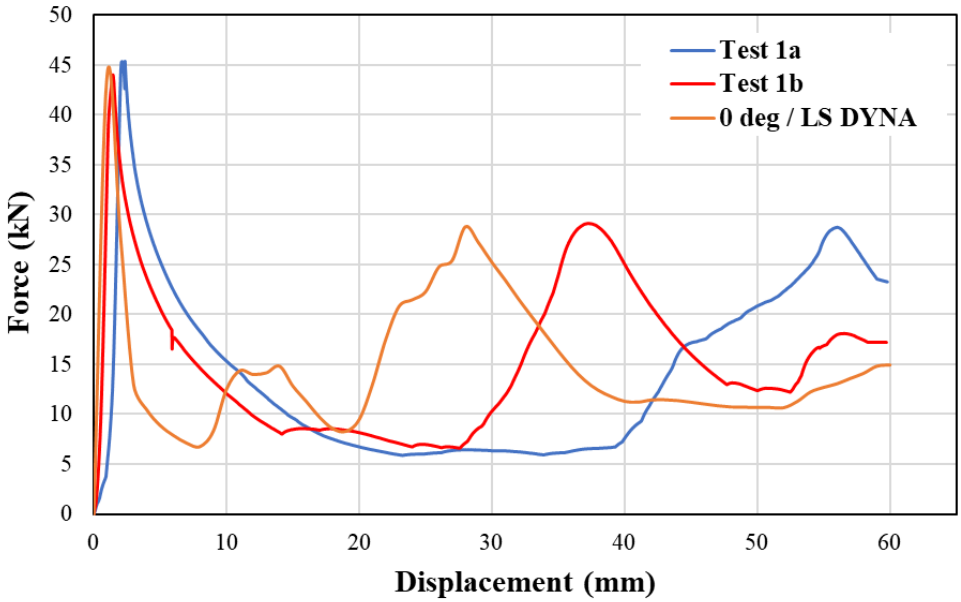


**Figure 153 Experimental vs. numerical F-x curves for axial loading**

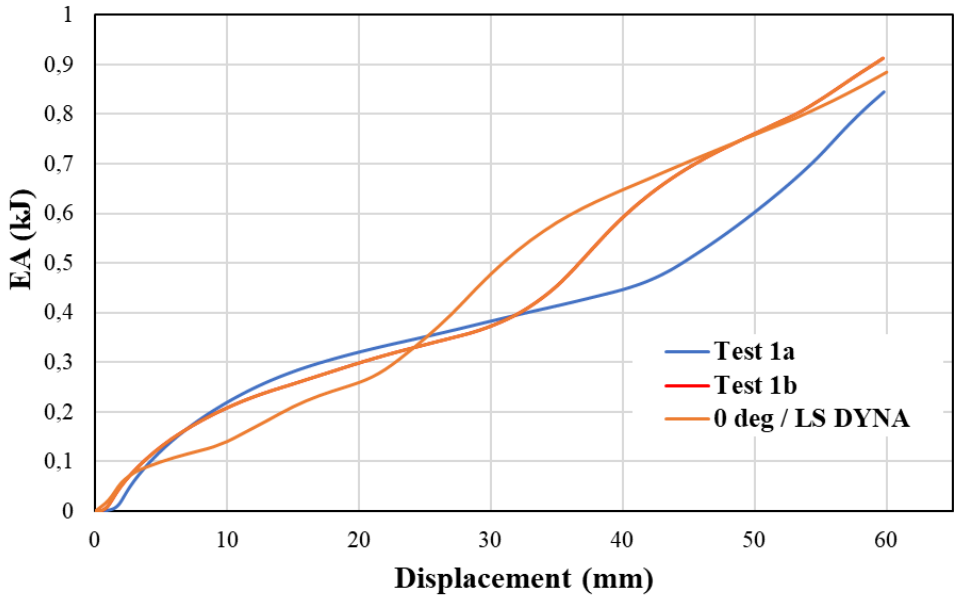


**Figure 154 Experimental vs. numerical EA-x curves for axial loading**

The occurred crushing force decrease is caused by the local tube tearing around its corners due to the high enough PCF which resulted in significant bending moment concentration around the corners of the squared cross-section. Further, the model shows an agreement with test 1b on the formulation of 2 more inextensional plastic folds reflected by the local force peaks in the post-buckling

region of F-x curves. Therefore, EA increase rate during plastic collapse shows an initial drop due to tube tearing which results in energy absorption decrease, however as the inextensional collapse mode progresses formulating folds EA increases linearly to the impactor displacement due to the progressive and stable behavior of the collapse mechanism. In fact, the above tendency is captured sufficiently between FE model and test 1b, while in contrast test 1a reflects the same tendency at higher impactor displacement as the formulation of the folds took place later during collapse in that case. CFE is also captured sufficiently by the finite element (FE) model showing an error about 3.4% as both PCF and EA are estimated accurately.

**Table 18 Results in comparison between tests and simulation for case 1**

| ***Axial loading – case 1*** | | | |
|---|---|---|---|
| | LS DYNA | Test 1a | Test 1b |
| **PCF (kN)** | 43.96 | 45.36 | 44.02 |
| **MCF (kN)** | 14.74 | 14.13 | 15.28 |
| **EA (J)** | 884.6 | 844.9 | 912.7 |
| **SEA (kJ/kg)** | 18.76 | 17.92 | 19.36 |
| **CFE (-)** | 0.34 | 0.31 | 0.35 |
| | | | |
| | LS DYNA – Test 1a error (%) | LS DYNA – Test 1b error (%) | |
| **PCF** | 3.07 | 0.13 | |
| **EA** | 4.70 | 3.07 | |
| **CFE** | 7.65 | 3.39 | |

Finally, regarding the plastic collapse mechanism, both FE models and experimental tests agreed on an inextensional collapse mode with a local tearing taken place around tube corners, while further FE model predicted accurately the 2 formulated folds during collapse as also revealed from test 1b.

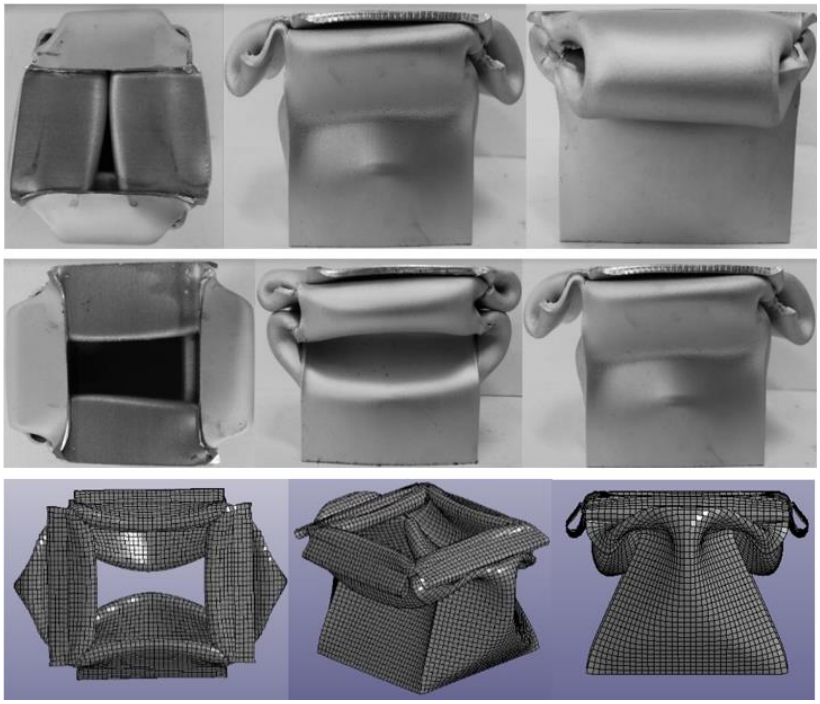

**Figure 155 Collapsed structures for case 1 (top: test 1a, mid: test 1b, bottom: LS DYNA)**

## 5.2.2 Oblique Loading under 5º – Case 2

### 5.2.2.1 Initial contact in edge

For the 5º obliquely loading tube under an initial contact-in-edge with the impactor, simulation and experimental tests revealed a sufficient agreement on crushing force distribution as depicted in Figure 156, showing an error in PCF of 7.5%, while EA error lied about 1.8%. Further, Figure 156 shows that the local peaks in crushing force are captured accurately by the FE model reflecting the formulation of plastic folds. In more specific, both simulation and tests revealed the formulation of 3 inextensional plastic folds, the progressive and stable behavior of which are reflected by the linear EA increase during plastic deformation. However, the two tests revealed further a slight tearing occurance around tube corners which are not captured by the FE model as the lower PCF compared to axial loading did not seem enough to predict the material failure around the tube corner as achieved by the axial loading simulation. Although, that did not prove to affect the accuracy level of the estimated energy absorption capability which is predicted sufficiently as the occurred tearing in tests did not prove to be enough for changing the progressive and stable behavior of inextensional mode of deformation which resulted in a uniform EA increase rate with respect to the impactor displacement.

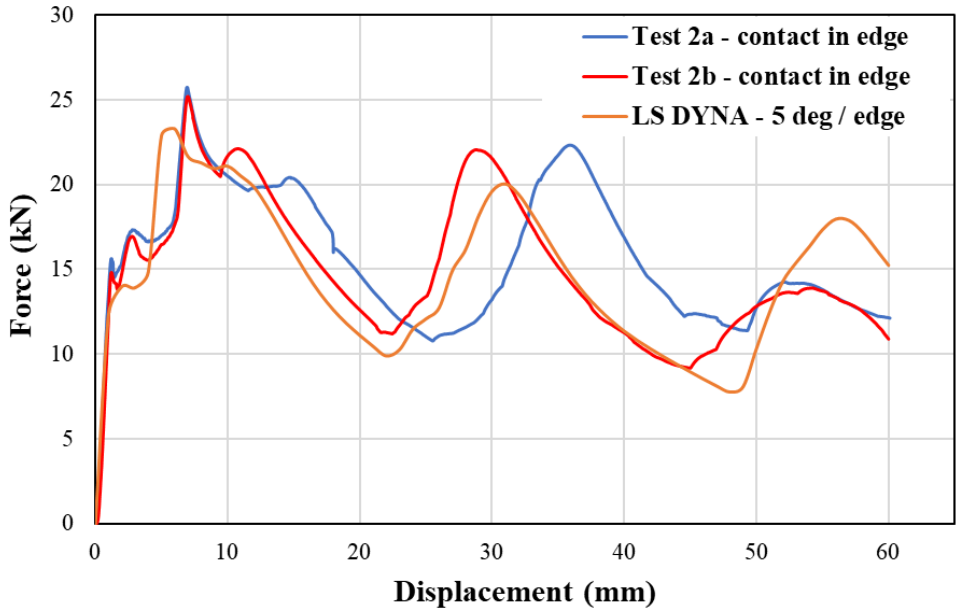


**Figure 156 Experimental vs. numerical F-x curves for 2-edge case**

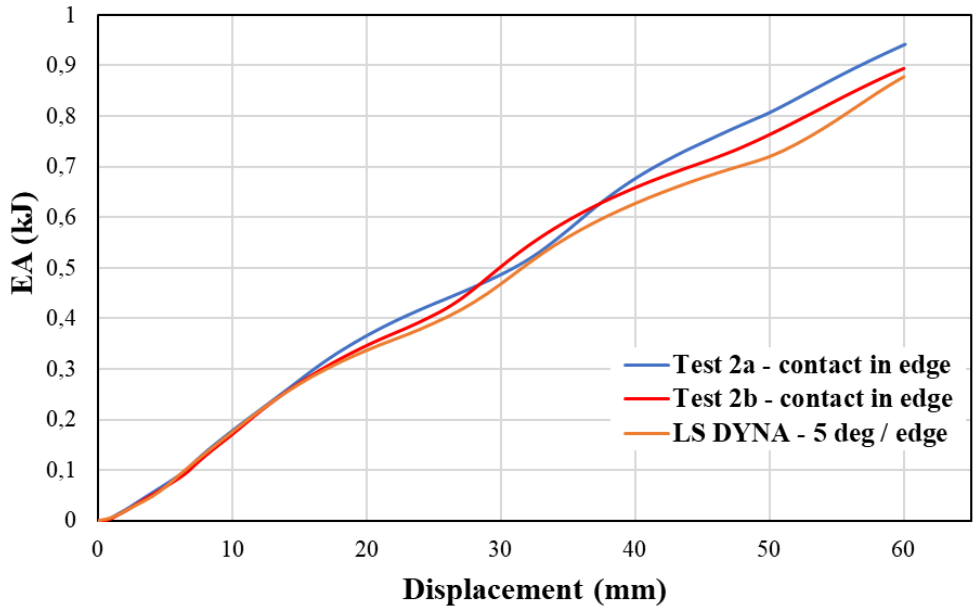


**Figure 157 Experimental vs. numerical EA-x curves for 2-edge case**

Finally, regarding the plastic collapse mechanism, both FE models and experimental tests agreed on an inextensional collapse mode under 3 inextensional formulated plastic folds. However, the occurred slight corner tearing in tests is not captured by the FE model due to the lower PCF which was not enough to result in material failure during the simulation, without although affecting the accuracy level of the EA prediction due to the weak magnitude of tearing effect which was not developed in significant extent.

**Table 19 Results in comparison between tests and simulation for case 2-edge**

| *5º oblique loading – case 2-edge* | | | |
|---|---|---|---|
| | LS DYNA | Test 2a-edge | Test 2b-edge |
| **PCF (kN)** | 23.3 | 25.75 | 25.21 |
| **MCF (kN)** | 14.6 | 15.68 | 14.90 |
| **EA (J)** | 878.0 | 942.1 | 894.2 |
| **SEA (kJ/kg)** | 18.62 | 19.98 | 18.97 |
| **CFE (-)** | 0.63 | 0.61 | 0.59 |
| | | | |
| | LS DYNA – Test 2a error (%) | LS DYNA – Test 2b error (%) | |
| **PCF** | 9.50 | 7.57 | |
| **EA** | 6.80 | 1.82 | |
| **CFE** | 3.15 | 6.23 | |

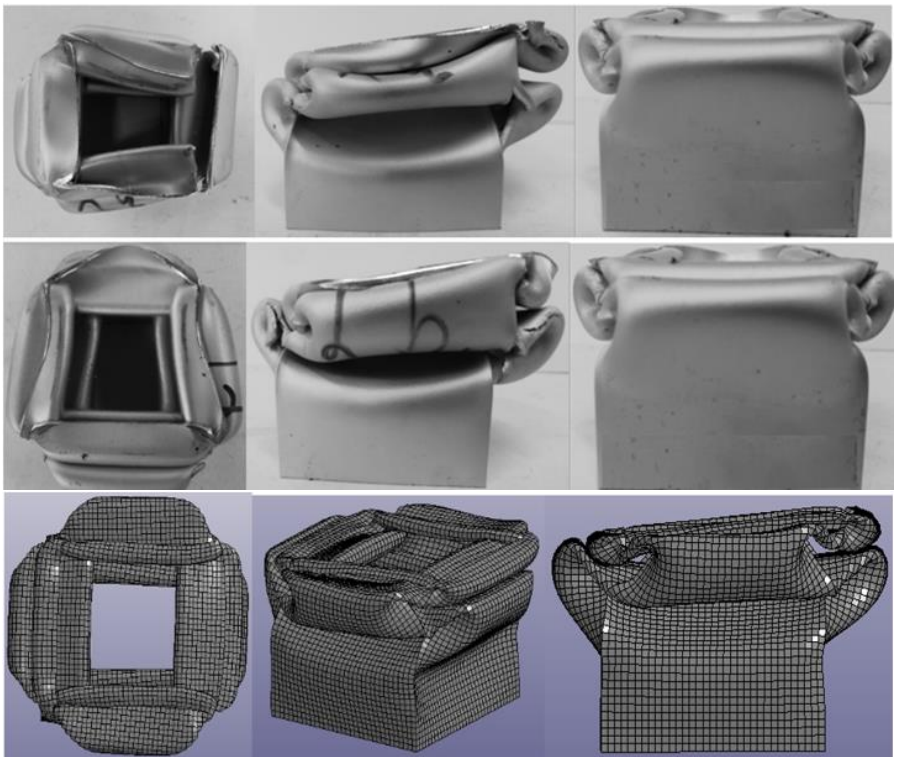

**Figure 158 Collapsed structures for case 2-edge (top: test 2a, mid: test 2b, bottom: LS DYNA)**

### 5.2.2.2 Initial contact in corner

For the 5º obliquely loading tube under an initial contact-in-corner with the impactor, simulation and experimental tests revealed a sufficient agreement on crushing force distribution as depicted in Figure 159, showing an absolute agreement in PCF between test 2a and simulation, while EA error lied about 1.8%. Further, Figure 159 shows that the local peaks in crushing force are captured sufficiently by the FE model reflecting the formulation of plastic folds. In more specific, both simulation and tests revealed the formulation of 3 inextensional plastic, folds the progressive and stable behavior of which are reflected by the linear EA increase during plastic deformation. However, the two tests revealed further a slight tearing occurance around tube corners which are not captured by the FE model as the lower PCF compared to axial loading did not seem enough to predict the material failure around the tube corner as achieved by the axial loading simulation. Although, that did not prove to affect the accuracy level of the estimated energy absorption capability which is predicted sufficiently as the occurred tearing in tests did not prove to be enough for changing the progressive and stable behavior of inextensional mode of deformation which resulted in a uniform EA increase rate with respect to the impactor displacement.

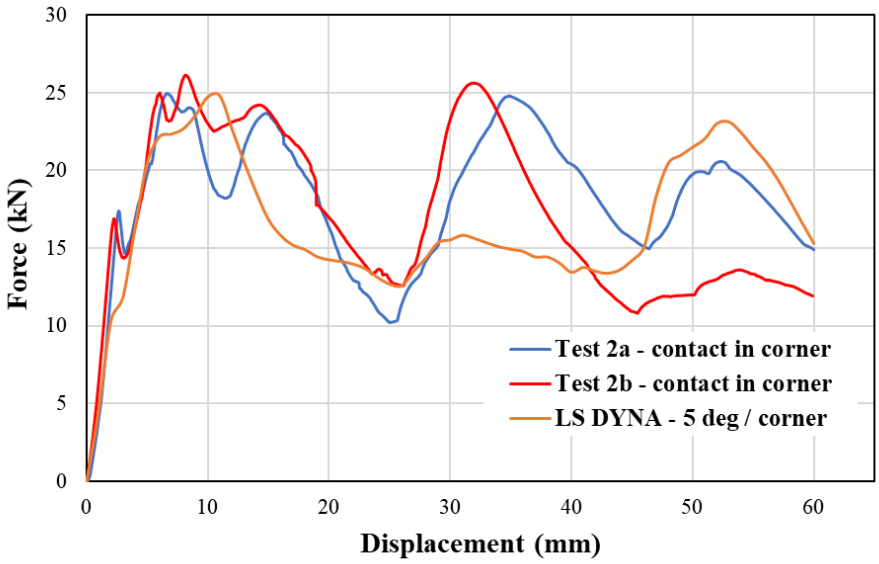


**Figure 159 Experimental vs. numerical F-x curves for 2-corner**

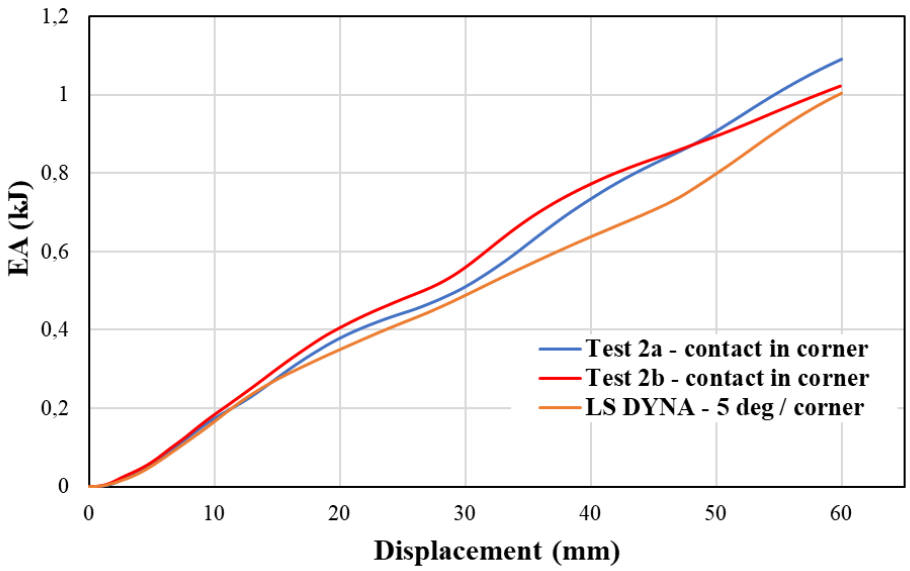


**Figure 160 Experimental vs. numerical EA-x curves for 2- corner**

**Table 20 Results in comparison between tests and simulation for case 2-corner**

| *5° oblique loading – case 2-corner* | | | |
|---|---|---|---|
| | LS DYNA | Test 2a-corner | Test 2b-corner |
| **PCF (kN)** | 24.80 | 24.95 | 26.14 |
| **MCF (kN)** | 16.73 | 18.17 | 17.06 |
| **EA (J)** | 1003.6 | 1090.4 | 1021.9 |
| **SEA (kJ/kg)** | 21.29 | 23.13 | 21.68 |
| **CFE (-)** | 0.67 | 0.73 | 0.65 |
| | | | |
| | LS DYNA – Test 2a error (%) | LS DYNA – Test 2b error (%) | |
| **PCF** | 0.63 | 5.15 | |
| **EA** | 7.96 | 1.79 | |
| **CFE** | 7.38 | 3.37 | |

Finally, regarding the plastic collapse mechanism, both FE models and experimental tests agreed on an inextensional collapse mode under 3 inextensional formulated plastic folds. However, the occurred slight corner tearing in tests is not captured by the FE model due to the lower PCF which was not enough to result in material failure during the simulation, without although

affecting the accuracy level of the EA prediction due to the weak magnitude of tearing effect which was not developed in significant extent.


**Figure 161 Collapsed structures for case 2-corner (top: test 2a, mid: test 2b, bottom: LS DYNA)**

## 5.2.3 Oblique Loading under 10º – Case 3

### 5.2.3.1 Initial contact in edge

For the 10º obliquely loading tube under an initial contact-in-edge with the impactor, both numerical and experimental results showed a sufficient agreement on crushing force distribution as depicted in Figure 162, revealing a deviation of about 2% in both PCF and EA. Further, Figure 162 shows that the local peaks in crushing force are captured accurately by the FE model reflecting the formulation of plastic folds. More specifically, both simulation and tests revealed the formulation of 3 inextensional plastic folds, while EA linear increase during collapse reflects the progressive and stable behavior of the inextensional deformation mode. However, the two tests revealed also a slight tearing occurance around tube corners which is not captured by the FE model as the lower PCF compared to axial loading did not seem enough to predict the

material failure around the tube corner. Although, that did not prove to affect the accuracy level of the estimated energy absorption capability which is predicted sufficiently as the occurred tearing in tests did not prove to be enough for changing the progressive and stable behavior of inextensional mode of deformation which resulted in a uniform EA increase rate with respect to the impactor displacement.

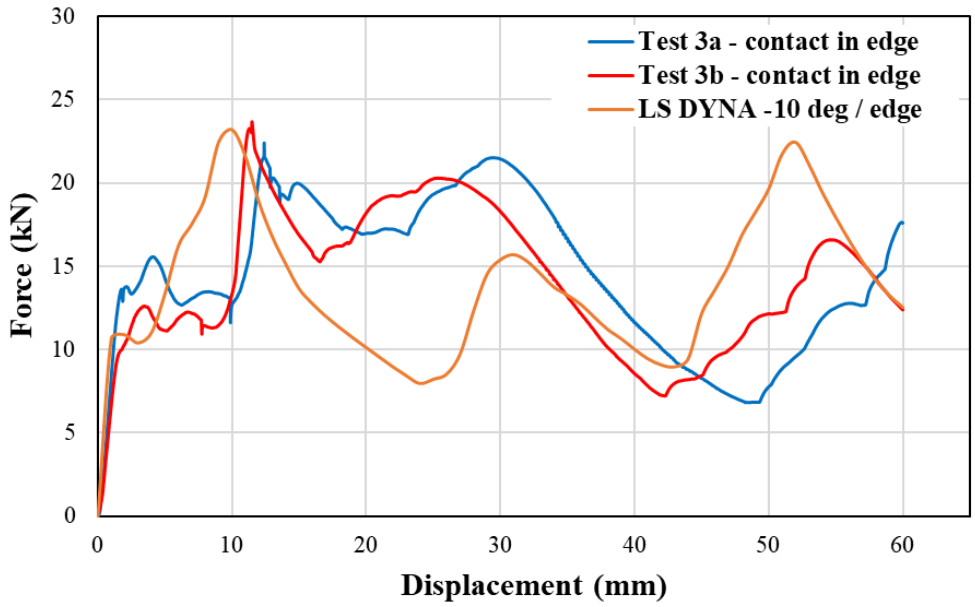


**Figure 162 Experimental vs. numerical F-x curves for 3-edge case**

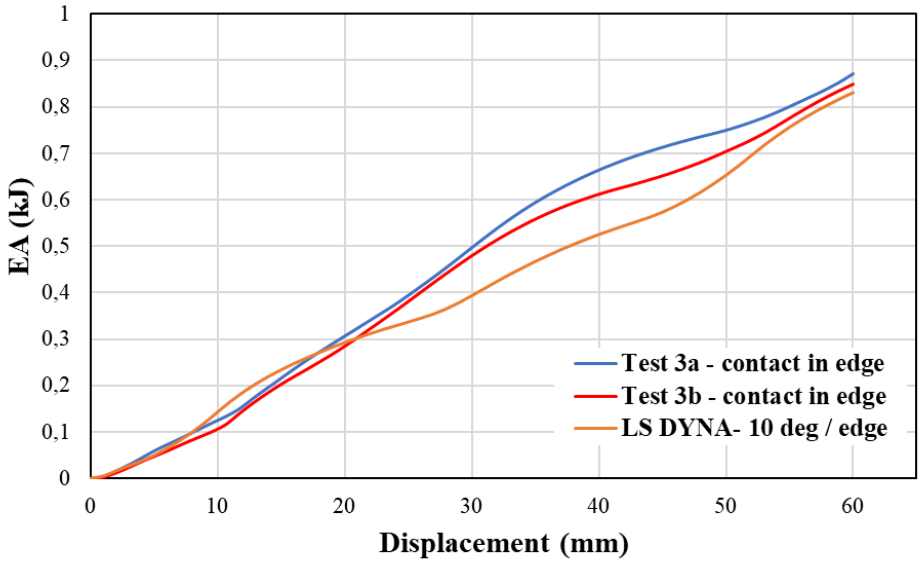


**Figure 163 Experimental vs. numerical EA-x curves for 3-edge case**

**Table 21 Results in comparison between tests and simulation for case 3-edge**

| *10º oblique loading – case 3-edge* | | | |
|---|---|---|---|
| | LS DYNA | Test 3a-edge | Test 3b-edge |
| **PCF (kN)** | 23.20 | 22.40 | 23.65 |
| **MCF (kN)** | 13.85 | 14.53 | 14.15 |
| **EA (J)** | 830.9 | 871.6 | 849.0 |
| **SEA (kJ/kg)** | 17.62 | 18.49 | 18.01 |
| **CFE (-)** | 0.60 | 0.65 | 0.60 |
| | | | |
| | LS DYNA – Test 3a error (%) | LS DYNA – Test 3b error (%) | |
| **PCF** | 3.57 | 1.97 | |
| **EA** | 4.66 | 2.12 | |
| **CFE** | 7.95 | 0.16 | |

Finally, regarding the plastic collapse mechanism, both FE models and experimental tests agreed on an inextensional collapse mode under 3 inextensional formulated plastic folds. However, the occurred slight corner tearing in tests is not captured by the FE model as PCF was not high enough to react to a material failure during simulation which although did not affect the predicted energy absorption capability.

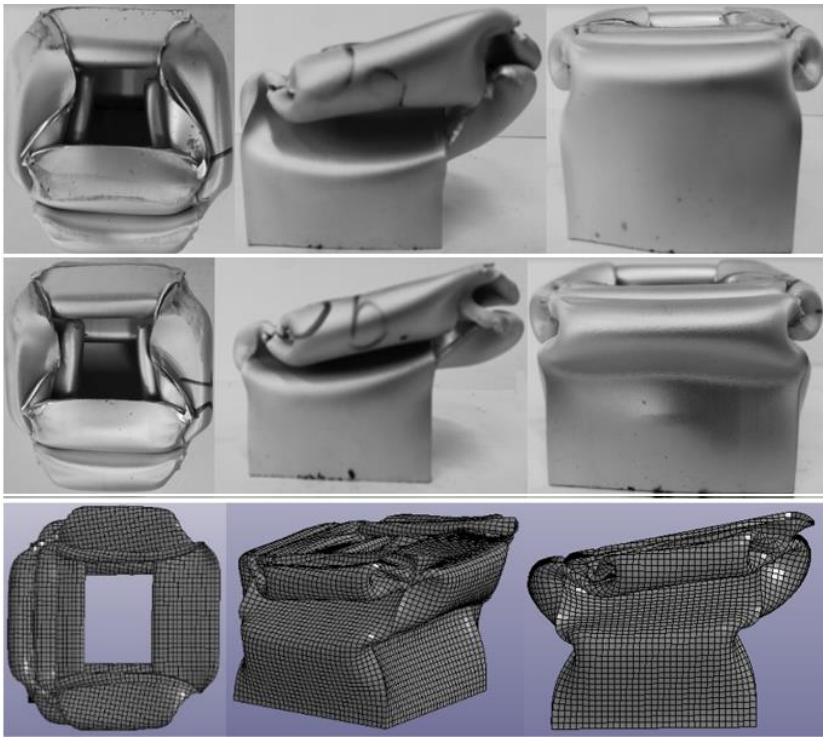

**Figure 164 Collapsed structures for case 3-edge (top: test 3a, mid: test 3b, bottom: LS DYNA)**

### 5.2.3.2 Initial contact in corner

For the 10$^{o}$ obliquely loading tube under an initial contact-in-corner with the impactor, simulation and experimental tests revealed a sufficient agreement on crushing force variance during collapse revealing a 1.4% error in PCF, while the deviation in EA lied about 8%. Further, Figure 165 shows that the local peaks in crushing force are captured sufficiently by the FE model reflecting the formulation of plastic folds. In more specific, both simulation and test 3b revealed the formulation of 3 inextensional plastic in contrast to test 3a in which 2 inextensional folds were observed. Moreover although, slight tearing was occurred around tube corners in both experimental tests which FE model failed to capture as PCF did not seem enough to bring material failure at the tube corners. However, the weak magnitude of the occurred tearing in tests did not manage to affect strongly the energy absorption capability of the crushed tube which is also reflected by the linear increase of EA during impactor displacement due to the progressive and stable behavior of inextensional plastic deformation mode. Therefore, that allowed simulation to capture sufficiently the energy absorption capacity of the 10$^{o}$ obliquely crushed tube under a contact-in-corner.

Regarding the plastic collapse mechanism, 3 inextensional plastic folds were revealed by FE model and test 3b, while test 3a showed 2 formulated folds. Finally, the occurred slight corner tearing in tests was not captured by the FE model without although affecting the accuracy level of the EA prediction due to

the weak magnitude of tearing effect which was not developed in significant extent.

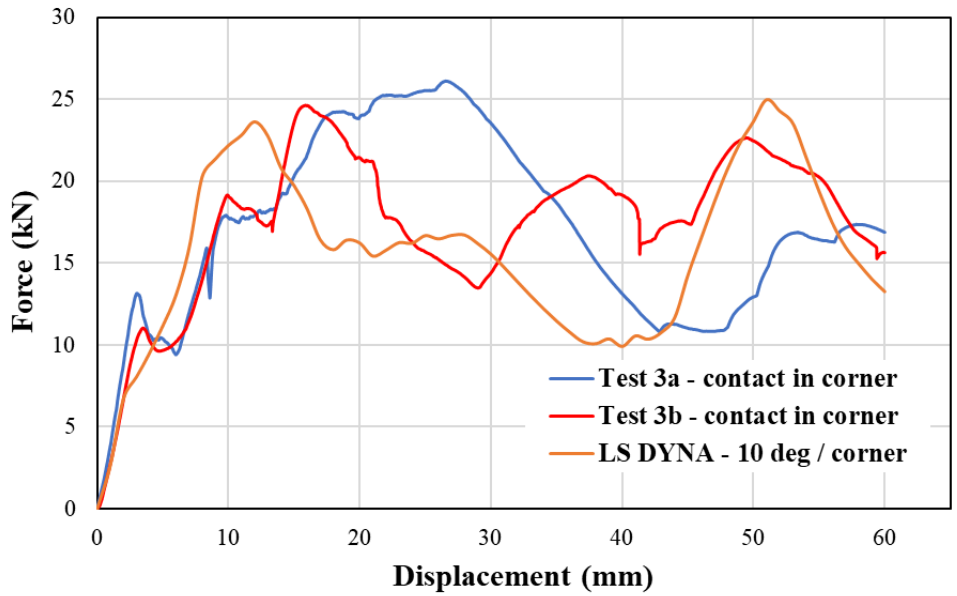


**Figure 165 Experimental vs. numerical F-x curves for 3-corner**

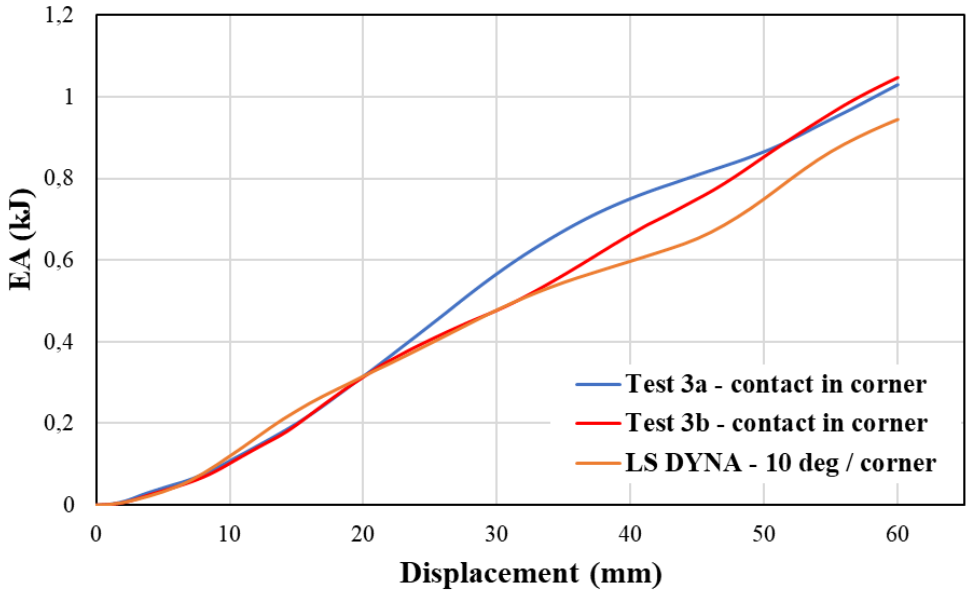


**Figure 166 Experimental vs. numerical EA-x curves for 3-corner**

**Table 22 Results in comparison between tests and simulation for case 3-corner**

| *10º oblique loading – case 3-corner* | | | |
|---|---|---|---|
| | LS DYNA | Test 3a-corner | Test 3b-corner |
| **PCF (kN)** | 24.98 | 26.11 | 24.62 |
| **MCF (kN)** | 15.74 | 17.16 | 17.45 |
| **EA (J)** | 944.6 | 1029.8 | 1047.3 |
| **SEA (kJ/kg)** | 20.04 | 21.84 | 22.22 |
| **CFE (-)** | 0.63 | 0.66 | 0.71 |
| | | | |
| | LS DYNA – Test 3a error (%) | LS DYNA – Test 3b error (%) | |
| **PCF** | 4.33 | 1.44 | |
| **EA** | 8.27 | 9.81 | |
| **CFE** | 4.11 | 11.08 | |

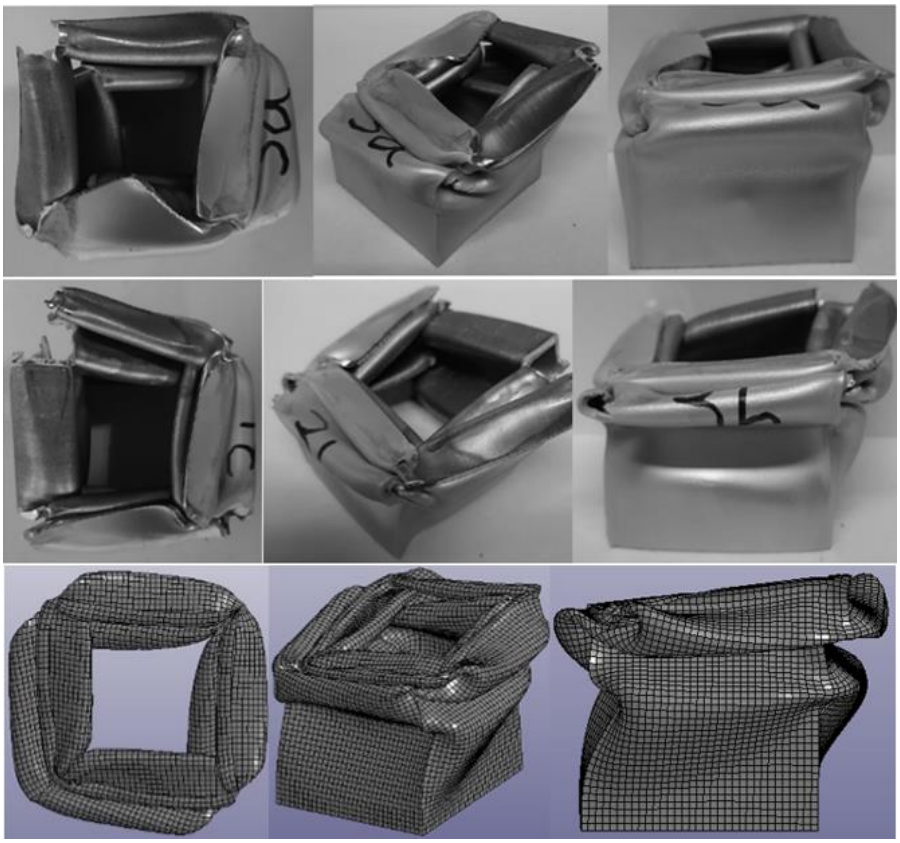

**Figure 167 Collapsed structures for case 3-corner (top: test 3a, mid: test 3b, bottom: LS DYNA)**

## 5.2.4 Oblique Loading under 15º – Case 4

### 5.2.4.1 Initial contact in edge

For the 15º obliquely loading tube under an initial contact-in-edge with the impactor, both numerical and experimental results showed a sufficient agreement on PCF revealing an error of 2.38%. In addition, the crushing force distribution during plastic collapse is captured accurately by the FE model allowing for an accurate prediction in EA capability where FE model and experimental results showed a deviation of 0.57% regarding test 4a. Moreover, the number of formulated folds is also predicted accurately by the FE model capturing two inextensional folds reflected further by the two local peaks in crushing force during collapse as depicted in the following figure.

Also, the inextensional mode of plastic deformation allowed for a stable and progressive behavior of collapse reflected by the linear EA increase with respect to impactor displacement showing a uniform increase rate. However, the slight tube corner tearing which occurred during the two tests is not captured by the FE model as PCF was not proved great enough to react to material failure around tube corners. Although that FE model failed to predict the tearing occurance, the EA is captured sufficiently as the tearing magnitude in the tests seemed to be low without thus reacting to a significant EA decrease.

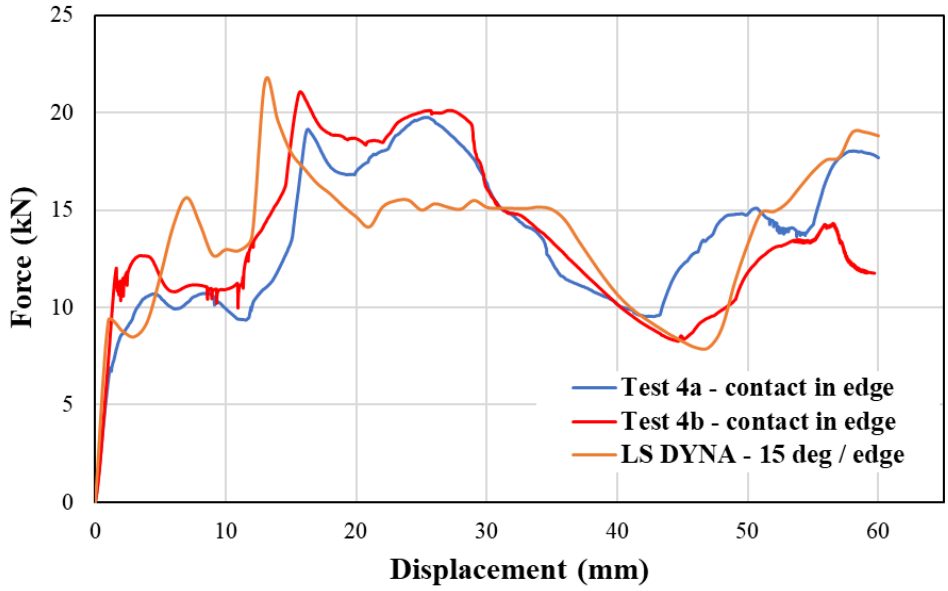


**Figure 168 Experimental vs. numerical F-x curves for 4-edge case**

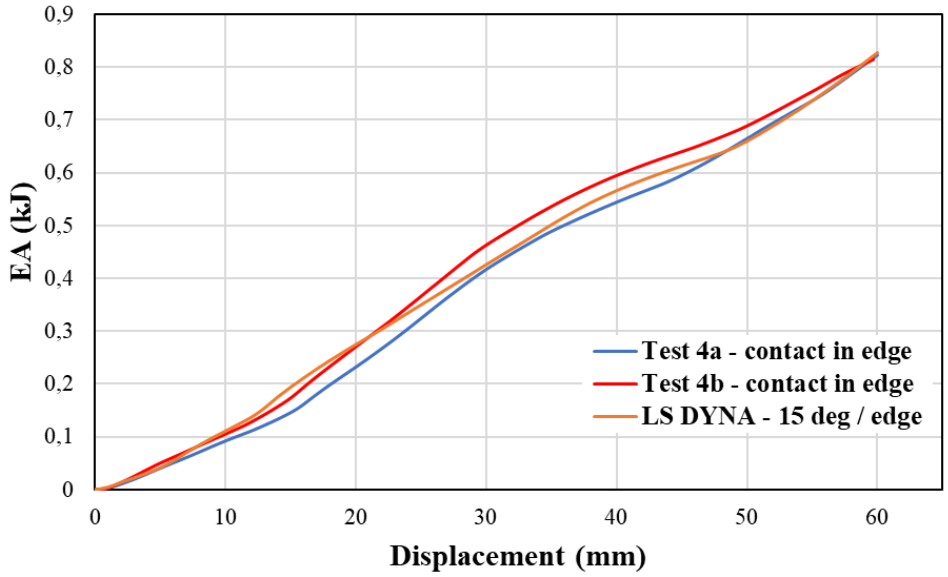


**Figure 169 Experimental vs. numerical EA-x curves for 4-edge case**

**Table 23 Results in comparison between tests and simulation for case 4-edge**

| *15º oblique loading – case 4-edge* | | | |
|---|---|---|---|
| | LS DYNA | Test 4a-edge | Test 4b-edge |
| **PCF (kN)** | 21.57 | 19.76 | 21.07 |
| **MCF (kN)** | 13.79 | 13.71 | 13.58 |
| **EA (J)** | 827.5 | 822.8 | 814.8 |
| **SEA (kJ/kg)** | 17.55 | 17.45 | 17.28 |
| **CFE (-)** | 0.64 | 0.69 | 0.65 |
| | | | |
| | LS DYNA – Test 4a error (%) | LS DYNA – Test 4b error (%) | |
| **PCF** | 9.16 | 2.38 | |
| **EA** | 0.57 | 1.56 | |
| **CFE** | 7.87 | 0.80 | |

Finally, regarding the plastic collapse mechanism, both FE models and experimental tests revealed a sufficient agreement on both deformation mode and the number of formulated folds showing an inextensional collapse mechanism under 2 plastic folds. However, the occurred slight corner tearing in tests is not captured by the FE model as PCF was not high enough to react to a

material failure during simulation which although did not affect the predicted energy absorption capability due to the low tearing extent.

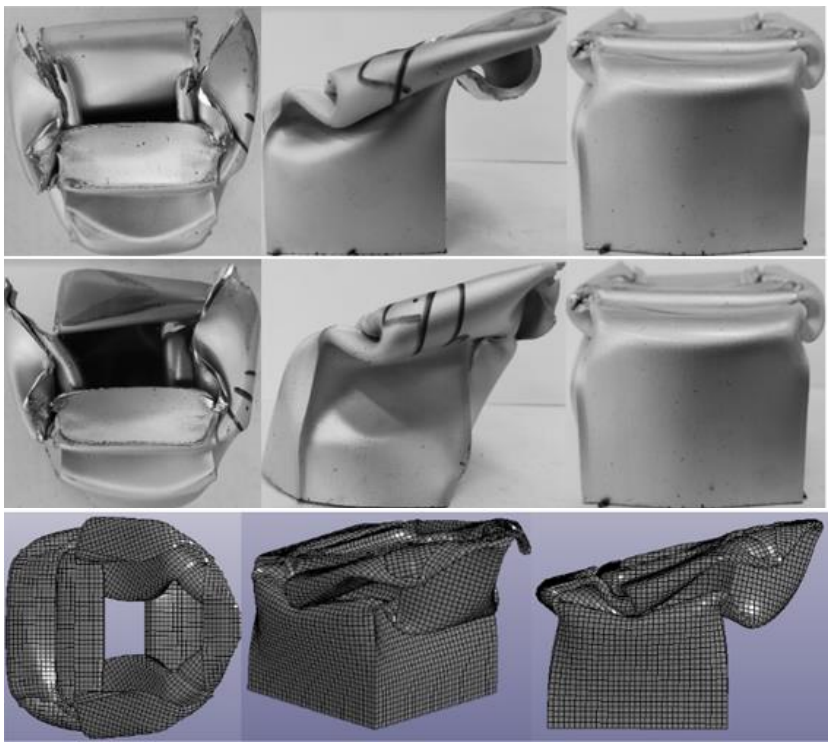

**Figure 170 Collapsed structures for case 4-edge (top: test 4a, mid: test 4b, bottom: LS DYNA)**

### 5.2.4.2 Initial contact in corner

For the 15º obliquely loading tube under an initial contact-in-corner with the impactor, both numerical and experimental results showed a sufficient agreement on PCF revealing an error of 2.8%. In addition, the crushing force distribution during plastic collapse is captured accurately by the FE model allowing for an accurate prediction in EA capability where FE model and experimental results showed a deviation of 6.8% regarding test 4a which reacted to an error in predicted CFE of 4.12% as although PCF was sufficiently predicted, the error in MCF was slightly higher affected by the accuracy in predicted EA. Moreover, the number of formulated folds is also predicted accurately by the FE model capturing two inextensional folds reflected further by the two local peaks in crushing force during collapse as depicted in the following figure. Also, the inextensional mode of plastic deformation allowed for a stable and progressive behavior of collapse reflected by the linear EA increase with respect to impactor displacement showing a uniform increase rate. However, the slight tube corner tearing which occurred during the two tests is not captured by the FE model as PCF was not proved great enough to react to material failure around tube corners. Although that FE model failed to predict

the tearing occurance, the EA is captured sufficiently as the tearing magnitude in the tests seemed to be low without thus reacting to a significant EA decrease.

Finally, regarding the plastic collapse mechanism, both FE models and experimental tests revealed a sufficient agreement on both deformation mode and the number of formulated folds showing an inextensional collapse mechanism under 2 plastic folds. However, the occurred slight corner tearing in tests is not captured by the FE model as PCF was not high enough to react to a material failure during simulation which although did not affect the predicted energy absorption capability due to the low tearing extent.

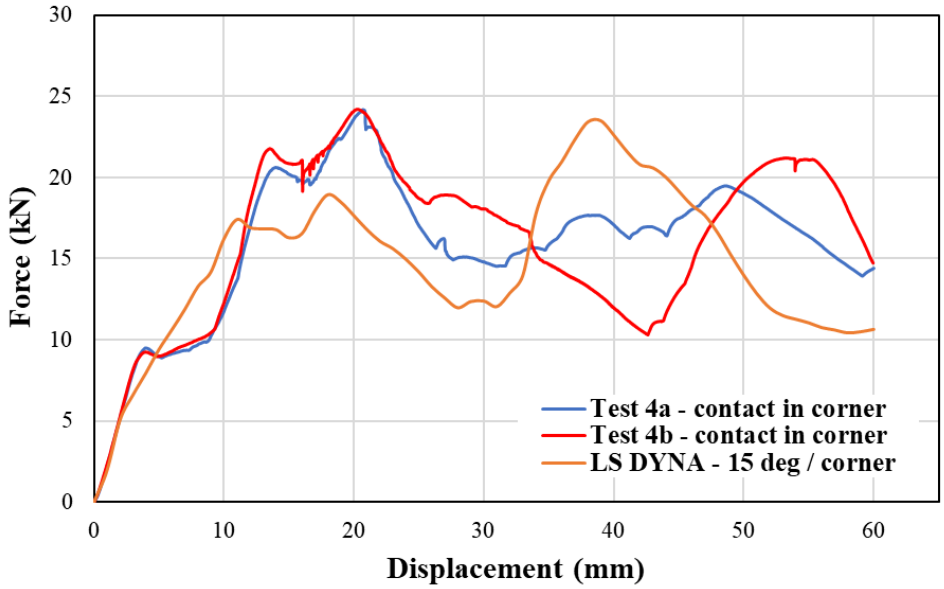


**Figure 171 Experimental vs. numerical F-x curves for 4-corner**

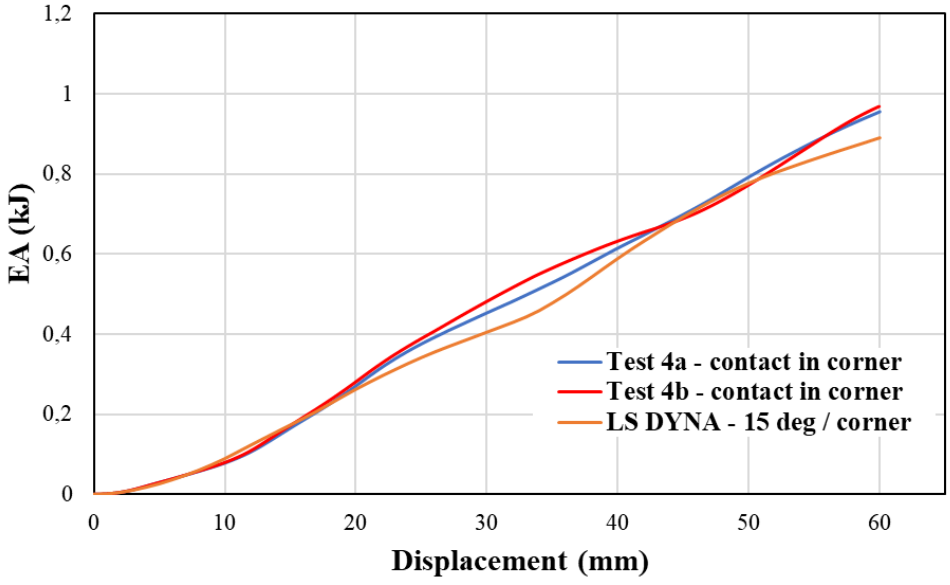


**Figure 172 Experimental vs. numerical EA-x curves for 4-corner**

**Table 24 Results in comparison between tests and simulation for case 4-corner**

| *15º oblique loading – case 4-corner* | | | |
|---|---|---|---|
| | LS DYNA | Test 3a-corner | Test 3b-corner |
| **PCF (kN)** | 23.49 | 24.17 | 24.20 |
| **MCF (kN)** | 14.84 | 15.93 | 16.16 |
| **EA (J)** | 890.5 | 955.7 | 968.8 |
| **SEA (kJ/kg)** | 18.89 | 20.27 | 20.55 |
| **CFE (-)** | 0.63 | 0.66 | 0.67 |

| | LS DYNA – Test 4a error (%) | LS DYNA – Test 4b error (%) |
|---|---|---|
| **PCF** | 2,81 | 2,91 |
| **EA** | 6,82 | 8,09 |
| **CFE** | 4,12 | 5,41 |

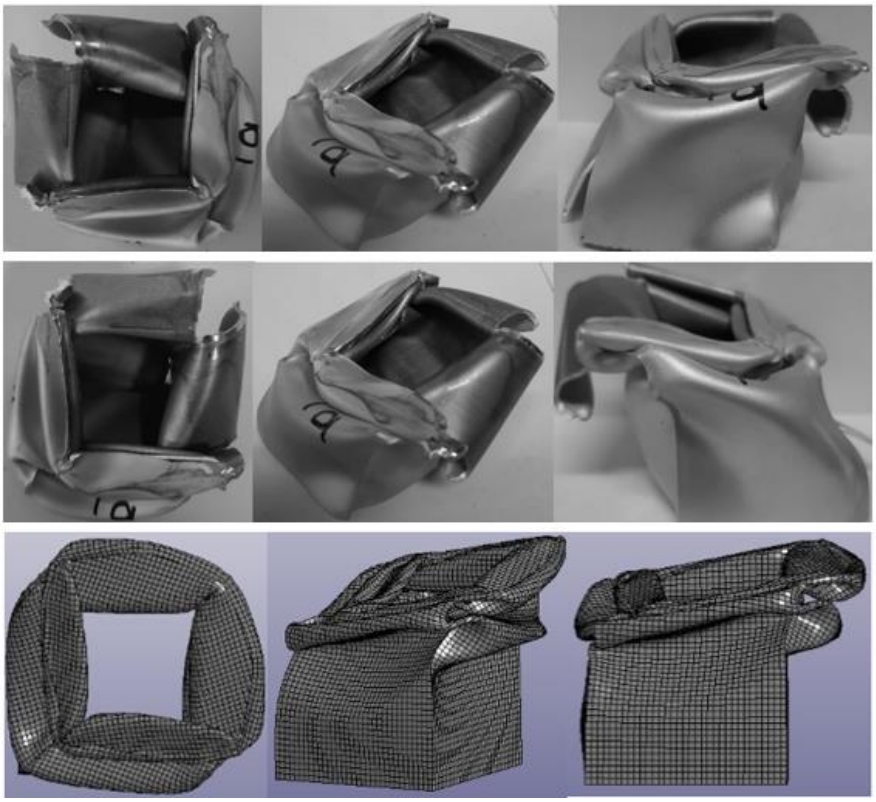

**Figure 173 Collapsed structures for case 4-corner (top: test 4a, mid: test 4b, bottom: LS DYNA)**

## 5.3 Conclusions

By summarizing the provided experimental and numerical results, critical conclusions can be extracted for the crashworthiness response of the examined square tube models subjected to axial and oblique impact loading regarding the loading angle effect and the effect of initial contact type between impactor and tube. In more specific, the comparison between the simulations and the experimental tests showed a sufficient agreement in both main crashworthiness response parameters like PCF and EA revealing errors below 7.5% and 8% respectively reflecting thus the validity of the developed FE models.

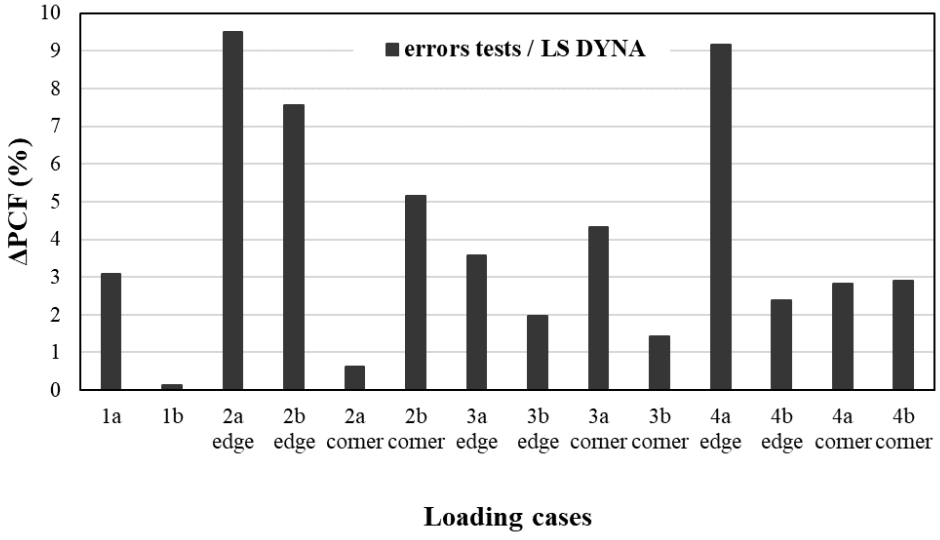


**Figure 174 PCF errors between tests and simulations**

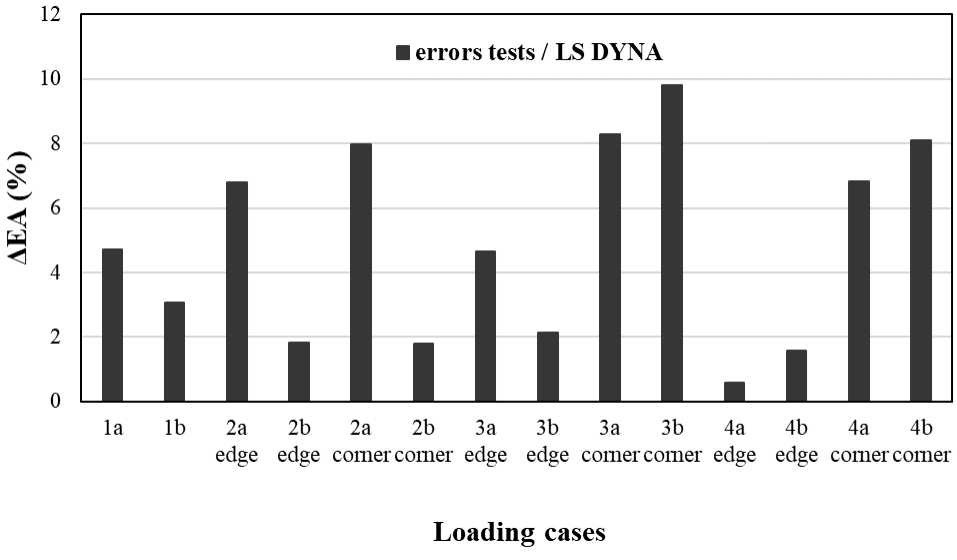


**Figure 175 EA errors between tests and simulations**

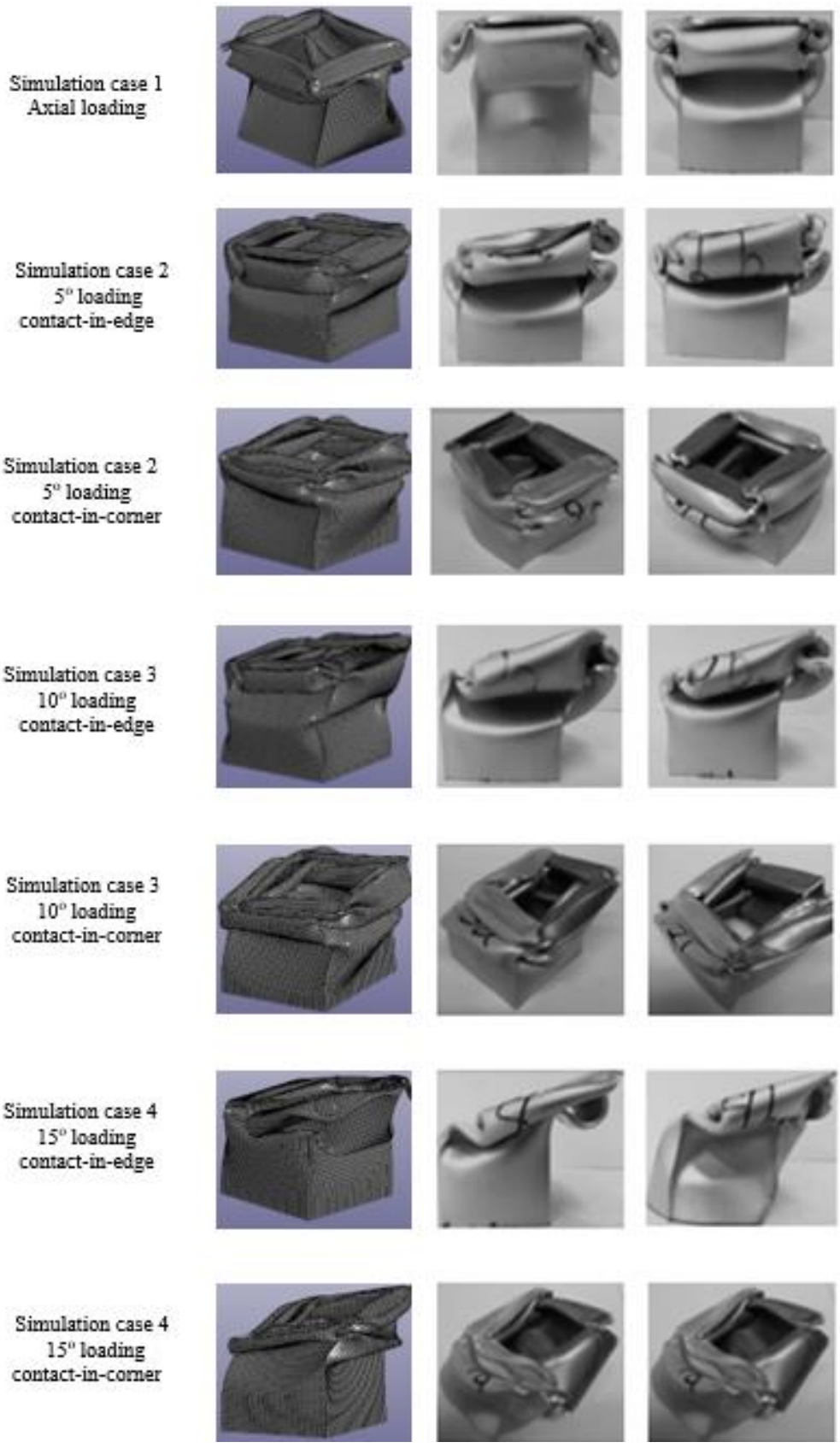


**Figure 176 Final views of crushed tubes (left: LS DYNA, mid: test a, right: test b)**

Regarding the predicted plastic collapse mechanism, all experimental tests revealed an inextensional collapse mode by formulating 2 or 3 inextensional plastic folds in the cases of 1&4 and 2&3 respectively. In addition, in all tests a slight tearing was occurred around tube corners without however being sufficient enough to result in a significant EA decrease as the increase rate of energy absorption with respect to impactor displacement remained uniform except the axial loading case where the occurred tearing during plastic deformation reacted to a significant decrease in EA. Further, all tube models predicted accurately both inextensional deformation mode and the number of formulated folds in all cases, while tearing occurance was captured only in axial loading simulation where the great enough PCF caused a high bending moment concentration around tube corners resulting in tearing. However, the obliquely crushed tube models did not succeed to predict tearing due to the lower PCF which did not seem enough to bring any material failure around tube corners without although affecting the accuracy in predicted EA by the FE models as the tearing effect magnitude on obliquely crushed tubes seemed weaker than the stable and progressive inextensional collapse behavior which reacted to a linear EA increase during plastic deformation.

Regarding the crashworthiness performance of the examined tubes, PCF reveals a decrease with respect to crushing angle especially in low loading angles as at higher ones PCF seems to flatten out. The PCF decrease is caused due to the additional bending moment which is introduced by the lateral force component facilitating the plastic collapse initiation, while also the tearing occurance also reacted to PCF decrease. Also, in all examined crushing angle range, PCF in contact-in-corner conditions proved to be slightly greater than the one under contact-in-edge conditions, while also the oblique crushing cases showed a weakened crushing angle effect on PCF due to tube tearing which restricted the required crushing force for plastic deformation by introducing material failure in lower force value.

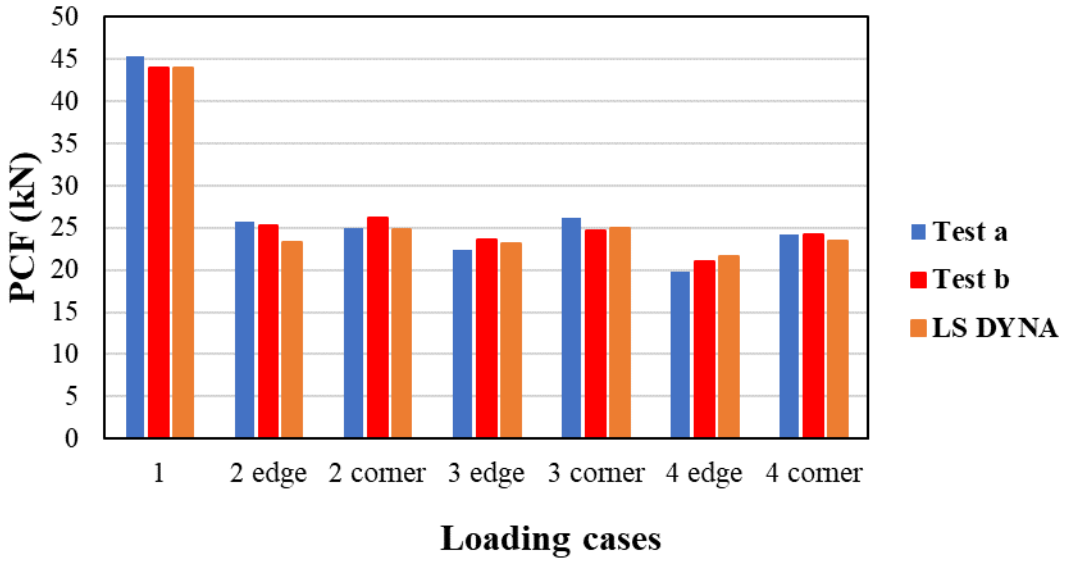


**Figure 177 PCF results**

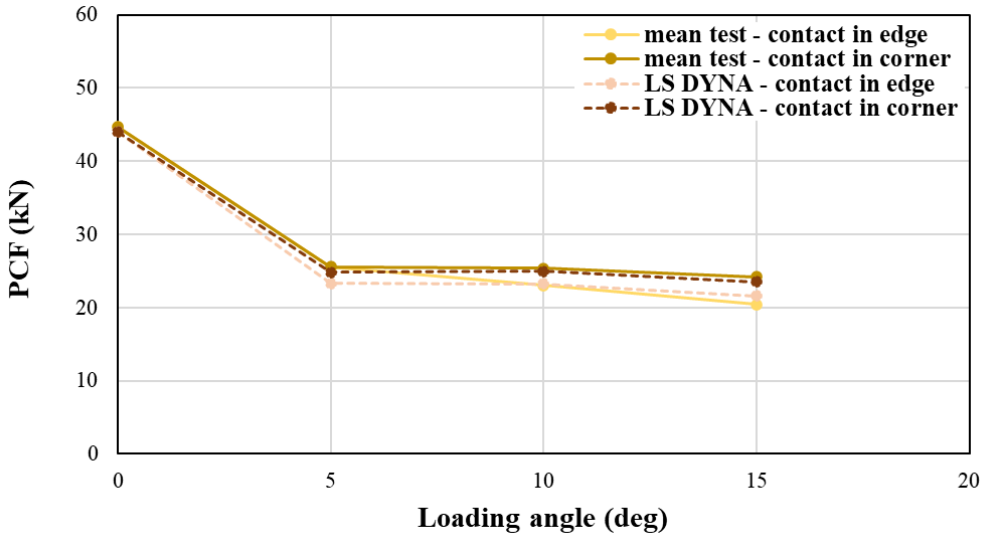


**Figure 178 PCF variation with loading angle and type of initial contact**

Regarding the provided energy absorption capacity \, MCF, EA and SEA are treated as the proper indicators in order to evaluate the crashworthiness performance of the tested tubes. The above response parameters reveal the same tendency with respect to the crushing angle and the initial type of contact as they are proportional metrics capturing thus similarly the tendency variations of the energy absorption capability. As depicted in the following figures, the maximum energy absorption capacity is revealed by the 5º oblique impact loading case under an initial contact-in-corner between impactor and tube. In fact, 5º cornered oblique crushing case revealed a greater EA compared to axial crushing due to tearing occurance in the last one which caused an EA drop, while 5º edged crushing showed slightly greater EA compared to axially crushed tube model. Therefore, at low crushing angle tearing effect seemed stronger than the one of crushing angle on EA as in the case of the absence of any tearing axial loading condition would react to greater EA. Furthermore, as the crushing angle getting higher, EA reveals a decrease due to the additional bending moment introduced by lateral crushing force component facilitating both plastic collapse initiation and progress for both examined cases of initial contact between tube and impactor.

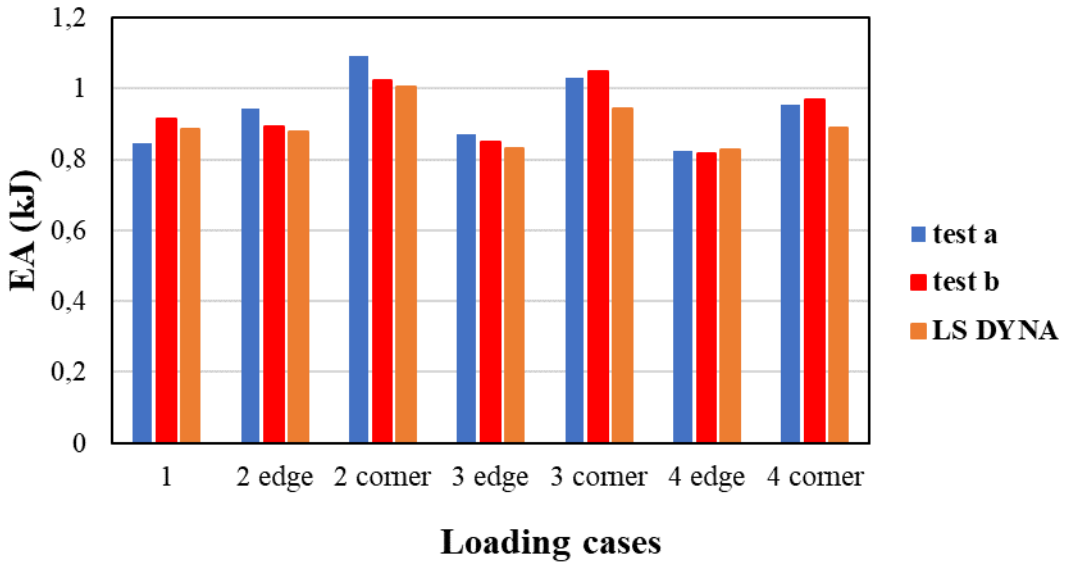


**Figure 179 EA results**

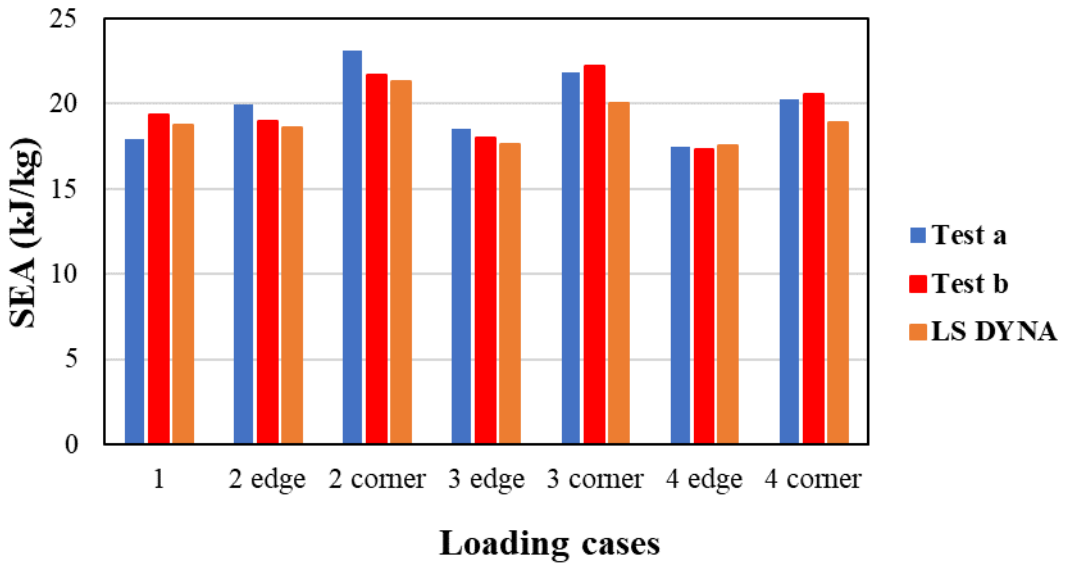


**Figure 180 SEA results**

In more detail, in all examined oblique crushing angles, the contact-in-corner type reveals greater energy absorption capacity compared to the contact-in-edge type. Also, the cornered oblique crushing revealed a linear decrease of EA with respect to crushing angle, while the edged oblique crushing showed a sigma variance in EA reduction according to the simulations revealing a weaker crushing angle effect on energy absorption. Thus, the numerical results showed that edged oblique crushing highlights $10^{o}$ as the critical crushing angle above from which slight bending mode is occurred during plastic collapse reducing EA, while cornered oblique impact loading does not reveal a critical crushing angle in the examined range until $15^{o}$ showing a linear drop in EA according to both

numerical and experimental results. Thus, cornered oblique crushing conditions can be considered as more beneficial providing greater energy absorption capacity and an increased critical crushing angle compared to edged oblique loading.

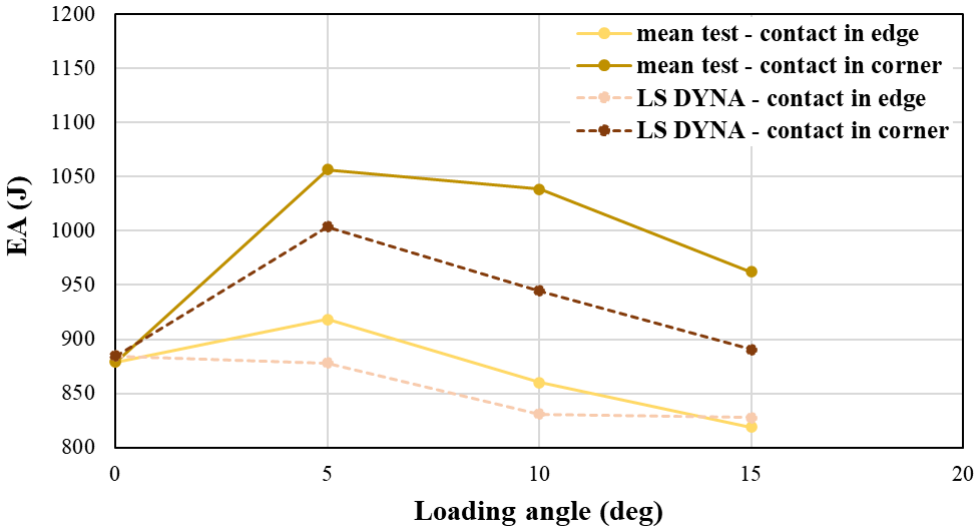


**Figure 181 EA variation with loading angle and type of initial contact**

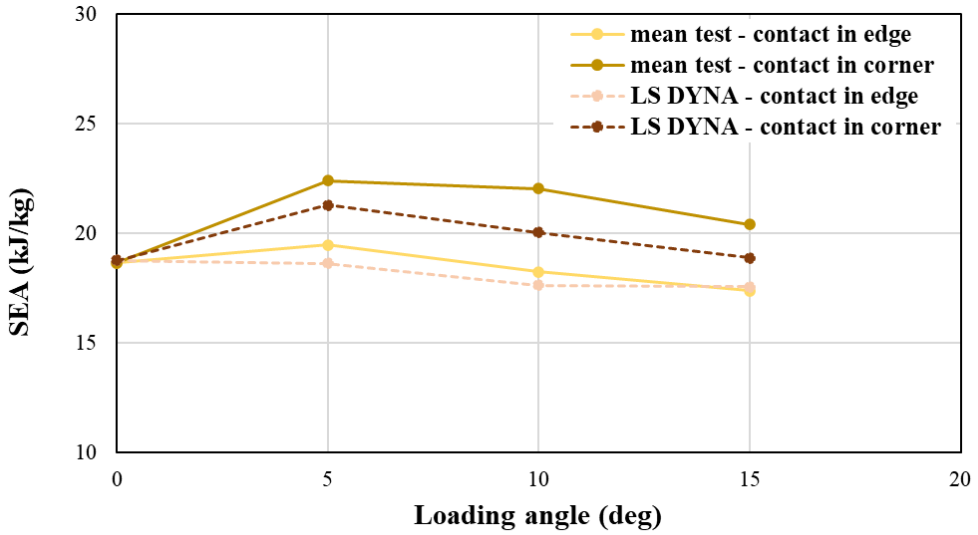


**Figure 182 SEA variation with loading angle and type of initial contact**

Moreover, both tests and simulation agreed that CFE is captured at higher levels in the case of cornered oblique crushing conditions compared to edged oblique crushing, while as the crushing angle getting higher, the difference in CFE between edged and cornered oblique loading is eliminated. Finally, a maximum CFE value is revealed for 5º cornered oblique impact as in axial crushing the occurred great enough PCF reacts to lower CFE due to lower energy

absorption caused by the significant tube tearing. Thus, 5º cornered oblique crushing conditions can be considered as the most efficient among the examined ones providing the highest EA, SEA and CFE levels.

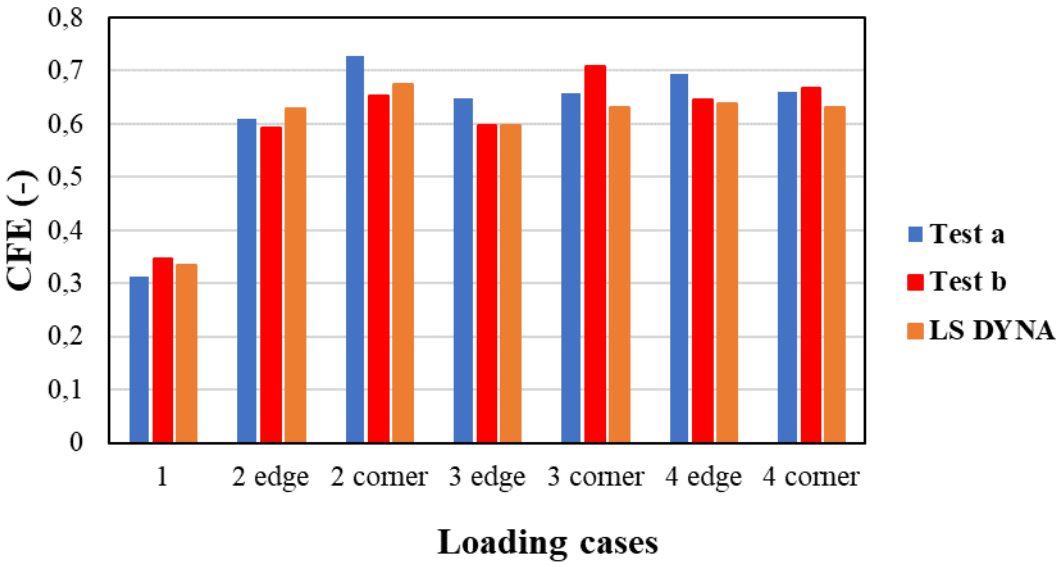


**Figure 183 CFE numerical results**

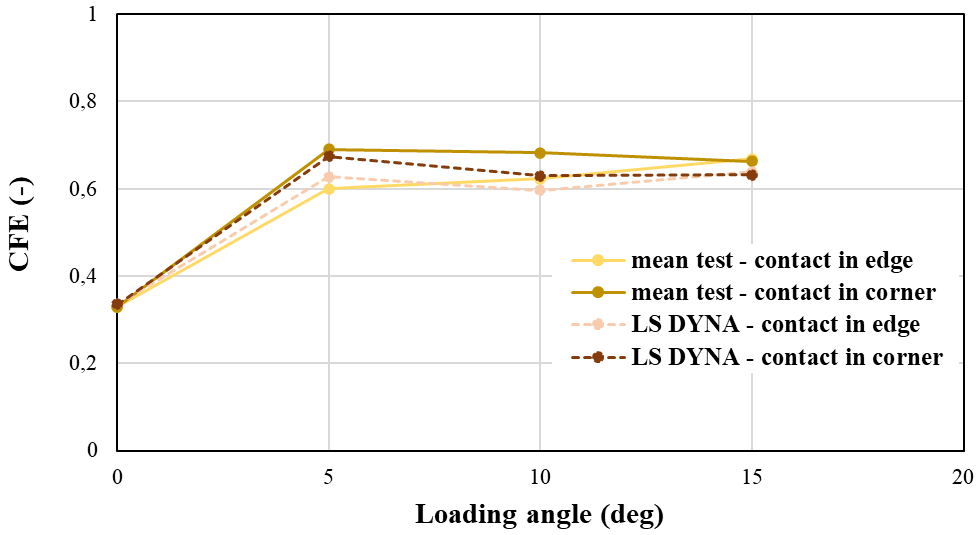


**Figure 184 CFE variation with loading angle and type of initial contact**

# 6. Summary, Conclusions and Recommendation for Future Work

## 6.1 Summary

The purpose of this study is to investigate the crashworthiness behavior of thin-walled square aluminium tubes under both axial and oblique impact loading in order to evaluate their crushing response in terms of efficiency by assessing their energy absorption capability and observing the occurred collapse mechanism. The examined cases consisted of axial and oblique loading scenarios under crushing angles of $0^o$ to $15^o$, while in the case of oblique crushing two different types regarding the initial contact between impactor and tube were examined. In the first case, the impactor initially compressed the tube alongside the top edge of its cross-section labelling that case as "contact-in-edge", while in the second case the initial contact took place around tube corner of its cross-section labelling that as "contact-in-corner". The aim of this thesis was to study the crushing behavior of the examined square tubes subjected to axial and oblique impact loading and evaluate their crashworthiness performance. The main focus was paid on capturing the effects of crushing angle and initial type of contact on energy absorption capacity and plastic collapse initiation. In more specific, the crushing angle effect was investigated around its influence on the collapse mode and the crashworthiness parameters, while an important goal was the identification of a critical crushing angle which reacts to a significantly lower energy absorbing levels by bringing an unstable behavior in the plastic collapse such as a bending mode. Regarding the influence of initial contact type ("in-edge" or "in-corner"), the two different cases were examined aiming to capture their effect on plastic collapse initiation and progress focusing on peak crushing force and further on energy absorption as it was consequently affected.

For the needs of current work, both experimental tests and numerical simulations were carried out in order to provide the force-displacement curve in each examined case and estimate the main crashworthiness response metrics such as the peak crushing force, the mean crushing force, the absorbed energy and the specific one corrected to the structure mass and finally the crushing force efficiency. Moreover, the occurred collapse mechanism was observed for each examined case capturing several states during plastic deformation in order to understand its characteristics which affect the structure crashworthiness response and in consequence its energy absorption capability.

During the experimental investigation, two experimental tests were carried out for each examined case in order to minimize the possible deviations which may occur due to data recording errors, varied material properties and unpredicted anisotropy, compression test variation etc. The examined specimens

consisted of thin-walled aluminium AA6060-T6 tubes with squared cross-section of 50 mm width, 1.5 mm wall thickness and 100 mm initial length, while the examined loading cases contained axial and oblique impact under the crushing angles $0^o/5^o/10^o/15^o$ labelling so the specimens from 1 to 4 respectively. All experimental compression tests were conducted in quasi-static conditions applying a constant loading rate of 10 mm/min until a maximum shortening of 60 mm, while the oblique compression tests represented off-axis oblique loading conditions with the tube and bottom base being rotated to the proper crushing angle. Finally, each experimental test was conducted twice for extracting more accurate and valid results, labelling so each test case as "a" and "b".

For the conducted numerical simulation, the explicit non-linear code of LS-DYNA software was utilized after the finite element models development. During modelling procedure, the bodies geometry was initially designed and a finite element mesh was next generated. Impactor and bottom base were modelled via 8-node solid elements which then were treated as undeformable and rigid bodies. In contrast, tube was modelled via 4-node shell elements which have been proved quite efficient in crashworthiness modelling considering the examination of thin-walled structures. At next, tube and plates material properties were applied, while experimental tension tests were carried out for AA6060-T6 tube in order to obtain its stress-strain curve and estimate its response behavior through plastic deformation. Following, the appropriate boundary conditions were applied at each interface in order to avoid any penetration between the tube surface and the plates, but also between tube folds too. Further, tube bottom end was treated as fixedly supported due to the base configuration which did not allow any sliding, and thus the respective nodes of tube bottom elements were constrained against any displacement or rotational degree of freedom. Finally, dynamic loading conditions were applied by adjusting a constant vertical loading velocity of 1 m/s to the upper plate. Both experimental and numerical investigation provided the force-displacement curve and the respective crashworthiness response metrics while also the occurred collapse mechanism was observed for the finite element validation procedure and the evaluation of crashworthiness performance in each case.

## 6.2 Conclusions

By summarizing the provided results of experimental tests and finite elements simulations, all developed finite element models showed a sufficient agreement with conducted tests in terms of PCF and EA revealing deviations below 7.5% and 8% respectively. Also, all FE models captured the inextensional collapse mechanism which was occurred by the tests, while an absolute agreement was also captured between tests and simulations regarding the number of formulated folds.

In more specific, all tubes revealed inextensional collapse mode with axial loading and $15^o$ oblique crushing showing 2 plastic folds and $5^o$ and $10^o$ oblique crushing revealing 3 inextensional plastic folds. Further, a slight tearing around

tube corners was occurred in all test cases due to high bending moment concentration at the final stages of collapse. However, only the FE model of axial loading simulation succeeded to capture tube tearing due to the great enough PCF, while in contrast FE models of obliquely crushed tubes did not manage to capture tearing effect due to lower PCF which proved not high enough to react to material failure around tube corners. However, although no tearing was capture by FE models of obliquely crushed tubes, the accuracy level in EA prediction was not affected as the stable and progressive behavior of inextensional deformation mode proved stronger than tearing effect which is also reflected by the constantly linear increase in EA during plastic collapse.

Further, the axially collapse tube revealed the greatest PCF among the others as in the case of oblique impact loading PCF showed a decrease due to the additional bending moment introduced by the lateral force component facilitating plastic collapse initiation. However, the magnitude of crushing angle effect on PCF seemed to weaken at higher angles where the tearing occurance revealed stronger restricting the required crushing force for plastic collapse at lower levels. Moreover, an initial contact-in-corner condition between impactor and tube revealed slightly greater PCF than the edged oblique crushing at all examined loading angle range where however at higher angles PCF seemed to flatten out.

Regarding the crashworthiness performance, $5^o$ cornered oblique crushing revealed the greatest energy absorption capacity among all examined cases as the occurred tearing in axially crushed tube resulted in a significant decrease in EA, while in the case of the absence of any tearing the axially crushed tube would be expected to reveal the greatest EA showing that tearing effect seemed stronger than the one of crushing angle at low crushing angles. However, regarding the oblique loading cases, the increase in crushing angle resulted in EA decrease due to the additional bending moment introduced by the angled loading which facilitated both plastic collapse initiation and progress. Thus, at higher crushing angles the magnitude of crushing angle effect seemed stronger than the one of tearing effect for both examined initial type of contact.

Regarding the last one, at all examined crushing angles, cornered oblique loading proved to be more beneficial compared to edged oblique crushing revealing greater EA and SEA, while further EA showed a linear decrease with crushing angle for cornered oblique loading. In contrast, EA decrease with loading angle revealed a sigma variance tendency highlighting a $10^o$ critical crushing angle above of which slight bending collapse mode started to occur reacting to EA drop. Therefore, cornered oblique loading revealed not only greater energy absorption capability compared to edged one, but further an increase in critical loading angle which was not captured in the examined loading angle range for cornered oblique loading. In addition, the highest CFE was also captured for loading case 2-corner revealing $5^o$ cornered oblique impact loading as the most beneficial crushing case under the greatest EA, SEA and CFE. Also, CFE showed an increase with loading angle as higher crushing angles reacted to PCF drop due to tearing and angled loading, while MCF was more flattened out.

Finally, cornered oblique crushing revealed a greater CFE than edged one, the difference of which however seemed to be eliminated at high crushing angles.

## 6.3 Recommendation for Future Work

Some research topics which are strongly recommended for future investigation in the field of crashworthiness response under oblique impact loading conditions similar to the topic of current work are developed following:

- Regarding the finite element modelling procedure, the utilization of T-shell elements for the tube is considerably valuable in order to assess its effect on crushing response characteristics. More specifically, a more direct consideration of wall thickness regarding the stiffness matrix elements will affect the plastic deformation mode during collapse revealing thus an effect on crashworthiness parameters and possibly on collapse mode regarding the type and the number of formulated convolutions. Furthermore, more complex material modeling formulas can be utilized considering the effect of strain rate on stress hardening or capturing the material failure by implementing penalties or failure criteria. Finally, the examination of different finite element deformation modes through the utilization of other stiffness formulas via ELFORM parameter is considered quite valuable as implements different approaches during elements deformation. Thus, interesting conclusions can be extracted regarding their effect on failure mechanism and in consequence the energy absorption capability.

- Examination of angled loading type for oblique crushing in order to estimate the revealed behavior, the crashworthiness metrics and the observed failure mechanism during collapse. Also, the investigation of the types of tube ends support is further interesting to identify their effect on plastic collapse initiation and progress affecting so the energy absorption capacity.

- Examination of different cross-section types such as circular or polygonal tubes for identifying the effect of the number of cross-section corners on energy absorption and peak crushing force. In addition, parametric analyses for wall thickness, tube length and its width can also be carried out to capture their influence on the occurred collapse mode and crashworthiness efficiency as further the impact of crushing angle on collapse mode map with respect to L/a and a/t ratios can be captured.

# 7. Bibliography


[1] **W.J. Hughes** (2016). "Crushing Behavior of Laminated Composite Structural Elements: Experiment and LS-DYNA Simulations." Federal Aviation Administration, U.S. Department of Transportation, DOT / FAA / TC-15/25

[2] **US Dept. of Transportation FAA** (2009). Advisory Circular 20-107b. pp: 1-37

[3] **F. Garattoni** (2011). "Crashworthiness and composite materials: development of an experimental test method for the energy absorption determination and implementation of the relative numerical model." PhD thesis. University of Bologna

[4] **H. Nikkhah, A. Baroutaji, A. Ghani Olabi** (2019). "Crashworthiness design and optimisation of windowed tubes under axial impact loading." ELSEVIER

[5] **F. Tarlochan, S. AiKhatib** (2017). "Energy absorption capabilities of complex thin walled structures." 4th Internacional Conference of Mechanical Engineering Research. IOP Publishing

[6] **W. Suzhen, Z. Gang, S. Guangyong, L. Qiang, L. Guangyao, L. Qing** (2016). "On design of milti-cell thin-walled structures for crashworthiness." ELSEVIER. Internacional Journal of Impact Engineering

[7] **The Aluminium Automotive Manual** (2013). Applications-Car Body-Crash Management Systems ELSEVIER. Internacional Journal of Impact Engineering. European Aluminium Association

[8] **A.Riccio, S.Saputo, A.Sellitto, A.Russo, F. Di Caprio, L.Di Palma** (2019). "An insight on the Crashworthiness Behavior of a Full-Scale Composite Fuselage Section at Different Impact Angles." Aerospace MDPI

[9] **G.L. Farley, R.M.Jones** (1989). "Energy-absorption capability of compsite tube and beams." NASA Technical Publications. TM 101634. pp: 1-248

[10] **C. Bisagni** (2009). "Experimental Investigation of the Collapse Modes and Energy Absorption Characteristics of Composite Tubes." Internacional Journal of Crashworthiness. Vol.14. No.4. pp: 365-378

[11] **A.G. Mamalis, D.E. Manolakos, M.B. Ioannidis, D.G. Chronopoulos, P.K. Kostazos** (2009). "On the crashworthiness of composite rectangular thin-walled tubes internally reinforced with aluminium or polymeric foams: Experimental and Numerical simulation." ELSEVIER. Composite Structures

[12] **M. Ptak, P.Kaczynski, F.A.O. Fernandes, R.J. Alves de Sousa** (2017). "Assessing impact velocity and temperature effects on crashworthiness properties od cork material." ELSEVIER. Internacional Journal of Impact Engineering

[13] **P.Florent, Y.Wenyi, W.Cui'e** (2007). "Crushing modes of aluminium tubes under axial compression." 5th Australian Congress on Applied Mechanics. Brisbane Australia

[14] **Z. Tang, S. Liu, Z. Zhang** (2013). "Analysis of energy absorption characteristics of cylindrical multi-cell columns." ELSEVIER. Thin-Walled Structures. Vol. 62. pp. 75-84

[15] **S. R. Reid** (1993). "Plastic deformation mechanisms in axially compressed metal tubes used as impact energy absorbers." ELSEVIER. International Journal of Mechanical Sciences. Vol. 35 (12). pp. 1035-1052

[16] **A. Reyes, M. Langseth, O. D. Hopperstad** (2001). "An experimental and numerical study on the energy absorbing capability of aluminium extrusions under oblique impact." 3rd European LS-DYNA Conference. Paris France

[17] **A. Baroutaji, M. Sajjia, A.G. Olabi** (2017). "On the crashworthiness performance of thin-walled energy absorbers: Recent advances and future developments." ELSEVIER. Thin-Walled Structures. Vol. 118. Pp. 137-163

[18] **E. Acar, M. Altin, M.A. Guler** (2019). "Evaluation of various multi-cell design conceptsfor crashworthiness design of thin-walled aluminium tubes." ELSEVIER. Thin-walled Structures

[19] **A.G. Mamalis, D.E. Manolakos, M.B. Ioannidis, D.P. Papapostolou** (2004). "Crashworthy characteristics of axially statically compressed thin-walled square CFRP composite tubes: experimental." ELSEVIER. Composite Structures

[20] **P. Shivdayal, R. V. Venkata, C. S. Guedes** (2019). "Crashworthiness analysis of polymer composites under axail and oblique impact loading". International Journal of Mechanics and Science. Vol. 156. pp. 221-234

[21] **H. R. Zarei** (2019). "Experimental and numerical crashworthiness investigation of hybrid composite aluminium tubes under dynamic axial and oblique loadings." Intern. Journal of Automative Engineering. Vol. 5. No.3. pp. 1084-1093

[22] **D. Fauzan, A. Shahrum, A. Ariffin, M. N. Zilkifli** (2016). "Finite element analysis and crashworthiness optimization of foam-filled double circular tubes under oblique loading." Latin American Journal of Solids and Structures. Vol. 13. pp. 2176-2189

[23] **H. S. Kim, T. Wierzbicki** (2000). "Numerical and analytical study on deep biaxial bending collapse of thin-walled beams." Latin American Journal of Solids and Structures. Vol. 13. pp. 2176-2189

[24] **D. C. Han, S. H. Park** (1999). "Collapse behavior of square thin-walled columns subjected to oblique loads." Thin-walled strctures. Vol. 35 (3). pp. 167-184

[25] **Y. Crutzen, A. Inzaghi, M. Mogilevsky, C. Albertini** (1996). "Computer modelling of the energy absorption process in box-type structures under oblique impact." Automotive Automation Limitied UK. pp. 1293-1298

[26] **S. Pirmohammad, S. E. Marzdashti** (2016). "Crushing behavior of new designed multi-cell members subjected to axial and oblique quasi-static loads." ELSEVIER. Thin-Walled Structures. Vol. 108. pp. 291-304

[27] **W. Liu, L. Jin, Y. Luo, X. Deng** (2020). "Multi-objective crashworthiness optimisation of tapered star-shaped tubes under oblique impact." International Journal of Crashworthiness. pp. 1-15

[28] **F. Tarlochan, F. Samer, A. M.S. Hamouda, S. Ramesh, K. Khalid** (2013). "Design of thin wall structures forenergy absorption applications: Enhancement of crashworthiness due to axial and oblique impact forces." ELSEVIER. Thin-Walled Structures. Vol. 71. pp. 7-17

[29] **C. Qi, S. Yang** (2014). "Crashworthiness and lightweight optimisation of thin-walled conical tubes subjected to an oblique impact." International Journal of Crashworthiness. Vol. 19 (4). pp. 334-351

[30] **T. Borvik, O. S. Hopperstad, A. Reyes, M. Langseth, G. Solomos, T. Dyngeland** (2003). "Empty and foam-filled circular aluminium tubes subjected to axial and oblique quasistatic loading." International Journal of Crashworthiness. Vol. 8 (5). pp. 481-494

[31] **Q. Gao, L. Wang, Y. Wang, C. Wang** (2016). "Crushing analysis and multiobjective optimisation of foam-folled ellipse tubes under oblique impact loading." ELSEVIER. Thin-Walled Structures. Vol. 100. pp. 105-112

[32] **C. Qi, S. Yang, F. Donf** (2012). "Crushing analysis and multiobjective crashworthiness optimization of tapered square tubes under oblique impact loading." Thin-walled Structures. 59. pp. 103-119

[33] **J. Song** (2013). "Numerical simulation on windowed tubes subjected to oblique impact and a new method for the design of obliquely loaded tubes." Intern. Journ. of Impact Engineering. 54. pp. 192-205

[34] **C. Baykasoglu, A. Baykasoglu, M. T. Cetin** (2019). "A comparative study on crashwortiness of thin-walled tubes wih functionally graded thickness under oblique loadings." Intern. Journ. of Impact Engineering. 24 (4). pp. 453-471

[35] **O. Mohammadiha, H. Ghariblu** (2016). "Crush behavior optimization of multi-tubes filled by functionally graded foam." ELSEVIER. Thin-walled Structures. Vol. 98. pp. 627-639

[36] **J.M. Alexander** (1960). "An approxiamte analysis of the collapse of thin cylindrical shells under axial loading." Imperial College of Science and Technology

[37] **W. Abramowicz, N. Jones** (1984). "Dynamic axial crushing of circular tubes." Intern. Journ. of Impact Engineering. Vol. 2. pp. 263-281

[38] **T. Wierzbicki, S. U. Bhat, W. Abramowicz, D. Brodkin** (1992). "Alexander revised – A two folding elements model of progressive crushing of tubes." Intern. Journ. od Solid Mechanics. Vol. 29 (2). pp. 3269-3288

[39] **W.Johnson, P.D. Soden, S.T.S. Al-Hassani** (1997). "Inextensional collapse of thin-walled tubes under axial compression." Journal of Strain Analysis. Vol. 12. No. 4

[40] **A.G. Mamalis, D.E. Manolakos, G.A. Demosthenous, W.Johnson** (1991). "Axial Plastic Collapse of Thin Bi-Material Tubes as Energy Dissipating Systems." Internacional Journal of Impact Engineering. Vol.11. No.2. pp: 185-196

[41] **T. Tran, S. Hou, X. Han, N. Nguyen, M. Chau** (2014). "Theoretical prediction and crashworthiness optimization of culti-cell square tubes under impact loading." Internacional Journal of Mechanical Sciences. Vol. 89. pp: 177-193

[42] **D. Kecman** (1983). "Bending collapseof rectangular and square section tubes." Intern. Journ. of Mech. Sciences. 25 (9-10). pp. 623-636

[43] **Livermore Software Technology Corporation** (2007). "LS-DYNA keyword user's manual." Vol. I. Version 971